MODELLING OF ADSORPTION-BASED REFRIGERATION SYSTEMS

Liu Yue

SCHOOL OF MECHANICAL AND AEROSPACE ENGINEERING

NANYANG TECHNOLOGICAL UNIVERSITY

2005

MODELLING OF ADSORPTION-BASED REFRIGERATION SYSTEMS

Submitted by

Liu Yue

SCHOOL

OF

MECHANICAL AND AEROSPACE ENGINEERING

A thesis submitted to the Nanyang Technological University

in fulfillment of the requirements for the degree of Doctor of Philosophy

2005

ABSTRACT

This thesis presents several numerical models including thermodynamic model, lumped model and heat and mass transfer model for different zeolite/water adsorption refrigeration cycles to investigate the effects of parametric and operating conditions on system performance. Experiments were also carried out to validate the heat and mass transfer model.

Firstly, a thermodynamic model based on the first and second laws of thermodynamics is presented. The effects of operating conditions on the coefficient of performance (COP) for different cycles were investigated using a first law approach. The results show that the COP can be greatly improved (about 44%) when compared with the intermittent cycle by using heat recovery, while the mass recovery cycle can only increase the COP by 6%. For a coupled heat and mass recovery cycle, the COP will increase by about 53%, which is greater than the sum of the contributions from the heat and mass recovery cycles. Second law analysis is also used to obtain the upper performance limits for several multi-bed cycles.

Secondly, a novel cascading adsorption refrigeration cycle is proposed to improve system performance. This cycle consists of two zeolite adsorbent beds and a silica gel adsorbent bed. The zeolite adsorbent bed is configured as the high temperature stage while the silica gel adsorbent bed acts as the low temperature stage. Both heat and mass recovery are carried out between the two zeolite adsorbent beds. In addition, heat is also exchanged between the zeolite adsorbent and the silica gel adsorbent beds. A lumped model is assumed for this cascading cycle. The COP for the base case is found to be 1.35, which is much higher than the COP of an intermittent cycle (about 0.5) and a two-bed combined heat and mass recovery cycle (about 0.8). However, its specific cooling power (SCP) is much lower than that of the intermittent cycle.

Thirdly, a detailed cylindrical two-dimensional non-equilibrium numerical model for an intermittent cycle describing the combined heat and mass transfer in adsorbent bed is also

presented. As the performance of this system is mainly influenced by heat and mass transfer properties, three sub-models of heat and mass transfer properties (gas flow in adsorbent bed model, linear force driven model and equivalent heat transfer conductivity of adsorbent bed model) of the adsorbent bed are proposed. The model is solved by the control volume method. The effects of main configuration parameters such as the heat and mass transfer coefficients, thickness of the bed, diameter of the particle and porosity, on the thermal performance of the system are investigated. The effect of operating temperature on performance is also studied based on this model. This model is then validated by an experimental study. Subsequently, this heat and mass transfer model is extended to simulate a combined heat and mass recovery adsorption cycle. The numerical results show that the combined heat and mass recovery cycle between two adsorbent beds can increase the COP of an adsorption cooling system by more than 47% compared to the single bed cycle. A parametric study based on this model shows that an increase in the driven temperature results in the increase of both the COP and SCP of the adsorption cycle. On the other hand, the system performance can be severely deteriorated for velocities of the heat exchange fluid smaller than a critical value. An increase in the bed thickness will result in an increase in COP and a decrease in the SCP. The results of the simulations will provide useful guidelines for the design of this type of advanced adsorption cooling cycle.

Lastly, a zeolite/water adsorption refrigeration and internal reforming solid oxide fuel cell (IRSOFC) cogeneration system is presented to broaden the application area of the adsorption refrigeration system. A mathematical model is developed to simulate this combined system under steady-state conditions. The effects of fuel flow rate, recycle ratio, fuel utilisation factor, mass of adsorbent and inlet air temperature on the performance are considered. The results of the simulation show that the IRSOFC-AC cogeneration system can achieve a total efficiency (combined electrical power and cooling power) of more than 75%.

ACKNOWLEDGEMENTS

The author would like to express his sincere gratitude to his supervisor, Prof. Leong Kai Choong for his invaluable advice and constant encouragement throughout this project.

Furthermore, the author would also like to express his appreciation to Prof. Chai Chee Kiong and Mr. Chen Xu Yang for all the assistance that they had rendered to make the project possible. In addition, the author would like to express his sincere thanks to Mr. Yuan Kee Hock for his continuous support and technical expertise, without whom the experiments in this project would never have been completed. The author would also like to thank Dr. Wang Kean for his help on some experimental measurements.

Lastly, the author is grateful to his parents and friends for all things that he would have taken for granted.

TABLE OF CONTENTS

LIST OF FIGURES

LIST OF TABLES

LIST OF SYMBOLS

a	Mass flow rate of fuel, kmol/h
A	Heat transfer area of the adsorbent bed (m^2)
C_p	Specific heat (J/kg·K)
COP	Coefficient of performance
COP_C	Carnot coefficient of performance
D_0	Reference diffusivity (m^2/s)
D_e	Equivalent diffusivity in the adsorbent particles (m^2/s)
D_{ek}	Equivalent Knudsen diffusivity (m^2/s)
D_{hr}	Degree of heat recovery (%)
D_k	Knudsen diffusivity (m^2/s)
D_m	Molecular diffusivity (m^2/s)
D_p	Pore diffusivity (m^2/s)
D_s	Surface diffusivity (m^2/s)
d	Particle diameter (m)
E	Cell voltage (V)
E_D	Activation energy for diffusion (J/mol)
F	Faraday constant = 96,487 (C/mol)
H	Thickness of adsorbent bed (m)
h	Heat transfer coefficient ($W/m^2·K$); Specific enthalpy (J/kg)
h_{ms}	Contact heat transfer coefficient between metal tube and adsorbent bed ($W/m^2·K$)
i	Current density (mA/cm^2)
I	Current (A)
K	Permeability of adsorbent bed (m^2)
K_{ap}	Apparent permeability (m^2)

K_D	Permeability in Ergun equation (m^2)
K_E	Coefficient of inertial effect term in Ergun equation ($N \cdot s^2$/ kg)
K_p	Equilibrium constant
L	Length of adsorbent bed (m); Latent heat of vaporization (J/kg)
m	Mass (kg)
$\dot{m}_{al}$	Mass flow rate of the liquid phase adsorbate into the receiver (kg/s)
$\dot{m}_w$	Mass flow rate of the water vapour from the adsorber to condenser (kg/s)
$\dot{\boldsymbol{m}}$	Total mass flow flux of water vapour ($kg/s \cdot m^2$)
$\dot{\boldsymbol{m}}_p$	Poiseuille flow flux of water vapour ($kg/s \cdot m^2$)
$\dot{\boldsymbol{m}}_k$	Knudsen flow flux of water vapour ($kg/s \cdot m^2$)
$\dot{\boldsymbol{m}}_s$	Surface flow flux of water vapour ($kg/s \cdot m^2$)
M	Molar weight (kg/mol)
n	Adsorbed amount, kg/kg
$\mathbf{n}$	Normal vector of the surface area
P	Pressure (Pa)
P_{cw}	Cooling power (W)
P_{ew}	Electrical power (W)
P_s	Saturation pressure (Pa)
q	Adsorbed amount (kg/kg)
q_{max}	The initial value of adsorbed amount (kg/kg)
q_{min}	Adsorbed amount at the end of the generation phase (kg/kg)
q_{ra}	Effective heat influx by radiation (W/m^2)
Q	Heat obtained from or rejected to the heat exchange fluid (J); Heat transfer rate between adsorber and heat exchange fluid (W)
Q_a	Heat output during the cooling and adsorption phases (J)

Q_{co}	Heat output in condenser during generation phase (J)
Q_{ev}	Heat obtained from outside cold media in evaporator during adsorption phase (J)
Q_h	Total heat input during the heating and generation phases (J)
r	Radial coordinate (m); Coefficient of heat or mass recovery
r^*	Dimensionless radial coordinate
r_a	Circulation ratio
r_{ms}	Heat capacity ratio of adsorber metal to adsorbent
r_p	Radius of the particle (m)
R	Universal gas constant (J/mol·K); Radius of adsorbent bed (m)
S	Area of adsorbent bed surface (m^2)
S_f	Cross-sectional area of heat exchange fluid (m^2)
SCP	Specific cooling power (W/kg)
t	Time (s)
t_c	Cycle time (s)
t_h	Heat recovery time (s)
t_{hc}	Half cycle time (s)
t_m	Mass recovery time (s)
t_{st1}	Time of Step 1 (s)
T	Temperature (K)
T_a	Adsorption temperature (K) ; Atmospheric temperature (K)
T_g	Generation temperature (K)
TCP	Total mean cooling power (W)
u	Gaseous velocity in axial direction (m/s)
u_f	Fluid velocity (m/s)
u^*	Dimensionless gaseous velocity in axial direction

$\mathbf{u}$	Gaseous velocity vector (m/s)
U	Overall heat transfer coefficient (W/m^2·K)
U_f	Fuel utilisation factor
v	Gaseous velocity in radial direction (m/s)
v^*	Dimensionless gaseous velocity in radial direction
V_c	The inside volume of the condenser (m^3)
V_f^*	Dimensionless fluid velocity
V_{max}	Reference velocity (m/s)
W_c	Mass of the condenser (kg)
y	Distance to the wall of adsorbent bed (m)
z	Axial coordinate (m)
z^*	Dimensionless axial coordinate

Greek symbols

ΔH	Heat of adsorption/desorption (J/kg); Enthalpy of formation (kJ/mol)
ΔS	Entropy production (J/K)
Δm	Mass of cycled refrigerant (kg)
ε	Total bed porosity
ε_a	Bed porosity
ε_i	Particle porosity
ϕ_{0-a}	Heat transferred from the heating and cooling medium (W)
η	Second law efficiency; Over-potential (V)
μ	Dynamic viscosity (N·s/m^2)
θ	Dimensionless temperature
ρ	Density (kg/m^3)
λ	Thermal conductivity (W/m·K)

σ	Collision diameter for Lennard-Jones potential (Å)
τ	Tortuosity factor; Dimensionless time
ω	Dimensionless pressure
Ω	Collision integral; Dimensionless adsorbed amount

Subscripts

0	Initial state
a	Adsorbed phase
a^*	Start of isobaric adsorption phase
ac	Isobaric adsorption phase
b, bed	Adsorbent bed
c	Cold or condensing
co	Condenser
cw	Cold water in condenser
e	Evaporating
ev	Evaporator
eq	Equivalent
f	Heat exchange fluid
f-a	From heat exchange fluid to adsorber
g	Adsorbate vapour
gh	Isobaric generation phase
g^*	Start of isobaric generation phase
h	Heating
i	Three different parts of the adsorber (metal part, adsorbent and adsorbed component)
hxf	Heat exchange fluid
ic	Isosteric cooling phase
ih	Isosteric heating phase

in	Inlet fluid
l	Liquid adsorbate
m	Metal tube
out	Outlet fluid
p	Particle
po	Pore
rec	Heat or mass recovery
s	Adsorbent
t	Total
w	Liquid water
vi	Inlet of adsorbate vapour in condenser
1, 2 and 3	Adsorbers 1, 2 and 3

Superscripts

$(\quad)'$	Silica gel adsorbent
$\overline{(\quad)}$	Average

PUBLICATIONS ARISING FROM THIS THESIS

Journal papers

1. K.C. Leong and Y. Liu, Numerical modelling of combined heat and mass transfer in the adsorbent bed of a zeolite/water cooling system, *Applied Thermal Engineering*, Vol. 24, pp. 2359-2374, 2004
2. K.C. Leong and Y. Liu, Numerical study of a combined heat and mass recovery adsorption cooling cycle, *International Journal of Heat and Mass Transfer*, Vol. 47, pp. 4761-4770, 2004
3. Y. Liu and K.C. Leong, The effect of operating conditions on the performance of zeolite/water adsorption cooling systems, *Applied Thermal Engineering*, Vol. 25, pp. 1403-1418, 2005
4. Y. Liu and K.C. Leong, Numerical study of a novel cascading adsorption cycle, *International Journal of Refrigeration*, Vol. 29, No. 2, pp. 250-259, 2006.
5. Y. Liu and K.C. Leong, Numerical study of an internal reforming solid oxide fuel cell and adsorption chiller cogeneration system, *Journal of Power Sources*, 2005 (in press)
6. K.C. Leong and Y. Liu, System performance of a combined heat and mass recovery adsorption cooling cycle: a parametric study, *International Journal of Heat and Mass Transfer*, 2005 (in press)

Conference papers

1. Y. Liu and K.C. Leong, The effect of operating conditions on the performance of zeolite/water adsorption cooling systems, *International Forum in Heat Transfer*, November 24 - 26, Kyoto, Japan, 2004

2. K.C. Leong and Y. Liu, Modeling of internal reforming solid oxide fuel cell and adsorption chiller cogeneration system, *Heat Transfer in Components and Systems for Sustainable Energy Technologies*, *Proceedings of the Heat SET 2005 Conference*, 5-7 April 2005, Grenoble, France, pp. 577 – 582, ed. B. Thonon.

CHAPTER 1 INTRODUCTION

1.1 BACKGROUND

The most effective refrigerants, chlorofluorocarbons (CFCs), used in conventional vapour compression refrigeration systems are not environment-friendly because they contribute to the depletion of the stratospheric ozone layer and global warming as a result of the greenhouse effect (Meunier, 1993; Picard, 1993). Although alternatives such as hydrochlorofluorocarbons (HCFC's) and hydrofluorocarbons (HFC's) are more ozone-friendly, their global warming potentials are relatively high (Lu and Leong, 1993). These environmental concerns have intensified global research efforts on the development of both ozone layer and global warming safe refrigeration technology.

The sorption refrigeration system is one of the most attractive environment-friendly refrigeration technologies. Sorption refrigeration equipment were developed and manufactured more than 70 years ago (Shelton, 1993). Absorption and adsorption cycles are the two types of sorption cycles used. Absorption cycles such as those using lithium bromide-water (LiBr-H_2O) or water-ammonia (H_2O-NH_3) pairs have many limitations in operating conditions (Douss and Meunier, 1989; Lu and Leong, 1993). Adsorption cycles, on the other hand, are based on the gas-solid adsorption process using porous adsorbents. Compared to the absorption system, the adsorption system is a more promising environment-friendly refrigeration or heat pump technology (Wang *et al.*, 2002A). Natural refrigerants such as water, ammonia, or methanol can be used in these systems. Waste heat (Suzuki, 1992; Zhang and Wang, 1999) and solar energy (Grenier *et al.*, 1988; Worsøe-Schmidt, 1983) can be used to drive the refrigeration systems. The adsorption system can be operated without moving parts and a rectifier or solution pump is not needed, resulting in lower cost. Because of the above-mentioned reasons, extensive research on adsorption refrigeration cycles, which

employ solids/gases pairs such as adsorbent/adsorbate pairs have being carried out. Figures 1.1 to 1.3 show some examples of adsorption refrigeration equipment driven by various heat sources.

Figure 1.1 Solar icemakers manufactured by BLM (Nantes, France)
http://www.limsi.fr/Individu/mpons/solaradsor.htm

Figure 1.2 Waste heat driven adsorption chiller manufactured by KRUM International / HIJC, USA
http://www.adsorptionchiller.bigstep.com

Figure 1.3 Hot water driven adsorption refrigeration system manufactured by HUNAN DY Refrigeration Co. Ltd., CHINA
http://www.dyrefrigeration.com

The general adsorption refrigeration cycle is an intermittent cycle as shown in Figure 1.4. The adsorption cycle is composed of an adsorber alternately connected to a condenser and an evaporator. The whole process consists of four phases, which are Isosteric heating, Isobaric generation, Isosteric cooling and Isobaric adsorption. This cycle can be represented on a Clapeyron diagram (ln$P$ vs. $-1/T$) as shown in Figure 1.5. The processes are described below. The points A, B, C and D refer to the status indicated in Figure 1.5.

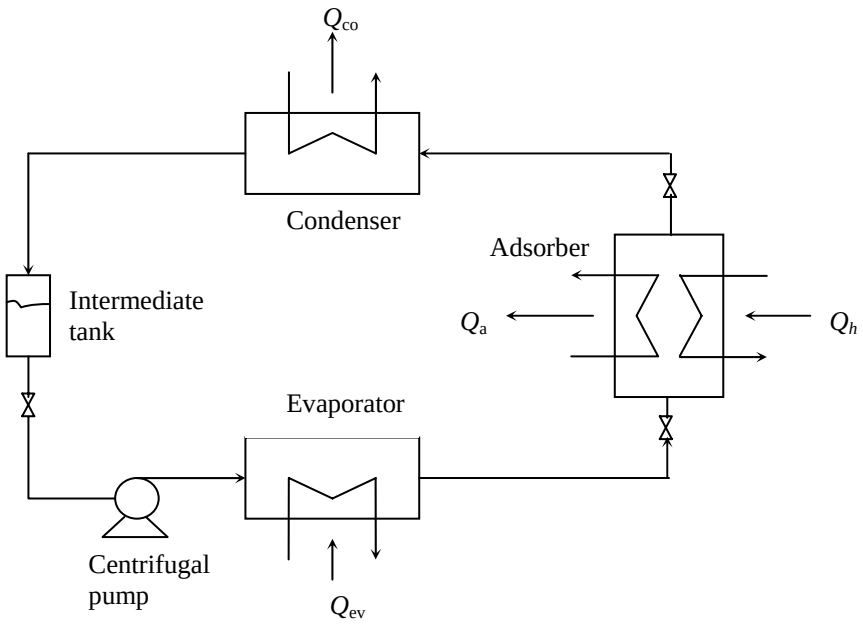

Figure 1.4 Schematic diagram of an intermittent adsorption cycle for refrigeration systems

(i) Isosteric heating (A-B): At the beginning of this phase, the adsorbent in the adsorber contains a high concentration of adsorbate (q_{max}) with an initial ambient temperature of T_a. During this phase, the adsorbent bed is heated at a constant concentration of adsorbate.

(ii) Isobaric generation (B-C): When the vapour pressure in the adsorber is equal to the condensing pressure (P_c), this phase begins with the opening of a valve between the adsorber and the condenser. The adsorbate gas desorbed from the adsorber is cooled to a temperature T_c until it condenses in either a water or an air-

cooled condenser. At the end of this phase, the maximum temperature (T_g) of the adsorbent bed is reached and the bed is disconnected from the condenser.

(iii) Isosteric cooling (C-D): During this phase, the adsorber is cooled at a constant adsorbed concentration (q_{min}). The pressure in the bed decreases from P_c to P_e.

(iv) Isobaric adsorption (D-A): The valve between the adsorber and evaporator is open and the adsorbate liquid evaporates from the evaporator and is adsorbed by the cooling bed.

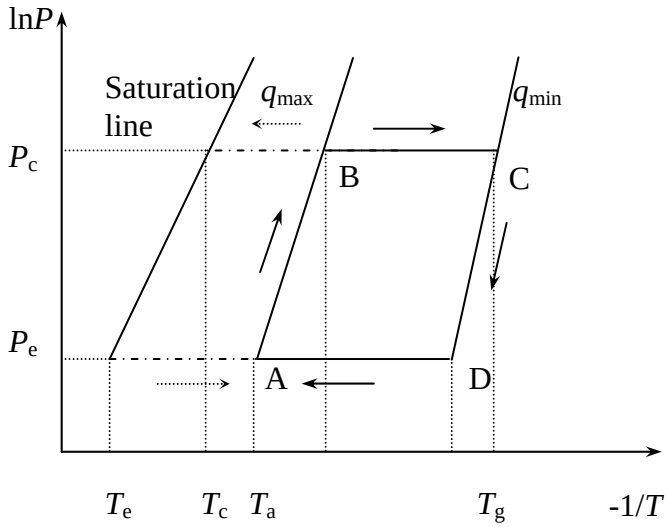

Figure 1.5 Clapeyron diagram of an adsorption refrigeration cycle

In order to assess the performance of a refrigerator, one must evaluate the Coefficient of Performance (COP) and Specific Cooling Power (SCP), which are defined as follows:

$$COP = \frac{Q_{ev}}{Q_h} \tag{1-1}$$

$$SCP = \frac{Q_{ev}}{m_s \cdot t_c} \tag{1-2}$$

where Q_h is the heat input from an outside heat source during the heating and generation phases, Q_{ev} is the heat obtained from the outside cold media required for the adsorbate to evaporate during the adsorption process, m_s is the mass of the adsorbent bed and t_c is the duration of adsorption cycle.

The biggest obstacle in the development of the adsorption cycle technology is its poor thermal performance. Extensive efforts have been made by many researchers to improve the performance of adsorptive cycles. These include the application of advanced cycles, consolidated adsorbents, and coated heat exchangers (Critoph, 1998; Qu *et al*., 2001; Groll, 1993, Restuccia *et al*., 2002). It is also very important to investigate the limitations on the system performance by numerical simulation in order to improve the performance. However, only limited numerical studies on adsorption cooling system were performed especially for advanced adsorption cycles. Available numerical studies are still not robust enough because the mechanisms of heat and mass transfer in adsorbent bed are not fully understood. This study is motivated by the need to achieve basic understanding of the transfer mechanisms of the adsorption cooling system. At the same time, it is meaningful to explain these mechanisms and obtain the general behaviour of the system performance by studying the effects of operating conditions and system parameters. This study also hopes to provide useful guidelines for optimising different adsorption cycles to obtain better performance. Furthermore, adsorption cycles driven by waste heat of high grade heat sources such as the solid oxide fuel cell (SOFC) can be explored. However, the literature is scarce for this coupled system. The coupled SOFC and adsorption cycle system will therefore be investigated numerically in this project. Although there are a large number of adsorptive pairs being employed in adsorption refrigeration system, the zeolite/water pair is selected as the adsorbent pair in this project because of its satisfactory refrigeration ability and suitability for use with a high temperature heat source (Srivastava and Eames, 1998).

1.2 OBJECTIVES AND SCOPE

The main objectives of this research are to develop effective numerical models of adsorption refrigeration cycles for refrigeration and to optimise system performance.

The scope of research includes the following:

i) Thermodynamic models of the adsorption cycles for single and multi-beds systems would be formulated to enable first and second law analyses of different adsorption cycles to be performed. This model would be compared with a heat and mass transfer model.

ii) A detailed numerical model based on heat and mass transfer considerations would be developed to predict several adsorption cycle processes. Some sub-models of thermal conductivity of the porous adsorbent, heat transfer resistance between the wall and adsorbent, and mass transfer resistance from the inter-pellet to intra-pellet would be formulated. The parametric effects of adsorption temperatures and bed configurations on the COP and SCP would be studied and the optimised conditions obtained.

iii) The heat and mass transfer model would be validated experimentally. Simultaneously, this model would be compared with some classical models proposed by other researchers.

iv) To improve system performance, numerical studies would be performed on some advanced adsorption cycles such as the heat and mass recovery cycle and cascading cycle.

v) Finally, a cogeneration system based on an adsorption refrigeration cycle coupled to a solid oxide fuel cell (SOFC) system would be proposed and studied by numerical simulation. The effect of operating conditions on the efficiency of electrical power and cooling power would be investigated.

1.3 LAYOUT OF THESIS

There are nine chapters in this thesis. Chapter 1 gives an introduction to the adsorption refrigeration system and a description of the objectives and scope of this project. In Chapter

2, a literature review which focuses on the numerical modelling of the adsorption refrigeration system is presented.

In Chapter 3, a thermodynamic model with first law and second law analyses for the adsorption refrigeration system is developed. The analyses are performed not only for the intermittent cycle but also for some advanced cycles.

In Chapter 4, a novel advanced adsorption refrigeration cycle is proposed and a lumped model is assumed for this cycle. This cycle consists of two zeolite adsorbent beds and a silica gel adsorbent bed. Both heat and mass recovery are carried out between the two zeolite adsorbent beds. In addition, heat is also exchanged between the zeolite adsorbent and the silica gel adsorbent beds. The COP and SCP for different operating conditions are studied by the lumped model. Furthermore, a comparison of the performances for this novel cycle and other cycles is also presented in this chapter.

In Chapter 5, a detailed cylindrical two-dimensional non-equilibrium numerical model describing the combined heat and mass transfer process in the adsorbent bed is presented. Three sub-models of heat and mass transfer properties *viz.* gas flow in adsorbent bed model, linear force driven model and equivalent heat transfer conductivity of adsorbent bed model of the adsorbent bed are proposed. The model is solved by the control volume method. The effects of main configuration parameters on the thermal performance of the system are investigated. The effects of operating temperature on performance are also investigated based on this model. The objective is to obtain the optimal operating conditions.

In Chapter 6, the heat and mass transfer model proposed in Chapter 5 is extended to simulate a combined heat and mass recovery adsorption cycle. Parametric studies based on this model are carried out to optimise this type of advanced adsorption refrigeration cycles.

In Chapter 7, an intermittent adsorption refrigeration system is set up. Some physical properties which are necessary inputs to the heat and mass transfer model are measured. A

comparison of experimental and simulation results is performed to validate the numerical model proposed in Chapter 5.

In Chapter 8, a zeolite/water adsorption refrigeration and internal reforming solid oxide fuel cell (IRSOFC) cogenerations system is presented. In this system, the adsorption cycle is driven by waste heat from the SOFC system. It is a good example to broaden the area of application for adsorption refrigeration systems. A mathematical model is developed to simulate this combined system under steady-state conditions. The effects of fuel flow-rate, recycle ratio, fuel utilisation factor, mass of adsorbent, and inlet air temperature on system performance are considered.

Chapter 9 gives the main conclusions drawn from this study and recommendations for future work.

CHAPTER 2 LITERATURE REVIEW

2.1 INTRODUCTION

In the last twenty years, there has been active research worldwide into adsorption refrigeration systems. Several research groups such as Jet Propulsion Laboratory of NASA (JPL/NASA), Shanghai Jiao Tong University (SJTU), Laboratoire d'Informatique pour la Mécanique et les Sciences de l'Ingénieur (LIMSI-CNRS) and Warwick University, have been focusing on the adsorption system for several years and have achieved encouraging results in their specific research areas. Recently, with advances in computer technology and numerical methods, more numerical studies have been carried out in this field (Marletta *et al*., 2002; Miltkau *et al*., 2002; Alam *et al*., 2000). This is because of the difficulty in testing many parameters experimentally, the high cost of experimental devices and the long time needed to obtain good results. In terms of time and cost savings, many new designs of adsorption cycles are first tested numerically before actual experimental investigation. In view of the above, the author has chosen to focus on numerical studies of adsorption cooling systems in this project. Therefore, this literature review will focus mainly on theoretical and numerical simulations of adsorption refrigeration systems. Numerical models of adsorption heat pump cycles are also reviewed in this chapter since their heat and mass transfer mechanisms and adsorption phenomena are similar to adsorption refrigeration systems.

2.2 FUNDAMENTALS OF ADSORPTION

Adsorption is a surface phenomenon that can be defined as the increase in concentration of a particular component at a surface or at the interface between two phases. During adsorption, solid or liquid atoms at the surface are subjected to unbalanced forces of attraction normal to the surface plane (Ruthven, 1984). There are essentially two types of

adsorption namely, chemisorption and physical adsorption. Physical adsorption is more commonly used in refrigeration applications for the following reasons (Turner, 1992):

(i) It has a low value of heat of adsorption/desorption which is comparable to the latent heat of the adsorbate.

(ii) The adsorption process is readily reversible.

(iii) Most pairs of solids and gases will undergo a certain amount of adsorption.

Because of the above-mentioned reasons, physical adsorption refrigeration or heat pump cycles, which employ solids/gases pairs as adsorbent/adsorbate pairs, have attracted much interest in recent years.

The adsorption characteristics of an adsorbent/adsorbate pair are very important to the performance of the refrigeration and heat pump cycles. Many underlying theories of adsorption are necessary for one to analyse the adsorption characteristics.

2.2.1 Equilibrium model of adsorption

For a given solid/gas pair, the amount adsorbed at equilibrium can be described by

$$q = f(P,T) \tag{2-1}$$

where q is the adsorbed amount of adsorbate and is a function of P and T.

All numerical models for adsorption cycles applied to refrigeration and heat pump systems are based on the adsorption phenomena regardless of whether the model are simple or complex. The adsorption equilibrium equations used in numerical models for various adsorption cycles are listed in Table 2.1.

Table 2.1 Adsorption equilibrium equations used in numerical simulation for adsorption cycle

	Equilibrium equation	Adsorbent/adsorbate pair	References
1	Modified Langmuir equation: $q = \frac{q_{s1}B_1P}{1+B_1P} + \frac{q_{s2}B_2P}{1+B_2P} + \frac{q_{s3}B_3P}{1+B_3P}$ $q_{si} = a_{0i} + \frac{a_{1i}}{T} + \frac{a_{2i}}{T^2} + \frac{a_{3i}}{T^3};\ B_i = B_{0i}\exp(E_i/T)$	Zeolite 13X/Water	Ben Amar *et al.*, 1996; Sward and Douglas, 2000
2	Freundlich equation: $q = K \cdot \left(\frac{P_s(T_v)}{P_s(T_b)}\right)^{\frac{1}{n}}$	Silica gel/Water	Sakoda and Suzuki, 1984; Cho *et al.*, 1992; Alam, 2000
3	Dubinin-Astakhow (D-A) equation: $q = \rho V_0 \exp\left[-D\left(T\ln\frac{P_s(T)}{P}\right)^n\right]$	Activated carbon/Methanol Activated carbon/Ammonia Zeolite/Water	Guilleminot and Meunier, 1987; Critoph, 1989; Sun and Meunier 1987; Zhu *et al.*, 1992; Chahbani *et al.*, 2002
4	$\ln(\frac{p}{p_s}) = \sum A_n q^n + \frac{1}{T}\sum B_n q^n$ where, A_n and B_n are empirical equilibrium coefficients, n = 1,2,3.	Zeolite 13x/Water Zeolite 13x/Mehanol Zeolite 13x/ammonia	Härkönen and Aittomäki, 1991; Aittomäki and Härkönen, 1992
5	$\ln(P) = a(q) + b(q)/T$ $a(q) = a_0 + a_1q + a_2q^2 + a_3q^3;\ b(q) = b_0 + b_1q + b_2q^2 + b_3q^3$	Zeolite 4A/Water Zeolite 13X/Water	Zhang, 2000; Marletta *et al.*, 2002
6	$\frac{q}{a_1} = a_2 \cdot \frac{[(a_3/\sqrt{T})\exp(a_4/T)]\cdot P}{1+[(a_3/\sqrt{T})\exp(a_4/T)\cdot P} + (1-a_2)\cdot\frac{\{[(a_5/\sqrt{T})\exp(a_6/T)]\cdot P\}^2}{1+\{[(a_5/\sqrt{T})\exp(a_6/T)]\cdot P\}^2}$	Zeolite-MgNaA/water	Miltkau and Dawoud, 2002
7	$q = A_1 + A_2T + A_3T^2 + A_4C + A_5C^2 + A_6TC + A_7T^2C + A_8TC^2 + A_9T^2C^2$ where C is the concentration of adsorbate and A_i is empirical coefficient	Silica gel/water	San *et al.*, 2002
8	$V = V_0\exp(-by)\cdot\exp(y^2\Delta^2/2)\cdot[1-erf(Z)]/2$ $Z = (y - b/a^2)a/\sqrt{2};\ y = (T/\beta)^2\ln^2(f_s/f)$ where V is the absorbed volume, β is the affinity coefficient, f_s and f are the saturation emissivity and emissivity, respectively	Activated carbon/Methanol	Wang *et al.*, 1998

2.2.2 Diffusion model of adsorption

The Diffusion Model is a very important model used in describing adsorption kinetics. All adsorbents employed in adsorption refrigeration or heat pump systems possess a porous structure and a large surface area. The gases are adsorbed on the surface beneath the particle of the absorbents. The adsorptive gases must penetrate into or out of the porous structure during adsorption or desorption, respectively. Three major diffusion mechanisms are involved *viz*. pore diffusion, surface diffusion and combined pore and surface diffusion (Ruthven, 1984). However, not all of these mechanisms have the same effect on the diffusion rate at different locations of the adsorbent. For diffusion in macro-pores between adsorbent particles, the dominant diffusion mechanism is pore diffusion while for diffusion in the micro–pores of the particle, surface diffusion is dominant (Yang, 1987).

Diffusion in macro-pores between adsorbent particles can reduce the mass transfer resistance, although this phenomenon has been considered only in very few investigations of heat and mass transfer phenomena in adsorption cycles (Marletta *et al*., 2002). Diffusion in macro-pores consists of molecular diffusion and Knudsen diffusion. To correlate macro-pore diffusion to molecular diffusion and Knudsen diffusion, a simple empirical equation was proposed by Yang (1987) as

$$D_p \approx \frac{\varepsilon}{\tau}\left[\frac{1}{(1/D_m)+(1/D_k)}\right] \tag{2-2}$$

where D_{m} is the molecular diffusivity, D_{k} is the Knudsen diffusivity, ε is porosity and τ is the tortuousity factor.

On the other hand, the micro-pore diffusion model has been addressed in some investigations. A common approximation solution of the mass balance equation in the micro-pores of particles given by the linear driven force (LDF) assumption of Gluekauf (1955) is

widely used in the transfer model of adsorption cycles (Sakoda and Suzuki, 1984; Passos and Escobedo, 1989; Härkönen and Aittomäki, 1991; Zhang, 2000). The solution is given as

$$\frac{\partial \bar{q}}{\partial t} = \frac{15 D_e}{r_p^2}(q_{eq} - \bar{q}) \tag{2-3}$$

where r_p is the radius of the particle, $\bar{q}$ is the mean adsorbed concentration within the particle, and q_{eq} is the adsorbed phase concentration in equilibrium with bulk fluid. Chahbani *et al.* (2002) studied the effect of micro-pore diffusion on adsorption refrigeration systems. They concluded that such diffusion could not be neglected because the performance of an adsorption cycles could be significantly reduced due to intra-particle diffusion limitations. They also reported that the LDF model could be used to simulate intra-particle diffusion with little error.

2.2.3 Heat of adsorption

Adsorption is always accompanied by evolution of heat termed as the heat of adsorption. The amount of heat depends on the magnitude of van der Waals forces involved, phase change and electrostatic energies. Heat of adsorption is a necessary component of the heat and mass transfer model. The heat of adsorption for some adsorbent/adsorbate pairs are listed in Table 2.2. There are two different ways of using the heat of adsorption in the modelling of adsorption cycles. One way is to consider the heat of adsorption as a constant (Grenier and Guilleminot, 1988; Douss *et al*., 1988; Luo, 1989; Chandra and Patwardhan., 1990; Cho *et al*., 1992; Miles *et al*., 1993; Ben Amar *et al*., 1996; Sun *et al*., 1997). The other way is to use the heat of adsorption derived from the Clausius-Clapeyron equation (Guilleminot and Meunier, 1987; Luo, 1992; Aittomäki and Härkönen, 1992; Sami and Tribes, 1996; Teng *et al*., 1997) as

$$\Delta H = RT^2 \left[\frac{\partial(\ln P)}{\partial T} \right]_q \qquad (2\text{-}4)$$

Table 2.2 Heat of adsorption of some adsorption/adsorbate pairs (Srivastava and Eames, 1997)

Adsorbent	Adsorbate	Heat of Adsorption, kJ/kg	Remarks
Silica gel	Methyl Alcohol	1000-1500	Unsuitable above 200ºC
	H_2O	2800	
Activated alumina	H_2O	3000	
Zeolite (various grades)	H_2O	3300-4200	Natural zeolites have values lower than synthetic ones
	NH_3	4000-6000	
	CO_2	800-1000	
	CH_3OH	2300-2600	Unsuitable: they react at 100ºC
Charcoal	C_2H_4	1000-1200	
	NH_3	2000-2700	
	H_2O	2300-2600	
	CH_3OH	1800-2000	
	C_2H_5OH	1200-1400	

2.3 ADSORBENT/ ADSORBATE PAIRS

The characteristics of adsorbent/adsorbate pairs can affect the efficiency of an adsorption system. The requirements of an adsorbate are as follows (Turner, 1992):

(i) A high latent heat is necessary to minimise the mass of adsorbent required.

(ii) The condensing pressure at the anticipated condensing temperature should be as low as possible to reduce the risk associated with high-pressure systems.

(iii) The evaporation pressure at the anticipated evaporating temperature should be slightly above atmospheric to avoid the risk of inward leak.

(iv) It must be non-toxic, non flammable and inexpensive.

(v) It should be chemically and thermally stable.

(vi) It should be non-environmentally polluting.

The basic requirements of an adsorbent are as follows:

(i) It has a large adsorbed capacity.

(ii) It has a low specific heat.

(iii) It has good heat transfer properties.

(iv) It is inexpensive and readily available.

Many adsorbent/adsorbate pairs are employed in adsorption refrigeration and heat pumps. Adsorbent/adsorbate pairs that are commonly used and investigated are zeolite and water, silica gel and water, active carbon and ammonia (Srivastava *et al*., 1998).

2.3.1 Zeolite/water pair

The zeolite/water pair is the most common adsorption pair used in adsorption refrigeration and heat pump systems. Such systems possess satisfactory refrigeration ability and can be driven by a high temperature heat source.

Zeolite is a crystalline alumino-silicate material with an exactly defined pore structure. The pores, which can occupy up to 50% of the volume, can be totally saturated with adsorbate during the adsorption process. Cacciola *et al*. (1993) used preformed zeolite products in an adsorption heat pump. They obtained some new zeolite material which has good potential to be used in adsorption heat pumps. Schwarz *et al*. (1991) analysed the application potential of zeolite/water adsorption cycles and concluded that the zeolite/water pair can be used in various applications such as energy storage, air conditioners and icemakers. Zanifé and Meunier (1992) in their experimental investigation used the zeolite/water pair and achieved a high COP_h of 1.45.

2.3.2 Silica gel/water pair

Silica gel is one of the synthetic amorphous silicas. It is a rigid, continuous network of spherical particles of colloidal silica. Silica gel has large surface area and high adsorption capacity. Silica gel/water systems can operate at a lower temperature than zeolite/water systems and can be driven by a low temperature heat source. Such systems have lower refrigeration capability compared to zeolite/water system. Sakoda and Suzuki (1984) performed a fundamental study on a solar-powered adsorption cooling system based on the silica gel/water pair. Cho *et al*. (1992) improved the refrigeration capacity up to 1.76 RT (1 RT = 3.528 kW) with a large heat transfer capacity condenser.

2.3.3 Activated carbon/ammonia pair

Activated carbons can be manufactured from raw materials such as wood, peat, coal, fruit nuts, and petroleum coke. By controlling some manufacturing steps, the activated carbon can attain desired pore structure and mechanical strength. Ammonia may be used in a wide range of operating temperatures. Turner (1992) reported that a COP of about 0.5 could be achieved for an intermittent refrigeration cycle using the activated carbon/ammonia pair at the evaporating temperature of 15°C. For the same operating temperature, Critoph (2002) reported that multi-bed systems could achieve a cooling COP of 0.60 with total cooling power of 291 W. He also concluded that a cooling COP of 0.85 with a total cooling power of 400 W was feasible.

2.3.4 Other adsorbent/adsorbate pairs

Many other adsorbent/adsorbate pairs are used in adsorption refrigeration and heat pump systems such as activated carbon/methanol (Passos *et al*., 1986; Hu, 1996), zeolite

composites and water (Pons *et al*., 1996; Liu *et al*., 1998), salts and ammonia or water (Chen *et al*., 2001).

The activated carbon/methanol pair has been considered as the best pair among those studied so far in terms of higher COP and lower cost (Hu, 1996). Pons *et al*. (1996) used composite adsorbents (zeolite and expanded natural graphite) with a thermal wave system. A cooling COP of 0.9 was achieved but the specific cooling power was only 35 W/kg of adsorbent. Liu *et al*. (1998) used a compound zeolite-activated carbon/water pair in adsorption solar cooling systems. They concluded that the use of zeolite-active carbon composites can enhance heat transfer in adsorbent bed and reduce the cycle time.

2.4 MATHEMATICAL MODEL OF ADSORPTION CYCLES

Many mathematical models of adsorption refrigeration/heat pump systems have been proposed to predict their performance. The models are classified under three main categories: thermodynamic models, lumped parameter models, heat and mass transfer models (Li and Sumathy, 2002). Heat and mass transfer processes are not considered in the thermodynamic model. Although heat transfer is considered in the lumped parameter model, temperature variation with space is not accounted for, which is considered in the heat and mass transfer model.

2.4.1 Thermodynamic model

The model based on thermodynamic analysis in which details of heat transfer are not considered is the simplest among the three models. This model can be used to predict the system performance based on limited data available for the adsorbent/adsorbate pairs.

Turner (1992) studied the single-bed adsorption cycles using the carbon/ammonia pair and obtained a simple model in order to assess the performance. In his model, the latent heat

of vaporization was considered as a constant, and the isosteric heat of adsorption was derived from the Clausius-Clapeyron equation. He obtained the variation rules of the coefficient of performance (COP) vs. carbon properties and operating parameters.

In order to analyse the performance of an intermittent adsorption cycle and determine the adsorbent/adsorbate behaviour under expected operating conditions, Luo and Feidt (1992) proposed a thermodynamic model. This model included evaluation of the cycled mass of the adsorbate, the isosteric heat of adsorption and its dependency on adsorbate properties and generator characteristics. They used the theory of Dubinin-Radushkevich and took into account the temperature dependency of the volumetric coefficient of expansion of the adsorbate to obtain an adsorption equilibrium equation. The latent heat of condensation or vaporization in their model is not a constant, but a function of temperature. They evaluated the coefficient of performance (COP), and the adsorbed amount of an adsorption cycle based on different modelling techniques with various simplifications of the Clapeyron equation, which can yield significantly different results. They concluded that calculations using a constant latent heat evaluated at some specific temperature yielded results with significant error.

Chandra and Patwardhan (1990) proposed a thermodynamic model for a novel intermittent zeolite/water cycle which consisted of two isothermal processes and two isosteric processes. The values of COP were computed for each system (two-tank system, three-tank system, four-tank system) for various temperatures of waste heat source. They concluded that the four-tank system gave the most improved COP value among the three systems and the COP value was sensitive to the temperature driving force for heat transfer.

A similar work was carried out by Douss and Meunier (1989) who proposed an equilibrium model based on heat and mass balances for a cascading adsorption cycle. Two adsorption pairs including zeolite/water and activated carbon/methanol were employed in this

cascading cycle. Neither the effects of kinetics nor temperature drop were taken into account. The cooling COP was predicted to be 0.95, which agreed with their experimental results to within 10%.

A thermodynamic model of a two-absorber regenerative heat pump was presented by Cacciola and Restuccia (1995). The main assumptions of their model are as follows:

(i) The heat capacity of the adsorbate in the adsorbed phases is equal to that in the vapour phases.

(ii) The enthalpy of adsorption (ΔH) is a function of the amount of adsorbed adsorbate, and is independent of temperature.

(iii) The equilibrium conditions can be represented by a set of isosteres.

(iv) The isosteres on a diagram of ln (P) vs. 1/T are straight lines.

The model had been used to calculate system performance and useful heat product of one adsorption/desorption cycle. Based on the model, they compared the performances of three different adsorbent/adsobate pairs including zeolite4A /water, zeolite13X /water and AC35 activated carbon/methanol. They concluded that zeolite/water is the most suitable pair for adsorption refrigeration machines to be used in domestic applications in southern Europe.

Teng *et al*. (1997) proposed a detailed model based on the Dubinin-Radushkevich equation and thermodynamic analyses. In their model, variable physical properties with temperature, such as the specific heats of working pairs, isosteric heat of adsorption, were considered. Several main factors affecting the performance were discussed according to the simulation results such as the characteristics of working pairs and operating conditions. The following assumptions were made in their analysis:

(i) No desorption took place until the condensing pressure was reached.

(ii) Heating the generator during an isosteric heat phase was considered to be a constant volume process.

(iii) Sensible heating to the adsorbate gas contained within the generator volume was negligible.

The model of Teng *et al*. (1997) was extended by Wang (2001) to simulate a more complex combined heat and mass recovery system. Wang's results showed that the COP can be improved by about 25% compared with the basic adsorption cycle system.

Llobet and Goetz (2000) modelled and analysed the continuous operation rotary system for solid sorption cold production systems. A thermodynamic model was proposed to estimate the performance of the rotary process in terms of COP and cold production capacity. The assumptions of their model are as follows:

(i) During the pressure increase and decrease phases of the elementary modules, the pressure was imposed by the adsorbent. The operation temperature of the evaporators and condensers determined the operating pressures.

(ii) It was assumed that mass and heat transfer in the adsorbent were negligible. The heat exchange surface and the heat exchange coefficient were assumed to be constant.

(iii) All the elementary adsorbers were treated as a continuous adsorbent ring rotating about the central axis of the frame and characterised by an equivalent flow rate.

By using the model, COP and cold production capacity were evaluated by varying the thermodynamic operation parameters such as the number of transfer units (NTU), temperature of heat source, and temperature of cold production. Their results showed that the regeneration temperature could be kept relatively low (about 170°C) for the PX21/NH_3 pair. Their theoretical study demonstrated that the rotary process showed its full advantage in air-conditioning applications with cold production temperatures above 0°C.

Recently, Gui *et al*. (2002) proposed a thermodynamic model for a heat-regenerative adsorption cycle. In their model, YK activated carbon was taken as the adsorbent, and

methanol as the refrigerant. They studied the influence of various parameters on the performance, such as temperature of the heat source, supply outlet air temperature, ambient temperature, heat capacity ratio of adsorber metal and working fluid to adsorbent. Their results indicated that the system performance was satisfactory and the experimental results agreed well with their simulation data.

Thermodynamic models can use limited data to predict cycle performance, which is very important for the design of adsorption cycle systems. These models can be used to simulate highly complex systems, which are difficult to be simulated by the heat and mass transfer model. There are many different thermodynamic models which can be derived by using different simplifications. The description of the performance of the adsorption process involving different models may be significantly different. Comparison with these different models should be carried out and validated with experimental data.

2.4.2 Lumped parameter model

The lumped parameter model is based on the following assumptions (Li and Sumathy, 2002):

(i) The temperature is uniform in the adsorbent layer.

(ii) The refrigerant is adsorbed uniformly in the adsorber.

(iii) Both solid and gas phases exit at thermodynamic equilibrium.

(iv) The resistances of heat and mass transfer in the adsorbent are neglected.

Sakoda and Suzuki (1984) studied the solar adsorption cooling system employing the silica gel/water pair. A simple lumped parameter model was proposed for quantitative interpretation of the experimental results. The model comprised some equations of mass and heat balances. The mass balance of the adsorbate was expressed as:

$$m_s \frac{dq}{dt} + \frac{dm_w}{dt} = 0 \qquad (2\text{-}5)$$

where m_s is the mass of the adsorbent, q is the adsorbed amount, and m_w is the mass of water vapour.

The heat balance equation in the packed beds of adsorbent was given by

$$m_s C_{ps} \frac{dT_s}{dt} = m_s \Delta H \frac{dq}{dt} - A_s h_s (T_s - T_a) + A_s q_{ra} \quad (2\text{-}6)$$

where C_{ps} is the specific heat of the adsorbent, T_s is the temperature in the beds, ΔH is the heat of adsorption, A_s is the heat transfer area of the beds, T_a is the atmospheric temperature and q_{ra} is the effective heat influx into the beds by radiation by considering the receiving area as A_s.

Suzuki (1992) used the model of Sakoda and Suzuki (1984) by considering the heat balance equation in the evaporator to investigate the application of adsorption refrigeration system on automobiles. It is concluded that the application of adsorption refrigeration system to automobiles would be possible if appropriate design of adsorbent beds achieved improved heat transfer characteristics.

Douss *et al*. (1988) presented a predictive model for a two-adsorber adsorption heat pump cycle. Each component (adsorber, evaporator, and condenser) was considered to be homogeneous and thermodynamic equilibrium was assumed to exist in each component. They analysed the heat transfer between the heat pump and outside heat sources. Three forms of heat exchange between the unit and the heat source were considered in the model *viz*. indirect coupling with power constraint, indirect coupling with temperature constraint and direct coupling with temperature constraint. The results derived from their model agreed well with the results of experiments employing the zeolite/water pair. Their study showed that the temperature of adsorbent was not a sensitive variable. Instead, the heat rates in the different components of the heat pump were found to be sensitive variables with the pressure being the most sensitive.

An improved model was developed by Sami and Tribes (1996) to predict the dynamic performance of adsorption cycles. The adsorption cycle employed a single or double adsorber with heat recovery. The basic governing equations of their model are outlined as follows:

Heating phase: $$\sum_{i=1}^{3}(m_i C_{Pi})\frac{dT}{dt} = \phi_{0-a} + m_s(-\Delta H)\frac{dq}{dt} \quad (2\text{-}7)$$

Cooling phase: $$\sum_{i=1}^{3}(m_i C_{Pi})\frac{dT}{dt} = \phi_{0-a} - m_s \Delta H \frac{dq}{dt} + m_s C_{pa}(T_e - T)\frac{dq}{dt} \quad (2\text{-}8)$$

The term $\sum_{i=1}^{3}(m_i C_{Pi})$ includes the sensible heat of the metallic parts of the adsorber, the fully regenerated adsorbent bed, and the adsorbed phase. The adsorbed phase was considered as liquid. The symbol ϕ_{0-a} refers to the heat transferred from the heating or cooling medium. Several constitutive relationships were integrated into the model to enhance its capability to predict the thermal phenomena that takes place inside the adsorber and the heat exchangers. New sub-models were added to predict the performance of air-cooled evaporators and condenser-type heat exchangers. The numerical results derived from the model were fitted well with experimental data, which indicates that the model can be used to predict the performance of the systems.

Critoph (2001) described a rotary adsorption refrigeration system which consisted of a number of simple tubular adsorption modules. A single module shown in Figure 2.1 was comprised of a generator and a receiver/condenser/evaporator. A simple lumped model was proposed to simulate many modules in a real system. The following assumptions were made in this model:

(i) The thermal resistance between the carbon and steel was neglected;

(ii) The pressure was assumed to be uniform through each module;

(iii) Heat conduction axially along the adiabatic zone was assumed to be negligible.

Critoph's model studied how the five key parameters of thermal capacity ratio, number of modules, temperature of air leaving the heater, generator heat transfer coefficient and the evaporator air inlet temperature affect the COP and SCP. Critoph also proposed that second law analysis of the system should be embarked on to explore the ideal limitations of the performance for this system.

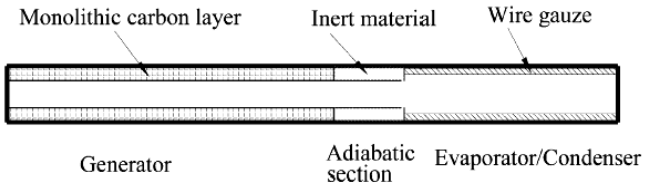

Figure 2.1 Sections through a sorption module (Critoph, 2001)

2.4.3 Heat and mass transfer model

The simulation model based on heat and mass transfer considerations is the most realistic among the three models since it gives insight into the dynamics of the adsorber in adsorption cycles. In this model, the temperature or mass content of adsorbate varies not only with time but also with space. It is very helpful for the design of adsorptive refrigeration or heat pump systems. A summary of the main features of each model is given in Table 2.3.

Guilleminot and Meunier (1987) proposed a uniform pressure non-isothermal model to describe the heat transfer in a fixed bed of solid adsorbent in a finned rectangular reactor (Figure 2.2). The assumptions of the model are as follows:

(i) Mass transfer within the bed occurred only in the vapour phase.

(ii) The reactor was considered to be symmetrical.

(iii) Convective heat transfer in the vapour phase was neglected.

(iv) Pressure was assumed to be uniform in the reactor.

(v) The resistance to mass diffusion through the inter-particle voids and the pores was neglected.

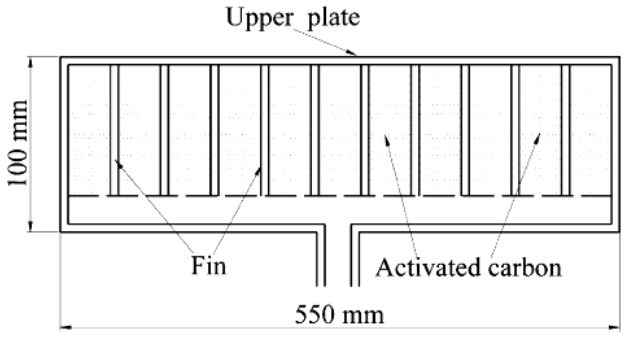

Figure 2.2 Cross section of the reactor showing the upper plate, the fins and the packing of the active carbon between the fins (Guilleminot and Meunier, 1987)

The model of this system is based on two energy conservation equations given as follows:

For metal part (copper): $$\rho_m C_{pm} \frac{\partial T_m}{\partial t} = k_m \nabla^2 T_m \quad (2\text{-}9)$$

For the adsorbent layer: $$\rho_s (C_{Ps} + qC_{Pa}) \frac{\partial T_s}{\partial t} = \rho_s \Delta H \frac{\partial q}{\partial t} + k_s \nabla^2 T_s \quad (2\text{-}10)$$

where k_m and k_s are the thermal conductivity of copper and adsorbent layer, respectively. By using the finite-difference technique, these governing equations had been solved. Experiments were also carried out by Guilleminot and Meunier to validate their model, and the numerical results fitted well with their experimental data. The thermal conductivity of the adsorbent bed and the heat transfer coefficient between the fin and adsorbent bed were obtained by an identification technique.

A similar model was proposed by Liu *et al*. (1994) to model a cylindrical adsorbent bed. They carried out experiments to validate the model and compare the effects of enhancement of heat transfer of adsorbent bed with and without fins. The unknown heat transfer coefficients were obtained by using the same identification method employed by Guilleminot and Meunier (1987).

Table 2-3 Features of reviewed heat and mass transfer models for adsorption cycle

	Governing equation characteristics	Bed geometry	Cycle type	References
1	Two- dimensional, equilibrium in adsorption	Rectangular	Intermittent	Guilleminot and Meunier,1987
2	Two-dimensional	Cylindrical	Intermittent	Liu *et al.*, 1994
3	Two-dimensional, LDF equation	Rectangular	Solar driven, intermittent	Passos and Escobedo, 1989
4	One-dimensional	Cylindrical	Thermal wave cycle	Sun *et al*., 1997; Pons and Feng, 1997
5	Two-dimensional, LDF equation, Darcy equation	Cylindrical	Thermal wave heat regeneration cycle	Ben Amar *et al.* 1996
6	Two-dimensional	Rectangular	Intermittent	Li *et al*., 2001
7	Two-dimensional	Cylindrical	Intermittent	Restuccia *et al*., 2002
8	Three-dimensional, LDF, Darcy equation	Cylindrical	Intermittent	Zhang and Wang, 1999; Zhang 2000
9	Two-dimensional, LDF equation	Rectangular	Two-beds	Alam *et al*., 2000
10	One-dimensional, Ergun equation	Cylindrical	Thermal wave cycle	Sun *et al*., 1995
11	Two-dimensional ,modified Darcy equation	Cylindrical	intermittent	Marletta *et al.* ,2002
12	One-dimensional, modified Darcy equation	Cylindrical	Heat and mass recovery cycle	Poyelle *et al.* ,1999
13	One-dimensional	Cylindrical	Thermal wave heat regeneration cycle	Sward *et al.* ,2000

Passos *et al*. (1989) presented a model of a solar-powered intermittent adsorptive cooling machine. This model was based on the simplifying assumptions that within the solid adsorbent bed, the pressure difference inside the adsorber was neglected and the mass transfer in the pellets was accounted for by the LDF equation. The performance of the system depended strongly on the adsorptive capacity of the solar collector and on its back insulation. For the activated carbon-methanol pair, it did not depend strongly on the heat transfer coefficient in the adsorbent bed and much less on the mass transfer coefficient in the reactor.

Sun *et al*. (1997) proposed a numerical model of thermal wave heat pump systems (shown in Figure 2.3) under uniform-pressure conditions. A new definition of the global coefficient was employed to allow the two-dimensional system to be solved as a one-dimensional model. Pons and Feng (1997) used a similar model to investigate parameters of the thermal wave heat regeneration heat pump. The number of transfer units (NTU) and the dimensionless outlet fluid temperature at the end of the cold front were found to be effective and meaningful parameters for characterising thermal wave adsorption cycles.

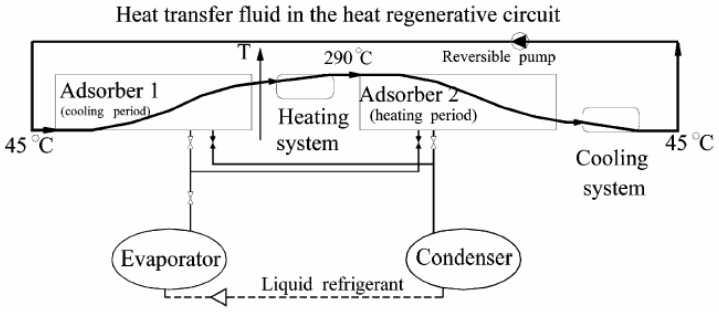

Figure 2.3 Basic thermal regeneration adsorption system (Sun *et al*., 1997)

A more basic model was presented by Ben Amar *et al*. (1996) for numerical analysis of adsorptive thermal wave regenerative heat pump system. The governing equations of the model are listed as follows:

Mass conservation: $$\varepsilon_t \frac{\partial \rho_g}{\partial t} + \nabla \cdot (\rho_g \mathbf{u}) + \rho_s \frac{\partial q}{\partial t} = 0 \qquad (2\text{-}11)$$

$$\text{Heat conservation: } \rho C_P \frac{\partial T_s}{\partial t} + \rho_g C_{pg} \mathbf{u} \cdot \nabla T_s = \nabla \cdot (\lambda_s \nabla T_s) + \rho_s \cdot \Delta H \frac{\partial q}{\partial t} \quad (2\text{-}12)$$

where ρC_P is total heat capacity of the bed, and $\mathbf{u}$ is the velocity vector of adsorbate vapour.

In order to solve Equations (2-11) and (2-12), Darcy's law was used to describe the velocity of the adsorbate vapour in the adsorbent bed. Darcy's law is given by

$$\mathbf{u} = -\frac{K}{\mu} \nabla P \quad (2\text{-}13)$$

where K is the permeability of the adsorbent bed and μ is the viscosity of the adsorbate vapour.

The two-dimensional model had been numerically solved using the alternating direction implicit (ADI) finite difference method, which is a method with high stability. Two types of adsorption systems were simulated *viz*. zeolite NaX/water and activated carbon AX21/ammonia.

The same model was also used by Li *et al*. (2001) to simulate a plate adsorptive cooling system. Restuccia *et al*. (2002) modified the above model to investigate a zeolite-coated bed for air-conditioning adsorption systems. The simulation results of the different types of adsorbent bed showed that the new bed proposed allowed the highest specific power of the adsorption-cooling device to be obtained. They also concluded that it was possible to enhance the competitiveness of adsorption air conditioning systems by changing the adsorbent material shape and thus its thermophysical properties.

Zhang and Wang (1999) and Zhang (2000) extended the models of Ben Amar *et al*. (1996) by considering the mass transfer resistance and non-equilibrium nature of the adsorption state and obtained a more complex, three-dimensional heat mass transfer model. The adsorber in their study comprised of cylindrical double-tubes as shown in Figure 2.4. The LDF equation was introduced to account for mass transfer resistance within the pellets. The vapour velocity in the pellets was determined by Darcy's law. The heat and mass transfer

mechanisms and their effects on the performance were evaluated by using this model. They found that the system performance was strongly influenced by the adsorber configurations such as the fin numbers, the adsorbent thickness, and the heat transfer coefficients. Furthermore, the performance of the system can be seriously deteriorated by poorer mass transfer in the adsorbent if its permeability is less than a critical value.

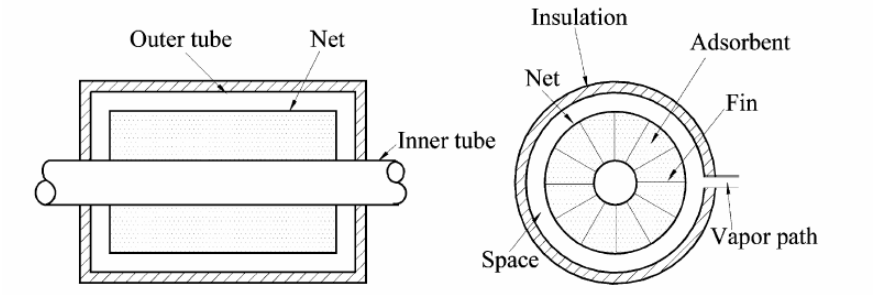

Figure 2.4 Schematic of the adsorber module showing the two tubes, the fins, the nets, the insulation and the adsorbent. (Zhang and Wang, 1999; Zhang, 2000)

A two-dimensional non-equilibrium model was proposed by Alam *et al*. (2000) to investigate the effect of the design parameters on the performances of a silica gel adsorption refrigeration system. This model is simpler than the previous model (Ben Amar *et al.*, 1996) since the convection term was neglected in their energy balance equations and macro mass transfer limitations were not considered. They concluded that the system performance was very sensitive to the switch frequency which indicates the cycle speed. In terms of system performance, there is an optimal switch frequency for a given set of design parameters.

Some assumptions of the model presented by Ben Amar *et al*. (1996) are questionable. Darcy's law, valid for incompressible fluid, was used to describe the velocity of compressible adsorbate vapour in the adsorbent bed. In actual fact, for gas flow through the porous adsorbent bed, the permeability in the Darcy equation (Equation 2-13) is higher than the intrinsic permeability of the bed, which is a result of the diffusion effect.

Sun *et al*. (1995) replaced the Darcy equation by the Ergun equation given by

$$\mathbf{u} + \frac{\rho_g}{\mu_g} K_E \mathbf{u}|\mathbf{u}| = -\frac{K_D}{\mu_g} \nabla P \tag{2-14}$$

where K_E is the coefficient of inertial effect term and K_D is permeability of the adsorbent bed. This equation is considered to be more general than the Darcy equation since it considers the effect of the inertial term at high velocities. Unfortunately, the effect of fluid compressibility was still not included in the momentum equation of flow through porous adsorbent particle. Recently, Marletta *et al*. (2002) introduced the following apparent permeability to account for this diffusion effect:

$$K_{aq} = K + \frac{D_g \mu}{P} \tag{2-15}$$

where K is the intrinsic permeability and D_g is the diffusivity in macro-pores in adsorbent bed. However, in the model of Marletta *et al.* (2002), micro mass transfer was neglected.

Advanced adsorption refrigeration cycles such as heat recovery, mass recovery and thermal wave cycles are rarely studied numerically. Poyelle *et al*. (1999) proposed a simple numerical model for the heat and mass recovery adsorption based air conditioning cycles. Mass transfer limitations were taken into account in their model. By assuming a parabolic pressure profile through the adsorbent bed, the average pressure inside the adsorbent can be predicted. Although the model fitted the experiment data very well, it is not a detailed model because of the assumption of the parabolic pressure profile and the need to know some empirical parameters in the model.

Sward *et al.* (2000) proposed a model for a thermal wave adsorption heat pump cycle. Local equilibrium was assumed to provide the asymptotic best-case performance. For each section of the bed, the mass balance consisted of an adsorbed phase term, a gas-phase term, a flow term and was given as:

$$\rho_b \frac{\partial n}{\partial t} + \frac{\partial(\varepsilon C)}{\partial t} + \frac{\partial(\varepsilon_a u C)}{\partial z} = f(z) \tag{2-16}$$

where n is the adsorbed phase concentration, C is the gas phase concentration and f(z) describes material flow into and out of the bed.

The energy balance for the bed which consisted of four similar terms and a term for heat transfer through the bed walls (J_b) was written as follows:

$$\rho_b \frac{\partial i_s}{\partial t} + \frac{\partial(\varepsilon i_v)}{\partial t} + \frac{\partial(\varepsilon_a uh)}{\partial z} = J_b + g(z) \qquad (2\text{-}17)$$

where i is internal energy and $g(z)$ are the energy fluxes through the bed.

The above equations were converted into dimensionless form, discretised into a number of individual cells and re-written as ordinary differential equations. The model was used to examine the performance of adsorption cooling cycles driven by low temperature waste heat sources of 373-393 K. Their results showed that the location of inlet/outlet valves in the bed had an impact on the shape of the temperature and loading fronts. The introduction of partitions within the bed was found to have only a small impact on the performance of the cycle for the temperatures examined, with sections of the bed undergoing pressurisation in a non-sequential order.

With the development of better computer hardware and numerical methodology, heat and mass transfer models are widely used to carry out critical investigation of adsorption cycles systems. Almost all the models fitted reasonably well with the experimental data, but with some deficiencies. More effort is required to enhance the existing models and new features of the adsorption cycles should be investigated.

2.5 SUMMARY

Adsorption cycles appear to be an attractive alternative for refrigeration and air conditioning applications because of environmental concerns in using the vapour compression cycle. There has been intensive research in the last few years to develop more efficient adsorption cycle systems.

The thermodynamic model, which is very important for the design of adsorption systems, predicts cycle performance by using limited data. Many different models resulting from various simplifications have been proposed by other investigators. Some of the assumptions used in their mathematical formulations appear to be too idealistic. Nevertheless, these models are useful in qualitative or semi-quantitative analysis of systems. Furthermore, these models can be used to simulate highly complex systems, which are difficult to be simulated by the heat and mass transfer model. Thermodynamic models based on second law analysis are useful to predict performance limits and give an insight on how to improve system performance. However, studies based on such thermodynamic models are scarce in the literature. Lumped models are considered to be transient models and are often expressed in terms of ordinary differential equations. The focus is primarily on the adsorbent bed without taking into account bed geometry.

With the development of high-speed computer hardware and numerical methodology, the heat and mass transfer model is widely used to carry out critical investigation of adsorption cycles. However, there are still some deficiencies in this model. The temperature component has received the most attention in the three fundamental quantities considered for modelling. Not much work has been done on models which considered mass transfer effects. Combined macro and micro mass transfer limitations in the adsorbent bed were not included in previous works. Advanced cycles which have been widely investigated by thermodynamic modelling have not attracted much interest in heat and mass transfer simulation. Detailed heat and mass transfer modelling have not been carried out on the heat and mass recovery adsorption refrigeration cycle, although the latter is very effective in improving system performance. Although adsorption cycles driven by low grade energy such as solar energy have been studied in detail, the literature is rather scarce on systems that couple the adsorption cycle to a high grade heat source such as the solid oxide fuel cell.

CHAPTER 3

THERMODYNAMIC MODELLING OF ADSORPTION REFRIGERATION CYCLES

3.1 INTRODUCTION

Much research has been carried out on the thermodynamic analysis of adsorption cooling cycles including not only first law analysis (Turner, 1992; Luo *et al*., 1992; Cacciola and Restuccia, 1995; Gui *et al*. 2002) but also second law analysis (Meunier *et al*., 1997; Chua *et al*., 1998). Different adsorption cycles were proposed and investigated thermodynamically, such as the intermittent (Turner, 1992), heat recovery (Cacciola and Restuccia, 1995), thermal wave (Miles, 1989), mass recovery (Wang, 2001), and continuous rotary system (Llobet and Goetz, 2000). Although there are many different thermodynamic models with different simplifications, they are all focused on predicting the system performance based on limited data available for the adsorbent/adsorbate pairs. The aim of these models was to obtain the variation rules of the system performance versus adsorbent/adsorbate properties and operating conditions, which are very important for the design of adsorption cycle systems. In this chapter, the cycle thermodynamics are investigated in detail with the aim of achieving an optimised design of the adsorption cycle system for zeolite/water pair, which approaches the ideal thermodynamic efficiency. The results will be compared to the results of a heat and mass transfer model.

3.2 INTERMITTENT ADSORPTION CYCLES

3.2.1 Numerical thermodynamic model

Figure 3.1 shows the Clapeyron diagram of an ideal intermittent adsorption cycle for zeolite/water pair. In order to evaluate the performance of this system, the amount of heat transfer for all phases has to be calculated.

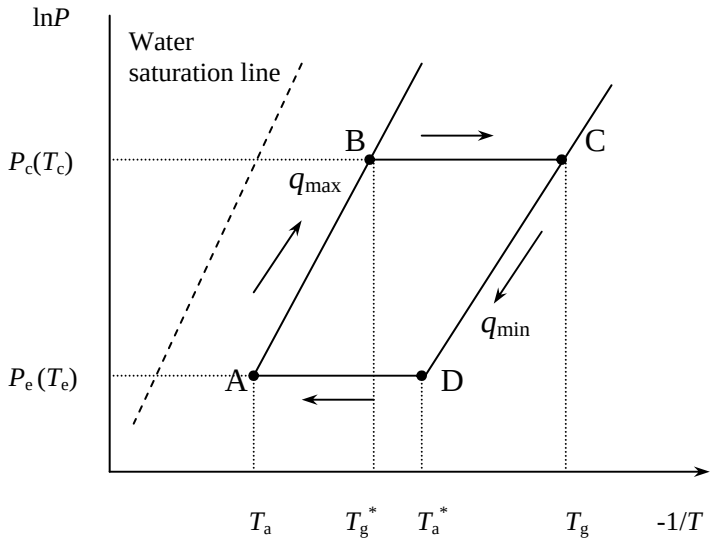

Figure 3.1 Clapeyron diagram of an ideal intermittent adsorption cycle

Isosteric heating phase (A-B):

The heat obtained from the heat exchange fluid is

$$Q_{ih} = \int_{T_a}^{T_g^*} [(1+r_{ms})C_{ps} + q_{\max}C_{pa} + (\varepsilon C_{pg}\rho_g / \rho_s)]m_s dT \qquad (3\text{-}1)$$

Assuming that the sensible heating of the water vapour within the adsorbent bed is negligible, Equation (3-1) becomes

$$\begin{aligned} Q_{ih} &= \int_{T_a}^{T_g^*} [(1+r_{ms})C_{ps} + q_{\max}C_{pa}]m_s dT \\ &= m_s[(1+r_{ms})C_{ps} + q_{\max}C_{pa}]\cdot(T_g^* - T_a) \end{aligned} \qquad (3\text{-}2)$$

Isobaric generation phase (B-C):

The heat obtained from the heat exchange fluid is

$$\begin{aligned} Q_{gh} &= \int_{T_g^*}^{T_g} [(1+r_{ms})C_{ps} + q(P_c,T)C_{pa} + \Delta H \frac{\partial q(P_c,T)}{\partial T}] m_s dT \\ &= m_s(1+r_{ms})C_{ps}(T_g - T_g^*) + m_s \Delta H (q_{\max} - q_{\min}) + m_s C_{pa} \int_{T_g^*}^{T_g} q(P_c,T) dT \end{aligned} \tag{3-3}$$

and the heat rejected to the condenser is

$$Q_{co} = \int_{T_g^*}^{T_g} [m_s C_{pg} \frac{\partial q(P_c,T)}{\partial T} \cdot (T - T_c)] dT + m_s (q_{\max} - q_{\min}) \cdot L(T_c) \tag{3-4}$$

Isosteric cooling phase (C-D):

The heat rejected to the heat exchange fluid is

$$Q_{ic} = -\int_{Tg}^{T_a^*} [(1+r_{ms})C_{ps} + q_{\min} C_{pa}] m_s dT = m_s [(1+r_{ms})C_{ps} + q_{\min} C_{pa}] \cdot (T_g - T_a^*) \tag{3-5}$$

Isobaric adsorption phase (D-A):

The heat rejected to the heat exchange fluid is

$$\begin{aligned} Q_{ac} &= -\int_{T_a^*}^{T_a} [(1+r_{ms})C_{ps} + q(P_e,T)C_{pa} + \Delta H \frac{\partial q(P_e,T)}{\partial T} - C_{pg}(T - T_e)\frac{\partial q(P_e,T)}{\partial T}] m_s dT \\ &= m_s [(1+r_{ms})C_{ps}(T_a^* - T_a) + \Delta H (q_{\max} - q_{\min})] \\ &- m_s \int_{T_a^*}^{T_a} [C_{pa} \cdot q(P_e,T) - C_{pg}(T - T_e)\frac{\partial q(P_e,T)}{\partial T}] dT \end{aligned} \tag{3-6}$$

and the heat obtained from the evaporator

$$Q_{ev} = m_s (q_{\max} - q_{\min})[L(T_e) - C_{pl}(T_c - T_e)] \tag{3-7}$$

The COP (coefficient of performance) can be defined as

$$COP = \frac{Q_{ev}}{Q_{ih} + Q_{gh}} \tag{3-8}$$

where m_s is the mass of adsorbent, q is adsorbed amount, L is the latent heat of vaporization, C_{ps} is specific heat of adsorbent, C_{pa} is specific heat of the adsorbed phase, C_{pg} is specific

heat of the adsorbate vapour, C_{pl} is specific heat of liquid adsorbate, ρ_s is the density of the adsorbent, $r_{ms} = \dfrac{m_m C_{pm}}{m_s C_{ps}}$ is the heat capacity ratio of adsorber metal to adsorbent, ε is the porosity of the adsorbent bed, and ΔH is the heat of adsorption. The physical properties of adsorbent bed are listed in Table 3.1.

Table 3.1 Some physical properties of adsorbent bed

Name	Symbol	Value
Density of adsorbent bed	ρ_s	620 kg/m^3
Specific heat of adsorbent bed	C_{ps}	836 J/kg·K
Specific heat of water vapour	C_{pg}	1880 J/kg·K
Specific heat of adsorbed water	C_{pa}	4180 J/kg·K
Specific heat of liquid water	C_{pl}	4180 J/kg·K
Heat of adsorption	ΔH	3200 kJ/kg
Total porosity of adsorbent bed	ε	0.64
Heat capacity ratio	r_{ms}	0.334

All physical properties listed in Table 3.1 are assumed to be independent of temperature

The latent heat of vaporization for pure adsorbate (water) is

$$L(T) = L_0 + L_1 T \tag{3-8}$$

where $L(T)$ is in kJ/kg and the values of the parameters are

$$L_0 = 3171.2 \text{ kJ/kg}; \quad L_1 = -2.4425 \text{ kJ/kg} \tag{3-9}$$

The saturation pressure for adsorbate liquid-vapour equilibrium (water) is written as

$$\ln P_s = 25.1948 - 5098.26/T \text{ Pa} \tag{3-10}$$

q_{eq} is the adsorbed phase concentration in equilibrium with bulk fluid defined by the following equation containing three Langmuir terms (Ben Amar *et al.*, 1996):

$$q_{eq} = \frac{q_{s,1} b_1 P}{1 + b_1 P} + \frac{q_{s,2} b_2 P}{1 + b_2 P} + \frac{q_{s,3} b_3 P}{1 + b_3 P} \tag{3-11}$$

where $q_{s,k}$ and b_k (k = 1, 2, and 3) are functions of temperature given by:

$$\begin{aligned} q_{s,k} &= a_{0,k} + \frac{a_{1,k}}{T} + \frac{a_{2,k}}{T^2} + \frac{a_{3,k}}{T^3} \qquad (k = 1, 2) \\ q_{s,3} &= 0.267 - q_{s,1} - q_{s,2} \\ b_k &= b_{0,k} \exp(E_k / T) \end{aligned} \tag{3-12}$$

The values of the parameters are given in Table 3.2 (Ben Amar *et al*., 1996).

Table 3.2 Parameter values used in the adsorption equilibrium Equation (3-12)

$a_{0,1}$ = 0.070	$a_{1,1}$ = -1.199 × 10^2	$a_{2,1}$ = 6.369 × 10^4	$a_{3,1}$ = -8.450 × 10^6
$a_{0,2}$ = -0.687	$a_{1,2}$ = 7.757× 10^2	$a_{2,2}$ = -2.542 × 10^5	$a_{3,2}$ = 2.775 × 10^7
$b_{0,1}$ = 1.508 × 10^{-10}	$b_{0,2}$ = 5.417×10^{-10}	$b_{0,3}$= 1.707×10^{-10}	
E_1 = 7726.58	E_2 = 6074.71	E_3 = 5392.17	

3.2.2 Effects of operating conditions on COP

For an adsorption cooling system, operating conditions are important in determining performance and machine design. In order to obtain the effects of operating conditions on system performance, a computer code has been written using Visual FORTRAN software to solve the above numerical model. The results are discussed in the following sections.

3.2.2.1 Effect of generation temperature (T_g)

The effect of the generation temperature on the COP is shown in Figure 3.2. From the figure, it can be seen that the COP has a maximum value at some value of T_g for a fixed T_c and T_a. COP (max) occurs at the temperature T_g (opt). Such variation of COP happens because q_{min} will decrease with an increase in T_g and the concentration change (q_{max}-q_{min}) that is proportional to the cooling energy produced in the evaporator (Q_{ev}) will be greater.

However when T_g increases beyond a certain point, the extra concentration change proportional to extra energy obtained from the heat source will decrease causing the COP to decrease.

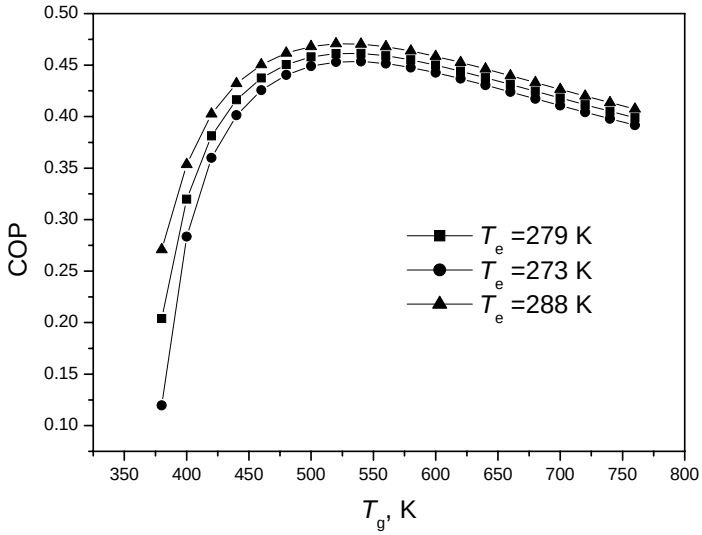

Figure 3.2 Effect of T_g on COP for $T_a = T_c = 318$ K; r_{ms}= 0.334

3.2.2.2 Effect of adsorption temperature (T_a) /condensing temperature (T_c)

It is assumed that T_c equals T_a because three heat reservoirs are used for the adsorption cooling system in this simulation. Figure 3.3 shows the effect of T_{ac} on the COP. It can be seen that the COP is inversely proportional to T_a. When T_c and T_a decrease, the adsorbed water concentration change will increase and the heat input will need to be increased. However, the gradient of the increase in concentration change compared to that in heat input will be greater and so does the COP.

3.2.2.3 Effect of evaporating temperature (T_e)

The effect of T_e on the COP is shown in Figure 3.4. As can be seen from this figure, the COP increases as T_e increases. From Figure 3.1, it can be observed that the concentration

change will increase as T_e is increased. Due to the fixed values of T_a and T_g, the heat input would have negligible change and hence, the COP will increase.

Figure 3.5 shows the effect of T_e on the COP (max) and T_g (opt). As can be seen in the figure, COP (max) increases with T_e, while T_g (opt) changes very little with T_e.

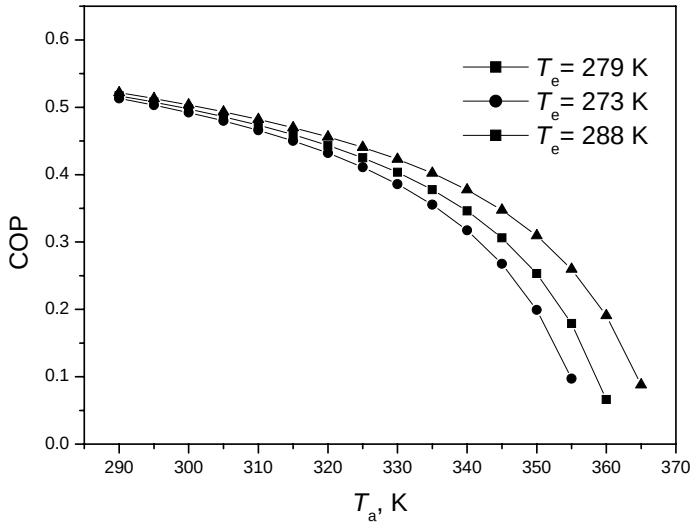

Figure 3.3 Effect of T_a on COP for T_g = 473 K; r_{ms} = 0.334

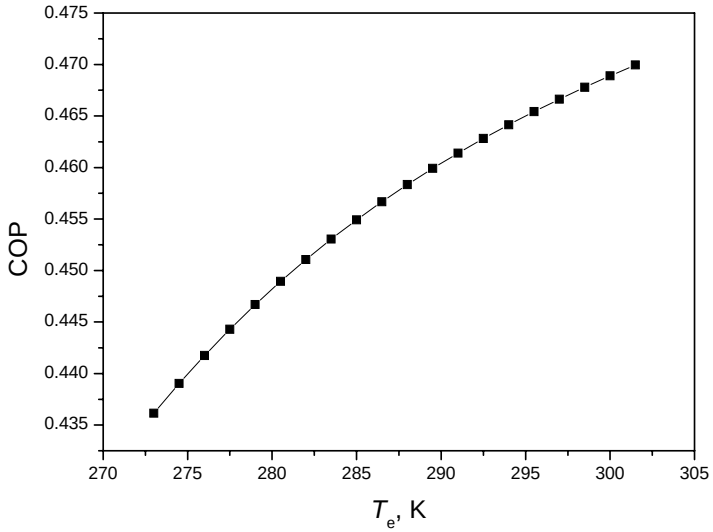

Figure 3.4 Effect of T_e on COP for T_a = T_c = 318 K; T_g= 473 *K*; r_{ms}= 0.334

3.2.2.4 Effect of heat capacity ratio of metal to adsorbent (r_{ms})

From Figure 3.6, it can be seen that the value of COP increases with a reduction of r_{ms}. This is because as r_{ms} increases, the heat absorbed by the metal media will increase. Thus, the effect of heat on the adsorbent bed compared to the whole heat input becomes lower, resulting in a reduction of the COP.

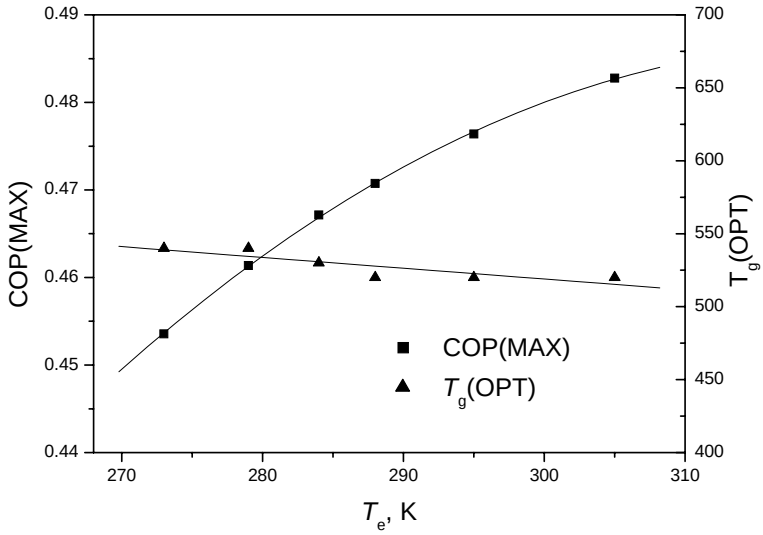

Figure 3.5 Effect of T_e on COP (max) and T_g (opt) for T_a=T_c=318 K; r_{ms}=0.334

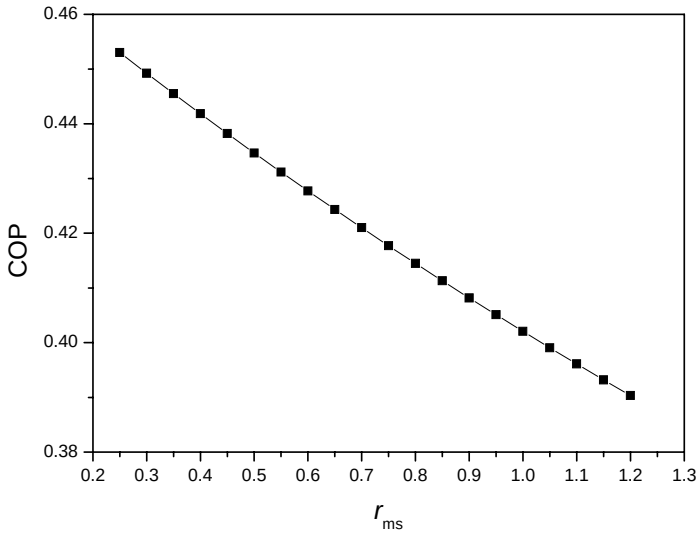

Figure 3.6 Effect of r_{ms} on COP for T_a = T_c = 318 K; T_g = 473 K; T_e =279K

3.2.3 Second law analysis

Using first and second law analyses for a closed intermittent cycle with three heat reservoirs ($T_a = T_c$) and following the approach of Meunier *et al*. (1997), the COP and second law efficiency can be obtained:

$$COP = \frac{Q_{ev}}{Q_h} = COP_C - \frac{\Delta S_t}{Q_h(\frac{1}{T_e} - \frac{1}{T_c})} \tag{3-13}$$

$$\eta = \frac{COP}{COP_C} = 1 - \frac{\Delta S_t}{Q_h(\frac{1}{T_c} - \frac{1}{T_g})} \tag{3-14}$$

where $COP_C = (\frac{1}{T_c} - \frac{1}{T_g}) \Big/ (\frac{1}{T_e} - \frac{1}{T_c})$ is the Carnot efficiency of the system performance, $Q_h = Q_{ih} + Q_{gh}$ is total heat input for the first two phases, ΔS_t is total entropy production and η is the second law efficiency.

The total entropy can be split into several parts as follows:

$$\Delta S_t = \Delta S_{bed} + \Delta S_{co} + \Delta S_{ev} \tag{3-15}$$

where ΔS_{bed}, ΔS_{co} and ΔS_{ev} are the entropy production in the adsorbent bed, condenser and evaporator, respectively.

The entropy production in the adsorbent bed can be further split into entropy production of four phases. It can be written as

$$\Delta S_{bed} = \oint (\frac{1}{T_{bed}} - \frac{1}{T_{hxf}}) dQ = \Delta S_{ih} + \Delta S_{gh} + \Delta S_{ic} + \Delta S_{ac} \tag{3-16}$$

where the entropy production of the four phases can be obtained as follows:

$$\begin{aligned} \Delta S_{ih} &= \int_{T_a}^{T_{g^*}} [(1 + r_{ms}) C_{ps} + q_{\max} C_{pa}] m_s (1/T - 1/T_g) dT \\ &= m_s [(1 + r_{ms}) C_{ps} + q_{\max} C_{pa}] \cdot [\ln(T_g^{\,*} / T_a) - (T_g^{\,*} - T_a) / T_g] \end{aligned} \tag{3-17}$$

$$\Delta S_{gh} = \int_{T_g^*}^{T_g} [(1+r_{ms})C_{ps} + q(P_c,T)C_{pa} + \Delta H \frac{\partial q(P_c,T)}{\partial T}] m_s (1/T - 1/T_g) dT$$
$$= m_s \cdot (1+r_{ms}) C_{ps} [\ln(T_g / T_g^*) - (T_g - T_g^*)/T_g] \quad (3\text{-}18)$$
$$+ \int_{T_g^*}^{T_g} [q(P_c,T)C_{pa} + \Delta H \frac{\partial q(P_c,T)}{\partial T}] \cdot m_s (1/T - 1/T_g) dT$$

$$\Delta S_{ic} = \int_{T_g}^{T_a^*} [(1+r_{ms})C_{ps} + q_{\min} C_{pa}] m_s / T dT - \{ \int_{T_g}^{T_a^*} [(1+r_{ms})C_{ps} + q_{\min} C_{pa}] \quad (3\text{-}19)$$
$$m_s dT\} / T_a = m_s [(1+r_{ms})C_{ps} + q_{\min} C_{pa}] \cdot [\ln(T_a^* / T_g) - (T_a^* - T_g)/T_a]$$

$$\Delta S_{ac} = \int_{T_a^*}^{T_a} [(1+r_{ms})C_{ps} + q(p_e,T) \cdot C_{pa} + \Delta H \frac{\partial q(P_e,T)}{\partial T}$$
$$- C_{pg}(T - T_e) \frac{\partial q(P_e,T)}{\partial T}] \cdot m_s (1/T - 1/T_a) dT \quad (3\text{-}20)$$
$$+ m_s \int_{T_a^*}^{T_a} \{ [C_{pg} \frac{\partial q(P_e,T)}{\partial T} \ln(T/T_e) - C_{pg}(T - T_e) \frac{\partial q(P_e,T)}{\partial T}] / T \} dT$$

and the entropy production in the evaporator and condenser can be obtained by

$$\Delta S_{co} = m_s \int_{T_g^*}^{T_g} [-\frac{\partial q(P_c,T)}{\partial T} \Delta H / T_c + \frac{\partial q(P_c,T)}{\partial T} C_{pg} \ln(T/T_c)] dT$$
$$= m_s (q_{\max} - q_{\min}) \Delta H / T_c - m_s \int_{T_g^*}^{T_g} [-\frac{\partial q(P_c,T)}{\partial T} \ln(T/T_c)] dT \quad (3\text{-}21)$$

$$\Delta S_{ev} = m_s (q_{\max} - q_{\min}) \cdot C_{pl} \int_{T_c}^{T_e} (1/T - 1/T_c) dT$$
$$= m_s (q_{\max} - q_{\min}) \cdot C_{pl} [\ln(T_e / T_c) - (T_e - T_c)/T_c] \quad (3\text{-}22)$$

All the entropy production terms are calculated by a FORTRAN programme written by the author. The following results are obtained for the basic operating conditions of T_a = T_c = 318 K; T_e = 279 K; T_g = 473 K; r_{ms}= 0.334: ΔS_t = 630.32 kJ/K, ΔS_{co} = 12.57 kJ/K, ΔS_{ev} = 5.86 kJ/K, ΔS_{bed} = 611.88 kJ/K. It is found that the entropy production in the adsorbent bed is the dominant term in the total entropy production. Hence, the heat exchange process in the

adsorbent bed is a controlled one for the performance of the adsorption cooling cycle. Figures 3.7 and 3.8 show the entropy production rate in the adsorbent bed for the heating and cooling phases. During the isosteric heating phase, the entropy production rate decreases with the increase of temperature. At the beginning of this phase, a large temperature gap between the adsorbent bed and HXF (heat exchange fluid) exists which decreases as the temperature increases while the heat exchange rate is almost unchanged (Figure 3.9). During the isobaric generation phase, the heat exchange rate increases greatly compared to that in the isosteric heating phase. Hence, at the beginning of the isobaric generation phase, the entropy production rate is very high (Figure 3.9). However, when the temperature of the adsorbent bed approaches the temperature of HXF, the temperature gap decreases resulting in a decrease in the entropy production rate.

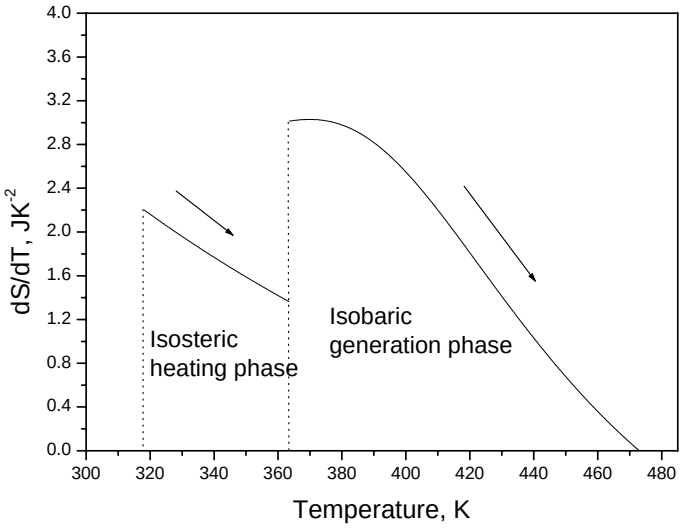

Figure 3.7 Entropy production rate in adsorbent bed during heating step

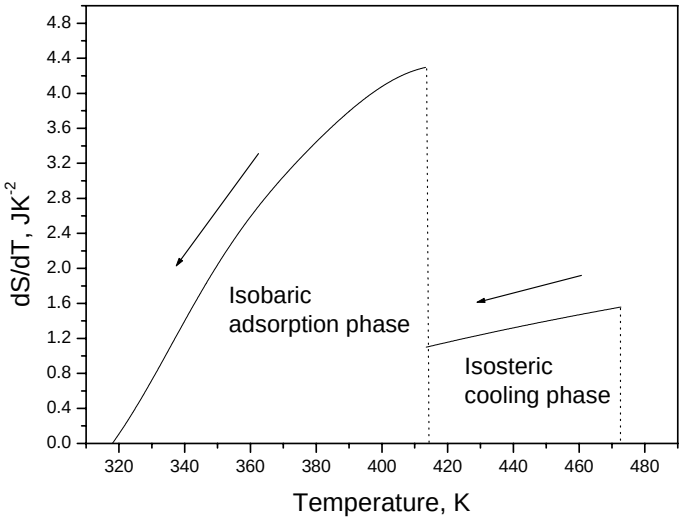

Figure 3.8 Entropy production rate in adsorbent bed during cooling step

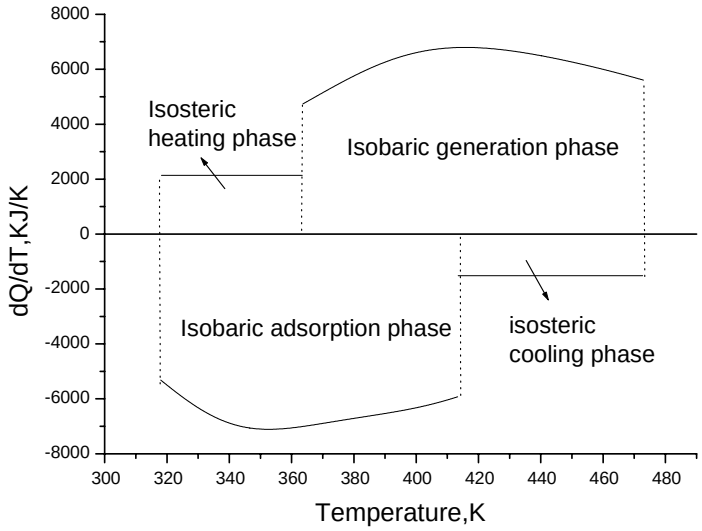

Figure 3.9 Heat exchange rate in adsorbent bed during entire intermittent cycle

3.3 HEAT RECOVERY CYCLE

It is recognised that the performance of the adsorption cycle can be improved by using a heat recovery cycle. For a two-bed system as shown in Figure 3.10, Adsorbent Bed 1 will be heated at the lowest temperature (Point A) and Bed 2 will be cooled at the highest

temperature (Point C). Heat recovery starts with heat exchange (Q_{rec}) from Bed 1 to the other bed (Bed 2). During this phase, no heat is supplied by the external heat source. The heat recovery will end when Bed 1 reaches Point E and Bed 2 reaches Point E'. From Figure 3.11, it can be easily seen how the heat recovery phase is carried out. The magnitude of area1 or area2 equals the value of the heat exchange between the two adsorbent beds. The COP will increase because the heat input from HXF decreases. For a two-bed heat recovery cycle, the COP can be defined as:

$$COP = \frac{Q_{ev}}{Q_{ih} + Q_{gh} - Q_{rec}} = \frac{Q_{ev}}{Q_h(1-r)} = \frac{COP_0}{1-r} \tag{3-23}$$

where COP_0 is the coefficient of performance without heat recovery and r is the coefficient of heat recovery.

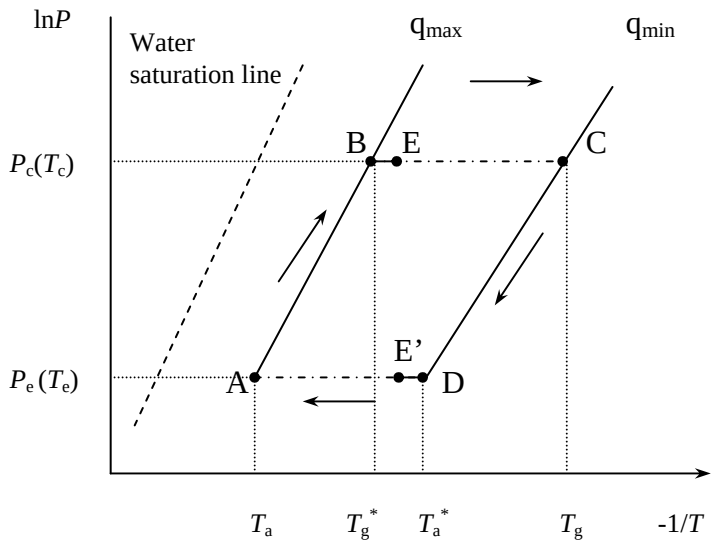

Figure 3.10 Clapeyron diagram of a two-bed heat recovery cycle

At the end of the heat recovery phase, Adsorbent Bed 1 is at the temperature of TE and Bed 2 is at the temperature of TE' (see Figure 3. 11). There is a temperature difference (ΔT) between the two beds. Figure 3.12 shows the effect of ΔT on the COP. It can be seen that

the COP decreases as ΔT increases. The degree of the heat recovery reduces with the increment of ΔT resulting in a decrease in COP.

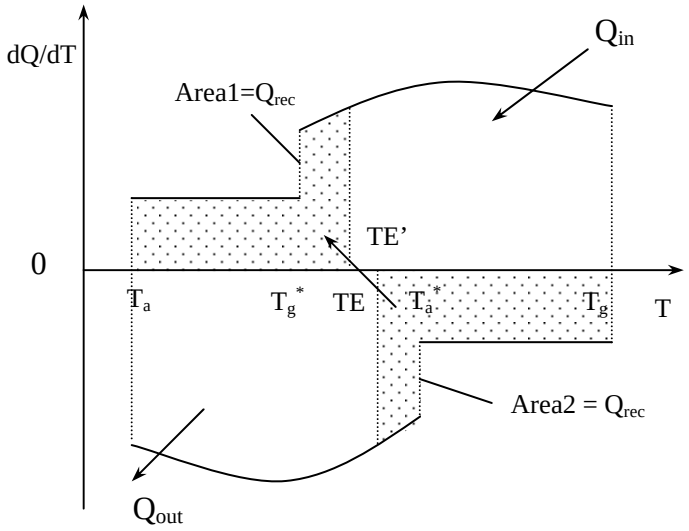

Figure 3.11 Heat exchange rate of a two-bed heat recovery cycle

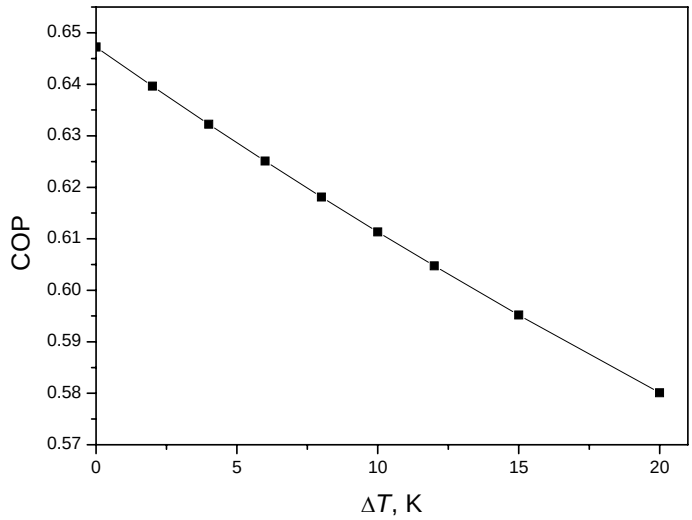

Figure 3.12 Effect of ΔT on COP for two-bed heat recovery cycle under basic operating conditions

Figure 3.13 shows how the heat recovery of a four-bed cycle can be achieved. The recovered heat of four beds compared to that of the two beds is greater with a larger COP. Meunier *et al*. (1997) investigated in detail the potential of better performance of multiple

bed heat recovery cycle. In order to study the potential of multiple bed heat recovery cycles, a second law analysis is performed. The results are shown in Table 3.3 for the following operating conditions: $T_a = T_c = 318$ K, $T_g = 473$ K, $T_e = 279$ K, $r_{ms} = 0.334$, $\Delta T = 0$ K.

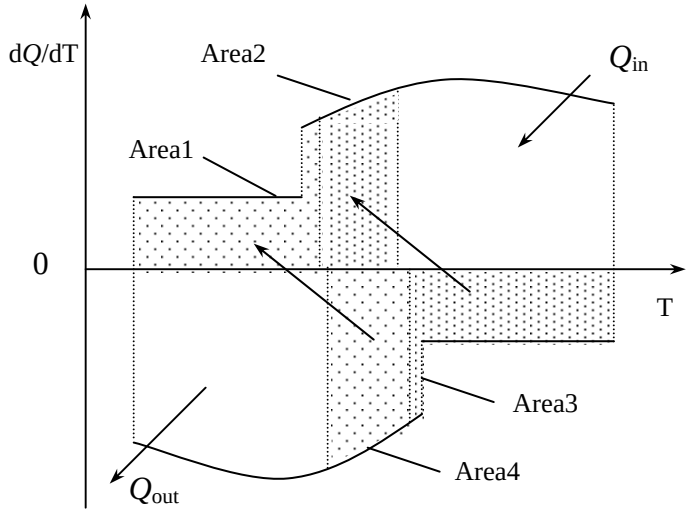

Figure 3.13 Heat exchange rate of four-bed heat recovery cycle Area1=Area4; Area2=Area3; Area1+Area2 = Q_{rec}

From Table 3.3, it can be seen that the recovered heat increases with an increase in the number of beds and thus the values of COP and η both increase. At the same time, with the increase in the number of beds for the heat recovery cycle, entropy production reduces due to the reduction in the temperature gap between the adsorbent and HXF.

Table 3.3 Results of a second law analysis for different multiple-bed heat recovery cycles ($\Delta T = 0$ K)

Number of adsorbent beds	Q_h (kJ)	Q_{rec} (kJ)	ΔS_t (J/K)	ΔS_{bed} (J/K)	ΔS_{rec} (J/K)	COP	η
1	777.316	0	630.319	611.822	0	0.447	0.191
2	536.466	240.850	382.149	272.379	91.334	0.647	0.276
4	452.871	324.445	295.982	189.986	87.559	0.767	0.327
∞	148.171	629.145	0	0	0	2.345	1

3.4 MASS RECOVERY CYCLE

The schematic of a two-bed adsorption cooling system with mass recovery is shown in Figure 3.14. At the beginning of this two-bed cooling cycle, one bed is hot and at high pressure (point C) and the other is cold and at low-pressure (Point A). The high-pressure adsorbent bed needs to be cooled down and depressurised while the low-pressure bed needs to be heated and pressurised. The two adsorbent beds can be interconnected directly with the opening of a valve and water vapour will flow from the high-pressure bed to the low-pressure bed. This is the mass recovery process. The pressure of higher-pressure adsorbent bed decreases due to mass outflow and this will again cause desorption. Meanwhile, the pressure of the lower-pressure bed increases due to mass inflow and will cause further adsorption. The process is maintained until the two beds reach points E and E'. Then the valve connecting the two beds is closed, and each bed goes on with the heating and cooling processes just as in the basic cycle.

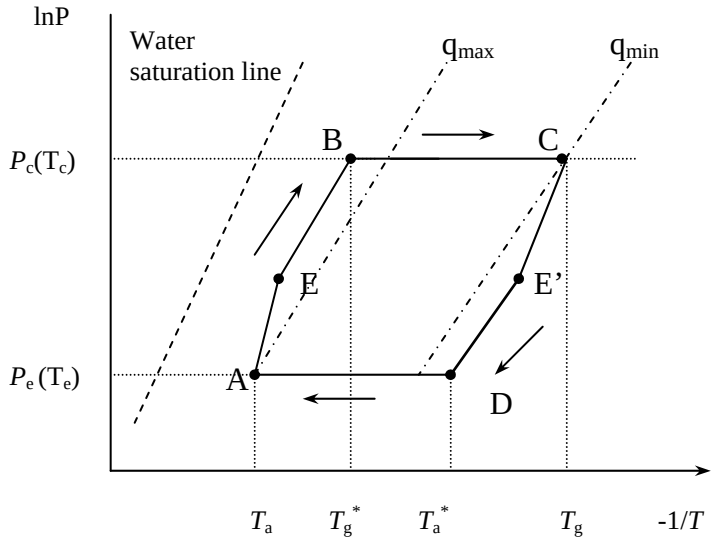

Figure 3.14 Clapeyron diagram of mass recovery cycle

This mass recovery process is expected to accelerate the circulation and enhance the performance of the cycle. By using mass recovery, the quantity of cycled refrigerant (Δm) in the evaporator is increased. The quantity of the cycled adsorbate vapour can be written as

$$\Delta m = m_s (q_{\max} - q_{\min}) + m_s \Delta q_{rec} = \Delta m_0 + \Delta m_{rec} \tag{3-24}$$

where Δm_0 is the quantity of the cycled adsorbate vapour without mass recovery and Δm_{rec} is the extra quantity of the cycled adsorbate vapour with mass recovery.

In a simple continuous cycle with two absorbent beds, the cooling energy produced in the evaporator can be calculated as

$$\begin{aligned} Q_{ev} &= \Delta m[L(T_e) - C_{pl}(T_c - T_e)] = (\Delta m_0 + \Delta m_{rec})[L(T_e) - C_{pl}(T_c - T_e)] \\ &= Q_{ev0} + Q_{evr} = Q_{ev0}(1+r) \end{aligned} \tag{3-25}$$

where Q_{ev0} is the cooling energy produced without mass recovery, Q_{evr} is the extra cooling energy with mass recovery and r is the coefficient of mass recovery.

The cooling coefficient of performance is defined as

$$COP = \frac{Q_{ev}}{Q_h} = \frac{Q_{ev0}(1+r)}{Q_h} \tag{3-26}$$

where Q_h is the heat supplied to the adsorbent bed during the two heating phases.

Because the difference of Q_h of the adsorption cycle with or without mass recovery is very small, Equation (3-26) can be rewritten as:

$$COP \approx COP_0 (1+r) \tag{3-27}$$

where COP_0 is the coefficient of the performance without mass recovery.

At the end of the mass recovery phase, Adsorbent Bed 1 is at the pressure of PE and the other bed is at the pressure of PE', where PE' - PE $= \Delta P$ is the pressure difference between beds. ΔP can be used to measure the degree of the mass recovery. From Figure 3.15, it can

be seen that an increase of ΔP causes a reduction of the COP. The degree of mass recovery decreases with the increase of ΔP, i.e. the cycled vapour quantities reduce, and so does the COP.

From Figures 3.12 and 3.15, it can be seen that the effect of heat recovery on the COP is larger than that of mass recovery. The COP can be greatly improved (about 44% for $\Delta T = 0$) by using heat recovery, while mass recovery cycle can only increase the COP by 6% for $\Delta P = 0$. Since the mass recovery phase takes a very short time (Wang *et al.*, 2002B), the improvement on the SCP as a result of mass recovery is obvious.

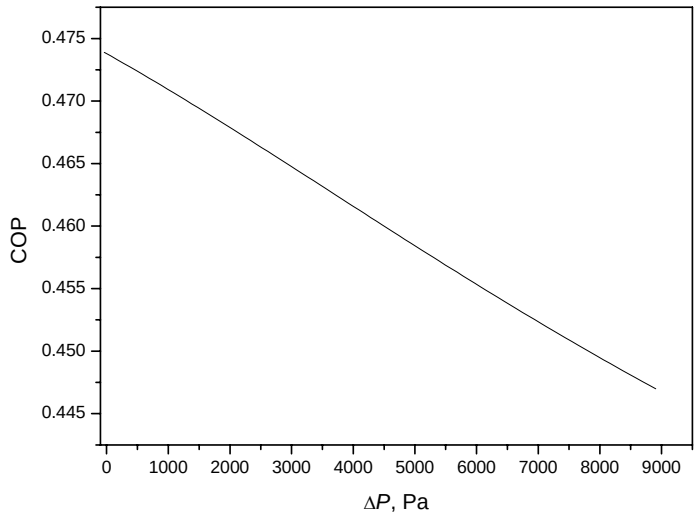

Figure 3.15 Effect of ΔP on COP for mass recovery cycle under basic operation conditions

3.5 COMBINED HEAT AND MASS RECOVERY CYCLE

In order to achieve both higher COP and SCP, mass recovery and heat regeneration can be simultaneously employed. The Clapeyron diagram of a combined heat and mass recovery cycle is shown in Figure 3.16. Initially one of the adsorbent beds is at the state of point A and the other bed is in the state of point C in Figure 3.16. The mass recovery phase then starts. At the end of this phase, the two beds are at the states of point E and point E',

respectively. Subsequently, the heat recovery phase is carried out from point E to point F for Adsorbent Bed 1 and from point E' to point F' for the other bed. Finally the two adsorbent beds are connected to the external heat source. Figure 3.17 shows the combined effect of heat and mass recovery on the COP. From this figure, the COP generally decreases with the growth of ΔP and ΔT. It can also be seen that the COP is affected mainly by heat recovery and to a lesser extent by mass recovery.

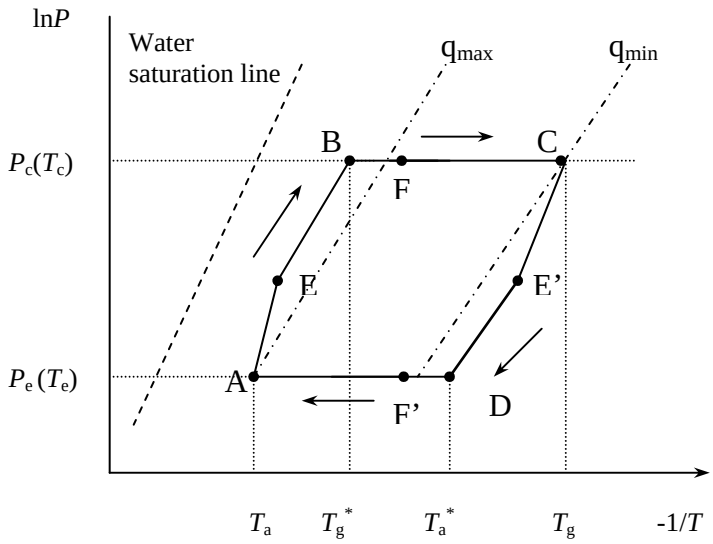

Figure 3.16 Clapeyron diagram of a combined heat and mass recovery cycle

Actually, the COP, SCP and total cooling power are all indices for evaluating the performance of an adsorption cooling system. In the thermodynamic model, only the COP can be investigated. Hence, a more complicated transient model of different adsorption cycle needs to be developed to investigate their comprehensive effects on the performance of an adsorption cooling system.

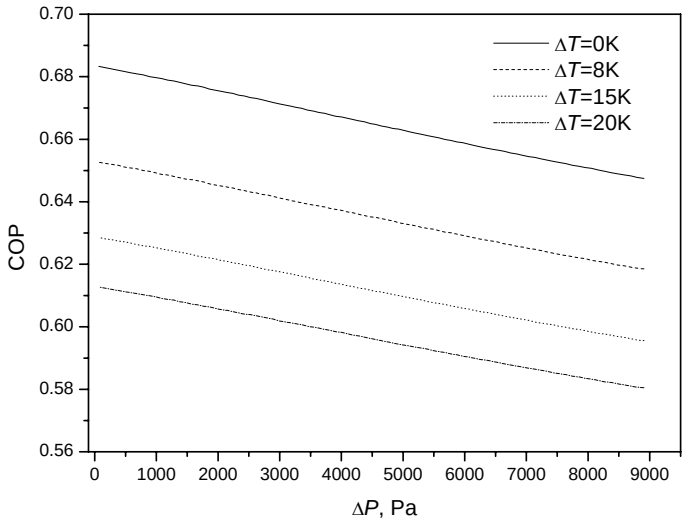

Figure 3.17 Combined effects of ΔP and ΔT on COP with heat and mass recovery for the basic operating conditions

3.6 SUMMARY

A thermodynamic model for different adsorption cycles incorporating intermittent, heat recovery, mass recovery and coupled heat and mass recovery cycles has been proposed. By using a computer programme based on this model, the effect of operating conditions on COP has been studied. The following conclusions can be drawn: (i) The COP has a maximum value at a certain value of $T_{g;}$ (ii) COP decreases as T_a/T_c increases; (iii) COP and COP(max) increase as T_e increases while T_{g2}(opt) changes very little with T_e; (iv) COP increases with the reduction of r_{ms}. The reduction of entropy production for the adsorption cycles results in a higher COP. The thermal exchange process in the adsorbent bed compared with other components is a controlled one for COP of the adsorption cooling cycle. The increase of COP results mainly from heat recovery.

CHAPTER 4

NUMERICAL STUDY OF A NOVEL CASCADING ADSORPTION REFRIGERATION CYCLE

4.1 INTRODUCTION

As mentioned previously, the main limitation in the commercial application of adsorption systems is its rather low coefficient of performance. In order to improve the performance of such cooling systems, several advanced cycles have been proposed such as the continuous cycle (Zanifé and Meunier, 1992; Cacciola and Restuccia, 1995), cascading cycle (Douss and Meunier, 1989), forced convection cycle (Critoph, 1998) and thermal wave cycle (Miles, 1989; Cho *et al*., 1992; Ben Amar *et al*., 1996; Sun *et al*., 1997; Sward and Douglas, 2000). Wang *et al.* (2002B) incorporated heat and mass recovery processes into the continuous cycle to improve its thermal performance. However, the resulting COP is still rather low being below < 1.0. Douss and Meunier (1989) proposed a cascading cycle with a higher COP of 1.06. In their cooling system, three adsorbers, two condensers and two evaporators were employed. The system configuration and operation are inherently more complex compared with the continuous cycle. The forced convection and thermal wave cycles are both capable of achieving high COP values. However, for actual engineering application, the operating conditions of these systems are difficult to control.

As an improvement of the cascading cycle proposed by Douss and Meunier (1989), a novel cascading cycle based on two zeolite adsorbent beds and a silica gel adsorbent bed is presented in this chapter. A lumped model is proposed to study the thermal performance of this cycle.

4.2 DESCRIPTION OF THE NEW CASCADING ADSORPTION CYCLE

The schematic of a new cascading adsorption system is shown in Figure 4.1. This cooling system consists of two zeolite/water adsorbers (Adsorbers 1 and 2) and a silica gel/water adsorber (Adsorber 3). The Clapeyron diagram which shows the working cycle of this cooling system is presented in Figure 4.2. The working cycle consists of four steps:

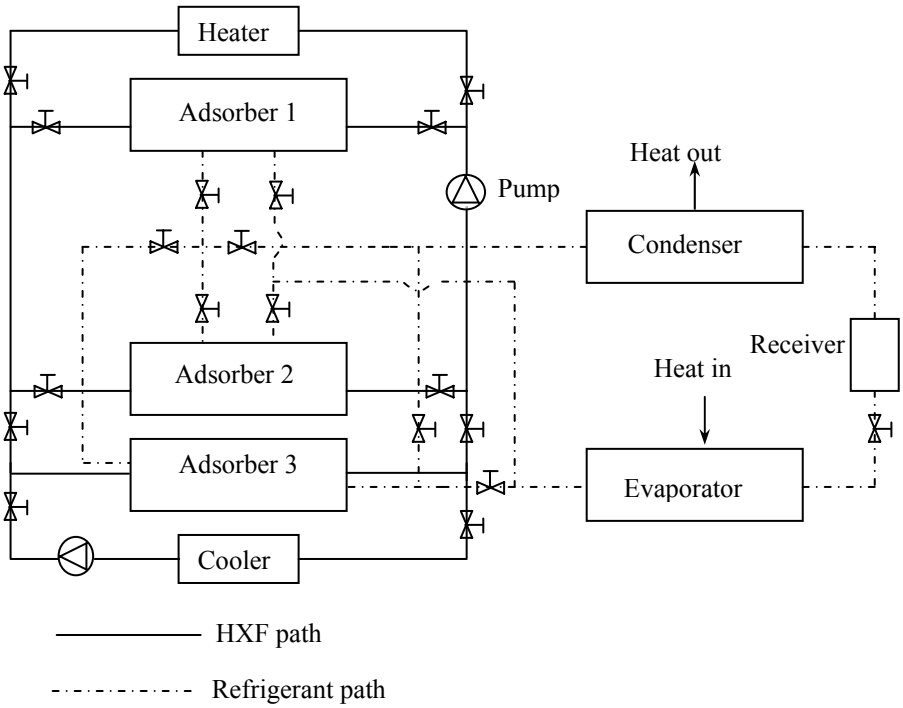

Figure 4.1 Schematic of cascading adsorption cooling system

First step: The cycle begins with the three adsorbers (Adsorbers 1, 2 and 3) at different temperatures (points I, E and C in Figure 4.2), respectively. Adsorbers 1 and 2 are then connected. The high-pressure adsorbate gas from Adsorber 1 is transferred to Adsorber 2 (Processes I-J and E-F), which is subsequently heated by energy drawn from Adsorber 1 through a heat exchange fluid (HXF) (Processes F-G-H for Adsorber 2 and J-K-M for Adsorber 1 in Figure 4.2). Adsorber 3 is cooled down (Process C-D-A in Figure 4.2). .

When the pressure in Adsorber 2 is higher than the condensing pressure (P_c), Adsorber 2 is connected to the condenser. In the condenser, the adsorbate gas will be cooled down and condensed. When the pressure equals to the evaporating pressure (P_e), Adsorbers 1 and 3 are connected to the evaporator.

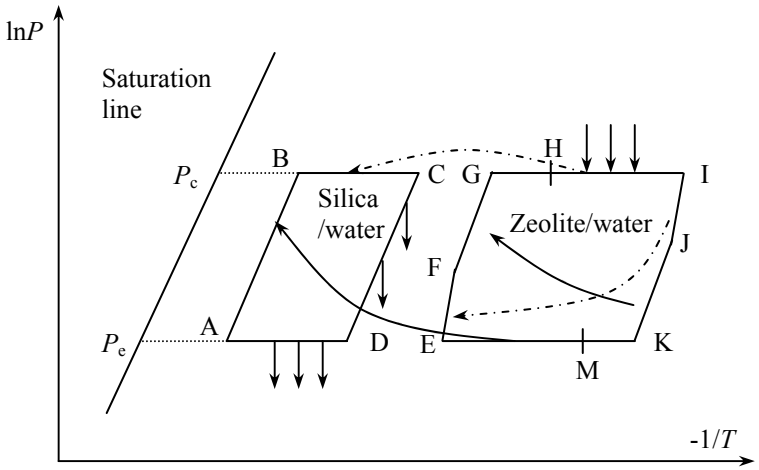

Figure 4.2 Clapeyron diagram of cascading adsorption cycle

Second step: During this step, Adsorber 3 is heated (Process A-B-C) by the energy from Adsorber 1 (Process M-E in Figure 4.2). Adsorber 2 is then heated by an external heat source through the HXF (Process G-H in Figure 4.2).

Adsorber 3 is connected to the condenser when its pressure reaches the condensing pressure. At the same time, Adsorber 2 is disconnected from the condenser and connected to Adsorber 3. The higher temperature adsorbate gas from Adsorber 2 flows through Adsorber 3 to the condenser.

When Adsorbers 1 and 2 are interchanged, the other two steps are the same as the first two steps.

The cascading cycle proposed by Douss and Meunier (1989) employed two different working pairs of active carbon/methanol and zeolite/water, three adsorbers, two condensers

and two evaporators. The configuration of the cascading adsorption cycle shown in Figure 4.1 is simpler than that proposed by Douss and Meunier (1989) since it uses only one type of refrigerant (water), and requires only one condenser and one evaporator. Furthermore, some of the sensible heat of high temperature adsorbate gas drawn from high temperature adsorber can be recovered.

4.3 NUMERICAL MODELLING

4.3.1. Adsorption equilibrium equations

Adsorption of the two working pairs is assumed to be in equilibrium. For the zeolite/water pair, the adsorption equilibrium is composed of three Langmuir terms, which are defined in Chapter 3.

Freundlich's equation (Sakoda and Suzuki, 1984) is chosen for the equilibrium adsorbed amount of silica gel/water pair and is defined by

$$q = k(P / P_s)^{1/n} \tag{4-1}$$

where P_s is the saturation vapour pressure and constants k and n have values of 0.346 kg/kg and 1.6, respectively.

4.3.2 Energy conservation equations

The energy conservation equations are based on the assumption that the pressure, temperature and adsorbed amount are uniform in the adsorber. In this analysis, heat losses to the external environment are not taken into consideration.

First step:

For the mass recovery process between Adsorbers 1 and 2, the heat conservation equations are expressed as

$$\sum m_i C_{pi} \frac{dT_{s1}}{dt} = m_s \cdot \Delta H \frac{dq}{dt} \qquad \text{(Adsorber 1)} \qquad (4\text{-}2)$$

$$\sum m_i C_{pi} \frac{dT_{s2}}{dt} = m_s \cdot \Delta H \frac{dq}{dt} + m_s \cdot \frac{dq}{dt} C_{pg} (T_{s1} - T_{s2}) \qquad \text{(Adsorber 2)} \qquad (4\text{-}3)$$

where ΔH is the heat of adsorption and $\sum m_i C_{pi}$ is the total heat capacity of the adsorbers which can be defined as

$$\sum m_i C_{pi} = m_s C_{ps} + m_m C_{pm} + m_s q C_{pa} = m_s (C_{pg} + r_{ms} C_{pm} + q C_{pa}) \qquad (4\text{-}4)$$

For the heat recovery process between Adsorbers 1 and 2, the heat balance equation for Adsorber 1 is defined by

$$\sum m_i C_{pi} \frac{dT_{s1}}{dt} = Q_{f-a,1} \quad \text{when disconnected from the evaporator} \qquad (4\text{-}5)$$

When Adsorber 1 is connected to the evaporator, the heat balance equation becomes

$$\sum m_i C_{pi} \frac{dT_{s1}}{dt} = Q_{f-a,1} + m_s \cdot \Delta H \frac{dq}{dt} + m_s \frac{dq}{dt} C_{pg} (T_e - T_{s1}) \qquad (4\text{-}6)$$

During this process, the heat balance equations for Adsorber 2 are given as

$$\sum m_i C_{pi} \frac{dT_{s2}}{dt} = Q_{f-a,2} \qquad \text{when disconnected from the condenser} \qquad (4\text{-}7)$$

$$\sum m_i C_{pi} \frac{dT_{s2}}{dt} = Q_{f-a,2} + m_s \cdot \Delta H \frac{dq}{dt} \qquad \text{when connected to the condenser} \qquad (4\text{-}8)$$

where $Q_{f-a,1}$ and $Q_{f-a,2}$ are the heat transfer rates from the heat exchange fluid to Adsorbers 1 and 2, respectively. These rates can be expressed as

$$Q_{f-a,1} = \dot{m}_f C_{pf} (T_{f1,in} - T_{s1})[1 - \exp(-NTU_1)] \qquad (4\text{-}9)$$

$$Q_{f-a,2} = \dot{m}_f C_{pf} (T_{f2,in} - T_{s2})[1 - \exp(-NTU_2)] \qquad (4\text{-}10)$$

where NTU_1 and NTU_2 are the number of heat transfer units of Adsorbers 1 and 2, respectively. $T_{f1,in}$ and $T_{f2,in}$ are the inlet temperatures of HXF for Adsorbers 1 and 2, respectively.

During the heat recovery process between Adsorbers 1 and 2, the HXF circulates between Adsorbers 1 and 2. Hence, the inlet temperature of HXF for one adsorber should be equal to the outlet temperature of the other adsorber. Thus $T_{f1,in}$ and $T_{f2,in}$ can be written as

$$T_{f1,in} = T_{f2,out} = T_{s2} + (T_{f2,in} - T_{s2}) \cdot \exp(-NTU_2) \tag{4-11}$$

$$T_{f2,in} = T_{f1,out} = T_{s1} + (T_{f1,in} - T_{s1}) \cdot \exp(-NTU_1) \tag{4-12}$$

If we neglect the sensible heat change of the HXF, we obtain

$$Q_{f-a,1} + Q_{f-a,2} = 0 \tag{4-13}$$

By solving Equations (4-9) – (4-13), we obtain

$$Q_{f-a,1} = -Q_{f-a,2} = \dot{m}_f C_{pf} (T_{s2} - T_{s1}) \cdot \frac{[1 - \exp(-NTU_1)] \cdot [1 - \exp(-NTU_2)]}{[1 - \exp(-NTU_1)\exp(-NTU_2)]} \tag{4-14}$$

Assuming that $NTU_1 = NTU_2$, Equation (4-14) can be rewritten as

$$Q_{f-a,1} = -Q_{f-a,2} = \dot{m}_f C_{pf} (T_{s2} - T_{s1}) \cdot \frac{[1 - \exp(-NTU_1)]^2}{[1 - \exp(-NTU_1)^2]} \tag{4-15}$$

When Adsorber 3 is disconnected from the evaporator during the first step, the heat balance equation for Adsorber 3 is given as

$$\sum m_i' C_{pi}{}' \frac{dT_{s3}}{dt} = Q_{f-a,3} \tag{4-16}$$

When Adsorber 3 is connected to the evaporator, the heat balance equations become

$$\sum m_i' C_{pi}{}' \frac{dT_{s3}}{dt} = Q_{f-a,3} + m_s' \cdot \Delta H' \frac{dq}{dt} + m_s' \frac{dq}{dt} C_{pg} (T_e - T_{s3}) \tag{4-17}$$

$$Q_{f-a,3} = \dot{m}_f C_{pf} (T_{c,in} - T_{s3})[1 - \exp(-NTU_3)] \tag{4-18}$$

Second Step:

During this step, heat is transferred between Adsorbers 1 and 3. The heat balance equation for Adsorber 1 is given as

$$\sum m_i C_{pi} \frac{dT_{s1}}{dt} = Q_{f-a,1} + m_s \cdot \Delta H \frac{dq}{dt} + m_s \frac{dq}{dt} C_{pg}(T_e - T_{s1}) \tag{4-19}$$

When Adsorber 3 is disconnected from the condenser, the heat balance equation becomes

$$\sum m_i' C_{pi}{}' \frac{dT_{s3}}{dt} = Q_{f-a,3} \tag{4-20}$$

When Adsorber 3 is connected to the condenser, Adsorber 2 will be disconnected from the condenser and connected to Adsorber 3. High temperature water vapour from Adsorber 2 will flow through Adsorber 3 to the condenser and release sensible heat to Adsorber 3 until its temperature is equal to the temperature at Adsorber 3. The heat balance equation is defined as

$$\sum m_i' C_{pi}{}' \frac{dT_{s3}}{dt} = Q_{f-a,3} + m_s' \Delta H' \frac{dq}{dt} + m_s \frac{dq}{dt}\Big|_{s2} \cdot C_{pg}(T_{s2} - T_{s3}) \text{ (Adsorber 3)} \tag{4-21}$$

where

$$Q_{f-a,1} = -Q_{f-a,3} = \dot{m}_f C_{pf}(T_{s3} - T_{s1}) \frac{[1-\exp(-NTU_1)] \cdot [1-\exp(-NTU_3)]}{[1-\exp(-NTU_1)\exp(-NTU_3)]} \tag{4-22}$$

Adsorber 2 in this step is heated by the external heat source. The heat balance equation is given by

$$\sum m_i C_{pi} \frac{dT_{s2}}{dt} = Q_{f-a,2} + m_s \Delta H \frac{dq}{dt} \tag{4-23}$$

where

$$Q_{f-a,2} = \dot{m}_f C_{pf}(T_{h,in} - T_{s2})[1-\exp(-NTU_2)] \tag{4-24}$$

The energy conservation equations for the other two steps are the same as the former two with Adsorbers 1 and 2 interchanged.

4.3.3 Mass conservation equations

In this analysis, the mass of water vapour is neglected. When the adsorber is disconnected from the condenser, evaporator and other adsorbers, the total mass of adsorber will not change. Thus

$$m_s \frac{dq}{dt} = 0 \tag{4-25}$$

When the adsorber is connected to the condenser or evaporator, we assume that the adsorber will maintain its condensing or evaporating pressure, respectively. Water vapour mass transfer limitation is neglected.

4.3.4 Performance equations

The system performance of an adsorption system can be characterised by its coefficient of performance (COP) and its specific cooling power (SCP), which are defined as

$$COP = \frac{Q_{ev}}{Q_h} \tag{4-26}$$

$$SCP = \frac{Q_{ev}}{t_{hc} \cdot m_t} \tag{4-27}$$

The heat Q_h supplied to Adsorber 2 during Step 2 can be calculated from

$$Q_h = \int_{t_{st1}}^{t_{hc}} \dot{m}_f C_{pf} (T_{f2,in} - T_{f2,out}) dt \tag{4-28}$$

The cooling energy produced in the evaporator can be calculated from

$$Q_{ev} = \int_0^{t_{hc}} \left[L(T_e) - C_{pl}(T_c - T_e) \right] \dot{m}_w dt \tag{4-29}$$

where $\dot{m}_w$ is the mass flow rate of the water vapour from the evaporator to the adsorber during the first half cycle.

$$\dot{m}_w = m_s \frac{dq}{dt}\Big|_{s1} + n \cdot m_s' \frac{dq}{dt}\Big|_{s3} \tag{4-30}$$

n is a flag number. If Adsorber 3 is connected to the evaporator, n = 1, otherwise n = 0.

4.4 RESULTS AND DISCUSSION

The governing equations are solved simultaneously using the finite difference method. Parameters and operating conditions for the base case in this model are shown in Table 4-1. In this analysis, the time taken for the mass recovery process is neglected being a very short duration compared to the total cycle time (Wang *et al*., 2002B).

Table 4-1 Parameter values and operating conditions for the base case

Name	Symbol	Value
Velocity of heat transfer fluid	u_f	1 m/s
Generation temperature of zeolite	T_g	473 K
Adsorption temperature of zeolite	T_a	373 K
Generation temperature of silica gel	T_g'	363 K
Adsorption temperature of silica gel	T_a'	303 K
Fluid inlet temperature during heating	$T_{h,in}$	483 K
Fluid inlet temperature during cooling	$T_{c,in}$	298 K
Evaporator temperature	T_e	279 K
Condenser temperature	T_c	303 K
Specific heat of adsorbent bed for zeolite	C_{ps}	836 J/kg·K
Heat of adsorption for zeolite/water pair	ΔH	3.2×10^6 J/kg
Specific heat of adsorbent bed for zeolite	C_{ps}'	924 J/kg·K
Heat of adsorption for zeolite/water pair	$\Delta H'$	2.8×10^6 J/kg
Specific heat of HXF	C_{pf}	2090 J/kg·K
Mass of zeolite	m_s	1.0 kg
Mass of silica	m_s'	1.0 kg
Number of heat transfer units for Adsorbers 1 and 2	NTU_1, NTU_2	0.004
Number of heat transfer units for Adsorber 3	NTU_3	0.004

4.4.1 Adsorption cycle for base case

The simulation results of the novel cascading cycle for the base case are shown in Figures 4.3-4.8. In these figures, only the situations for the first half cycle are presented since the process of the first half cycle is the same as that of the other half cycle with the two zeolite adsorbers interchanged. The coefficient of performance (COP) calculated by the model is 1.35 and the specific cooling power (SCP) is 42.7 W/kg. For similar operating conditions, Douss and Meunier (1989) reported values of 1.06 and 37.5 W/kg for the COP and SCP, respectively for their cascading cycle.

Figure 4.3 shows the numerical cascading cooling cycle for the base case. It can be seen that the numerical cascading cooling cycle is the same as the ideal cycle (Figure 4.2). Since mass transfer limitation is not included in the present model, the pressure is kept constant in the numerical cycle when the adsorber connected to an evaporator and the numerical results will differ from the experimental results of Douss and Meunier (1989).

The temperature variations with time for the three adsorbers are shown in Figure 4.4. It can be seen that the temperature drop during the heat recovery process between the two zeolite adsorbers is lower than that during the heat recovery process between the zeolite adsorber and the silica gel adsorber. This is due to the smaller temperature difference between the two zeolite adsorbers when compared to the difference between the zeolite adsorber and the silica gel adsorber. The heat rate for the heat recovery in Step 1 is lower than the heat rate for heat recovery in Step 2 (see Figure 4.7). It can also be seen from Figure 4.4 that the time taken for heating of Adsorber 2 is shorter than that for cooling of Adsorber 1 and heating of Adsorber 3 because of the higher heat transfer rate of Adsorber 2 (see Figure 4.7).

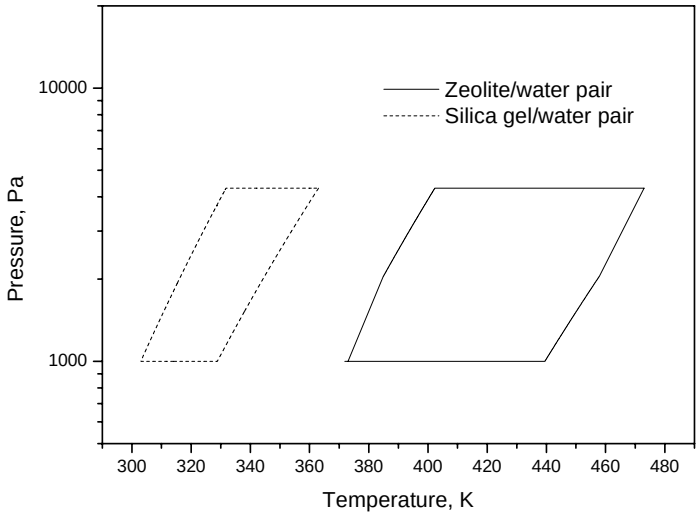

Figure 4.3 Numerical cascading adsorption cycles

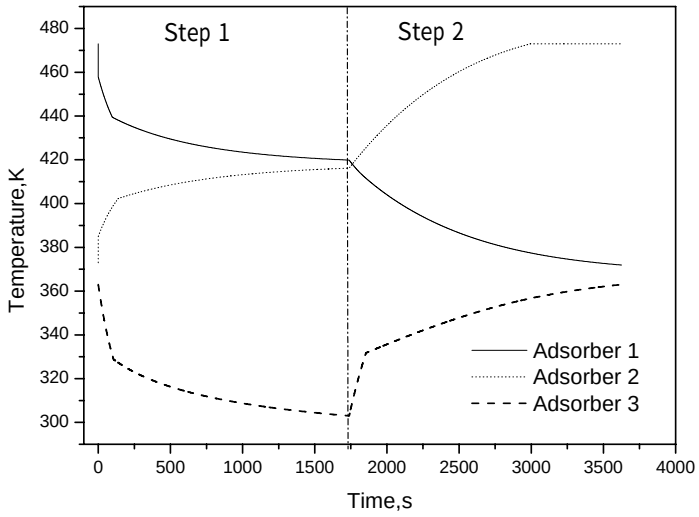

Figure 4.4 Variation of adsorbent temperature with time for three adsorbers

Figures 4.5 and 4.6 show the adsorbed amount variation with time for the zeolite and silica gel adsorbers, respectively. From Figure 4.5, it can be clearly seen that the quantity of cycled water vapour increases by using mass recovery at the beginning of Step 1. The second heat recovery process is more efficient than the first cycle. The adsorbed amount profile of

Adsorber 3 is similar to that of the intermittent cycle proposed by Marletta *et al.* (2002) since the profile of heat transfer rate for Adsorber 3 in two different steps are similar in the reverse direction (see Figure 4.7).

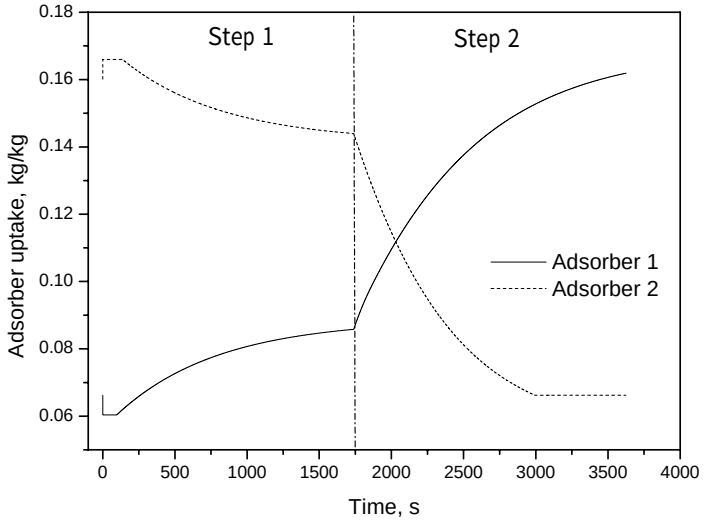

Figure 4.5 Variation of adsorbed amount in Adsorbers 1 and 2

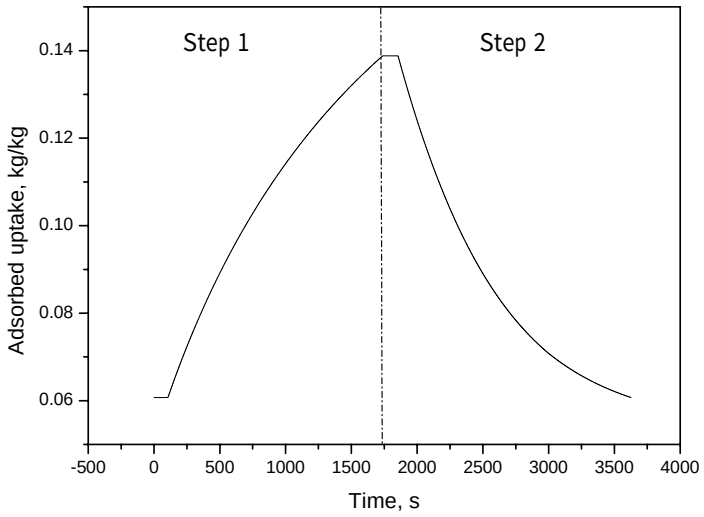

Figure 4.6 Variation of adsorbed amount in Adsorber 3

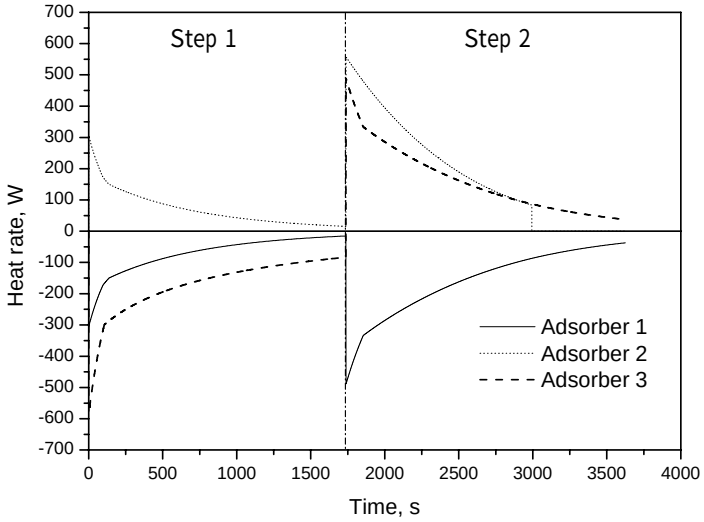

Figure 4.7 Variation of heat transfer rates of adsorbers

The variation of heat transfer rates of the evaporator and condenser is presented in Figure 4.8. The heat rate is the sum of the heat rates for all three adsorbers. It can be seen that the cooling energy produced is more stable compared with that of the intermittent cycle (Marletta *et al*., 2002).

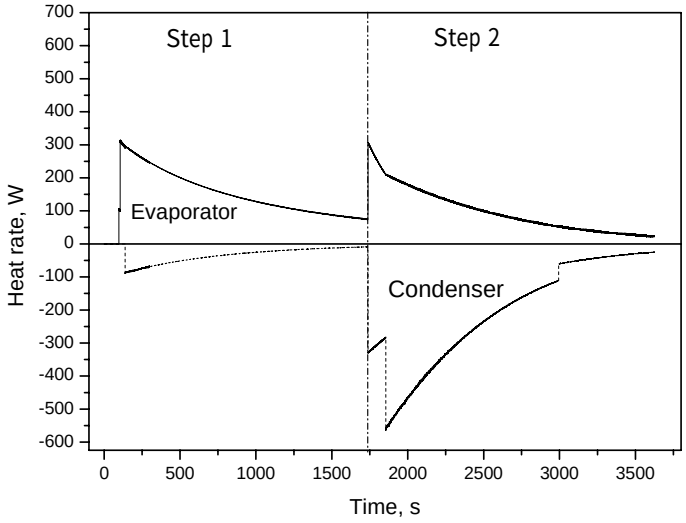

Figure 4.8 Variation of heat transfer rates of the evaporator and the condenser

4.4.2 The middle temperature

The middle temperature (T_m) in this analysis is defined as the average value of maximum generation temperature of the silica gel adsorber (T_g') and the initial adsorption temperature (T_a). The temperature gap of T_g' and T_a is assumed as 10 K. The effect of the middle temperature on performance is shown in Figure 4.9. From this figure, it can be seen that there is a maximum value of COP within the range of T_m investigated. However, when the COP reaches its highest value, the SCP becomes a minimum. If the middle temperature is lower than a certain value, the silica gel/water cycle (Adsorber 3) completes Step 2 in a shorter time than Adsorber 1. Subsequently, the second heat recovery process stops and Adsorber 1 is cooled by the external fluid. Therefore, the energy from the Adsorber 1 is not fully recovered, which leads to a reduction in COP. When the middle temperature is higher than this certain value, Adsorber 3 will take a longer time in Step 2 than Adsorber 1. The second heat recovery process also ceases before the end of Step 2. Adsorber 3 needs the external heating fluid to heat it to maximum temperature. Thus the recovered heat also reduces which will result in a decrease in COP. In the above two cases, either Adsorber 1 or Adsorber 2 is connected to the external heating or cooling fluid during Step 2 resulting in a reduction in the cycle time. Its SCP will therefore increase.

4.4.3 Driven temperature

The driven temperature is defined as the temperature of the external heating fluid. In this analysis, a constant temperature difference of 10 K is maintained between the generation temperature and the driven temperature. The variations of performance with driven temperature, T_m at maximum COP are shown in Figure 4.10. It can be seen that both the COP and SCP increases with an increase in the driven temperature. However, when the driven temperature increases beyond 503 K, the change in COP is very small.

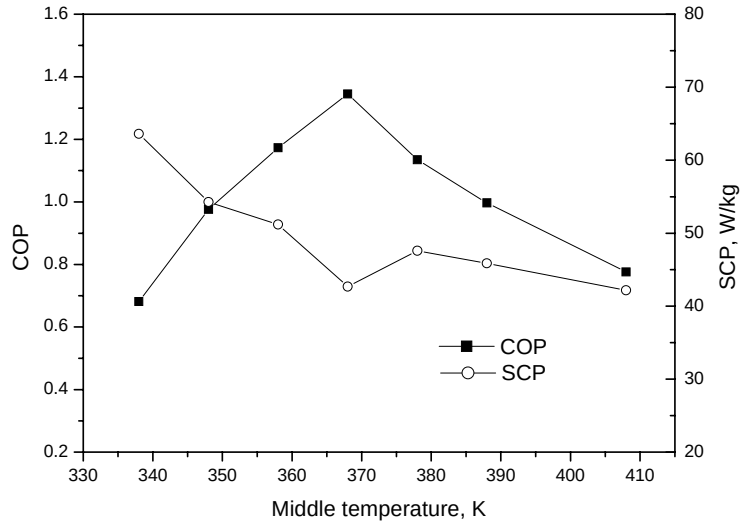

Figure 4.9 Variation of performance with the middle temperature

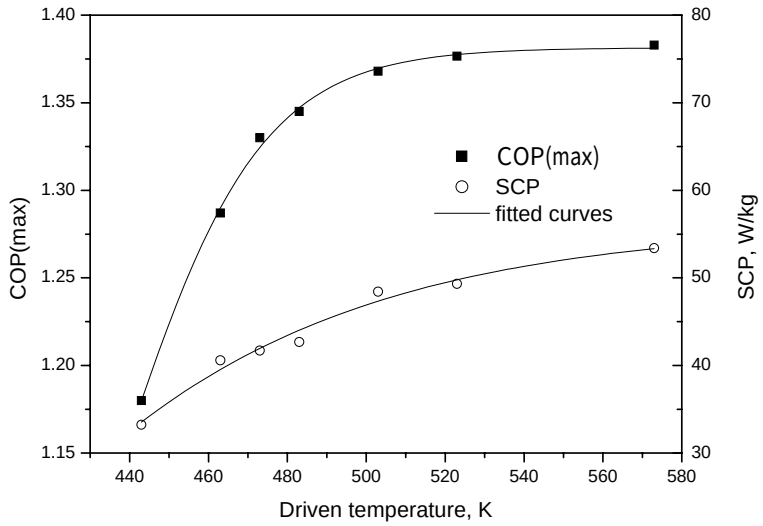

Figure 4.10 Variation of performance with driven temperature

4.4.4 Performance compared with other cycles

Figures 4.11 and 4.12 show the variation of COP and SCP for various cycles *viz.* the cascading cycle, heat and mass recovery cycle and the intermittent cycle. It is noted that both

the heat and mass recovery cycle and intermittent cycle employs zeolite/water as the working pair. From Figure 4.11, under the same base driven temperature and heat sink temperature it can be seen that the value of COP (about 1.3) for this cascading cycle is more than two times that of the intermittent cycle (about 0.5). Furthermore, the COP for the cascading cycle is also much higher than that of the heat and mass recovery cycle (about 0.8). However, its SCP is about 40 W/kg, which is much smaller than that of the other cycles (see Figure 4.12). Based on the analysis of Stitou *et al*. (2000), the overall COP of a cascading cycle is defined as:

$$COP = COP_1 + \left(\frac{Q_i}{Q_h}\right) COP_2 \tag{4-31}$$

where Q_i is the heat obtained from the high temperature stage to the low temperature stage and COP_1 and COP_2 are the coefficient of performance for the two stages. Note that Q_i is the heat input from the zeolite adsorber to the silica gel adsorber, COP_1 is the coefficient of performance of the heat and mass recovery zeolite/water system and COP_2 is the coefficient of performance of the intermittent silica gel/water system. The calculated values of COP_1 and COP_2 are about 0.8 and 0.5, respectively. It can be seen from Figure 4.7 that the value of Q_i is almost equal to that of Q_h. Thus, the overall COP calculated by Equation (4-31) is of the same order of magnitude as the numerical COP value. The Carnot COP for base operating conditions obtained by the approach of Meunier *et al*. (1997) is 2.539. The second law efficiency of this cascading cycle is 0.532. The COP value is of the same order of magnitude as that of the triple-effect cascading cycle but is lower than that of the quadruple-effect cascading cycle studied by Stitou *et al*. (2000). However, the second law efficiency of the proposed system in this study is slightly higher than those of the triple-effect and quadruple-effect cascading cycles.

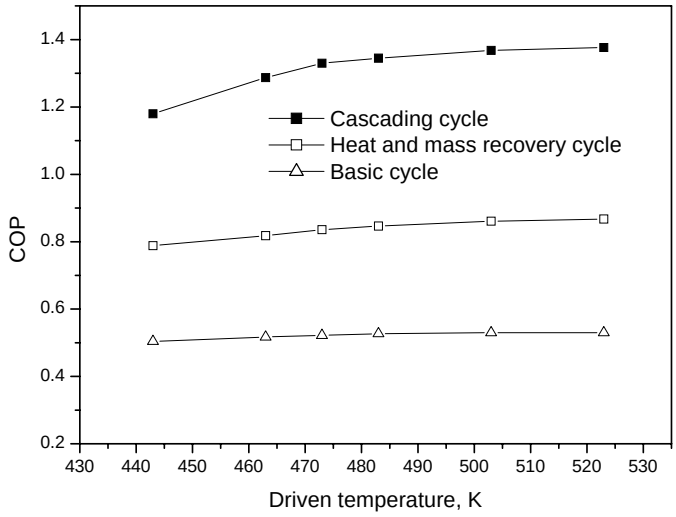

Figure 4.11 Variation of COP for different cycle types

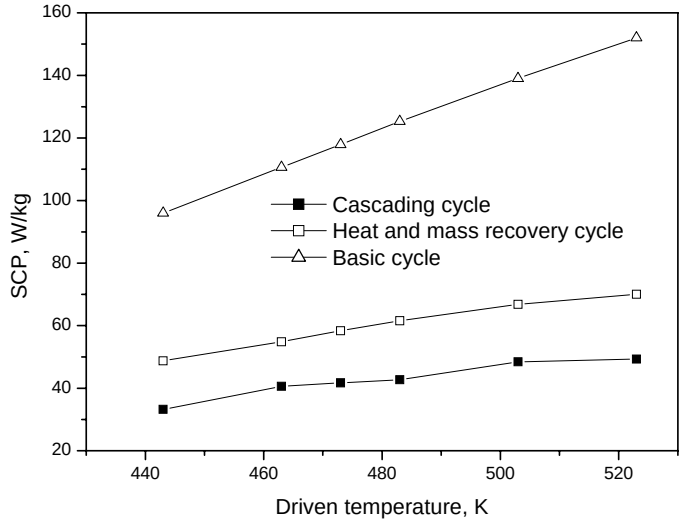

Figure 4.12 Variation of SCP for different cycle types

5. SUMMARY

A novel cascading adsorption cooling cycle is proposed in this chapter. This cycle consists of two zeolite adsorbent beds and a silica gel adsorbent bed. The zeolite adsorbent

bed is at the high temperature stage while the silica gel adsorbent bed is at the low temperature stage. Since only one refrigerant is employed, its configuration is simpler than the cascading cycle proposed by Douss and Meunier (1989). A lumped model is proposed to investigate the thermal properties and performances for this cycle. The following conclusions can be drawn:

1. The first and second heat recovery processes are very effective thus resulting in a higher COP.
2. There is a maximum value of COP within the range of T_m investigated for a prescribed driven temperature. However, when the COP reaches its highest value, the value of the SCP is at its lowest.
3. Both the COP and SCP increases with an increase in the driven temperature. However, when the driven temperature increases beyond 503 K, the change in COP is very small.
4. The COP value of 1.3 for this cascading cycle is more than twice of an intermittent cycle (about 0.5). It is also much higher than that of the heat and mass recovery cycle (about 0.8). However, the SCP of about 40 W/kg is much lower than those of the other two cycles.

CHAPTER 5

HEAT AND MASS TRANSFER MODELLING OF AN INTERMITTENT CYCLE

5.1 INTRODUCTION

The environment-friendly adsorption refrigeration system presents an attractive alternative to the conventional vapour-compression refrigeration system. However, the widespread application of adsorption systems is limited by its rather low coefficient of performance. The performance of these systems is largely determined by the heat transfer process in the adsorbent bed. In recent years, many investigators have studied the enhancement of adsorbent bed thermal conductivity to improve thermal performance of such systems (Groll, 1993; Pons *et al*., 1996; Liu *et al*., 1998; Restuccia *et al*., 2002). In addition, mass transfer limitations are also important in influencing the performance of these systems although its effect has been neglected by many researchers (Guilleminot and Meunier, 1987; Passos and Escobedo, 1989; Hajji and Worek, 1991). Since high mass transfer properties contribute to poor thermal transfer properties, it is important to optimise the heat transfer properties of adsorption systems. It is only recently that some numerical studies with combined heat and mass transfer have been presented (Ben Amar *et al*., 1996; Zhang, 2000; Marletta *et al*., 2002). In these studies, the Darcy law (Ben Amar *et al*., 1996; Zhang, 2000) and the extended Darcy-Ergun equation (Marletta *et al*., 2002) were adopted as the momentum equation for adsorbate gas flow in the adsorbent. However, the Darcy law is applicable only for incompressible fluid and its use in the above models is subject to question. For compressible adsorbate vapour, the diffusion and adsorption effects should also be considered in the momentum equation.

In most of the previous studies, the equilibrium adsorption model has been assumed and the internal mass transfer resistance between solid and adsorbate gas phases is neglected. In

actual systems, the solid and adsorbate would not reach equilibrium instantly. Hence, the internal mass transfer resistance can only be neglected for systems with long cycle times. Chahbani *et al.* (2002) studied the effect of internal mass transfer on the performance of adsorption cycles and concluded that the performance can be significantly reduced because of internal mass transfer. They pointed out that the linear force driven model (LDF) could be used to describe internal mass transfer limitations with minor error.

Most past studies have not clearly addressed the equivalent thermal conductivity of porous adsorbent bed in terms of the effect of the presence of the adsorbate gas within the adsorbent. Onyebueke and Feidt (1991) studied the equivalent thermal conductivity of activated carbon in the presence of alcohol vapour. However, no theoretical study was mentioned in their publication. Since the heat and mass transfer properties are greatly affected by the configuration of the adsorbent bed, the equivalent thermal conductivity should be defined as a function of the configuration parameters.

Operating conditions also have a significant effect on the performance of adsorption cooling cycle. However, the effects of operating conditions on the thermal performance of such systems especially those pertaining to operating temperature effects are scarcely reported in the literature. The effect of operating conditions on the adsorption cooling cycle based on thermodynamic analyses has been investigated by a number of researchers (Turner, 1992; Luo, and Feidt, 1992; Cacciola and Restuccia, 1995). These studies, however, did not account for the transient heat and mass transfer processes present in the adsorbent bed. Their results were therefore not presented in terms of the specific cooling power (SCP). Saha *et al.* (1995) proposed a lumped model and investigated the effects of operating conditions on the thermal performance of a silica gel/water adsorption cycle. However, they excluded the effect of the adsorption temperature. Recently, Critoph and Metcalf (2004) presented a one-dimensional transient model to study the effect of operating conditions on a carbon-ammonia

system. The initial adsorption temperature effect was not considered in their investigation and micro-mass transfer limitations were neglected.

In this chapter, a two-dimensional non-equilibrium numerical model describing the combined heat and mass transfer in adsorbent bed is presented to evaluate the effect of adsorbent bed configuration and operating conditions on the performance. The results of the numerical model can be used to optimise the configuration of the bed and the operating conditions.

5.2 NUMERICAL MODEL

A schematic of the adsorbent bed is shown in Figure 5.1. The adsorbent bed is a hollow cylinder, which encloses a metal tube for the purpose of heat exchange between the solid adsorbent, and heating or cooling fluid within the tube. The adsorbate gas transfers heat to or from the adsorbent bed.

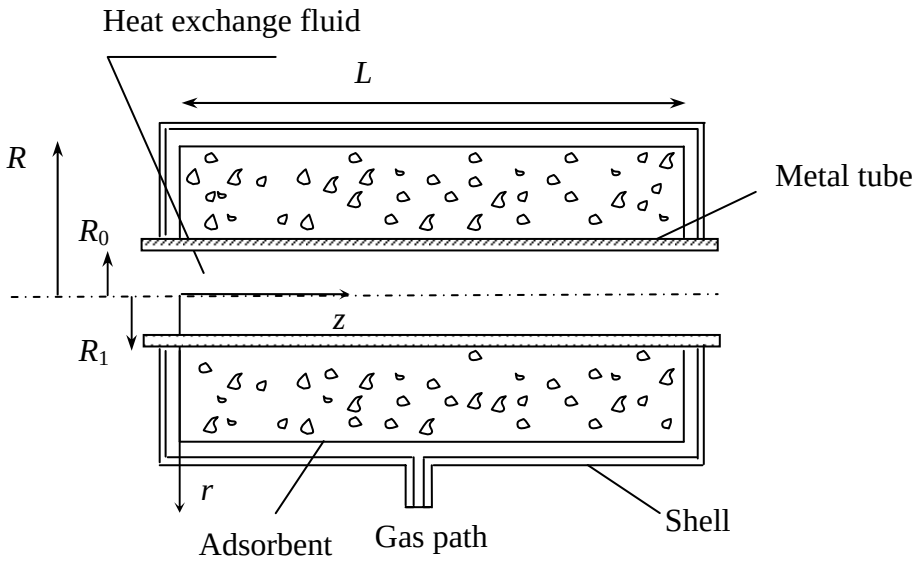

Figure 5.1 Schematic diagram of adsorber

The following assumptions are considered:

(1) The adsorbed phase is considered as a liquid, and the adsorbate gas is assumed to be an ideal gas.

(2) The adsorbent bed is composed of uniform-size particles and has isotropic properties.

(3) Except for the density of adsorbate vapour, the properties of the fluid, metal tube, adsorbent and adsorbate vapour are constant.

(4) There are no heat losses in the adsorption cycle.

(5) The thermal resistance between the metal tube and the adsorbent bed is neglected.

5.2.1 Sub-models of the system

5.2.1.1 Gas flow in adsorbent bed model

The flow between the adsorbent particles in the adsorbent bed includes Poiseuille flow, Knudsen flow and surface flow. Assuming that the adsorbate is an ideal gas and has low velocity, we obtain

$$\dot{m} = \dot{m}_p + \dot{m}_k + \dot{m}_s \tag{5-1}$$

where $\dot{m}_p$, $\dot{m}_K$ and $\dot{m}_s$ are the mass flow fluxes resulting from Poiseuille flow, Knudsen flow and surface flow, respectively. The Poiseuille flow mass flux in porous media can be described as:

$$\dot{m}_p = -\frac{K}{\mu}\frac{PM}{RT}\nabla P \tag{5-2}$$

K is permeability of the porous media which can be obtained from the semi-empirical Blake-Kozeny equation (Bird *et al*., 1960) as

$$K = \frac{\varepsilon_a{}^3 \times d^2}{150 \times (1-\varepsilon_a)^2} \tag{5-3}$$

Knudsen flow is dominated by molecular collisions, which include both the collisions between the gas molecules and the collisions between the gas molecules with surfaces. For a single component gas, the mass flux of Knudsen flow is defined as

$$\dot{m}_k = -\frac{\varepsilon_a}{\tau} D_{ek} \nabla \rho = \frac{\varepsilon_a}{\tau} D_{ek} \frac{M}{RT} \nabla P \tag{5-4}$$

The equivalent Knudsen diffusivity, D_{ek} , can be represented by the following equation (Ruthven, 1984):

$$D_{ek} = 1/(1/D_m + 1/D_k) \tag{5-5}$$

where

$$D_m = 0.2628\times10^{-6}\frac{\sqrt{T^3/M}}{P\sigma^2\Omega} \tag{5-6}$$

and $$D_k = \frac{2r_{po}}{3}\left(\frac{8RT}{\pi M}\right)^{1/2} = 0.97 r_{po}\left(\frac{T}{M}\right)^{1/2} \tag{5-7}$$

By using the Hydraulic Radius Model (Carman, 1937), the hydraulic radius of the porous media is defined as

$$r_{po} = \frac{4\varepsilon_a}{A_0(1-\varepsilon_a)} = \frac{2\varepsilon_a d}{3(1-\varepsilon_a)} \tag{5-8}$$

Thus $$D_k = 0.647\frac{\varepsilon_a d}{(1-\varepsilon_a)}\left(\frac{T}{M}\right)^{1/2} \tag{5-9}$$

Surface flow is dominated by the adsorbed substance gradient. The surface flow mass flux is defined as

$$\dot{\boldsymbol{m}}_s = \frac{(1-\varepsilon_a)}{\tau} D_s \nabla \rho_{ad} \tag{5-10}$$

For adsorbate vapour flow in porous adsorbent bed, the concentration of absorbed substance is very low on the macro-pore surface. Hence, the surface flow can be neglected in the macro-pores between adsorbent particles. Equation (5-10) can be rewritten as

$$\dot{\boldsymbol{m}} = \rho_g \mathbf{u} = -\left[\frac{K}{\mu}\frac{PM}{RT} + \frac{\varepsilon_a}{\tau} D_{ek}\frac{M}{RT}\right]\nabla P \tag{5-11}$$

If we introduce an apparent permeability defined as

$$K_{ap} = K + \frac{\varepsilon_a \mu}{\tau P} D_{ek} \tag{5-12}$$

then the gas velocity vector **u** is given by

$$\mathbf{u} = -\frac{K_{ap}}{\mu}\nabla P \tag{5-13}$$

5.2.1.2 Equivalent thermal conductivity and contact resistance

The thermal conductivity values used in many numerical models were obtained from experiments. Hence, these models cannot be used to predict system performance without experimental inputs. In addition, it is not possible to optimise the adsorbent configurations. The simplest model describing the equivalent thermal conductivity is given by

$$\lambda_{eq} = \lambda_g \varepsilon + \lambda_S (1-\varepsilon) \tag{5-14}$$

This simple model is not suitable for the particle bed under certain circumstances because the tortuousity effect is presumably neglected. Hsu *et al*. (1995) proposed a lumped parameter model based on the assumption of arrays of touched square cylinders (see Figure 5.2), which showed excellent agreement with the experimental data. Their model is defined as

$$\lambda_{eq}/\lambda_g = \frac{r_a r_c}{\Lambda} + \frac{r_a(1-r_c)}{1+(\Lambda-1)r_c} + \frac{(1-r_a)}{1+(\Lambda-1)r_a r_c} \tag{5-15}$$

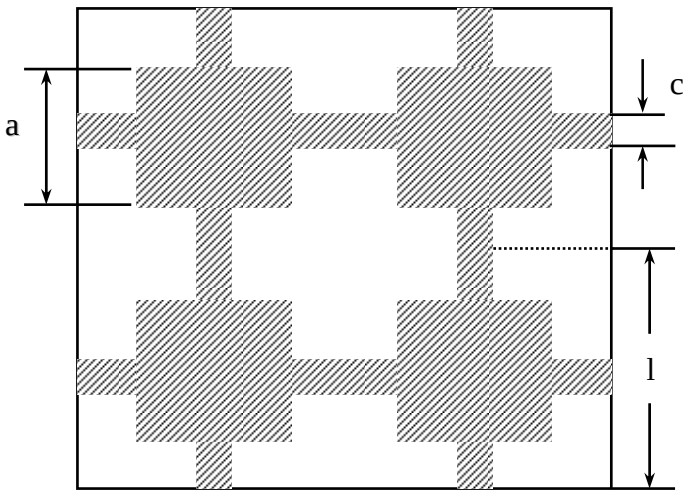

Figure 5.2 Arrays of touched square cylinders

where $\Lambda = \lambda_g / \lambda_s$; $r_a = a/l$; and $r_c = c/a$.

It is shown that results computed based on Equation (5-15) for r_c = 0.01 are in excellent agreement with the experimental data. Hence using $r_a \approx (1-\varepsilon)^{1/2}$, Equation (5-15) becomes

$$\lambda_{eq}/\lambda_g = \frac{0.01(1-\varepsilon)^{1/2}}{\Lambda} + \frac{0.99(1-\varepsilon)^{1/2}}{1+(\Lambda-1)(1-\varepsilon)^{1/2}} + \frac{1-(1-\varepsilon)^{1/2}}{1+0.01(\Lambda-1)(1-\varepsilon)^{1/2}} \qquad (5\text{-}16)$$

The thermal contact resistance was taken into account in most studies by previous investigators because of the higher porosity of adsorbent near the wall compared to other parts of the adsorbent bed. Coulibaly *et al*. (1998) reported that the thermal contact resistances of a loose granular adsorbent had an important effect on the heat transfer rate between the adsorber and external heat source. However, Zhu and Wang (2002) showed that the thermal contact resistance of the zeolite adsorbent bed as a block shape is very low (in the magnitude of 10^{-4} m^2·K/W). Tamaninot-Telto and Critoph (2001) reported a high contact heat transfer coefficient of carbon as 800 W/m^2·K for small particle size. The thermal contact resistance is therefore neglected in this study, since a compressed zeolite adsorbent bed with small particle size similar to the block-shaped adsorbent bed of Zhu and Wang (2002) is assumed.

5.2.1.3 LDF model and adsorption equilibrium

The adsorption rate is controlled by the adsorbate gas diffusion in the adsorbent particle. The linear driving force equation (LDF) is used to account for mass transfer resistance within the adsorbent particles as proposed by Sakoda and Suzuki (1984). In this model, the concentration profile within the particle is parabolic. The terms of the model are given by

$$\frac{\partial \bar{q}}{\partial t} = \frac{15 D_e}{r_p^2}(q_{eq} - \bar{q}) \qquad (5\text{-}17)$$

where $\bar{q}$ is the mean adsorbed concentration within the particle and q_{eq} is the adsorbed phase concentration in equilibrium with bulk fluid which is defined in Chapter 3. D_e is the equivalent diffusivity in the adsorbent particles which can be calculated by

$$D_e = D_0 \exp(-E_D / RT) \tag{5-18}$$

where D_0 and E_D can be obtained from experimental data available in the literature (Wang *et al.*, 2001).

5.2.2 Governing equations

The model describes the process which is related to heat transfer between different components of the whole cooling system, and mass transfer of adsorbate vapour in adsorbent bed. Thus, the model can be developed as follows:

An energy balance on the thermal-fluid system yields

$$\frac{\partial(\rho_f C_{pf} T_f)}{\partial t} + u_f \frac{\partial(\rho_f C_{pf} T_f)}{\partial z} = \frac{\partial}{\partial z}(\lambda_f \frac{\partial T_f}{\partial z}) + \frac{1}{r}\frac{\partial}{\partial r}(r\lambda_f \frac{\partial T_f}{\partial r}) \tag{5-19}$$

Energy balance for the metal tube:

$$\frac{\partial(\rho_m C_{pm} T_m)}{\partial t} = \frac{\partial}{\partial z}(\lambda_m \frac{\partial T_m}{\partial z}) + \frac{1}{r}\frac{\partial}{\partial r}(r\lambda_m \frac{\partial T_m}{\partial r}) \tag{5-20}$$

Energy balance for the adsorbent:

$$\begin{aligned}&(\rho_s C_{p_s} + \rho_s q C_{pa} + \varepsilon\rho_g C_{pg})\frac{\partial T_s}{\partial t} + \frac{\partial(\rho_g C_{pg} u T_s)}{\partial z} + \frac{1}{r}\frac{\partial}{\partial r}(r\rho_g C_{pg} v T_s)\\ &= \frac{\partial}{\partial z}(\lambda_{eq}\frac{\partial T_s}{\partial z}) + \frac{1}{r}\frac{\partial}{\partial r}(r\lambda_{eq}\frac{\partial T_s}{\partial r}) + \rho_s \Delta H \frac{\partial \bar{q}}{\partial t}\end{aligned} \tag{5-21}$$

Mass balance for the adsorbent:

$$\frac{\partial \varepsilon \rho_g}{\partial t} + \nabla \cdot (\rho_g \mathbf{u}) + \rho_s \frac{\partial \bar{q}}{\partial t} = 0 \tag{5-22}$$

Substituting Equation (5-13) into Equation (5-22), we obtain

$$\frac{\partial(\frac{\varepsilon M}{RT}P)}{\partial t} = \frac{\partial}{\partial z}(\frac{\rho_g K_{ap}}{\mu}\frac{\partial P}{\partial z}) + \frac{1}{r}\frac{\partial}{\partial r}(\frac{r\rho_g K_{ap}}{\mu}\frac{\partial P}{\partial r}) - \rho_s \frac{\partial \bar{q}}{\partial t} \tag{5-23}$$

The initial and boundary conditions are listed below to complete the numerical formulation of the problem.

Initial conditions:

$$t = 0 \quad T_f(z,r) = T_m(z,r) = T_s(z,r) = T_0 \quad ; P = P_0 \tag{5-24}$$

Boundary conditions for the heat exchange fluid are given as:

$$T_f\big|_{z=0} = T_{h,in} \qquad \text{during heating process} \tag{5-25}$$

$$T_f\big|_{z=0} = T_{c,in} \quad \text{during cooling process} \tag{5-26}$$

$$\frac{\partial T_f}{\partial z}\Big|_{z=L} = 0 \tag{5-27}$$

Equation (5-25) states that during the heating process (isosteric heating and isobaric generation phases), the inlet temperature of the fluid is constant. Equation (5-26) gives the same situation during the cooling process (isosteric cooling and isobaric adsorption phases). Equation (5-27) shows that the adiabatic condition is set for the outlet fluid because there is no heat exchange at $z = L$ in the z direction.

For this system, the shell of the adsorbent bed is covered with insulation. The following boundary conditions for the metal tube and adsorbent bed describe the adiabatic conditions:

$$\frac{\partial T_m}{\partial z}\Big|_{z=0} = \frac{\partial T_m}{\partial z}\Big|_{z=L} = 0 \tag{5-28}$$

$$\frac{\partial T_s}{\partial z}\Big|_{z=0} = \frac{\partial T_s}{\partial z}\Big|_{z=L} = \frac{\partial T_s}{\partial r}\Big|_{r=R} = 0 \tag{5-29}$$

The boundary conditions of pressure for water vapour in the adsorbent bed are

$$\frac{\partial P}{\partial z}\Big|_{z=0} = \frac{\partial P}{\partial z}\Big|_{z=L} = \frac{\partial P}{\partial r}\Big|_{r=R} = 0 \tag{5-30}$$

$$P\big|_{z=0} = P\big|_{z=L} = P\big|_{r=R} = P_e \qquad \text{when connected to evaporator} \qquad (5\text{-}31)$$

$$P\big|_{z=0} = P\big|_{z=L} = P\big|_{r=R} = P_c \qquad \text{when connected to condenser} \qquad (5\text{-}32)$$

When the adsorbent bed is not connected to evaporator or condenser, no vapour can flow in or out, and hence, the velocity of water vapour at the boundary equals zero. From Equation (5-13), the gradient of pressure in boundary is also zero. During the isobaric generation phase, the adsorbent bed is connected to the condenser, and it is assumed that the pressure can reach the equilibrium state quickly. Hence, the pressure at the boundary is equal to the pressure in the condenser. It is the same as that for the isobaric adsorption phase.

5.2.3 Performance of cooling cycle

The heat supplied to the adsorbent bed during the two heating phases, Q_h, can be calculated by

$$Q_h = \int_0^{t_{hc}} \rho_f C_{pf} u_f S_f (T_{h,in} - T_{h,out}) dt \qquad (5\text{-}33)$$

where t_{hc} is the time of the first half cycle.

The cooling energy produced in the evaporator can be calculated as

$$Q_{ev} = \int_{t_{hc}}^{t_c} \left[L(T_e) - C_{pl}(T_c - T_e) \right] \dot{m}_w dt \qquad (5\text{-}34)$$

where $\dot{m}_w$ is the mass flow rate of the water vapour from evaporator to the adsorbent bed. which is

$$\dot{m}_w = \iint_S \rho_g \mathbf{u} \cdot \mathbf{n} dS \qquad (5\text{-}35)$$

where S is the area of adsorbent bed surface, and $\mathbf{n}$ is the normal vector of the surface area.

The cooling coefficient of performance (COP) and the specific cooling power can be calculated by Equations (1-1) and (1-2) defined in Chapter 1, respectively. The total mean cooling power (TCP) can be calculated by

$$TCP = \frac{Q_{ev}}{t_c} \tag{5-36}$$

5.3 NUMERICAL METHOD

The governing equations are solved in primitive variables. In the discretisation of the physical domain, a two-dimensional, non-uniform and staggered grid is used with a control volume formulation and the power law scheme for the difference of dependent variables in the discrete formulation. The finite volume technique has been described in detail by Patankar (1980). This algorithm provides a remarkably successful implicit method for simulating heat transfer in fluid flow. The finite difference mesh consists of many cylindrical control volumes using a staggered grid system. Different control volumes are used for *x*- and *r*-directions. All scalar quantities (such as pressure and temperature) are defined at the intersection of any two-grid lines. The discrete equations are solved by the line-by-line procedure, which is the combination of the Tri-Diagonal Matrix Algorithm (TDMA) and the Gauss-Seidel iteration technique.

5.3.1 Finite Volume Method

In the finite volume method, the conservation principles are applied to a fixed region in space known as a control volume (CV). This method is also referred to as the control volume method. The domain is divided into a number of control volumes such that there is one control volume surrounding each grid point. The grid point is located at the centre of the CV. The integral form of the governing equation is integrated over each control volume [see Equation (5-43)] to derive an algebraic equation containing the grid point values of ϕ. The discretisation equation then expresses the conservation principle for a finite control volume just as the partial differential equation expresses it for an infinitesimal control volume. The

resulting solution implies that the integral conservation of quantities such as mass, momentum and energy is exactly satisfied for any group of control volumes and of course for the whole domain.

A typical two-dimensional cylindrical control volume is shown in Figure 5.3. The CV interface is subdivided into four plane faces, denoted by lower case letters corresponding to their direction (e, w, n, and s) with respect to the central node P. The nodes are denoted by upper case letters E, W, N, S. The discretisation of the governing equations using the finite volume method is described in the next section.

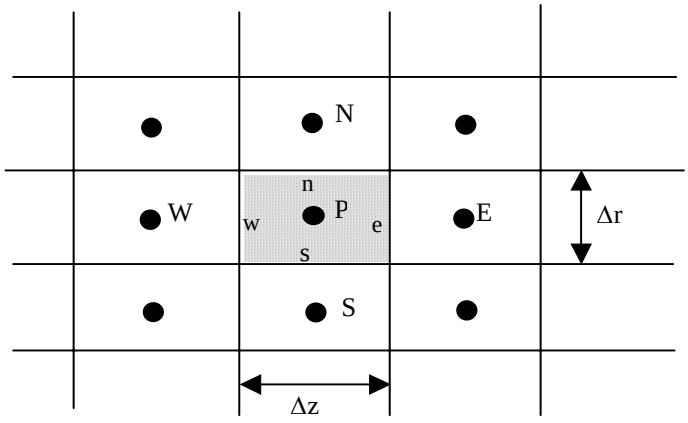

Figure 5.3 A typical CV and notation used for 2D cylindrical grid

5.3.2 Discretised equations

The computed domain is divided into three zones, which are the fluid zone, metal zone and adsorbent bed zone. The two-dimensional unsteady form of the governing equations in cylindrical coordinates can be written as

$$\underbrace{\frac{\partial}{\partial t}(\rho'\phi)}_{\text{Unsteady term}}+\underbrace{\frac{\partial}{\partial z}(\rho u\phi)+\frac{1}{r}\frac{\partial}{\partial r}(r\rho v\phi)}_{\text{convection term}}=\underbrace{\frac{\partial}{\partial z}(\Gamma\frac{\partial\phi}{\partial z})+\frac{1}{r}\frac{\partial}{\partial r}(r\Gamma\frac{\partial\phi}{\partial z})}_{\text{diffusion term}}+\underbrace{S_\phi}_{\text{source term}} \qquad (5\text{-}37)$$

The governing equations include the energy and continuity equation. For the energy equation, ϕ represents temperature and for the continuity equation, ϕ represents pressure. ρ' and ρ are the density of the unsteady and convection terms, respectively and Γ is the diffusivity of the diffusion term.

The energy equations are

$$\rho' = \rho = \rho_f C_{pf};\ \ \Gamma = \lambda_f;\ \ S = 0 \qquad \text{(Fluid zone)} \qquad (5\text{-}38)$$

$$\rho' = \rho = \rho_m C_{pm};\ \ \Gamma = \lambda_m;\ \ S = 0 \qquad \text{(Metal zone)} \qquad (5\text{-}39)$$

$$\begin{aligned} &\rho' = \rho_s C_{ps} + \rho_s q C_{pa} + \varepsilon \rho_g C_{pg} \\ &\rho = \rho_g C_{pg} \\ &\Gamma = \lambda_{eq} \qquad \text{(Adsorbent bed zone)} \\ &S = \rho_s \Delta H \frac{\partial \overline{q}}{\partial t} \end{aligned} \qquad (5\text{-}40)$$

The continuity equation is given by

$$\rho' = \varepsilon \rho_g;\ \ \rho = 0;\ \ \Gamma = \rho_g \frac{K_{ap}}{\mu};\ \ S = -\rho_s \frac{\partial \overline{q}}{\partial t} \qquad (5\text{-}41)$$

Let J_z and J_r be the total (convection and diffusion) fluxes defined by

$$J_z = \rho u \phi - \Gamma \frac{\partial \phi}{\partial z} \qquad (5\text{-}42a)$$

$$J_r = \rho v \phi - \Gamma \frac{\partial \phi}{\partial r} \qquad (5\text{-}42b)$$

Integration of Equation (5-37) over the control volume gives

$$\frac{(\rho'_p \phi_p - \rho'^0_p \phi^0_p)\Delta V}{\Delta t} + J_e A_e - J_w A_w + J_n A_n - J_s A_s = \overline{S}_\phi \Delta V \qquad (5\text{-}43)$$

where superscript 0 denotes the known value of $\rho'\phi$ at the beginning of the time step Δt, the *J's* are the integrated total fluxes over the control-volume faces, $\overline{S}$ is the average source term over the control volume, ΔV is the volume of the control volume, and the *A*'s are the areas of the control volume faces.

By using the expression of the total fluxes (*J's*) (Tao, 2001), an unsteady two-dimensional discretisation equation based on Equation (5-43) can now be written as

$$a_P\phi_P = a_E\phi_E + a_W\phi_W + a_N\phi_N + a_S\phi_S + b \tag{5-44}$$

where

$$a_E = D_e A(|P_e|) + [|-F_e, 0|] \tag{5-45a}$$

$$a_W = D_w A(|P_w|) + [|F_w, 0|] \tag{5-45b}$$

$$a_N = D_n A(|P_n|) + [|-F_n, 0|] \tag{5-45c}$$

$$a_S = D_s A(|P_s|) + [|F_s, 0|] \tag{5-45d}$$

$$b = \bar{S}_\phi r\Delta z\Delta r + \frac{\rho'^0_p \phi^0_p r\Delta z\Delta r}{\Delta t} \tag{5-45e}$$

$$a_P = a_E + a_W + a_N + a_S + \frac{\rho'_p r\Delta z\Delta r}{\Delta t} \tag{5-45f}$$

In the above expressions, the corresponding conductances are defined by

$$D_e = \frac{\Gamma_e r\Delta r}{(\delta z)_e},\ D_w = \frac{\Gamma_w r\Delta r}{(\delta z)_w},\ D_n = \frac{\Gamma_n r\Delta z}{(\delta r)_n},\ D_s = \frac{\Gamma_s r\Delta z}{(\delta r)_s} \tag{5-46}$$

and the mass flow rates through the faces of the control volume are defined as

$$F_e = (\rho u)_e r\Delta r,\ F_w = (\rho u)_w r\Delta r, F_n = (\rho v)_n r\Delta z, F_s = (\rho v)_s r\Delta z \tag{5-47}$$

The following Peclet numbers express the ratio of the strengths of convection to diffusion:

$$P_e = \frac{F_e}{D_e}, \qquad P_w = \frac{F_w}{D_w}, \qquad P_n = \frac{F_n}{D_n}, \qquad P_s = \frac{F_s}{D_s} \tag{5-48}$$

In general, there are five schemes, namely central difference, upwind, hybrid, exponential and power-law for formulation of convection diffusion. The power-law scheme is adopted in the present study as follows because of its stability:

$$A(|P|) = [|0,\ (1-0.1|P|)^5|] \tag{5-49}$$

5.3.3 The grid and time step generation

The influence of time step and grid size on the model results should be analysed. Too low or too high a time step and grid size is not acceptable. A non-uniform mesh with a large concentration ranging from 10×40 to 30×100 and a time step ranging from 0.01 to 1 s has been set up. The differences at different average temperatures and pressures from the 24×40 and 30×100 grids are less than 5%. The differences at different average temperatures and pressures using 0.1 s and 0.01s time step are less than 5%. Based on the above analysis, a time step of 0.1 s and a 24×40 grid were chosen to ensure the reliability of the results.

A staggered grid as shown in Figure 5.6 is used as follows: velocity components *u*, *v* are fields are stored at staggered grids which are placed at the centre of the CV interfaces, while pressure, temperature and the fluid properties are stored in the main grid point P. The velocity components are calculated for the points that lie on the surface of the main control volume. Thus the *z*-direction velocity component *u* (Figure 5.4a) is stored at the faces that are normal to the *z*-direction. Similarly, the *r*-direction velocity component *v* (Figure 5.4b) is stored at the faces that are normal to the *r*-direction. The control volume for *u* is staggered on a half grid in the *z*-direction and the control volume for *v* is staggered on a half grid in the *r*-direction.

5.3.4 Under-relaxation

Under-relaxation is a very useful technique for nonlinear problems. It is employed to avoid divergence in the iterative solution of strongly nonlinear phenomena. In this respect, a weighted average of the newly calculated value and the previous value are taken at each point. $\tilde{\phi}^{n+1}$ represents the newly calculated value of ϕ at the $n + 1$ iteration. The weighted average value is

$$\phi_P^{n+1} = \alpha \tilde{\phi}_P^{n+1} + (1-\alpha)\phi_P^n \qquad (5\text{-}50)$$

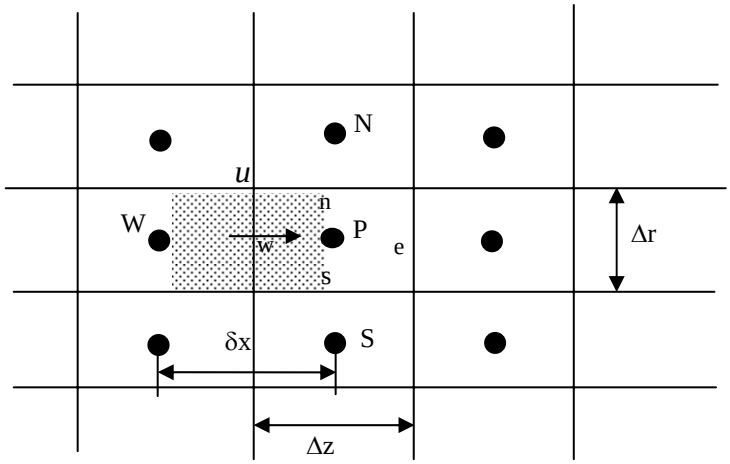

(a)

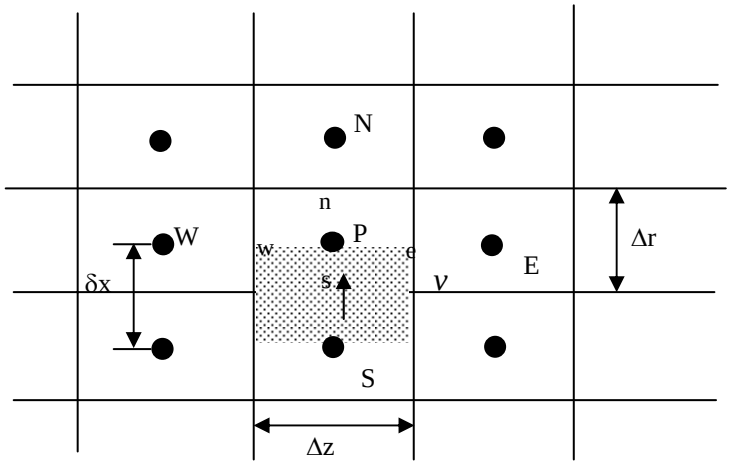

(b)

Figure 5.4 Staggered grids

where ϕ_P^{n+1} represents the under-relaxed value of ϕ_P at the n+1 iteration and α $(0 < \alpha \leq 1)$ is the under-relaxation parameter. The effect of under-relaxation factor on convergence rate is considerable. Unacceptably slow convergence or divergence of the solution is obtained if the factors are too low or too high, respectively. The under-relaxation factors for the pressure and temperature are set to 0.5- 0.8 and 0.8, respectively.

5.3.5 Solution Procedures

The above discretisation equation [Equation (5-44)] for each variable is solved by the line-by-line procedure, which is the combination of the Tri-Diagonal Matrix Algorithm (TDMA) and the Gauss-Seidel iteration technique. The sequence of operations is as follows:

1. Solve the modified Darcy equation to obtain *u*, and *v*.
2. Solve the adsorption equations and obtain the adsorbed amount (q) and adsorbed rate (dq/dt).
3. Solve the continuity equation and obtain the value of pressure (P).
4. Solve the energy equation.
5. Repeat the whole procedure until a converged solution is obtained.
6. With next increment of time step, repeat operations 1-5 for a time step, (time = time + time step).

Figure 5.5 shows the flow diagram of the computer programme. The parameters of geometry are given or calculated in SETUP1. The coefficients of the discretisation equations are established in SETUP2, where the SOLVE routine is called upon to solve the equations. In DIFLOW, the formulation of the convection diffusion $A(|P|)$ is calculated. In the SOLVE block, the equations are solved by using TDMA. The grid is generated in UGRID, and results are printed in PRINT. The grid points and surface of the control volume are generated in GRID. The initial conditions are set up for the unsteady problem in START. The density in the convection term (ρ) is set in DENSE and the density in the unsteady term (ρ') is set in DENSE2 while the boundary conditions are written in BOUND. The transport coefficient Γ and source term *S* are set in GAMSOR. The value of velocity of *u* and *v* are solved by the modified Darcy equation in UVCOM. The adsorbed amount and the adsorption rate are computed in ADSCOM. The main part of this programme is shown in the Appendix.

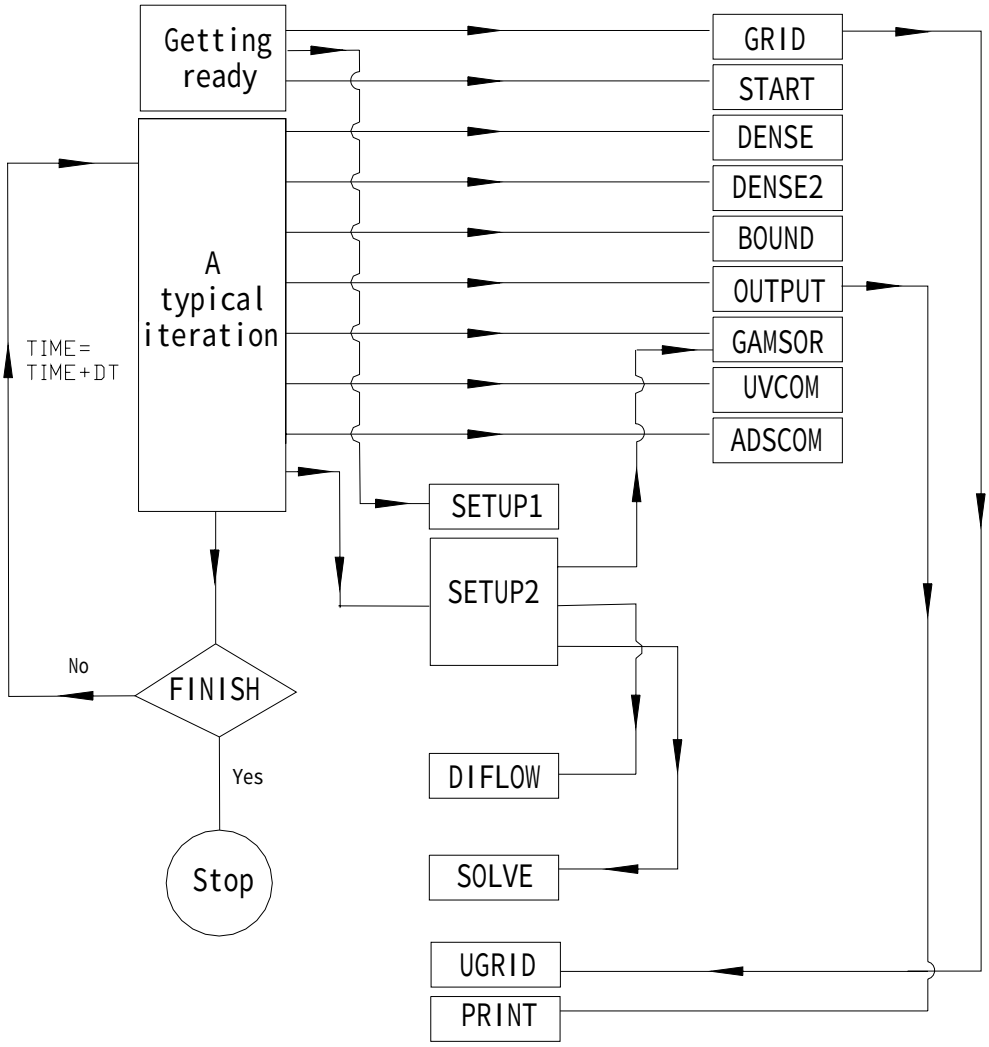

Figure 5.5 Flow chart of computer programme

5.3.6 Convergence Criterion

Convergence of the computational scheme is declared when the following convergence criterion is satisfied:

$$\left|\frac{\phi_p^{n+1}-\phi_p^{n}}{\phi_p^{n+1}-\phi_p^{0}}\right|_{\max} \le 10^{-6} \qquad \text{for all } \phi \tag{5-51}$$

where ϕ represents any dependent variable, and n refers to the value of ϕ at the nth iteration level.

5.4 RESULTS AND DISCUSSION

5.4.1 Adsorption cooling cycle - Base case

The zeolite-13X/water system is selected as the adsorbent /adsorbate pair. The parameter values and operating conditions of the given base case used in the model are listed in the Table 5.1. A computer programme has been written based on the above numerical scheme to solve the model. The cooling COP and SCP for the base case calculated by the numerical model are 0.442 and 48.75 W/kg, respectively. These results are close to the values of 0.43 and 32.1 W/kg obtained by Zhang and Wang (1999). The value of COP is also very close to the value of 0.447 obtained by thermodynamic model.

Table 5.1 Parameter values and operating conditions used in the model

Name	Symbol	Value
Velocity of heating transfer fluid	u_f	1 m/s
Initial temperature	T_0	318 K
Generation temperature	T_g	473 K
Adsorption temperature	T_a	318 K
Fluid inlet temperature during heating	$T_{h,in}$	493 K
Fluid inlet temperature during cooling	$T_{c,in}$	298 K
Evaporator temperature	T_e	279 K
Condenser temperature	T_c	318 K
Initial pressure	P_0	1000 Pa
Density of adsorbent bed	ρ_s	620 kg/m^3
Density of metal tube	ρ_m	7850 kg/m^3
Density of fluid	ρ_f	800 kg/m^3
Specific heat of adsorbent bed	C_{ps}	836 J/kg·K
Specific heat of metal tube	C_{pm}	460 J/kg·K
Specific heat of fluid	C_{pf}	2090 J/kg·K
Specific heat of water vapour	C_{pg}	1880 J/kg·K

Specific heat of adsorbed water	C_{pa}	4180 J/kg·K
Thermal conductivity of adsorbent bed	λ_s	0.2 W/m·K
Thermal conductivity of metal tube	λ_m	15.6 W/m·K
Thermal conductivity of heat exchange fluid	λ_f	0.1 W/m·K
Viscosity of water vapour	μ_g	9.09×10^{-6} N·s/m^2
Heat of adsorption	ΔH	3.2×10^{6} J/kg
Particle diameter	d	0.2 mm
Internal radius of metal tube	R_0	0.020 m
External radius of metal tube	R_1	0.021 m
External radius of adsorbent bed	R	0.036 m
Length of adsorbent bed	L	0.6 m
Macro-porosity of adsorbent bed	ε_a	0.38
Micro-porosity of adsorbent particle	ε_i	0.42
Total porosity of adsorbent bed	ε	0.64
Reference diffusion coefficient	D_0	3.92×10^{-6} m^2/s
Equivalent activation energy	E_D	28035 J/mol

Figure 5.6 shows the comparison between numerical thermodynamic cycle and ideal cycle. It can be seen that the path of numerical thermodynamic cycle does not agree well with that of the ideal cycle especially in the isosteric heating and isobaric adsorption phases. For the ideal cycle, the pressure and the temperature are kept as uniform in the adsorbent bed, and mass transfer resistance is neglected. During the isosteric heating phase, the difference between the numerical cycle and ideal cycle is a result of mass resistance in the adsorbent particles (mass resistance in micro-pores), and the difference between the numerical cycle and ideal cycle during the isobar adsorption phase is mainly due to the mass resistance between the adsorbent particles (mass resistance in macro-pores). In the model of Marletta *et al*. (2002), mass resistance in the adsorbent particles is neglected, and hence, their results are in good agreement with the ideal cycle in the isosteric heating phase.

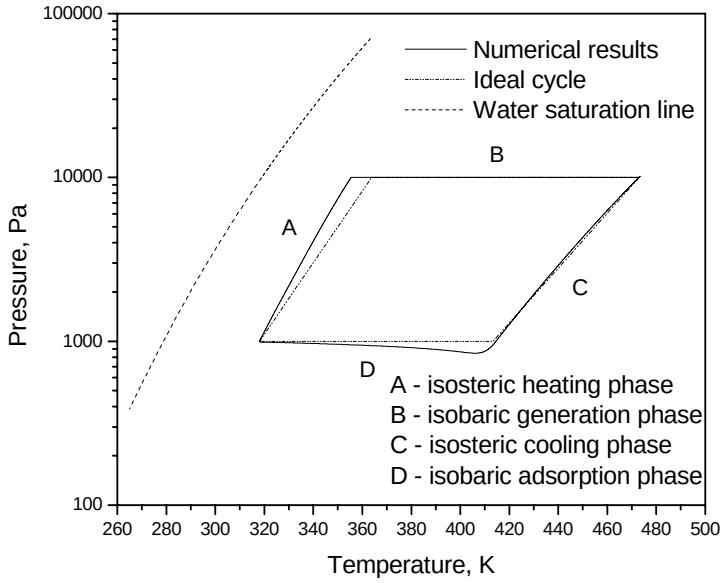

Figure 5.6 Comparison of numerically simulated adsorption cycle and ideal cycle

Figure 5.7 shows the variation of the average temperature with time. It can be observed that during the isosteric heating phase (A), the slope of the curve is larger than that during the isobaric generation phase (B). During isosteric heating, the heat adsorbed from the heating fluid goes mainly to increasing the temperature of the adsorbent bed because of the small change in the adsorbed amount. In the isobar generation phase, the heat adsorbed from the heating fluid not only increases the temperature of the adsorbent bed but also contributes to the heat of desorption. The isosteric cooling and isobaric adsorption phases behave in the same way. Figure 5.8 shows the variation of the average pressure of adsorbent bed with time. It can be seen that in the isosteric heating and isosteric cooling phases, the pressure changes very quickly and in the isobar heating phase, the pressure was kept nearly constant. The pressure in the isobaric adsorption phase increases slightly with time, which is different from the ideal case. For an ideal cycle, the pressure in the isobar adsorption phase is a constant, which is the same as the pressure in the evaporator. The difference results from the mass transfer resistance between the particles. The variations of the average adsorbed amount with

time are shown in Figure 5.9. During the isosteric heating phase, the total adsorbed amount of adsorbent bed is almost constant (Figure 5.9) and the pressure in Figure 5.6 during the isosteric heating phase is higher than the pressure of the ideal cycle. Hence, the real pressure is not equal to the equilibrium pressure because of mass transfer resistance in the particle.

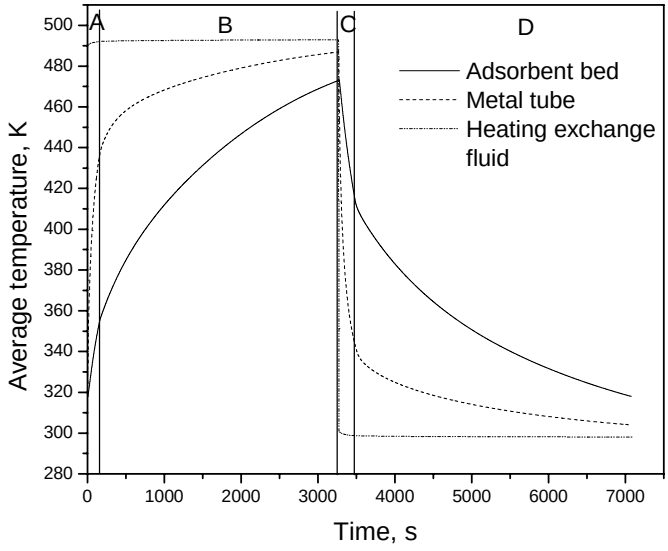

Figure 5.7 Variations of the average temperature with time

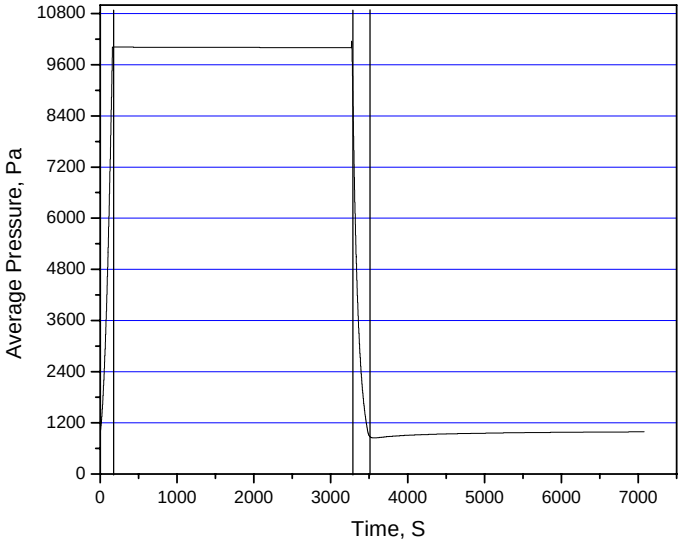

Figure 5.8 Variations of the average pressure with time

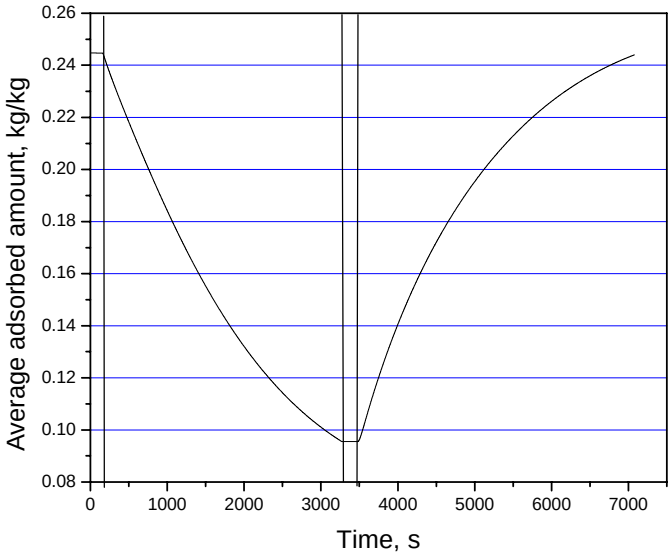

Figure 5.9 Variations of the average adsorbed amount with time

Figure 5.10 shows the variation of heat exchange rates with time for the four phases of the cycle. It can be seen that the thermal power for heat exchange fluid increases quickly and then decreases slowly. This is due to the large temperature difference at the initial phase, which subsequently reduces with time.

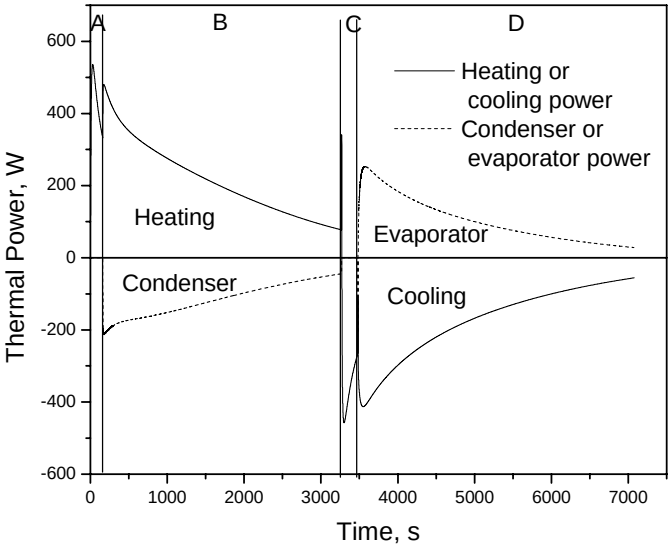

Figure 5.10 Variation of thermal power with time

Figure 5.11 shows the temperature, pressure, velocity and adsorbed amount distribution in the adsorbent bed during the isosteric heating phase. From Figure 5.11 (a), the temperature decreases from the inner to outer part and from left to right side, but the temperature gradient is very low from left to right side. It can also be seen that at the inner part of the adsorbent bed, the temperature gradient is higher than that at other portions of the adsorbent bed. There is a need to increase the density of the grids around the bottom of the adsorbent bed during numerical computation. In Figure 5.11 (b), the pressure in the adsorbent bed is not uniform, and hence, the importance of including the effect of the mass transfer resistance in the adsorbent bed can be seen. From Figures 5.9 and 5.11 (c), it can be seen that there is very little change in the total adsorbed amount in adsorbent bed during the isosteric heating phase. During heating, a part of the adsorbed phase migrates from the hot zones *via* the vapour phase to the cold zones with a desorption-adsorption process.

Figure 5.12 shows the temperature, pressure, velocity and adsorbed amount distributions in the adsorbent bed during the isobaric heating phase. From Figure 5.12 (a), it can be seen that in the isobaric heating phase, the temperature gradient is lower than that in the isosteric heating phase (Figure 5.11a). This is because of the fact that the temperature gap between heat exchange fluid and adsorbent bed in the isobaric heating phase is decreased compared with that in the isosteric heating phase. In the isobaric heating phase, the pressure difference at different sides in the adsorbent bed is very small and the value of pressure is about 1000 Pa (see Figure 5.12b). It can also be seen that the amount of water vapour rejected from the adsorbent bed in the outer part is more than that from the inner part. From Figure 5.12(c), it can be seen that the absorbed amount in the outer part is higher than that in the inner part. Hence, the adsorbed amount in the adsorbent bed tends to become uniform.

Figure 5.13 shows the distribution of all variables in the isosteric cooling phase. Figure 5.14 shows the distribution of all variables in isobaric adsorption phase. The distributions of

all variables in isosteric and isobaric heating phases are similar to the isosteric cooling and isobar adsorption phases but in the opposite direction.

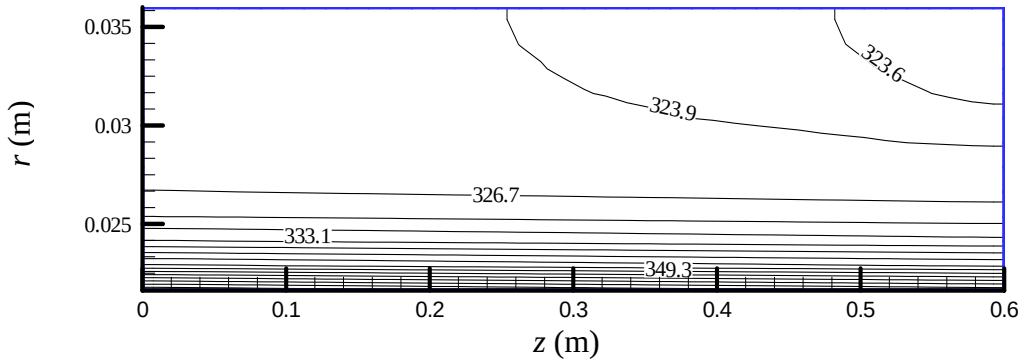

(a)

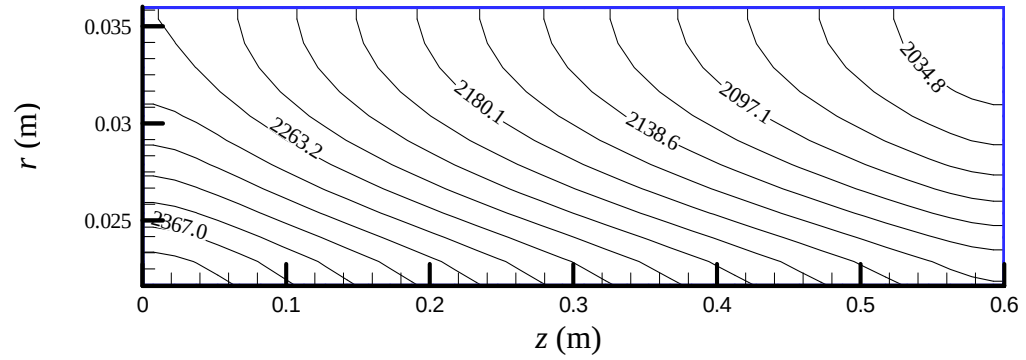

(b)

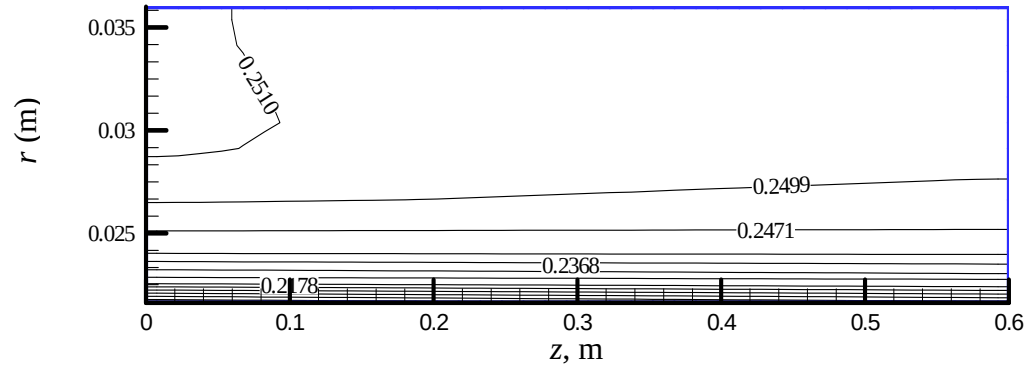

(c)

Figure 5.11 Distribution of variables of the adsorbent during isosteric heating phase
(a) Temperature, K; (b) Pressure, Pa; (c) Adsorbed amount, kg/kg

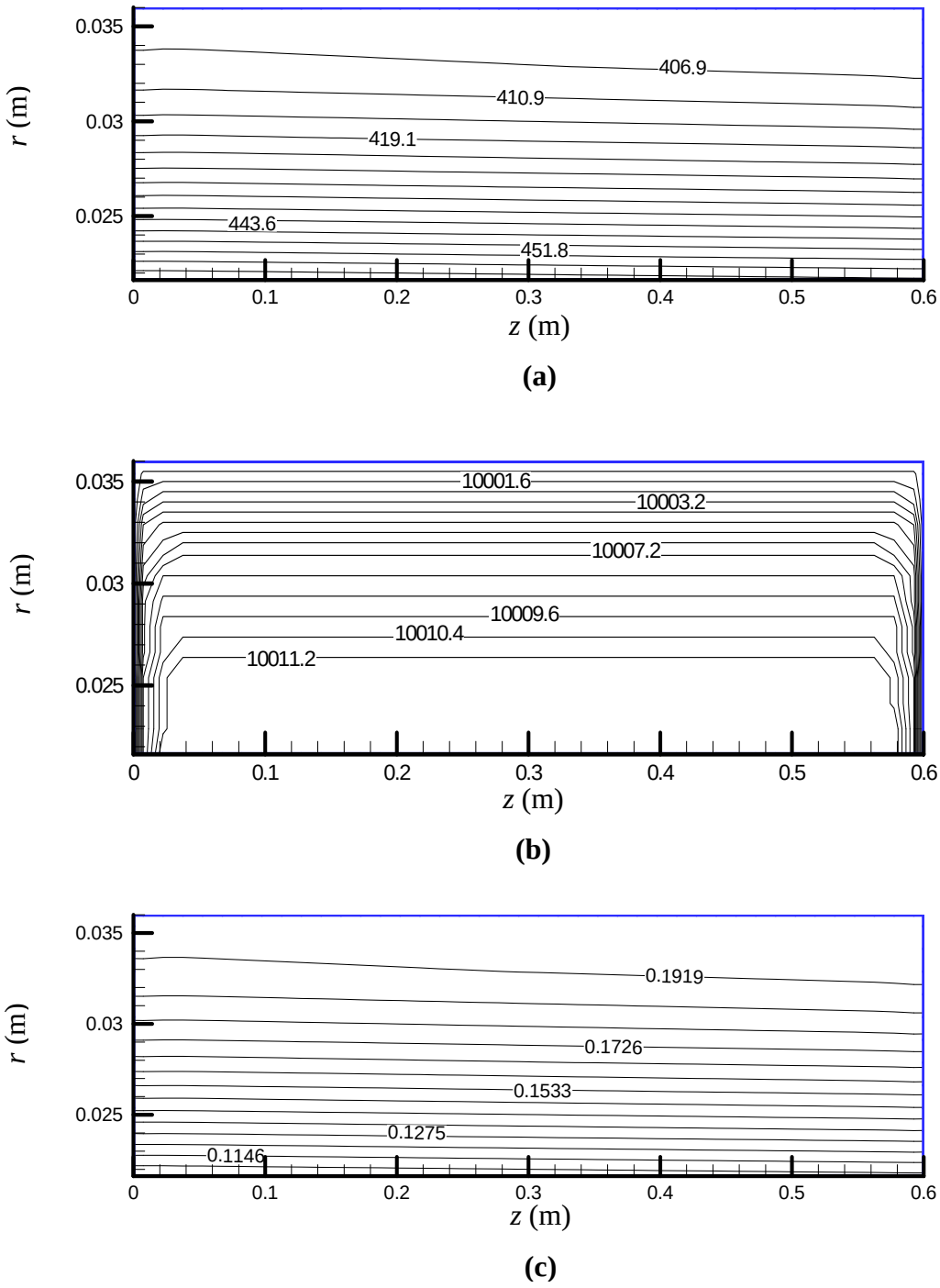

Figure 5.12 Distributions of variables of the adsorbent during isobaric heating phase
(a) Temperature, K; (b) Pressure, Pa; (c) Adsorbed amount, kg/kg

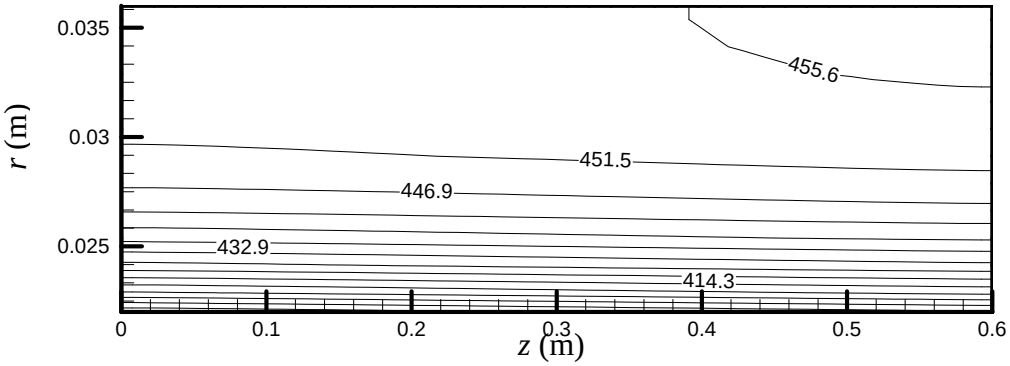

(a)

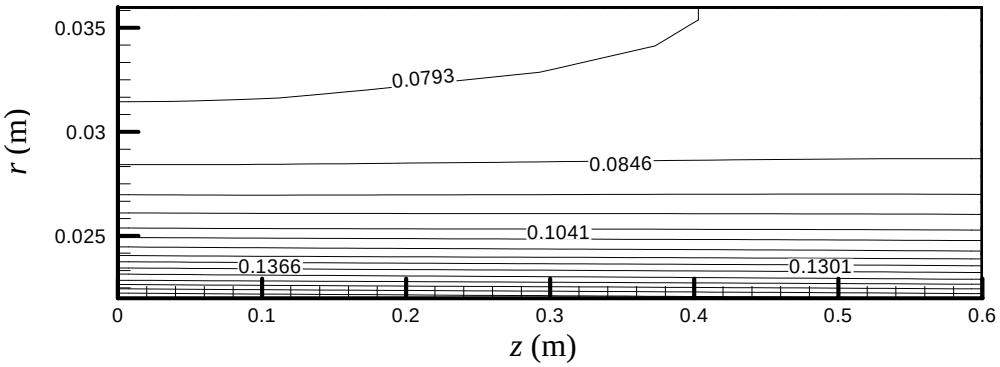

(b)

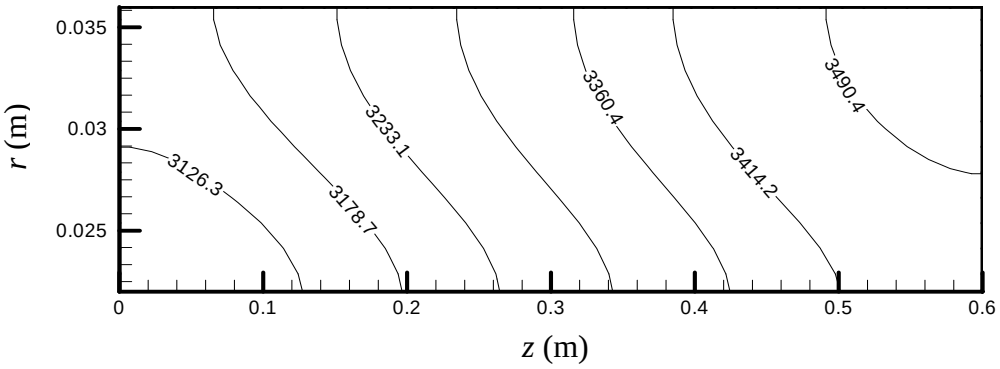

(c)

Figure 5.13 Distributions of variables of the adsorbent during isosteric cooling phase
(a) Temperature, K; (b) Pressure, Pa; (c) Adsorbed amount, kg/kg

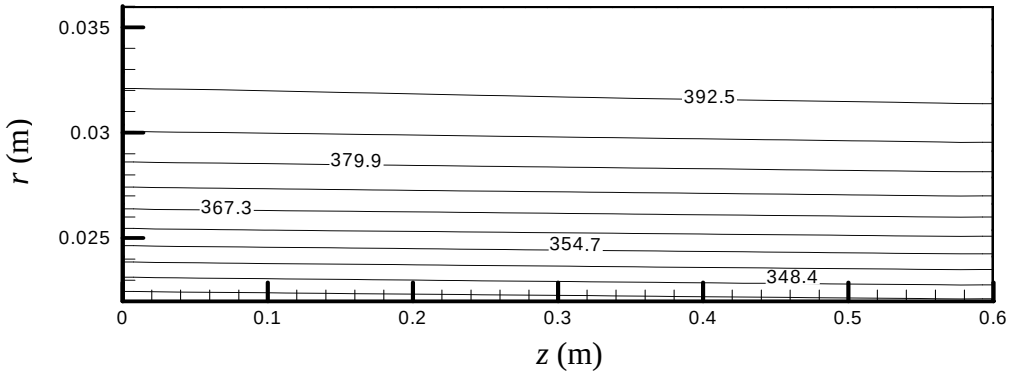

(a)

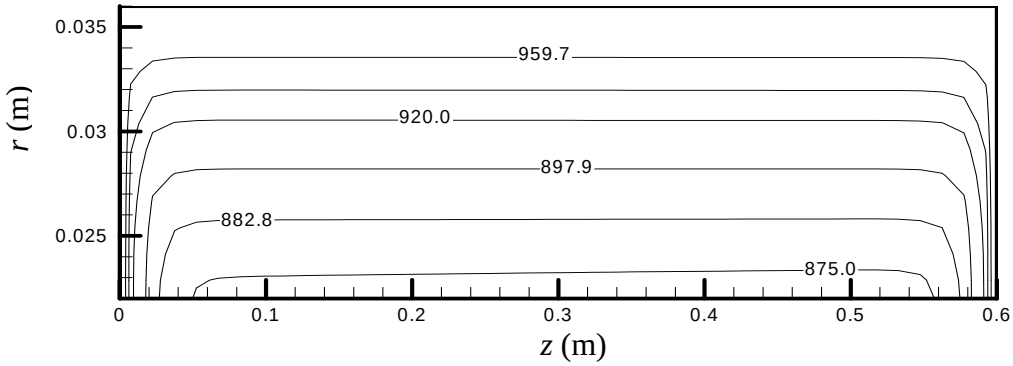

(b)

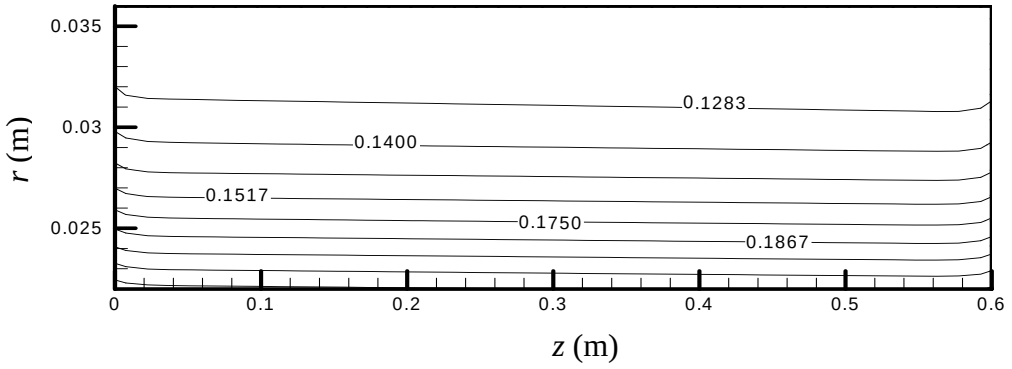

(c)

Fig 5-14 Distributions of variables of the adsorbent during isobaric adsorption phase
(a) Temperature, K; (b) Pressure, Pa; (c) Adsorbed amount, kg/kg

5.4.2 Parametric study

5.4.2.1 Effect of thickness of the adsorbent bed

The adsorbent bed thickness is an important parameter which has great influence on the performance of the adsorption cooling cycle. Figure 5.15 shows the influence of adsorbent thickness on the COP and SCP. Figure 5.16 shows that the cycle time and total cooling power (TCP) varies with the thickness of adsorbent bed. It can be seen that COP increases with an increase in adsorbent thickness. On the contrary, SCP reduces with an increase in adsorbent thickness, and so does TCP. For a large thickness, the heat capacity ratio of metal tube to adsorbent bed will decrease which leads to the increase in COP. However, a larger thickness means more adsorbate can be driven into the cycle resulting in increased thermal resistance and contributing to a longer cycle time (Figure 5.16) and a reduction in SCP.

5.4.2.2 Effect of adsorbent particle diameter

Figure 5.17 shows the adsorption cycles for different particle sizes. The diameter of adsorbent particle plays an important role in mass transfer resistance. If the particle size were to increase, the mass transfer resistance in micro-pores will increase while the mass transfer in macro-pores will decrease. It can be seen from Figure 5.17 that in the isosteric heating phase, the slope for D_p = 0.5 mm is higher than those for other diameters. This is because the mass transfer resistance in micro-pores for D_p = 0.5 mm is greater than those corresponding to the other two diameters. It can also be seen that the pressure for D_p = 0.1 mm in the isobaric adsorption phase is lower than the other two diameters. The reason for this is that the mass resistance in macro-pores for D_p = 0.1mm is greater than that of the other two diameters. The calculated values of COP and SCP for different particle sizes are listed in Table 5.2.

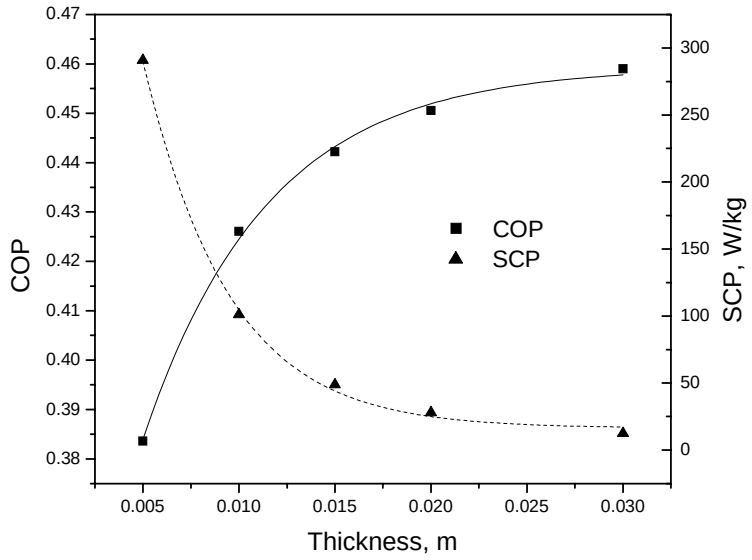

Figure 5.15 Variation of COP and SCP with thickness

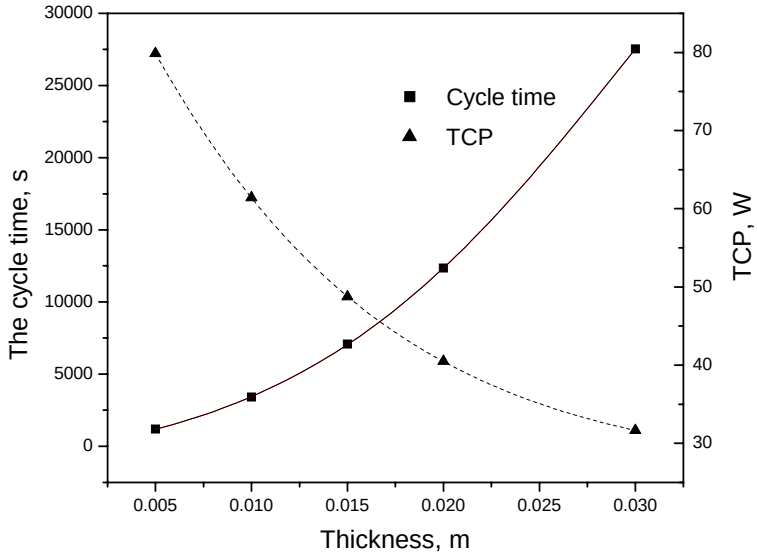

Figure 5.16 Variation of cycle time and TCP with thickness

The simulation results of Table 5.2 show that the COP and SCP are approximately the same for the three particle sizes investigated. The mass transfer resistance in the macro-pores increases with a reduction in particle size, and the mass transfer resistance in micro-pores

decreases with a decrease in particle size. The influence of the macro and micro-mass transfer resistances cancel each other out. Hence, the variation of the particle size has almost no effect on the performance of the cooling cycles.

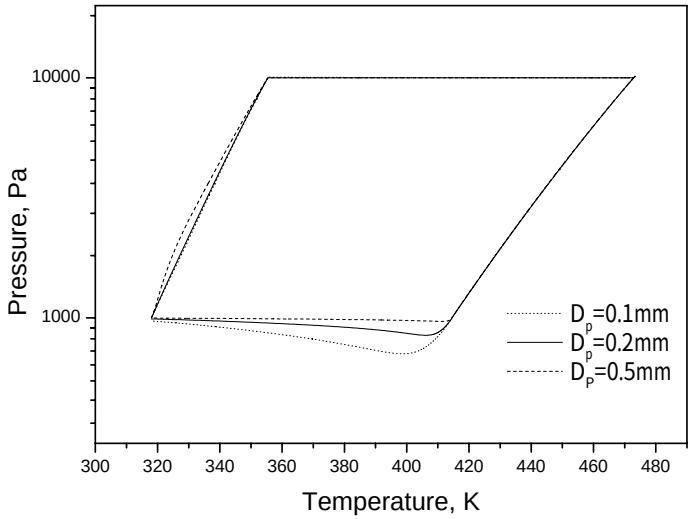

Figure 5.17 Adsorption cycles for different particle size

Table 5.2 Values of COP and SCP for different particle sizes

D_p, mm	0.1	0.2	0.5
COP	0.441	0.442	0.441
SCP, W/kg	48.37	48.75	48.80

5.4.2.3 Effect of porosity of the adsorbent bed

Liu (1994) studied the performance of compressed adsorbent particles with the motivation of higher performance based on higher equivalent thermal conductivity of the bed. The effect of mass transfer resistance was neglected in his study. However, when the adsorbent particles are compressed, the mass transfer resistance in macro-pores of the bed is also increased. Figure 5.18 shows the Clapeyron diagram of the adsorption cycle for different macro-porosities. The effect of mass resistance in macro-pores can be seen from this figure. The pressure in the isobar adsorption phase decreased with decrease of porosity

because there is a higher mass transfer resistance in macro-pores for a lower porosity. The calculated performance values of the cooling cycle and their corresponding values of equivalent thermal conductivity for various adsorbent bed porosities are shown in Table 5.3.

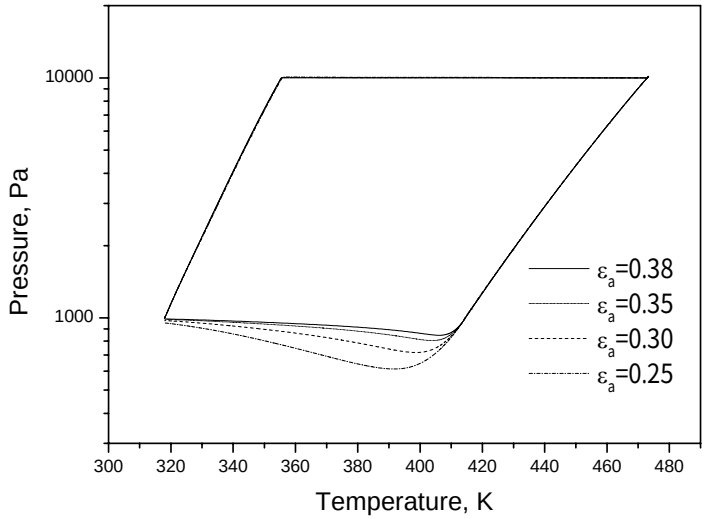

Figure 5.18 Adsorption cycles for different macro-porosities

Table 5.3 Performance values for various adsorbent bed porosities

ε_a	0.25	0.30	0.35	0.38
COP	0.445	0.445	0.443	0.442
SCP, W/kg	42.8	45.0	47.3	48.8
Cycle time, s	8022	7648	7292	7076
TCP, W	51.7	50.8	49.5	48.7
λ_{eq}, W/m·K	0.223	0.214	0.205	0.200

From Table 5.3, it can be seen that the COP does not change with the variation of adsorbent bed porosity, while the SCP reduces with a decrease in bed porosity. The total cooling power (TCP) increases for a more compact adsorbent bed. With the reduction of bed porosity, the adsorbent density increases leading to a longer cycle time. Hence, the SCP is reduced. At the same time, the mass of cycled refrigerant vapour and the TCP increases with

the reduction in bed porosity. The effect of the mass transfer resistance is insignificant when compared to the effect of heat transfer resistance for the range of porosities investigated. Thus, the performance of the adsorption cooling cycle can be improved by compressing the adsorbent bed when the adsorbent bed porosity is between 0.25 to 0.38.

5.4.3 Operating conditions

5.4.3.1 Effect of condensing temperature (T_c)

Figure 5.19 shows the effect of T_c on the system performance. It can be seen that both COP and SCP decreases linearly with increasing condensing temperature over the range shown. When T_c increases, the condensing pressure also increases. From the Clapeyron diagram of the adsorption cycle (Figure 1.5), it can be seen that the cycled adsorbate mass (q_{max} - q_{min}) decreases for a lower condensing pressure with a fixed generation temperature. Equation (5-34) shows that the cooling energy (Q_{ev}) is proportional to the cycled adsorbate mass. Thus, an increase in T_c will result in a reduction of COP. The cycle time also decreases with an increase in T_c. However, the decrease rate of cycle time is smaller than that of cooling energy when T_c increases. Hence, SCP also decreases with an increase in condensing temperature. Figure 5.19 also suggests that a low condensing temperature would result in better performance. Since the condenser is usually cooled by either atmospheric air or water, the evaporating temperature is normally not lower than the room temperature.

5.4.3.2 Effect of evaporating temperature (T_e)

The effect of T_e on system performance is shown in Figure 5.20. As can be seen from this figure, both the COP and SCP increases as evaporating temperature increases. The Clapeyron diagram of the adsorption cycle (Figure 1.5) also shows that the cycled adsorbate mass will increase as T_e is increased. The heat input from the heat exchange fluid (Q_h) will

also increase with T_e. Its increase however is not as large as the increase of cycled adsorbate mass leading to an increase in the COP. Due to the fixed adsorption and generation temperatures, there is very little change in heat input from the heat exchange fluid. The difference in cycle time would be very small (within 3%) resulting in an increase in the SCP.

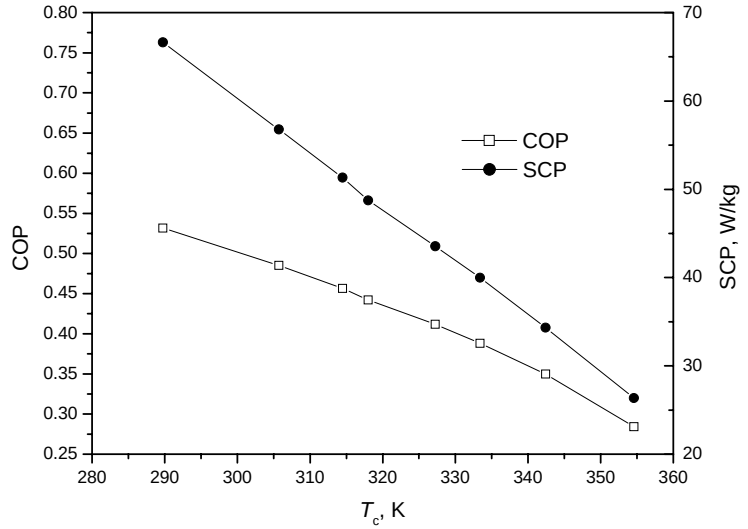

Figure 5.19 Variation of performance coefficients with condensing temperature

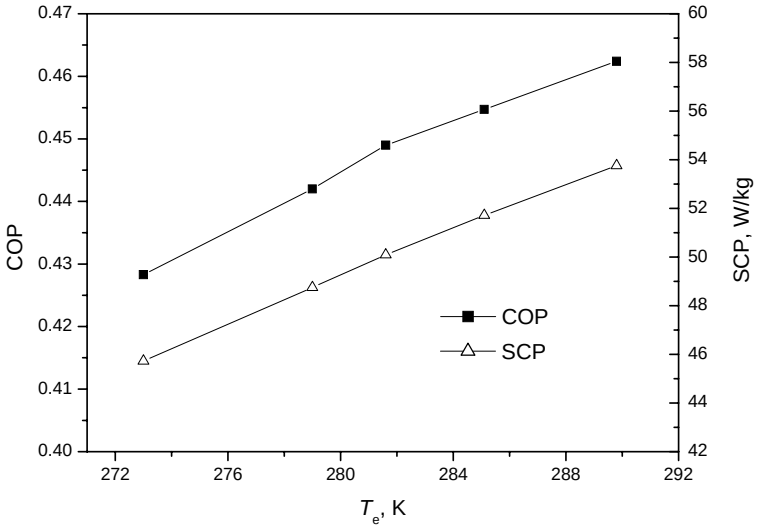

Figure 5.20 Variation of performance coefficients with evaporating temperature

5.4.3.3 Effect of adsorption temperature (T_a)

From Figure 5.21, it can be seen that the COP first increases slightly and then decreases with T_a. It can also be observed that there is a maximum value of SCP over the range of T_a investigated. From Figure 1.5, when adsorption temperature decreases, the cycle adsorbate mass will increase and the heat input will need to be increased. The cycle time also increases with the reduction of T_a. The cycled adsorbate mass relative to heat input will first change very little and then decreases greatly contributing to a reduction in the COP. Starting from a high value of T_a, the ratio of cycled adsorbate mass change to the cycle time will be greater with a reduction of T_a, which causes SCP to increase. However, when T_a decreases below a certain value, the ratio of additional cycled adsorbate mass change to the additional cycle time change will decrease causing the SCP to decrease. It can also be seen from this figure that T_a has an optimal value with regards to system performance when other operating conditions are fixed. For the case under study, an adsorption temperature in the range of 320-340 K will result in both high COP and SCP values. A suitable operating point in this temperature range will give a COP of about 0.43 and a SCP of about 50 W/kg.

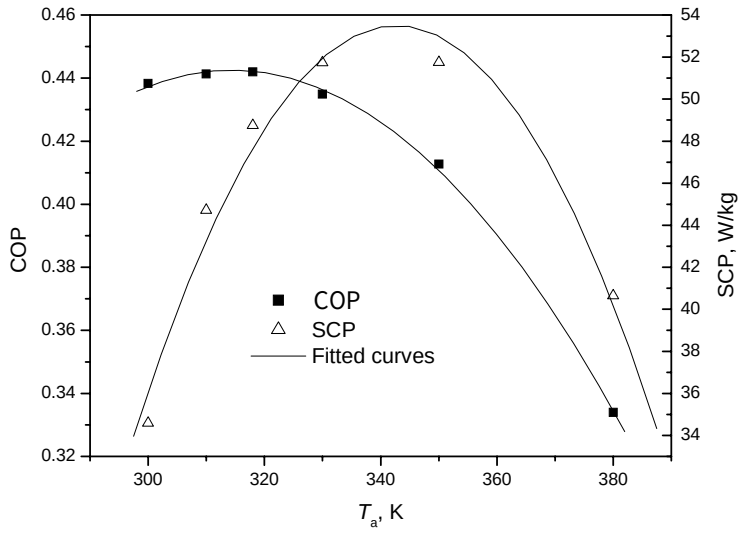

Figure 5.21 Variation of performance coefficients with adsorption temperature

The three-heat reservoir system (high temperature reservoir, low temperature reservoir and medium temperature reservoir) is often employed in adsorption cooling systems. In this system, the adsorption and condensing temperatures are assumed to be the same because of the common medium temperature reservoir. Figure 5.22 shows the effect of adsorption temperature on the system performance. From this figure, it can be seen that the optimal adsorption temperature and condensing temperature is about 310 K.

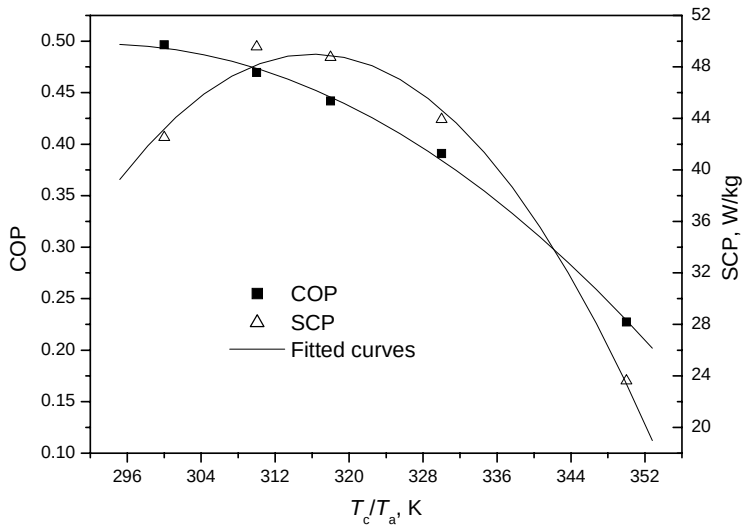

Figure 5.22 Variation of performance coefficients with adsorption temperature in a three-temperature reservoir system

5.4.3.4 Effect of generation temperature (T_g) and driven temperature ($T_{h,in}$)

The effects of generation temperature on SCP with different driven temperatures (the temperature of heat exchange fluid during the heating process) are shown in Figure 5.23. From this figure, it can be seen that SCP has a maximum value for every driven temperature. The reason is that the ratio of cycle adsorbate mass to cycle time increases with an increase in generation temperature at low temperature. However, when the generation temperature approaches the driven temperature, the heat transfer rate between HXF and the adsorbent bed

decreases. Thus, the cycle adsorbate mass will increase very slightly and the cycle time becomes longer, resulting in a decrease of SCP.

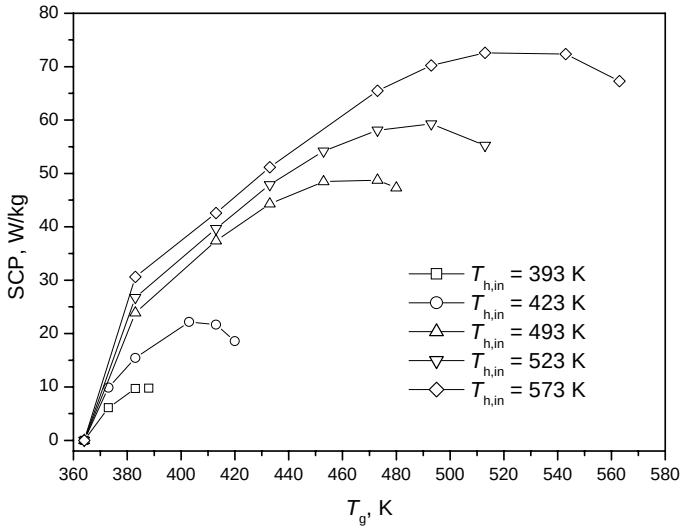

Figure 5.23 Variation of SCP with generation temperature for different driven temperatures

Figure 5.24 shows the effects of generation temperature on the COP for different driven temperatures. It can be seen from this figure that the COP is affected directly by the generation temperature and that the driven temperature has a negligible effect on COP. COP values increase asymptotically to a constant value for generation temperatures beyond 480 K. The results agree with the findings of Cacciola and Restuccia (1995). The variation of heat input from HXF and cycled adsorbate mass with generation temperature T_g are shown in Figure 5.25. From this figure, it can be seen that the heat input increases almost proportionately with cycled adsorbate mass. During isosteric heating phase, no cycled adsorbate is generated as the adsorber was disconnected from the condenser and the heat input in this phase is about 6×10^4 J. For the large value of T_g, the heat input during isosteric heating phase compared to the total heat input is very small. For example, it can be seen from Figure 5.25 that the total heat input is more than 10 times that of the heat input in

isosteric heating phase when the generation temperature exceeds 480 K. The COP tends to a constant value as the generation temperature exceeds 480 K.

The variation of performance coefficients with driven temperature, T_g at maximum SCP, is shown in Figure 5.26. It can be seen that COP increases very sharply with driven temperature until approximately 493 K and assumes a constant value of about 0.45 beyond that temperature. The variation of maximum SCP with driven temperature is linear for the range of driven temperature investigated. It appears that using a higher driven temperature would result in a higher SCP. However, when the driven temperature exceeds 493 K, COP values higher than 0.45 cannot be attained.

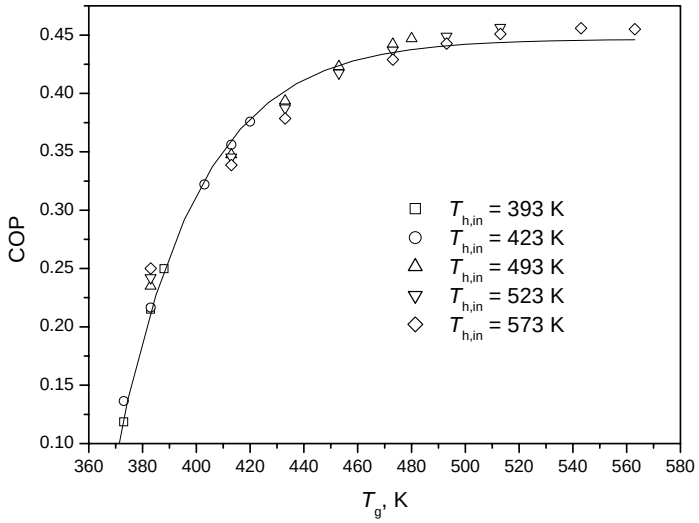

Figure 5.24 Variation of COP with generation temperature for different driven temperatures

5.4.3.5 Effect of velocity of the heat exchange fluid

Table 5.4 shows the effect of the velocity of heat exchange fluid on the performance coefficients. The COP changes very little with the velocity of heat exchange fluid. For fluid velocities smaller than 0.1 m/s, the cycle time will increase very quickly with an increase in fluid velocity. Hence, the SCP increases significantly with an increase in fluid velocity.

However, for velocities larger than 0.5 m/s, the cycle time does not change with velocity leading to very little change in SCP. To reduce operating energy cost, the optimal velocity of the heat exchange fluid should be in the range of 0.1 - 0.5 m/s.

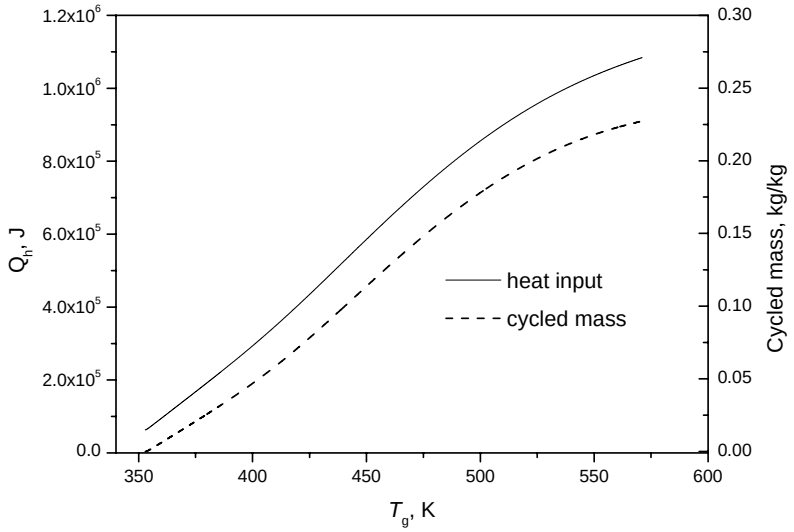

Figure 5.25 Variation of heat input and cycled adsorbate mass with generation temperature

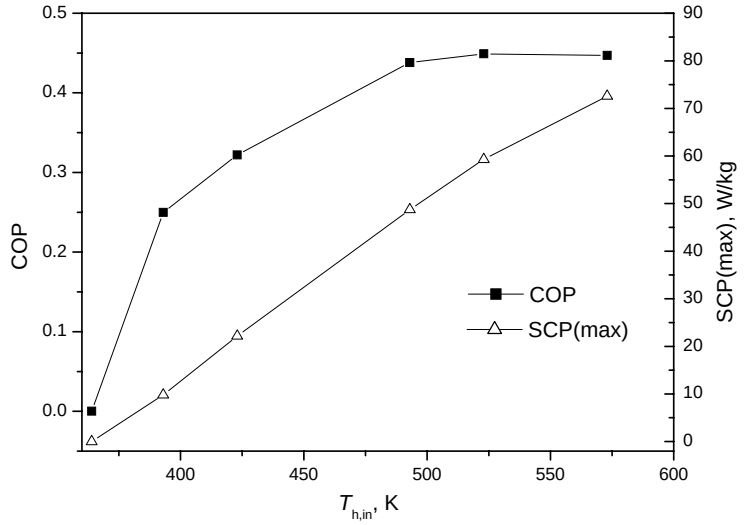

Figure 5.26 Variation of performance coefficients with driven temperature, T_g at maximum SCP

Table 5.4 Variation of system performance with velocity of heat exchange fluid

Velocity of HXF, m/s	0.01	0.1	0.5	1	2	5
COP	0.426	0.441	0.442	0.441	0.441	0.441
SCP, W/kg	21.5	40.6	47.4	48.8	49.2	49.6
t_c, s	15424	8448	7258	7076	6984	6926

5.4.4 Heat transfer limits in condenser

In most numerical models, heat transfer limits in condenser are not considered. The condensing pressure (P_c) in their model is assumed to be a constant during the isobaric generation phase. Actually, the pressure in condenser will change with time because the condensing thermal power is not constant during this phase (see Figure 5.10). To study the effect of these limits, a lumped model of the heat transfer in condenser is proposed in this section. This model will be related to the heat and mass transfer model through the pressure boundary condition during the isobaric generation phase (Equation 5-32).

The schematic of the condenser is shown in Figure 5.27. The adsorbate vapour in the condenser is cooled by water and condenses into a liquid. The mass balance equation in the condenser can be obtained as

$$V_c \frac{d\rho_{cg}}{dt} + \dot{m}_{al} = \dot{m}_w \tag{5-52}$$

where V_c is the inside volume of the condenser, ρ_{cg} is the density of adsorbate vapour and $\dot{m}_{al}$ is the mass flow rate of the liquid phase adsorbate into the receiver.

The heat balance equation for the condenser is given by

$$C_{pm} W_c \frac{dT_c}{dt} + \dot{m}_{al} h_{al} + \frac{d(\rho_{cg} V_c h_{cg})}{dt} + \dot{m}_w h_{vi} = \dot{m}_{cw} C_{pw} (T_{cw,in} - T_{cw,out}) \tag{5-53}$$

h_{al} is the enthalpy of the liquid phase adsorbate which can be written as

$$h_{al} = h_{cg} - L(T_c) \tag{5-54}$$

and h_{vi} is the enthalpy of inlet adsorbate vapour, which is given by

$$h_{vi} = h_{cg} + C_{pg}(T_{vi} - T_c) \tag{5-55}$$

By substituting Equations (5-59) and (5-58) into Equation (5-57), we have

$$\begin{aligned} &C_{pm}W_c\frac{dT_c}{dt} + \frac{\rho_{cg}V_cC_{pg}dT_c}{dt} + V_c \cdot L(T_c)\frac{d\rho_{cg}}{dt} + \dot{m}_w[L(T_c) + C_{pg}(T_{vi} - T_c)] \\ &= \dot{m}_{cw}C_{pw}(T_{cw,in} - T_{cw,out}) \end{aligned} \tag{5-56}$$

where T_{vi} is the temperature of the inlet adsorbate vapour. It is defined as

$$T_{vi} = \frac{\oiint_S \rho_g T_s \mathbf{u}\cdot\mathbf{n}dS}{\dot{m}_w} \tag{5-57}$$

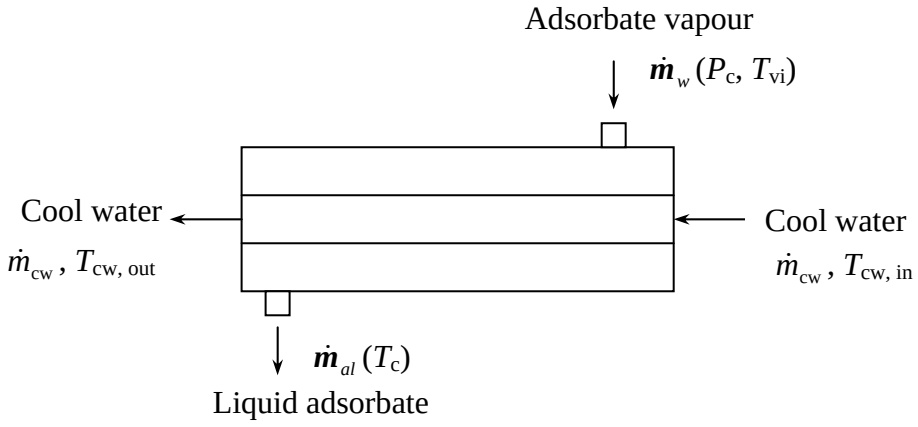

Figure 5.27 Schematic of condenser

The adsorbate gas is assumed to be an ideal gas. Hence the density of adsorbate can be written as

$$\rho_{cg} = \frac{P_c M}{RT_c} = \frac{M \cdot \exp(25.1948 - 5098.26/T_c)}{RT_c} \tag{5-58}$$

Thus, Equation (5-56) can be rewritten as

$$\begin{aligned} &\{C_{pm}W_c + \rho_{cg}V_cC_{pg} + V_cL_{cv}\rho_{cg}(-\frac{1}{T_c} + \frac{5098.26}{T_c^2})\}\frac{dT_c}{dt} + \dot{m}_w[L_{cv} + C_{pg}(T_{vi} - T_c)] \\ &= \dot{m}_{cw}C_{pw}(T_{cw,in} - T_{cw,out}) \end{aligned} \tag{5-59}$$

where

$$T_{cw,out} = T_c + (T_{cw,in} - T_c) \cdot \exp(-\frac{UA}{\dot{m}_{cw} C_{pw}}) \quad (5\text{-}60)$$

Equation (5-59) is discretised by using the forward difference method. The calculation block of the discretized equation is inserted into the main programme shown in Figure 5.5. The parameters values of condenser used in this calculation block are listed in Table 5.5.

Table 5.5 Parameter values of condenser

Name	Symbol	Value
Overall heat transfer coefficient of condenser	U	4000 W/m^2·K
Specific heat of the metal shell of condenser	C_{pm}	460 J/kg·K
Specific heat of cooling water	C_{pw}	4180 J/kg·K
Mass of the metal shell	W_c	0.8 kg
Surface area of the condenser	A	0.1 m^2
Inside volume of the condenser	V_c	0.4×10^{-3} m^3
Inlet water temperature	$T_{cw,in}$	318 K

Figure 5.28 shows the variations of average pressure of adsorbent with time taking into consideration the heat transfer limits in the condenser ($\dot{m}_{cw}$ = 0.003 kg/s). From this figure, it can be seen that the pressure decreases with time during the isobaric generation phase whereas the pressure in Figure 5.8 is almost a constant. This is because the condensing pressure (P_c) is not a constant in this case but instead will decrease with time. In the condenser, the cooled water will absorb more heat than condensing heat under constant pressure as shown in Figure 5.10. This will cause the condensing pressure to decrease, which in turn will reduce the pressure in the adsorber. The simulated adsorption cycles for different mass flow rates of cooling water in the condenser are shown in Figure 5.29. It can be seen that the pressure during the isobaric adsorption phase will increase with a reduction of mass flow rate of cool water in condenser. For a higher value of $\dot{m}_{cw}$, the condensing heat will increase. Hence, the pressure will decrease. Figure 5-30 shows the variation of adsorbed

amount with time in half cycle. It can be seen that the mass of adsorbate generated from adsorber to condenser will increase with an increase in $\dot{m}_{cw}$ for a fixed generation temperature. A reduction of pressure will result in the decrease in adsorbed amount, which leads to an increase in cycled adsorbate mass.

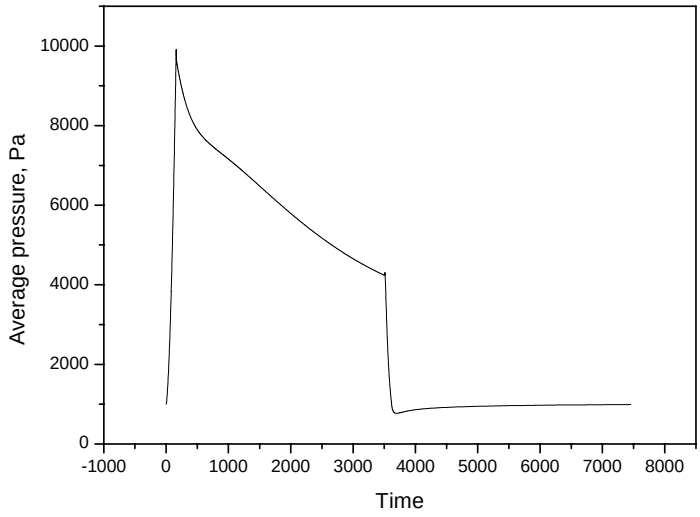

Figure 5.28 Variation of average pressure with time (non-constant condensing pressure)

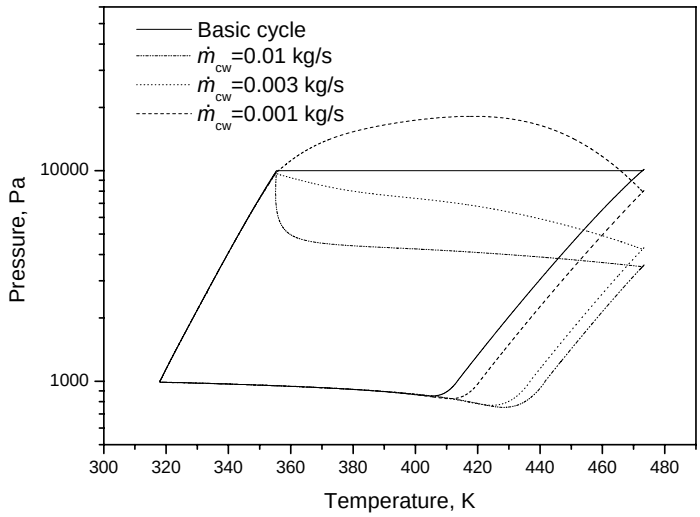

Figure 5.29 Simulation adsorption cycles for different mass flow rates of cooling water in condenser

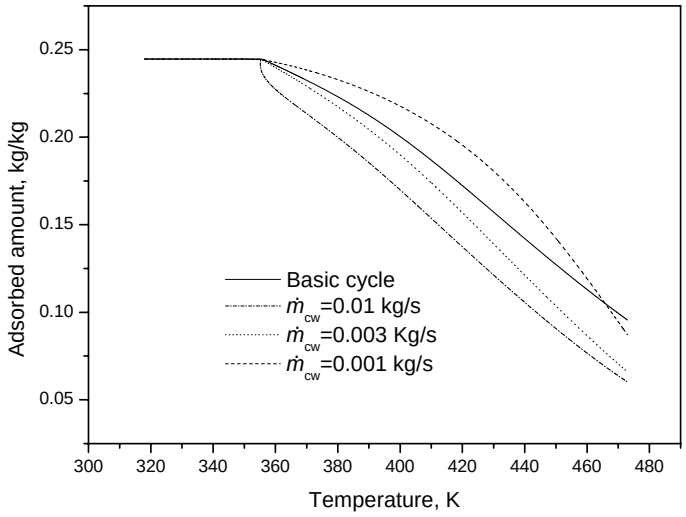

Figure 5.30 Variations of adsorbed amount with temperature for different mass flow rates of cool water in condenser

The calculated system performance values of the cooling cycle for various mass flow rates of cooling water ($\dot{m}_{cw}$) in the condenser are shown in Table 5-6. It can be seen that the both the COP and SCP increases with an increase in $\dot{m}_{cw}$. The cycled adsorbate mass will therefore increase with an increase in $\dot{m}_{cw}$. The cooling energy (Q_{ev}) is proportional to the cycled adsorbate mass (see Equation 5-34). For fixed adsorption and generation temperatures, the change in heat input (Q_h) is very small. Thus, an increase in $\dot{m}_{cw}$ will result in an increase in COP. It can also be seen from Table 5.6 that the cycle time will decrease with an increase in $\dot{m}_{cw}$. Therefore, the value of SCP will increase when $\dot{m}_{cw}$ increases (see Equation 1-2).

Table 5.6 Performance values for various mass flow rates of cool water

$\dot{m}_{cw}$, kg/s	0.01	0.003	0.001	Basic cycle
COP	0.487	0.477	0.448	0.442
SCP, W/kg	58.25	55.50	48.25	48.75
Cycle time, s	7336	7456	7560	7076

5.5 Summary

A two-dimensional non-equilibrium numerical model describing the combined heat and mass transfer in the adsorbent bed has been developed. Mass transfer resistances in both micro-pores and macro-pores are considered in the model. The process paths of the thermodynamic cycle resulting from the numerical computation differ from that of the ideal cycle especially in the isosteric heating and isobar adsorption phases due to the effect of mass transfer resistance. COP increases with an increase in adsorbent thickness while the SCP reduces with an increase in adsorbent thickness. Particle size has very little effect on the performance of the cooling cycle. The performance of the adsorption cooling cycle can be improved slightly by compressing the adsorbent bed when adsorbent bed porosity varies from 0.25 to 0.38. The system performance in terms of both its COP and SCP varies almost linearly with condensing temperature (T_c) and evaporating temperature (T_e). The performance coefficients increase with a reduction in T_c but with an increase in T_e. The adsorption temperature, T_a has an optimal value between 320 K and 340 K based on system performance for fixed operating conditions. The optimal T_a for the given case yields a COP of about 0.43 and a SCP of about 50 W/kg. SCP has a maximum value within the range of generation temperature (T_g) investigated for a given driven temperature ($T_{h,in}$). The maximum value of SCP increases linearly with an increase in $T_{h,in.}$ COP is directly affected by the generation temperature for different driven temperatures. It increases and tends to a constant value with an increase in $T_{g.}$ The cycle time increases significantly when the velocity of the HXF is smaller than 0.1 m/s but changes very little for velocities of HXF larger than 0.5 m/s. The optimal value of velocity of the heat exchange fluid lies within the range of 0.1 - 0.5 m/s. Heat transfer limitations in condenser affect the performance of adsorption cycle. The performance will increase with an increase in the mass flow rate of cooling water ($\dot{m}_{cw}$) in the condenser.

CHAPTER 6

NUMERICAL STUDY OF A COMBINED HEAT AND MASS RECOVERY ADSORPTION CYCLE

6.1 INTRODUCTION

As stated previously, the widespread application of adsorption refrigeration system is limited by its poor performance in terms of COP. Hence, some advanced cycles are proposed in order to improve the system performance (see Section 4.1 in Chapter 4). Among these advanced cycles, the continuous cycle, which incorporates heat and mass recovery cycles have been verified to be a simple and effective method to improve thermal performance (Wang *et al*., 2002B). The function of the heat recovery cycle is to recover thermal energy from the temperature difference between the two adsorbent beds while mass recovery can increase the cycled refrigerant mass, which leads to improved performance. In order to achieve higher performance, mass recovery and heat regeneration can be simultaneously employed.

Thermodynamic investigations of the two-bed heat and mass recovery adsorption cycle have been carried out in recent years by several researchers (Wang *et al*., 2002B; Wang, 2001; Qu *et al*., 2001). In Chapter 2, thermodynamic analysis of a combined heat and mass recovery cycle is described. Although some good results are obtained, the models gave only the COP values without any information on the transient heat and mass transfer process. Numerical studies for intermittent cycle single bed systems with combined heat and mass transfer were performed by many investigators to predict the thermal performance of such systems (Ben Amar *et al*., 1996; Zhang, 2000, Marletta *et al*., 2002). However, these studies also did not take into account the transient heat and mass transfer processes in these advanced cycles. Poyelle *et al*. (1999) proposed a simple one-dimensional numerical model for a heat and mass recovery adsorption-based air conditioning cycles. Mass transfer limitations were

taken into account in their model. By assuming a parabolic pressure profile through the adsorbent bed, the average pressure inside the adsorbent was predicted. Although their model fitted the experimental data very well, there was a need to specify some empirical parameters *a priori*. From the above brief literature review, it can be seen that it is necessary to set up a more detailed model for the combined heat and mass recovery cycle. Based on the numerical model for intermittent cycle proposed in Chapter 5, this chapter presents a two-dimensional heat and mass transfer model of a combined heat and mass recovery adsorption cycle.

6.2 SYSTEM DESCRIPTION

The adsorption cooling system based on the zeolite-NaX/water pair modelled in this study is shown in Figure 6.1. This system consists of six major components including two adsorbers, external heat and cooling systems, a condenser and an evaporator. Compared to the one-adsorber system, a two-adsorber cycle provides cooling on a more continuous basis (see Figure 6.2). At the beginning of this two-bed cooling cycle, the adsorbent bed is at the state of point a and another bed is in the state of point c in Figure 6.2. The mass recovery phase then starts. The two adsorbers are interconnected directly and the refrigerant vapour will flow from the high-pressure to the low-pressure adsorber. This process is maintained until the two beds reach the same pressure (points e and e') and the two adsorbers are disconnected. Subsequently, the heat recovery phase is carried out from point e to point f for Adsorbent Bed 1 and from point e' to point f' for the other bed. During this phase, no heat is supplied by the external heating system and an amount of heat of Q_r is exchanged between the two adsorbers. Finally, the two adsorbent beds are connected to the external heating or cooling system, respectively. It can be seen from Figure 6.2 that the mass of cycled refrigerant will be increased by using the mass recovery cycle compared with the basic cycle, which leads to an increased value of cooling energy (Q_{ev}). Figure 6.2 also shows that the

amount of heat from external heat source Q_h will decrease by using a heat recovery phase between two of the adsorbers. Therefore, the COP will be increased for the combined heat and mass recovery cycle compared to the basic cycle (See Equation 1-1 in Chapter 1).

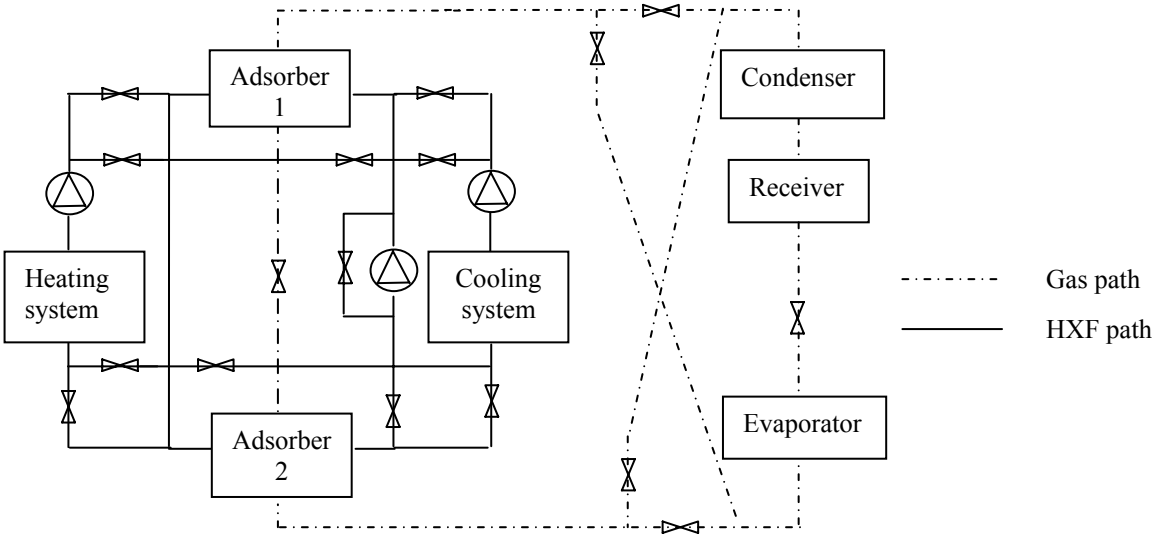

Figure 6.1 Schematic diagram of two-bed adsorption refrigeration system with heat and mass recovery

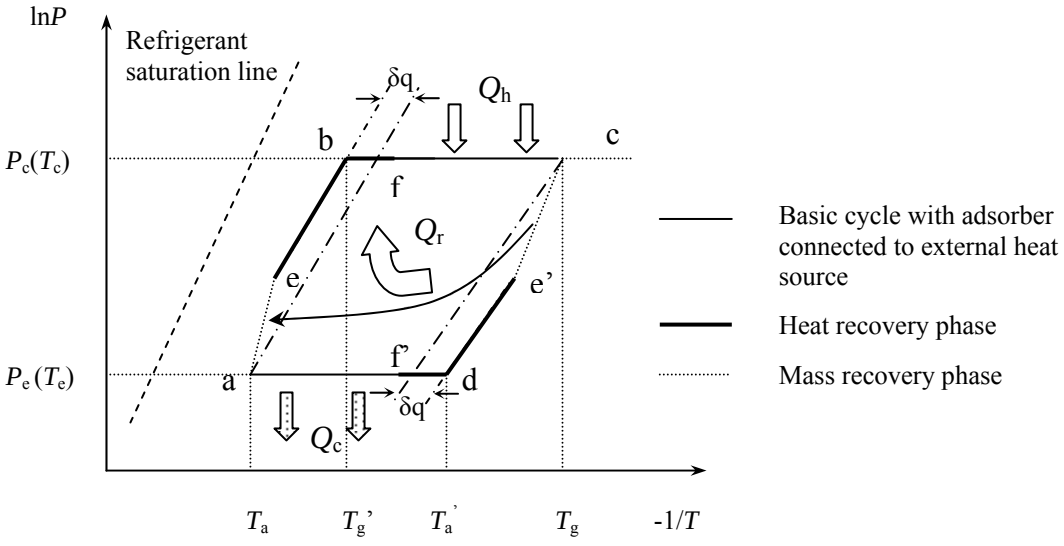

Figure 6.2 Clapeyron diagram of combined heat and mass recovery cycle

6.3 MATHEMATICAL MODELLING

The adsorber modelled in this study is the same as that described in Chapter 5 (see Figure 5.1). The mathematical model describes the process, which is related to heat transfer between different components of the entire cooling system and mass transfer of refrigerant vapour in or between the two adsorbers. The energy and mass conservation equations of this model are the same as those described in Chapter 5 [Equations (5-23)-(5-27)], while the boundary conditions are different during the heat and mass recovery phases.

The initial and boundary conditions are listed below to complete the numerical formulation of the problem.

Initial conditions:

For $t = 0$ $T_f(z,r) = T_{cin}$; $T_m(z,r) = T_s(z,r) = T_a$; $P = P_e$ (Adsorber 1) (6-1)

For $t = 0$ $T_f(z,r) = T_m(z,r) = T_s(z,r) = T_g$; $P = P_c$ (Adsorber 2) (6-2)

Boundary Conditions:

$$\frac{\partial T_f}{\partial z}\Big|_{z=0} = \frac{\partial T_f}{\partial z}\Big|_{z=L} = 0 \quad \text{during mass recovery phase} \tag{6-3}$$

$$T_{f1}\big|_{z=0} = T_{f2}\big|_{z=L}; \quad T_{f2}\big|_{z=0} = T_{f1}\big|_{z=L} \quad \text{during heat recovery phase} \tag{6-4}$$

$$T_f\big|_{z=0} = T_{hin} \quad \text{when connected to external heating system} \tag{6-5}$$

$$T_f\big|_{z=0} = T_{cin} \quad \text{when connected to external cooling system} \tag{6-6}$$

$$\frac{\partial T_m}{\partial z}\Big|_{z=0} = \frac{\partial T_m}{\partial z}\Big|_{z=L} = 0 \tag{6-7}$$

$$\frac{\partial T_s}{\partial z}\Big|_{z=0} = \frac{\partial T_s}{\partial z}\Big|_{z=L} = \frac{\partial T_s}{\partial r}\Big|_{r=R} = 0 \tag{6-8}$$

$$P_1\big|_{z=0} = P_1\big|_{z=L} = P_1\big|_{r=R} = P_a \quad \text{during mass recovery phase for Adsorber 1} \tag{6-9}$$

$$P_2\big|_{z=0} = P_2\big|_{z=L} = P_2\big|_{r=R} = P_a \quad \text{during mass recovery phase for Adsorber 2} \tag{6-10}$$

$$\frac{\partial P}{\partial z}\Big|_{z=0} = \frac{\partial P}{\partial z}\Big|_{z=L} = \frac{\partial P}{\partial r}\Big|_{r=R} = 0 \tag{6-11}$$

$$P\big|_{z=0} = P\big|_{z=L} = P\big|_{r=R} = P_e \quad \text{when connected to evaporator} \tag{6-12}$$

$$P\big|_{z=0} = P\big|_{z=L} = P\big|_{r=R} = P_c \quad \text{when connected to condenser} \tag{6-13}$$

where the symbols with subscripts 1 and 2 represent the properties of Adsorbers 1 and 2, respectively. Otherwise, these boundary conditions are suitable for the two adsorbers. During the heat recovery phase, the outlet temperature of heat exchange fluid in the high temperature adsorber is equal to the inlet temperature of the fluid in the low temperature adsorber. P_a is the pressure in the space between the adsorbent and the shell during the mass recovery phase, and it is assumed to be equal for the two adsorbers during the mass recovery phase. During the mass recovery phase, the water vapour will be transferred from Adsorber 2 to Adsorber 1, and the entire system is closed. Thus, the total mass flux for the system is zero and is presented as

$$\iint_{S1} \rho_g \boldsymbol{u}\cdot\boldsymbol{n}dS + \iint_{S2} \rho_g \boldsymbol{u}\cdot\boldsymbol{n}dS = 0 \tag{6-14}$$

where S1 and S2 are the boundary surfaces for the two different adsorbers, respectively and $\boldsymbol{n}$ is the outward normal vector of the surface area. Substituting Darcy's equation into Equation (6-14), we have

$$\iint_{S1} \rho_g \frac{K_{ap}}{\mu}\nabla P\cdot\boldsymbol{n}dS + \iint_{S2} \rho_g \frac{K_{ap}}{\mu}\nabla P\cdot\boldsymbol{n}dS = 0 \tag{6-15}$$

The first term in Equation (6-15) can be simplified as

$$\begin{aligned}\iint_{S1} \rho_g \frac{K_{ap}}{\mu}\nabla P\cdot\mathbf{n}dS &= \int_{s1}(2\pi r \frac{\rho_g K_{ap}}{\mu}\frac{\partial P}{\partial z})_{z=0}dr \\ &+ \int_{s1}(2\pi r \frac{\rho_g K_{ap}}{\mu}\frac{\partial P}{\partial z})_{z=L}dr + \int_{s1}(2\pi R \frac{\rho_g K_{ap}}{\mu}\frac{\partial P}{\partial r})_{r=R}dz\end{aligned} \tag{6-16}$$

The simplification of the second term of Equation (6-15) is the same as Equation (6-16) with subscript 1 changed to 2. By using Equation (6-16), Equation (6-15) is discretized as follows:

$$\begin{aligned}&\sum_{r=R_1,R}^{s1}\left\{2\pi r\left(\frac{\rho_g K_{ap}}{\mu}\right)\Big|_{w2}^{0}\cdot\frac{(P_a-P|_{w2}^{0})}{\Delta z}+2\pi r\left(\frac{\rho_g K_{ap}}{\mu}\right)\Big|_{e2}^{0}\cdot\frac{(P_a-P|_{e2}^{0})}{\Delta z}\right\}\\&+\sum_{z=0,L}^{s1}\left\{2\pi R\left(\frac{\rho_g K_{ap}}{\mu}\right)\Big|_{n2}^{0}\cdot\frac{(P_a-P|_{n2}^{0})}{\Delta r}\right\}=\sum_{r=R_2,R}^{s2}\left\{2\pi r\left(\frac{\rho_g K_{ap}}{\mu}\right)\Big|_{w2}^{0}\cdot\frac{(P|_{w2}^{0}-P_a)}{\Delta z}+2\pi r\left(\frac{\rho_g K_{ap}}{\mu}\right)\Big|_{e2}^{0}\cdot\frac{(P|_{e2}^{0}-P_a)}{\Delta z}\right\}\\&+\sum_{z=0,L}^{s2}\left\{2\pi R\left(\frac{\rho_g K_{ap}}{\mu}\right)\Big|_{n2}^{0}\cdot\frac{(P|_{n2}^{0}-P_a)}{\Delta r}\right\}\end{aligned}\tag{6-17}$$

where superscripts s1 and s2 represent Adsorber 1 and Adsorber 2, respectively. Superscript 0 refers to the value of the last time step. Subscripts w2, e2 and n2 represent the control volume beside the boundary in the west, east and north directions, respectively. The value of P_a can be calculated from Equation (6-17).

To simplify the solution of the governing equations, the heat and mass conservation equations in this numerical model are arranged in dimensionless forms as follows:

$$\frac{\partial\theta_f}{\partial\tau}+v_f^*\frac{\partial\theta_f}{\partial z^*}=\frac{\partial}{\partial z^*}\left(\frac{1}{Pe_f}\frac{\partial\theta_f}{\partial z^*}\right)+\frac{1}{Ar^2}\cdot\frac{1}{r^*}\frac{\partial}{\partial r^*}\left(\frac{r^*}{Pe_f}\frac{\partial\theta_f}{\partial r^*}\right)\tag{6-18}$$

$$\frac{\partial\theta_m}{\partial\tau}=\frac{\partial}{\partial z^*}\left(\frac{1}{Pe_m}\frac{\partial\theta_m}{\partial z^*}\right)+\frac{1}{Ar^2}\cdot\frac{1}{r^*}\frac{\partial}{\partial r^*}\left(\frac{r^*}{Pe_m}\frac{\partial\theta_m}{\partial r^*}\right)\tag{6-19}$$

$$\begin{aligned}&(1+r_a\Omega+r_g)\frac{\partial\theta_s}{\partial\tau}+r_g\left(u^*\frac{\partial\theta_s}{\partial z^*}+\frac{v^*}{Ar}\cdot\frac{\partial\theta_s}{\partial r^*}\right)=\frac{1}{Pe_s}\left[\frac{\partial^2\theta_s}{\partial z^{*2}}+\frac{1}{Ar^2}\frac{\partial\left(r^*\frac{\partial\theta_s}{\partial r^*}\right)}{r^*\cdot\partial r^*}\right]\\&+\left[(\theta_s-\theta_r)\cdot(r_g'-r_a)+\beta\right]\frac{\partial\Omega}{\partial\tau}\end{aligned}\tag{6-20}$$

$$\Lambda_1\frac{\partial\omega}{\partial\tau}-\Lambda_2\frac{\partial\theta_s}{\partial\tau}=\frac{\partial}{\partial z^*}\left[\frac{1}{Pe_s'}\frac{\partial\omega}{\partial z^*}+\frac{1}{Ar^2}\cdot\frac{1}{r^*}\frac{\partial}{\partial r^*}\left(\frac{r^*}{Pe_s'}\frac{\partial\omega}{\partial r^*}\right)\right]-\frac{\partial\Omega}{\partial\tau}\tag{6-21}$$

where the following dimensionless variables are introduced:

$$\tau=\frac{V_{\max}\cdot t}{L},\quad z^*=\frac{z}{L},\quad r^*=\frac{r}{R},\quad \omega=\frac{P-P_0}{\Delta P},\quad \Omega=\frac{\bar{q}}{q_{\max}}$$

$$\theta_s = \frac{T_s - T_0}{\Delta T}, \quad \theta_m = \frac{T_m - T_0}{\Delta T}, \quad \theta_f = \frac{T_f - T_0}{\Delta T}$$

$$V_f^* = \frac{V_f}{V_{\max}}, \quad u^* = \frac{u}{V_{\max}}, \quad v^* = \frac{v}{V_{\max}}$$

where *0* refers to the initial value, $q_{\max}$ is the reference adsorbed amount, $V_{\max}$ is the reference velocity, ΔT is the reference temperature variation and ΔP is the reference pressure variation. The dimensionless parameters are

$$Ar = \frac{R}{L}, \quad Pe_s = \frac{V_{\max} L \rho_s C_{ps}}{\lambda_s}, \quad Pe_m = \frac{V_{\max} L \rho_m C_{pm}}{\lambda_m}, \quad Pe_f = \frac{V_{\max} L \rho_f C_{pf}}{\lambda_f}$$

$$Pe_s' = \frac{V_{\max} L \rho_s q_{\max} \mu}{\Delta P \cdot \rho_g K_{ap}}, \quad r_g = \frac{\rho_g C_{pg}}{\rho_s C_{ps}}, \quad r_a = \frac{C_{pa}}{C_{ps}} \cdot q_{\max}, \quad , r_g' = \frac{C_{pg}}{C_{ps}}, \quad \theta_R = \frac{T_0}{\Delta T}, \quad \omega_R = \frac{P_0}{\Delta P}$$

$$\beta = \frac{\Delta H \cdot q_{\max}}{\Delta T \cdot C_{ps}}, \quad \Lambda_1 = \frac{\varepsilon \cdot \rho_g}{\rho_s (\omega + \omega_R) q_{\max}}, \quad \Lambda_2 = \frac{\varepsilon \cdot \rho_g}{\rho_s (\theta_s + \theta_R) q_{\max}}$$

6.4 BASE-CASE STUDY

A computer programme was written based on the numerical methodology mentioned in Section 5.3 (Chapter 5) to solve the model. Some operating conditions of the base case used in the model are listed in Table 6.1.

6.4.1 Analysis of mass recovery phase

The mass recovery phase is expected to accelerate the circulation and enhance the performance of the cycle. By using the mass recovery process, the quantity of refrigerant (Δm) in the evaporator is increased. The entire quantity of the cycled refrigerant can be written as

$$\Delta m = m_s (q_{\max} - q_{\min}) = m_s \Delta q \tag{6-22}$$

where Δq is the adsorbed amount change during the cooling cycle, which is given by $\Delta q = \Delta q_0 + \delta q$. δq is the increase in adsorbed amount due to mass recovery.

Table 6.1 Operating conditions for the base case

Name	Symbol	Value
Average velocity of heat transfer fluid	u_f	1 m/s
Adsorption temperature	T_a	318 K
Generation temperature	T_g	473 K
Fluid inlet temperature during heating	T_{hin}	493 K
Fluid inlet temperature during cooling	T_{cin}	298 K
Evaporator temperature	T_e	279 K
Condenser temperature	T_c	318 K
Mass recovery time	t_m	55 s
Heat recovery time	t_h	3700 s
Reference velocity	V_{max}	2 m/s
Reference adsorbed amount	q_{max}	0.2447 kg/kg
Reference temperature variation	ΔT	155 K
Reference pressure variation	ΔP	9000 Pa

As mentioned in Section 6.2, the mass recovery phase starts with the connection of the two adsorbers. The refrigerant vapour will be transferred from Adsorber 2 to Adsorber 1 because of the difference in pressure of both adsorbers. This phase will end when the pressure is equalised in the two adsorbers. The variations of the average pressure for both adsorbers with time are shown in Figure 6.3. It can be seen that the pressure of the low temperature adsorber (Adsorber 1) increases to a maximum value in a very short time. At the same time, the pressure change is not as large as that in the higher temperature adsorber (Adsorber 2). When the two adsorbers are connected, the refrigerant is transferred from Adsorber 1 to Adsorber 2. The mass of refrigerant vapour will increase quickly and cannot be adsorbed in time in Adsorber 1 because of intra-particle mass transfer limitation for the adsorption process. This will lead to a rapid increase in the pressure. Compared with Adsorber 1, Adsorber 2 has higher diffusivity [see Equation (5-22)] because of its higher temperature. Thus the intra-particle mass transfer resistance in Adsorber 2 is smaller than that of Adsorber 1. Hence, the pressure change in the higher temperature adsorber is smaller than that of the other adsorber. With increasing time, the refrigerant vapour will be adsorbed in the adsorbent

and will tend towards the equilibrium state with adsorbed phase. Therefore, the pressure will decrease slowly.

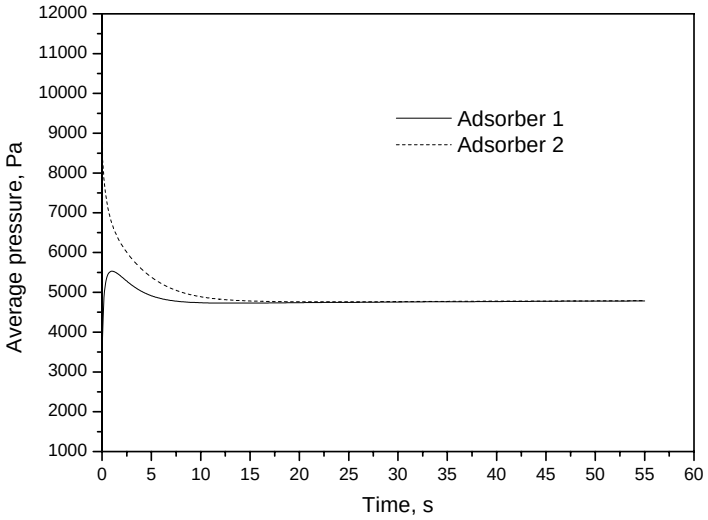

Figure 6.3 Variation of average pressure with time during the mass recovery phase

Figure 6.4 shows the variations of average adsorbed amount of the two adsorbers with time during the mass recovery phase. From Figure 6.4, the adsorbed amount of Adsorber 1 increases and that of Adsorber 2 decreases with time during the mass recovery phase, with both adsorbed amounts tending to a constant value. It can also be seen that the adsorbed amount change for Adsorber 1 is almost equal to that of Adsorber 2. This also verifies the accuracy of the results because the entire system is closed and total mass flux is zero [Equation (6-14)]. The trend of pressure variation with the time (Figure 6.3) is very different from the trend of increase in adsorbed mass (Figure 6.4) because of internal mass transfer limitation.

Figure 6.5 shows the variation of temperature of the two adsorbers during mass recovery phase. It can be seen that the temperature in Adsorber 1 increases very quickly at the beginning of mass recovery phase and then decreases slightly. The variation of temperature in Adsorber 2 also behaves in the opposite manner. This is because the increase in adsorbed amount in Adsorber 1 which releases adsorption heat causes the temperature of the adsorbent

bed to rise. During the mass recovery phase, the adsorbent bed in Adsorber 1 is cooled by heat exchange fluid which absorbs heat from the adsorbent bed. When the adsorption process is almost completed, no more adsorption heat will be released causing the temperature of adsorbent bed to decrease.

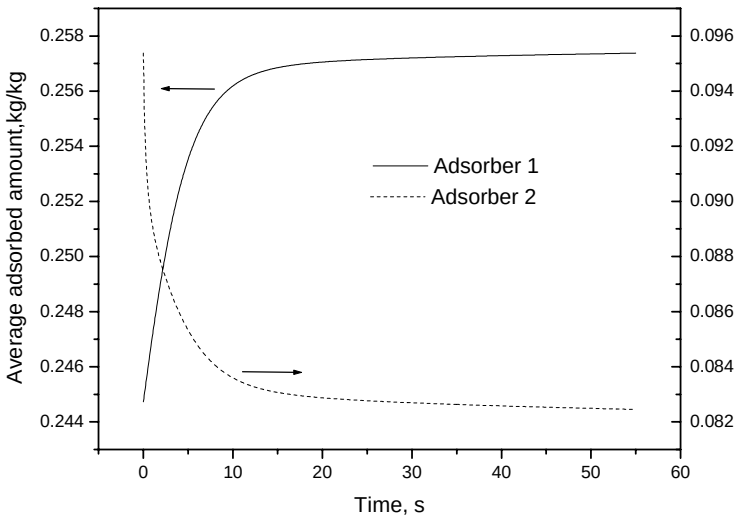

Figure 6.4 Variation of average adsorbed amount with time during the mass recovery phase

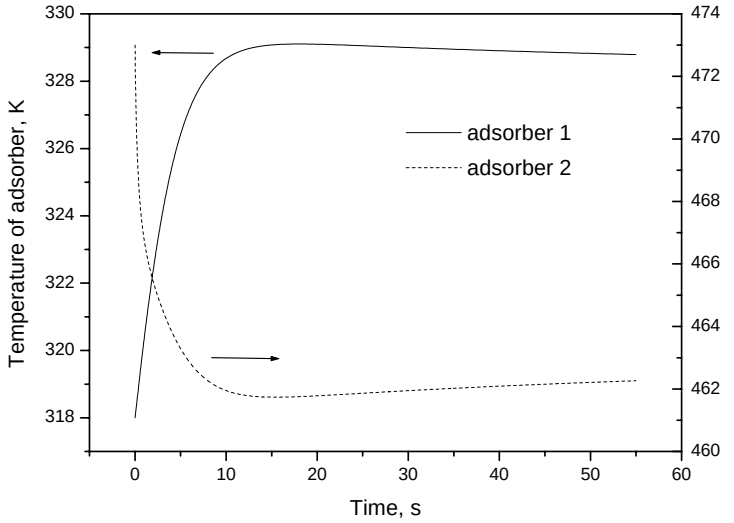

Figure 6.5 Variation of average temperature with time during the mass recovery phase

The mass recovery process happens very quickly. The 99% adsorbed amount is completed in less than 35 s. This means that the performance can be improved by using a mass recovery phase without significant increase in the cycle time.

6.4.2 Results of combined heat and mass recovery cycle

In this section, the numerical simulation results of the adsorption cooling cycle with combined heat and mass recovery phase are presented.

The profiles of temperature, pressure and adsorbed amount of adsorbate with time are shown in Figures 6.6 to 6.8. From Figure 6.6, it can be seen that temperature increases rapidly during the mass recovery phase. The adsorption process carried out during the mass recovery phase and the adsorption heat released to adsorbent caused the adsorbent temperature to increase. The same figure also shows that the slope of the heat recovery phase will be lower than that of the basic cycle phase. For the heat recovery phase, the temperature gap between the two adsorbers is not as high compared to the gap between the adsorber and external heat source or heat sink. The variation of pressure shown in Figure 6.7 is similar to the ideal case. The pressure becomes a constant after a rapid and significant change for every half cycle. It can be deduced from Figure 6.8 that the adsorbed amount will be almost a constant after mass recovery until the adsorber is connected to evaporator or condenser. The quantity of refrigerant vapour is also increased by the mass recovery phase as can be seen from the same figure.

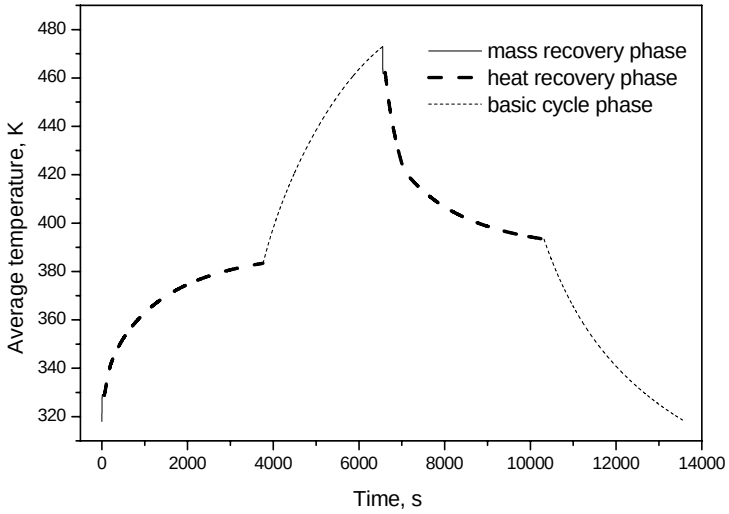

Figure 6.6 Variation of average temperature with time for the whole cycle

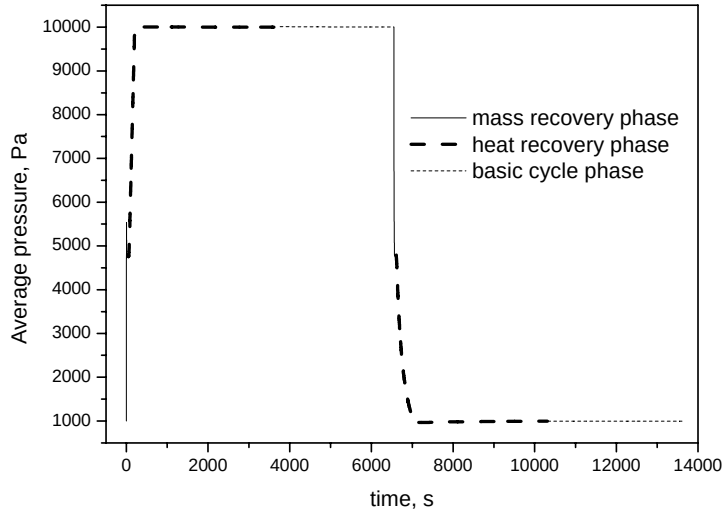

Figure 6.7 Variation of average pressure with time for the whole cycle

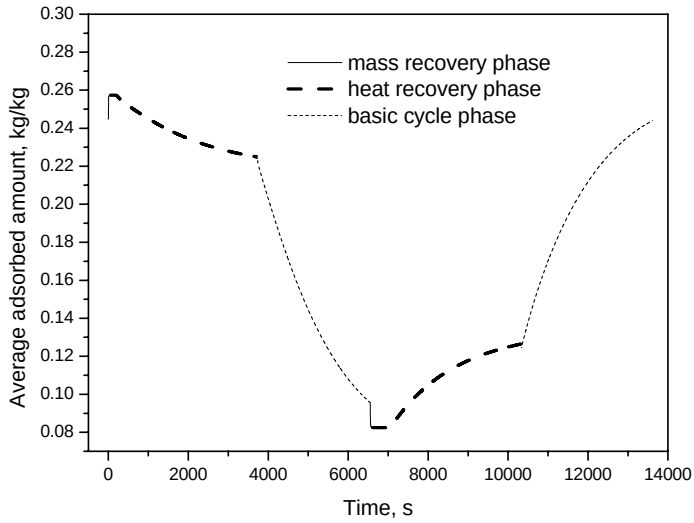

Figure 6.8 Variation of average adsorbed amount with time for the whole cycle

Figure 6.9 shows a comparison between the combined heat and mass recovery adsorption cycle and the basic cycle. It can be clearly seen that the gap of the two isosteric lines (see Figure 1.5 phase a-b and phase c-d) is increased. This means that more refrigerant vapour is recycled compared with the basic cycle leading to an increase in cooling power produced. From Figure 6.9, it can also be seen that pressure is not a constant during the isobaric adsorption phase (see Figure 1-5 phase d-a) for the basic cycle. Marletta *et al.* (2002) suggested that this phenomenon could be the result of mass transfer limitation. However, for a cycle incorporating a combined heat and mass recovery phase, this phenomenon is not obvious. The effect of mass transfer limitation is reduced. When the adsorber is connected to the evaporator, the temperature gap between adsorber with heat exchange fluid for heat and mass recovery cycle is smaller than that for a basic cycle. Hence, the mass flux of vapour from the evaporator to the adsorber of this advanced cycle is smaller than that of the basic cycle. Based on the same permeability, the pressure gradient in the adsorbent bed of this

advanced cycle is also smaller than that of basic cycle. Thus the average pressure in the heat mass recovery cycle is closer to the ideal pressure.

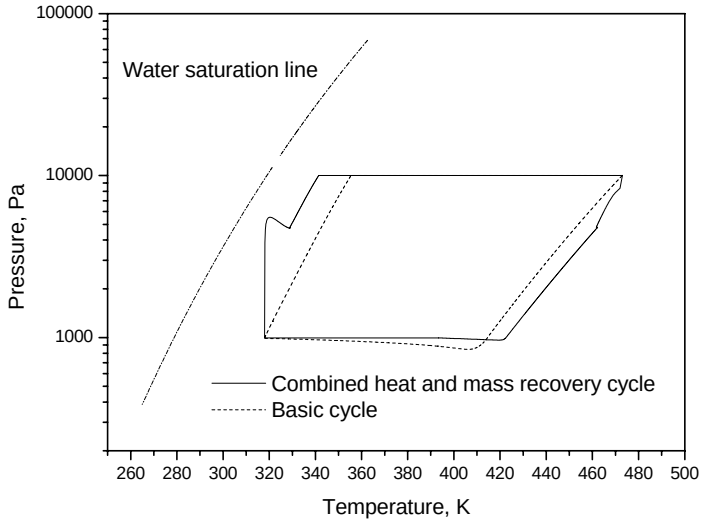

Figure 6.9 Comparison of combined heat and mass recovery adsorption cycle and basic cycle

The variations of heat transfer rate between adsorber and heat exchange fluid for different phases are shown in Figure 6.10. From this figure, it can be clearly seen that the heat transfer rate during the heat recovery phase is lower than that during the basic cycle phase. This is because of the lower temperature gap between the adsorber and heat exchange fluid during the heat recovery phase compared with the basic cycle phase. In Figure 6.10, area A represents the heat recovery energy (Q_r) and area B represents the heat input (Q_h). For fixed operating temperature, the heat input (Q_h) will decrease while the heat recovery energy (Q_r) increases since the total heat needed should be a constant. Hence, the COP will increase with an increase in Q_r.

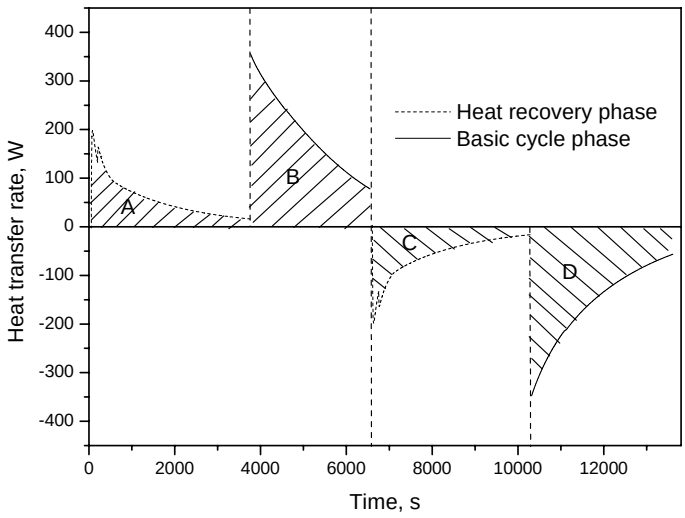

Figure 6.10 Variation of heat transfer rate between adsorber and heat exchange fluid

6.4.3 Cycle Performance

The main aim of using a combined heat and mass recovery cycle is to improve system performance. Table 6.2 shows the calculated performance for different cycle types. It can be seen that for a cycle employing only mass recovery, the values of COP and SCP are both increased compared with the basic cycle. However, for a combined heat and mass recovery cycle, the significant increase in COP (by 47%) is accompanied by a reduction of about 40% in the SCP.

Table 6.2 Performance for different cycle types

Cycle Type	COP	SCP, W/kg	Remarks
Basic cycle	0.44	48.8	t_c = 7076 s
Adsorption cycle with only mass recovery	0.47	52.0	t_m = 55 s
Adsorption cycle with combined heat and mass recovery	0.65	27.6	

The results of the numerical simulation for the base case shown in Table 6.2 can be compared with the results of Poyelle *et al*. (1999). For about the same operating temperature, the COP obtained in this study is 0.65, which is the same as that calculated by Poyelle *et al*. (1999) without considering mass transfer resistance. Their experimental COP is 0.41, which is lower than that calculated in this study. This can be explained by the fact that the permeability (10^{-13} m^2) used in their adsorbent bed is almost 5 times less than the permeability used in this study. Thus, the effect of mass transfer resistance in Poyelle *et al*.'s work is more significant and this effect resulted in a reduction in the COP.

Since the mass recovery phase can be completed very quickly, heat recovery time becomes a very important control parameter for system performance. Figure 6.11 shows the effect of heat recovery time on the performance of an adsorption cycle employing heat and mass recovery. It can be seen that COP increases and tends to a constant value with an increase in heat recovery time. This is due to the decrease in Q_h with an increase of heat recovery time. The temperature difference between the two adsorbers will become smaller compared with the temperature difference between the adsorber and external heat source. Hence, the heat exchange rate during the heat recovery phase is small compared to the basic cycle. The total cycle time will then increase with an increase in the heat recovery time leading to a reduction in SCP (See Figure 6.12). Both COP and SCP should be considered in the design of an adsorption cooling system. For different systems, the COP and SCP may be assigned different weights depending on their relative importance. For systems utilising waste heat, SCP is more important as the user is only concerned with the cooling power produced since the cost of producing the heat is negligible. For other systems, COP may be more important compared to SCP since the heat input is fixed. Thus, the selection of operating conditions should consider the specific demands of the system.

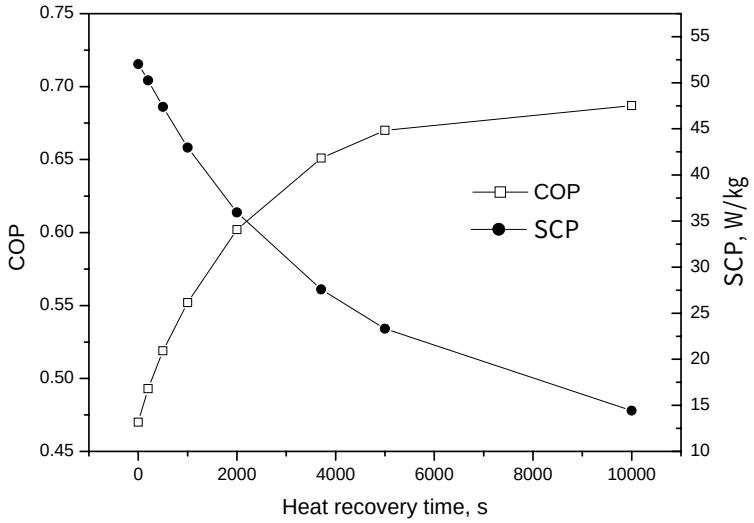

Figure 6.11 Variation of performance parameters with heat recovery time

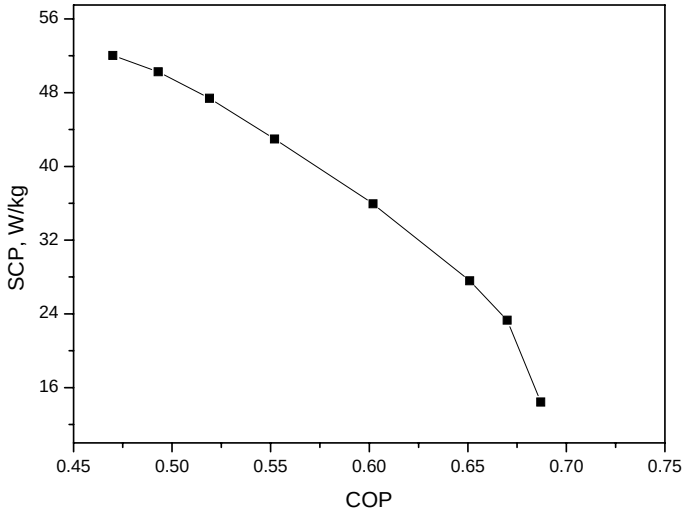

Figure 6.12 Variation of the value of SCP with COP

6.5 EFFECTS OF PARAMETERS AND OPERATING CONDITIONS

6.5.1 Degree of heat recovery

It is established in Section 6.4 that the temperature gap between the two adsorbers will decrease with an increase in heat recovery time. It is also mentioned that there is less heat recovery produced with the increase of heat recovery time. When the temperature gap becomes zero, heat recovery will be completed since no heat energy can be produced. Here, a parameter, D_{hr}, is defined to describe the degree of the fulfillment of the heat recovery process:

$$D_{hr} = \left(1 - \frac{\Delta T}{T_g - T_a}\right) \times 100\% \qquad (6\text{-}23)$$

where ΔT is the temperature gap between the two adsorbers, T_g is the generation temperature and T_a is the initial adsorption temperature.

Figure 6.13 shows the variation of degree of heat recovery and heat recovery power with heat recovery time. It can be seen that D_{hr} increases quickly with heat recovery time at the beginning of heat recovery. However, when D_{hr} is greater than 90%, the rate of increase slows down. At that time, the value of the heat recovery power is less than 10% of the maximum value. From Figure 6.14, it can be seen that when D_{hr} becomes greater than 90%, the marginal increase in COP brings about a severe decrease in SCP. This is due to the much smaller heat exchange rate between the two beds when the degree of the heat recovery process is over 90%. A small increase in COP will lead to a large increase in the heat recovery time, which in turn increases the total cycle time significantly.

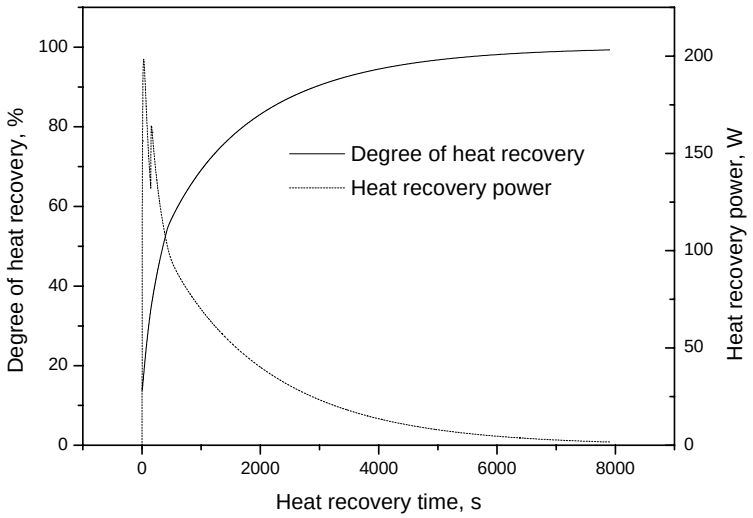

Figure 6.13 Variation of degree of heat recovery and heat recovery power with heat recovery time

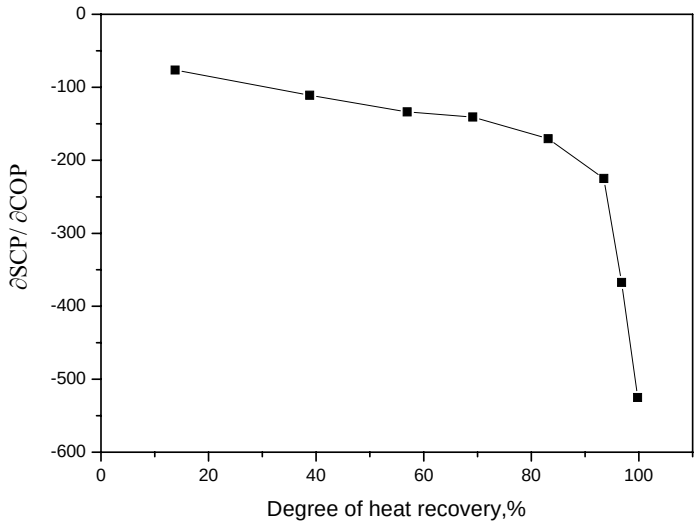

Figure 6.14 Variation of ∂SCP/ ∂COP with degree of heat recovery

6.5.2 Driven temperature

The driven temperature is defined as the temperature of the heat exchange fluid. In this analysis, a constant temperature difference of 20 K is maintained between the generation temperature and the driven temperature. Variations of COP and SCP with driven temperature for different degrees of heat recovery are shown in Figures 6.15 and 6.16, respectively. It can be seen that both COP and SCP increases with an increase in the driven temperature of heat exchange fluid which will in turn lead to an increase in the generation temperature. It is known that the COP value of the basic cycle will increase with an increase in the generation temperature as discussed in Chapter 5. From the simulation results, the ratio of heat recovery energy to heat input of the basic cycle will increase with generation temperature for the same degree of heat recovery. The heat recovery process reduces the value of the heat input from external heat source but does not change the value of the cooling energy. Hence, the COP of the combined heat and mass recovery cycle becomes larger for a higher driven temperature. The cycled mass of refrigerant will increase with an increase in the generation temperature. Therefore, the cooling energy will also increase. Since the total cycle time does not increase very much with the increase of driven temperature of the heat exchange fluid, the value of SCP also increases. Although a high driven temperature can improve the system performance, safety issues and heat loss for the high temperature heat exchange fluid need be addressed in actual applications.

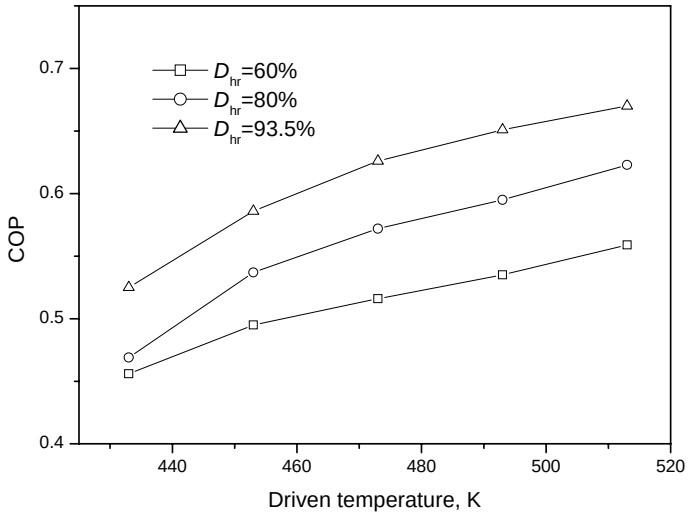

Figure 6.15 Variation of COP with driven temperature

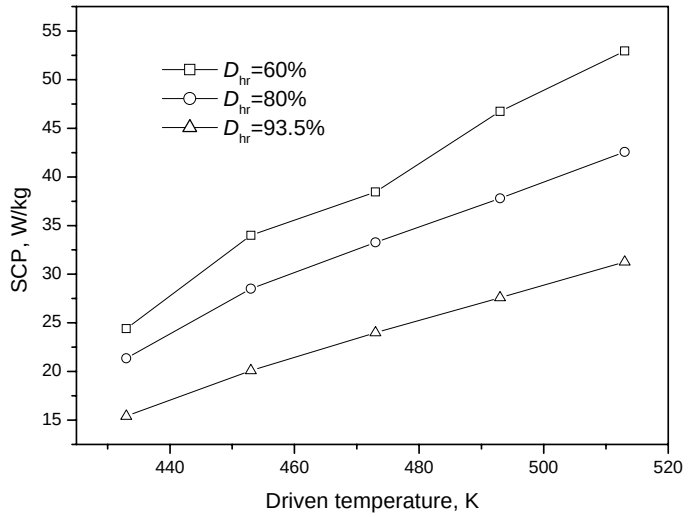

Figure 6.16 Variation of SCP with driven temperature

6.5.3 Thermal conductivity of adsorbent bed

Many researchers (Groll, 1993; Pons *et al.*, 1996; Marletta *et al.*, 2002) have investigated the enhancement of heat transfer in the adsorbent bed in order to improve the performance of adsorption cooling systems. One way to enhance the heat transfer in the adsorbent bed is to

use adsorbents of higher thermal conductivity. Figures 6.17 and 6.18 show the variations of COP and SCP with thermal conductivity of the adsorbent bed for a combined heat and mass recovery cycle. It can be seen from Figure 6.17 that thermal conductivity has negligible effect on the magnitude of the COP but it has a significant effect on the SCP. This is primarily because of the fact that the bed thermal conductivity has no effect on the heat input and cooling energy produced under fixed operating temperatures. In addition, the heat transfer rate between the adsorbent bed and heat exchange fluid will increase with an increase in the thermal conductivity of adsorbent bed resulting in a reduction of cycle time. Thus, the value of SCP increases with an increase in bed thermal conductivity (see Figure 6.18). In general, an increase in thermal conductivity has a positive effect on the system performance of the combined heat and mass recovery cycle.

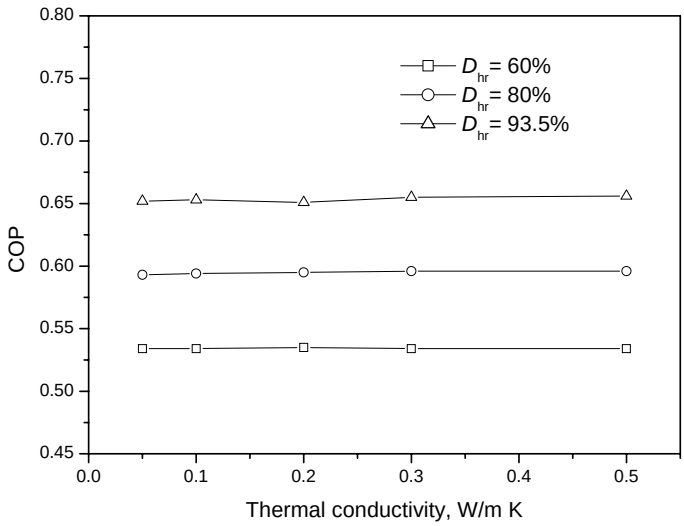

Figure 6.17 Variation of COP with thermal conductivity of adsorbent bed

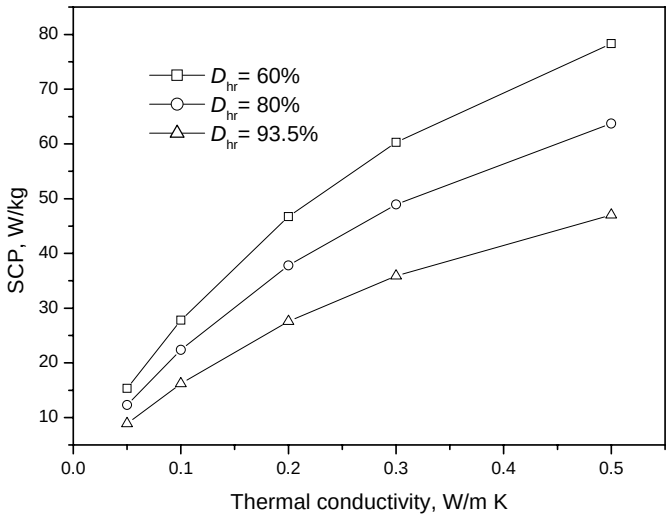

Figure 6.18 Variation of SCP with thermal conductivity of adsorbent bed

6.5.4 Velocity of heat exchange fluid

The effect of the velocity of heat exchange fluid on the performance coefficients are shown in Figures 6.19 and 6.20. Since the heat input and cooling energy are not affected by the velocity of the heat exchange fluid, there will also be very little effect on the COP (see Figure 6.19). When the fluid velocity is smaller than 0.01 m/s, the cycle time will increase very quickly with an increase in fluid velocity. The temperature gradient of the fluid inside the metal tube in the axial direction will increase for a lower fluid velocity. Therefore, the total heat exchange rate between the two beds and between the bed and external heat source will decrease, resulting in an increase in the cycle time. Hence, when the velocity is smaller than a certain value, the SCP decreases significantly with the reduction of velocity (Figure 6.20). However, for velocities larger than 0.5 m/s, the cycle time does not change with velocity thus leading to negligible change in SCP. The optimal velocity of the heat exchange fluid should be in the range of 0.1 – 0.5 m/s.

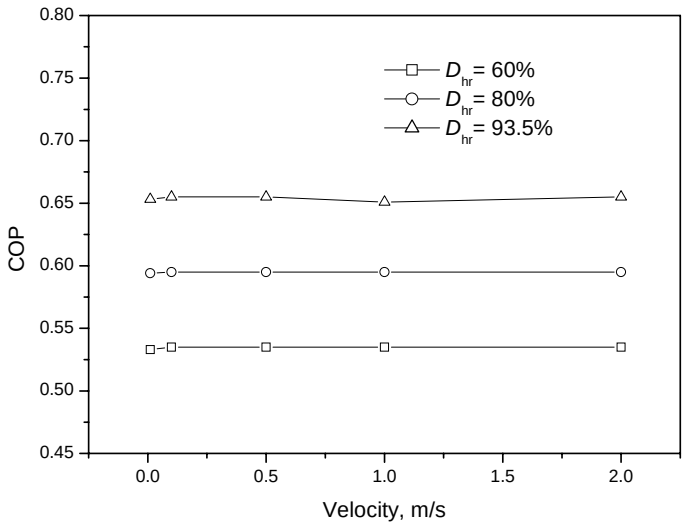

Figure 6.19 Variation of COP with velocity of heat exchange fluid

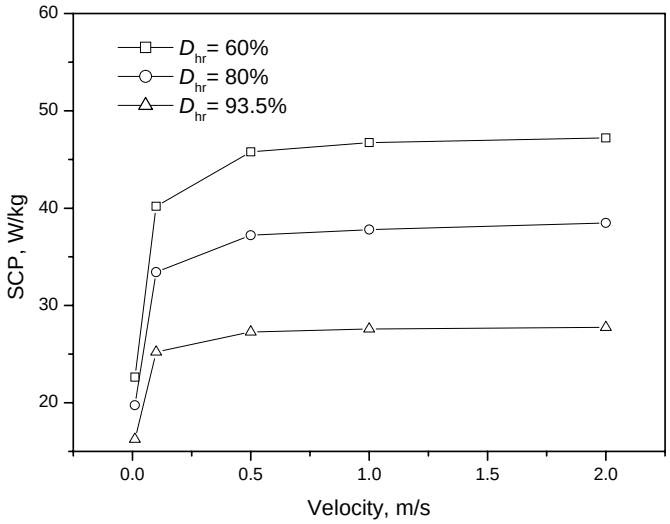

Figure 6.20 Variation of SCP with velocity of heat exchange fluid

6.5.5 Thickness of adsorbent bed

The adsorbent bed thickness is an important parameter that has great influence on the performance of an adsorption cooling cycle. Figures 6.21 and 6.22 show the effect of bed

thickness on the COP and SCP for a combined heat and mass recovery cycle. It can be seen that the COP increases with an increase in adsorbent thickness. On the contrary, the SCP reduces with an increase in adsorbent thickness. For a large thickness, the heat capacity ratio of the metal tube to adsorbent bed will decrease. This means that the heat input to the metal tube will decrease leading to an increase in COP. When the thickness is increased beyond a certain value, the heat energy consumed by the metal tube is rather small compared with the total heat input. Therefore, the COP tends to a constant value for a large thickness of the adsorbent bed. Although a larger thickness means more adsorbate can be driven into cycling, the thermal resistance is also larger. Consequently, the heat exchange rate during the basic cycle process and heat recovery process is reduced contributing to a longer cycle time and a reduction in the SCP.

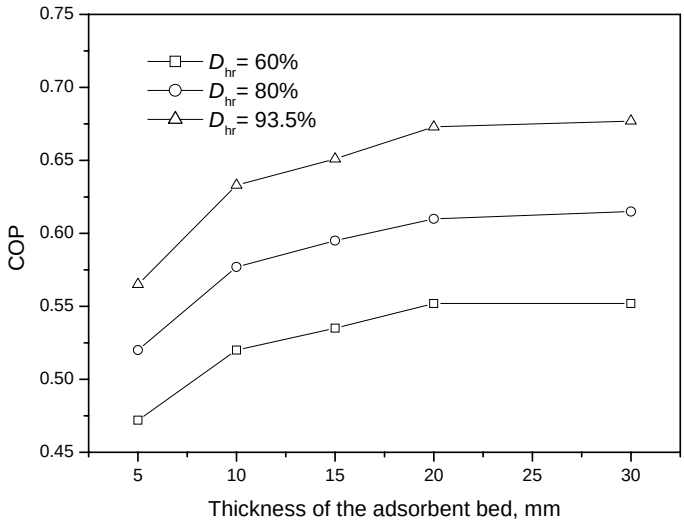

Figure 6.21 Variation of COP with thickness of adsorbent bed

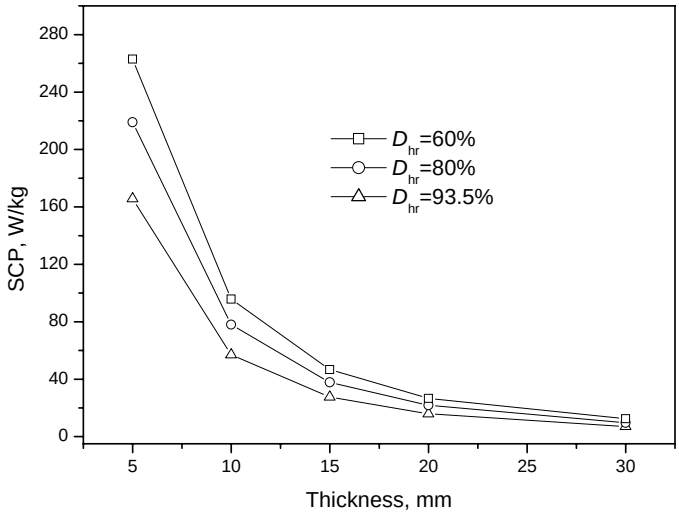

Figure 6.22 Variation of SCP with thickness of adsorbent bed

6.6 SUMMARY

In this chapter, the numerical transient model proposed in Chapter 5 is extended to describe an adsorption refrigeration system based on the zeolite/water pair and incorporating a combined heat and mass recovery cycle. The resulting heat and mass transfer balance equations in two dimensions are solved by the control volume method.

The mass recovery phase is very short (about 50 seconds) compared to the entire cycle time for the specified operating conditions. By using only the mass recovery cycle, the COP and SCP can be improved by about 6% and 7%, respectively compared to the basic cycle. The COP will increase and tend to a constant value while the SCP reduces with an increase in heat recovery time for the combined heat and mass recovery cycle. For the combined heat and mass recovery cycle with the given conditions, the calculated values of COP and SCP are 0.651 and 27.58 W/kg, respectively. Although there is a significant increase in COP (by about 47 %) as compared with the basic cycle, there is an accompanied reduction in SCP by

about 40 %. Therefore, the selection of the operating conditions should consider the specific situations of the different systems.

The results of the parametric study of system performance yield the following conclusions: (i) The COP of the system increases while its SCP decreases with an increase in the degree of heat recovery (D_{hr}). When D_{hr} becomes greater than 90%, the increase of COP results in a severe decrease in the SCP; (ii) Both COP and SCP increases with an increase in the driven temperature of heat exchange fluid. For very high driven temperatures, safety issues and heat loss should be addressed in actual applications; (iii) Increasing the thermal conductivity of the bed can enhance the heat transfer in the adsorbent bed and reduce the cycle time. It has a positive effect on the system performance; (iv) The SCP of the system can be severely deteriorated when the fluid velocity is below 0.1 m/s. However, for velocities larger than 0.5 m/s, any change in fluid velocity will result in negligible change in the SCP. The optimal velocity of the heat exchange fluid lies within the range of 0.1–0.5 m/s; (v) The COP of the system increases while its SCP decreases with an increase in adsorbent bed thickness.

CHAPTER 7

EXPERIMENTAL STUDY OF AN INTERMITTENT ADSORPTION REFRIGERATION SYSTEM

7.1 INTRODUCTION

Recently, several investigators have proposed detailed heat and mass transfer models for the adsorption refrigeration system without experimental validation (Alam *et al*., 2000; Chahbani *et al*., 2002; Marletta *et al*., 2002). Other researchers validated their models indirectly since parameters such as thermal conductivity and contact resistance were unknowns in their models (Guilleminot *et al*., 1987, Liu *et al*., 1994). In their investigations, these parameters were identified by minimising the errors between simulation results and experiments. Poyelle *et al.* (1999) proposed a simple numerical model and obtained good agreement with their experimental data. However, their model is not comprehensive because they assumed a parabolic pressure profile. This chapter describes an experimental facility set up based on the model proposed in Chapter 5. The parameters required in the model will be measured. The main aim is to validate the model with experimental results.

7.2 MEASUREMENT OF ADSORBENT PROPERTIES

Zeolite 13X was selected as the adsorbent in the project since it possesses satisfactory adsorption ability for use in adsorption refrigeration systems. It has stable adsorption properties under high temperature and possesses high water adsorption capacity. The zeolite adsorbent used in the experimental unit of this study was purchased from Best Chemical Co. Pte Ltd. A photograph of the zeolite adsorbent particles used is shown in Figure 7.1. Table 7.1 shows the thermophysical properties of the zeolite adsorbent.

Figure 7.1 Zeolite 13x adsorbent particles

Table 7.1 Physical properties of zeolite adsorbent particles

Properties	Value
Molecular formula	$Na_2O{\cdot}Al_2O_3{\cdot}ySiO_2{\cdot}zH_2O$
Size	2-3 mm
Bulk density	About 660 kg/m^3
BET surface area	504.6 m^2/g
Micropore volume	0.2123 cm^3/g
Pore size	10 Å
Water capacity	> 28 % kg/kg
PH	9.0-11.5
Flash point	Not flammable
Ignition temperature	Not flammable
Change of physical state	Does not soften below 700°C

7.2.1 Thermal conductivity

A major problem with the solid adsorbents used in adsorption refrigeration system is their poor thermal conductivity. Their adsorption performance is very sensitive to the heat transfer rate between external heat source and adsorbent bed. The equivalent thermal conductivity of adsorbent filled with adsorbate is a necessary input in every heat and mass transfer simulation

of the adsorption refrigeration system. Thermal conductivity tests were performed in the Fluid Mechanics Laboratory of the School of Mechanical and Aerospace Engineering, Nanyang Technological University. The instrument used is Lambda 2300V (see Figure 7.2) which is suitable for testing low thermal conductivity materials based on ASTM 518 and ISO 8310 standards at temperature ranging from 0°C to 200°C.

Figure 7.2 Lambda 2300V thermal conductivity test instrument

The determination of the effective thermal conductivity λ is based on the measurement of the heat flow through the sample from the hot plate and the cold plate under a fixed temperature difference ΔT across the specimen. Figure 7.3 shows a schematic of the test section. In the test, the temperature difference was set at 20°C. Calculations were done when the test section reached equilibrium. The effective thermal conductivity is given by

$$\lambda = N\frac{V}{\Delta T}\cdot\Delta x \qquad (7\text{-}1)$$

where N is the calibration factor that relates the voltage signal of the heat flow transducer to the heat flux, V is the voltage of heat flow transducer, and Δx is the thickness of the specimen.

Firstly, the calibration factor is determined (0.01085) and then the thermal conductivity is obtained as 0.103 W/m·K (±5%) when the specimen temperature varies from 25°C -75°C**.** The value of the zeolite particles is lower than the value (0.2 W/m·K) used in the literature (Ben Amar *et al*., 1996), since the porosity of the zeolite bed in this study is higher. Note that the gas around the pellets is air and the pressure is atmospheric pressure, which is different from the case in the adsorption experiments. Since the thermal conductivities of air and water vapour are very small compared to that of zeolite, the effect of the gas around the pellets on the thermal conductivity can be neglected.

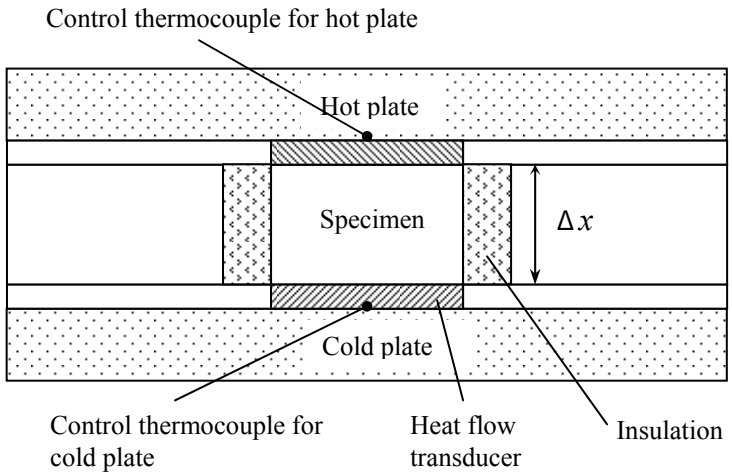

Figure 7.3 Schematic of the thermal conductivity test section

7.2.2 Density and porosity

The bulk density, ρ_b is given by the supplier of the zeolite is about 660 kg/m^3. The real density (ρ_r) of zeolite can be measured using the Ultrapycnometer 1000 equipment available in the Thermal and Fluids Research Laboratory of the School of Mechanical and Aerospace Engineering, NTU (see Figure 7.4).

Figure 7.4 Ultrapycnometer 1000

The Ultrapycnometer uses pressurised helium (1.25bar) which filled the space surrounding the sample. Since the size of helium atoms is very small, helium can enter into all micro-pores in the porous media. The measured real density of zeolite is 2286 kg/m^3 ±5%. The total porosity, ε_t is thus given by

$$\varepsilon_t = 1 - \rho_b / \rho_r = 0.711 \pm 2\% \tag{7-2}$$

The macroporosity of the adsorbent, ε_a can be obtained as follows:

$$\varepsilon_a = \varepsilon_t - v_p \cdot \rho_b = 0.571 \pm 2.5\% \tag{7-3}$$

where v_p is the micropore volume.

7.2.3 Permeability

The permeability of the adsorbent was measured by the constant head method. The experimental setup is shown in Figure 7.5. This test comprises measurements of the flow rate, F_w, through the sample under a constant pressure drop.

Figure 7.5 Experiment setup of a permeability test

The permeability can be computed from

$$K = \frac{\mu L R_T}{\rho g h} \cdot \frac{F_w}{A} \tag{7-4}$$

where h is the head loss in piezometer reading, A is the cross-sectional area of the sample, L is the distance between piezometer taps and R_t is the temperature correction factor.

Three readings were taken and an average permeability value of $K = 1.91 \times 10^{-8}$ m^2 (±10%) was obtained. The permeability of the adsorbent can also be determined mathematically using the Blake-Kozeny equation [Equation (5-3)]. The value which lies between 2.70 - 5.83 $\times 10^{-8}$ m^2 is of the same order of magnitude as the experimental results.

7.3 EXPERIMENTAL SETUP

To validate the numerical model, a laboratory-scale experimental intermittent adsorption cooling system was developed. A schematic diagram of this facility is shown in Figure 7.6. The main experimental unit consists of a zeolite adsorbent containing 1.82 kg of zeolite as well as a condenser/evaporator. Figure 7.7 shows the photograph of the experimental test facility.

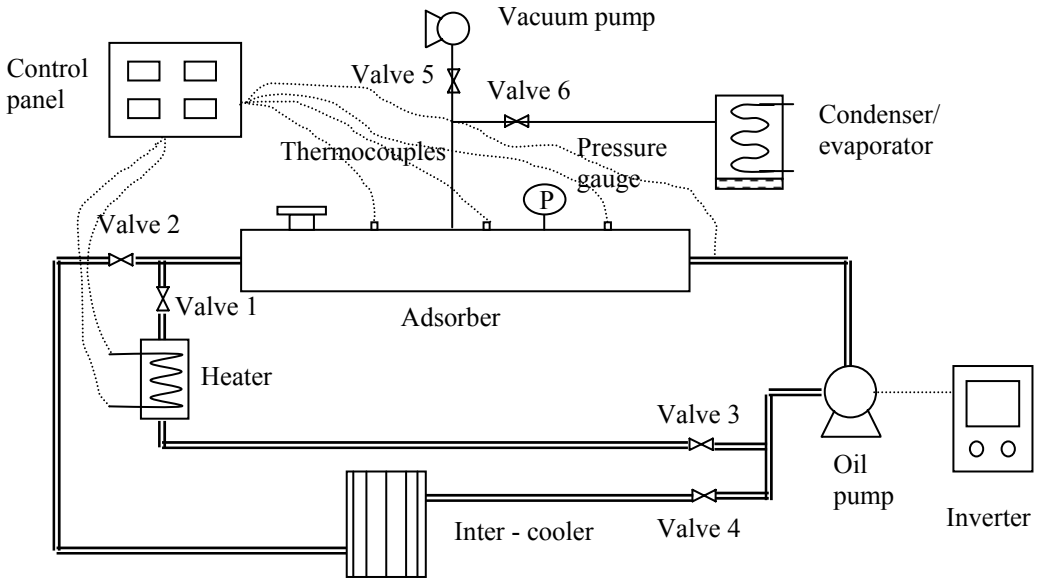

Figure 7.6 Schematic diagram of experimental adsorption cooling system

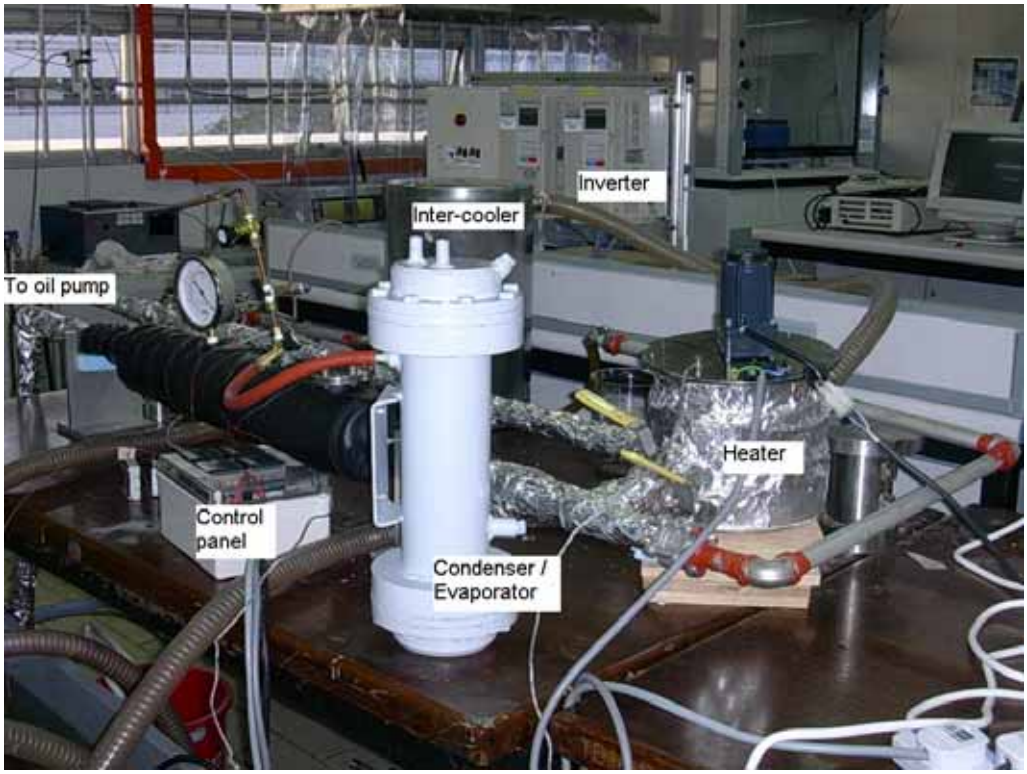

Figure 7.7 Photograph of the experimental test facility

Adsorbers: The configuration of the zeolite adsorber is shown in Figure 7.8. The adsorber is a 0.6m-long cylindrical double-tube. Alam *et al.* (2000) mentioned that the optimal ratio of the length to the width for an adsorber should be around 10. Thus, the radius of adsorber was designed to be 0.052 m. The ratio of length to the radius, *R/L*, is about 10. The diameter of the inner tube through which the heat exchange oil (Benolin Therm 300) flows, is 0.040 m. The locations (in the axial and radial directions) of three thermocouples placed in the zeolite adsorbent bed are (0.15 m, 0.033 m), (0.30 m, 0.037 m) and (0.45 m, 0.041 m), respectively. Thermocouples were also placed at the inlet and outlet of the heat exchange oil to measure the oil temperatures in order to determine the heat input by the external heat source. Heat exchange oil flows through the inner tube to supply or remove heat to or from the adsorber. Foam tape insulation (Superlon) was used to cover the outside of the tube to decrease heat loss to the environment.

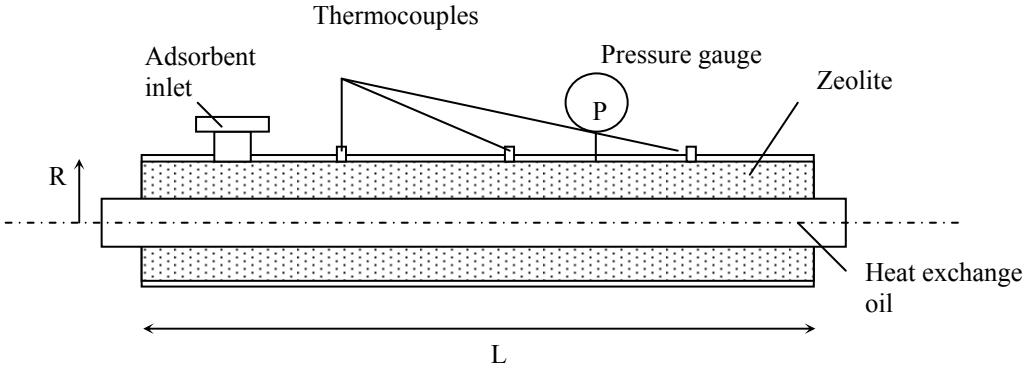

Figure 7.8 Schematic diagram of adsorber in experiment

Condenser/Evaporator: In this experimental study, the condenser and evaporator were constructed as a single component (see Figure 7.6) since the operation of the experiment cycle is intermittent. This component was used as a condenser during the heating process and as an evaporator during the cooling process. The evaporator/condenser is also a water-finned tube heat exchanger. The heat exchange surface area is 0.12 m^2.

Heater: In this setup, an electric heater (2.5 kW) was used to simulate conditions of solar heating or energy from a waste heat source. The heater was placed in a tank of volume 5.0×10^{-3} m^3 to deliver heat to the heat exchange oil (Benolin Therm 300). The temperature of the heating oil was set and controlled by the control panel.

Inter-cooler: During the cooling process, the heat exchange oil was cooled by the shell and tube heat exchanger (inter-cooler). Water at a temperature of 25°C was drawn from a small reservoir to cool the heated oil that enters the cooler.

Other Component: The heat exchange oil was circulated and driven by a high temperature oil pump with a maximum volume rate of 7.1m^3/h (Varisco, POMPA V 30-2). A frequency inverter was used to regulate the speed of the pump and hence the flow rate of the heat exchange oil. The main function of the vacuum pump (E2M1.5) was to draw out the air in the adsorber at the beginning of the experiments. All thermocouples used in the experiments were calibrated by a "Thermocal 18b" thermocouple calibrator available in the Thermodynamics Laboratory of the School of Mechanical and Aerospace Engineering, NTU.

7.4 EXPERIMENTAL PROCEDURE

The operation of the adsorption cooling system is similar to the basic adsorption system described in Section 1.1. The operating procedures for the experimental adsorption cycle are shown in the following steps.

Initial Preparation: Zeolite adsorbent filled with water was fed into the adsorber. The pressure of the adsorber was maintained as a constant value (P_e) by using the vacuum pump. At the same time, the heater was switched on to heat up the heating fluid. Valves 1 and 2 (see Figure 7.6) were opened and the oil pump switched on. Thus the heat exchange fluid will flow through the adsorber to heat up the zeolite adsorbent. When the average temperature of

three thermocouples reaches the initial adsorption temperature (T_a), the valves and oil pump were turned off. Air in the condenser/ evaporator was also removed by vacuum pump.

Isosteric heating: The heat exchange oil in the heater tank was heated until its temperature reached a desired temperature ($T_{h,in}$). This step was commenced with the Valves 1 and 3 and oil pump turned on again. This will cause the adsorption bed to be heated up. Isosteric heating phase begins. The temperature and pressure readings along the adsorption bed were recorded at fixed positions along the adsorption bed.

Desorption-Condensation: When the vapour pressure in the adsorbent bed equaled the condensing pressure (P_c), desorption began with the opening of Valve 6 between the adsorber and the condenser. The water vapour desorbed from the adsorber was cooled until it condensed into a liquid in the condenser. The process was then stopped when the temperature of adsorbent bed reached a maximum value (T_g).

Isosteric cooling: The heating process was ceased for the isosteric cooling step to proceed. Valves 1 and 3 were closed and Valves 2 and 4 were opened to allow the circulating heat exchange oil flowing through the heat exchanger to be cooled down. Subsequently, the adsorber will be cooled by heat exchange oil.

Adsorption- Evaporation: Valve 6 was again opened to allow evaporation to take place when the pressure in the adsorber reached evaporating pressure (P_e). The entire cycle ceased when the temperature of adsorbent bed reached the initial adsorption temperature (T_a).

7.5 EXPERIMENTAL RESULTS

The experimental runs were based on the four processes proposed in Chapter 1 with different driven temperatures of heat exchange oil. The operating conditions and some parameters are listed in Table 7.2.

Table 7.2 Parameters and operating conditions in experiments

Name	Symbol	Value
Mass flow rate of heating transfer fluid	$\dot{m}_f$	0.78 kg/s
Initial temperature	T_0	318 K
Fluid inlet temperature during cooling	T_{cin}	298 K
Evaporator pressure	P_e	1000 Pa
Condenser pressure	P_c	10000 Pa
Thermal conductivity of adsorbent bed	λ_s	0.103 W/m·K
Contact heat transfer coefficient	h_{ms}	25 W/m^2·K*
Permeability of adsorbent bed	K	1.91×10^{-8} m^2
Particle diameter	d	2-3 mm
Internal radius of metal tube	R_0	0.020 m
External radius of metal tube	R_1	0.024 m
External radius of adsorbent bed	R	0.045 m
Length of adsorbent bed	L	0.6 m
Macro-porosity of adsorbent bed	ε_a	0.57
Total porosity of adsorbent bed	ε	0.71

* Source: Zhang (2000)

Figure 7.9 shows the temperature variation with time measured by three thermocouples for a driven temperature, $T_{h,in}$ of 403 K. The numerical simulation based on the model proposed in Chapter 5 was carried out under this condition. It is noticed that in this simulation the particle diameter was estimated as an average value of 2.5 mm. Since the particle diameter here is relatively large, the thermal contact resistance between the bed and metal tube should be considered in the simulation. From Figure 7.9, the simulation results fit well with the experiment results for the inner layer location (Thermocouple 1). For the outer layer of adsorbent bed (Thermocouples 2 and 3), there is a maximum difference of 8.5 K between the simulation and numerical results. This could be due to heat loss by radiation and convection from the adsorbent bed to the environment (see Figure 7.10). The variation of heat input power with time for the experiments and simulation is shown in Figure 7.10. It can be seen that the heat input in the experiments is greater than the calculated heat input. The difference between the experimental heat input power and simulation results increases

with the increase of bed temperature due to the increased heat loss by convection and radiation when the bed temperature is increased. Figure 7.11 shows the Clapeyron diagrams obtained experimentally and from the simulation cycles the location of Thermocouple 1. From this figure, it can be seen that during the desorption and condensing processes, the pressure is not constant and is in fact slightly higher than the theoretical condensing pressure. This is a result of the heat transfer resistance in the condenser. It can also be seen that the experimental evaporating pressure is higher than the simulation value. Because the same component was used as either an evaporator or condenser, the high pressure water vapour in the evaporator will cause an increase in the pressure in the adsorber when it is connected to the evaporator during adsorption and evaporator processes.

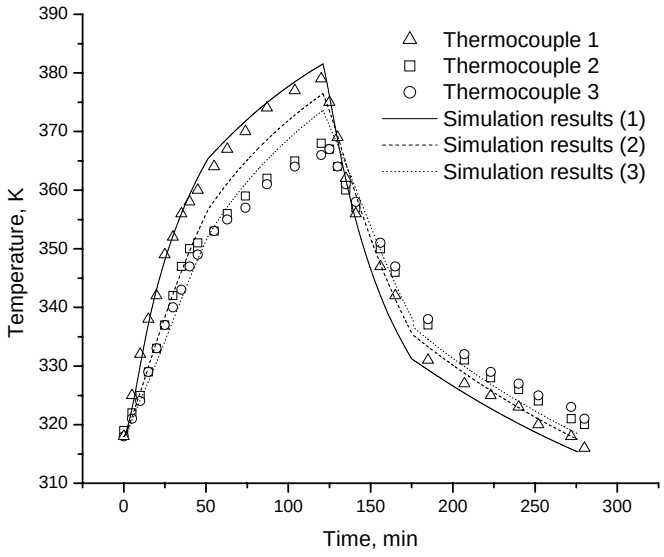

Figure 7.9 Temperature variations with time;

$T_{h,in}$ = 403 K

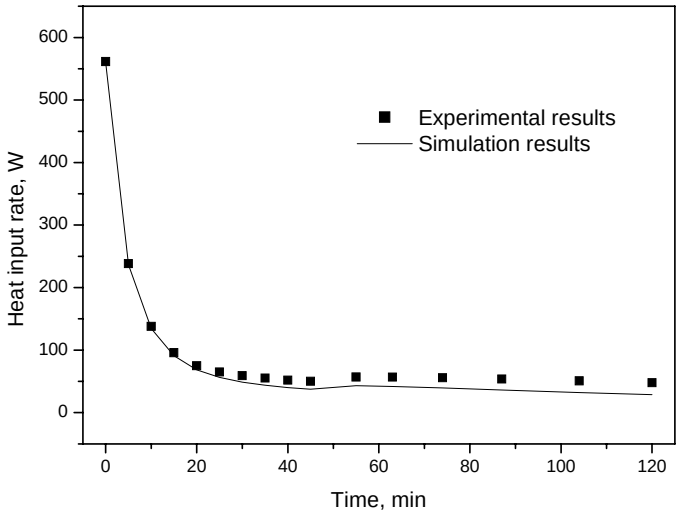

Figure 7-10 Variation of heat input rate with time; $T_{h,in}$ = 403 K

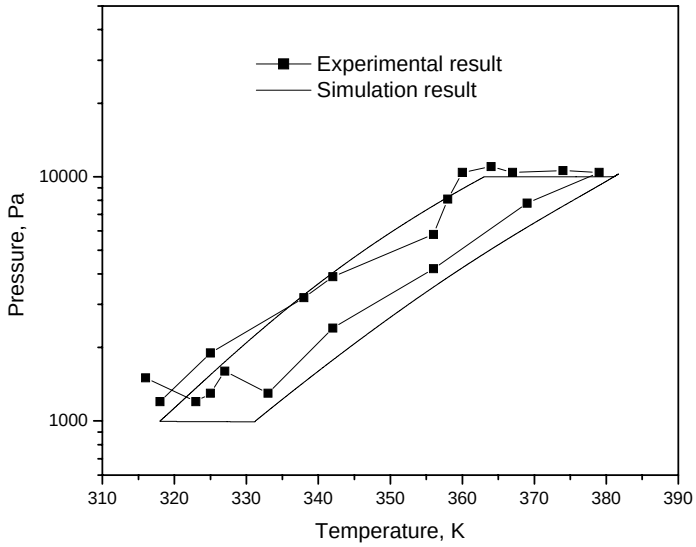

Figure 7.11 Comparison between experimental cycle with simulation cycle; $T_{h,in}$ = 403 K

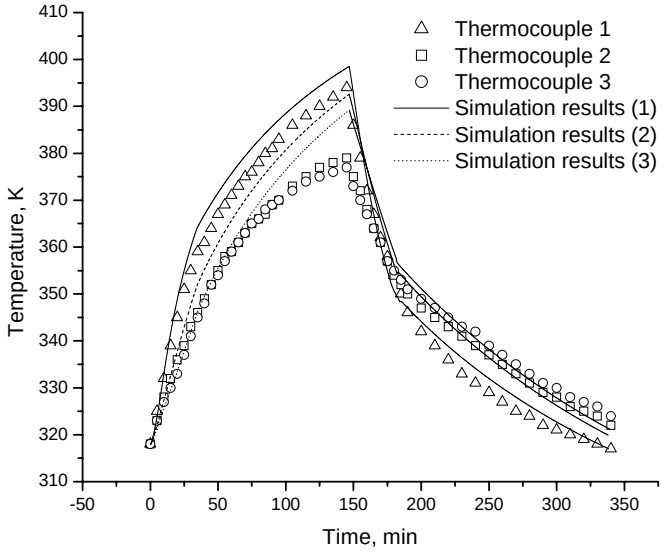

Figure 7.12 Temperature variations with time;

$T_{h,in}$ = 423 K

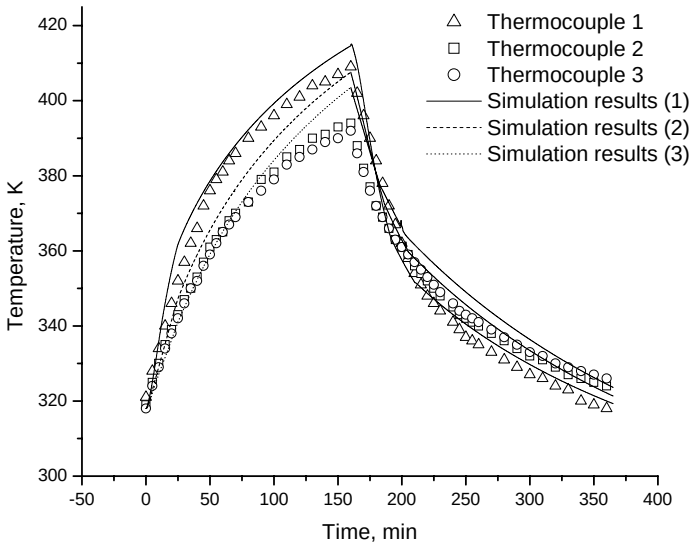

Figure 7.13 Temperature variations with time;

$T_{h,in}$ = 443 K

The variations of bed temperature with time for $T_{h,\ in}$ = 423 K and 443 K are shown in Figures 7.12 and 7.13, respectively. The maximum difference between the experimental

results and simulation is about 12 K for these two cases. The difference will be larger than the low driven temperature case (Figure 7.9). This could be due to higher heat loss for high bed temperature.

The performance coefficients (COP and SCP) obtained in the experiments are defined as:

$$COP = \frac{Q_{ev}}{Q_h} = \frac{m_w[L - C_{pw}(T_c - T_e)]}{\sum_i \dot{m}_f C_{pf}(T_{h,in} - T_{h,out})\Delta t_i} \tag{7-5}$$

$$SCP = \frac{Q_{ev}}{t_c \cdot m_s} = \frac{m_w[L - C_{pw}(T_c - T_e)]}{t_c \cdot m_s} \tag{7-6}$$

where m_w is the mass of water vapour condensed in the condenser during the desorption process, L is the latent heat of evaporation of water and Δt is the time interval.

The uncertainties of the COP and SCP values can be calculated using the following expressions:

$$\delta COP = \sqrt{\delta^2 Q_{ev} + \delta^2 Q_h} = \sqrt{\delta^2 m_w + \delta^2 \dot{m}_f + \delta^2 (T_{hin} - T_{hout}) + \delta^2 \Delta t} \tag{7-7}$$

$$\delta SCP = \sqrt{\delta^2 Q_{ev} + \delta^2 m_s + \delta^2 t_c} = \sqrt{\delta^2 m_w + \delta^2 m_s} \tag{7-8}$$

Here the uncertainty of the cycle time (t_c) is neglected since it is very small. The maximum uncertainties in m_w, $\dot{m}_f$, (T_{hin}-T_{out}) and Δt were calculated to be $\delta m_w = 5\%$, $\delta \dot{m}_f = 2\%$, $\delta(T_{hin} - T_{hout}) = 4\%$ and $\delta \Delta t = 0.7\%$. Using Equation (7-7), the maximum uncertainty in the COP was estimated to be 6.8 %. The maximum uncertainty in m_s and δm_s are estimated as 0.6 %. Thus, the maximum uncertainty value of SCP is 5.1%. It is noted that no uncertainty was assumed for the physical properties of the adsorbent, metal tube and heat exchange fluid. Since these properties will change with temperature, the uncertainties may be somewhat higher than indicated.

The performance coefficients (COP and SCP) obtained for the experiments and simulation are listed in Table 7.3. It can be seen that the experimental performance

coefficients are lower than those obtained by simulation. The maximum difference in COP values between the numerical simulations and the experiments is less than 15 %, while the maximum difference in the SCP values is less than 3 %. It appears that the differences of cooling energy (Q_{ev}) between the experimental and simulation results are small. The difference in the COP value between the simulation and experiments is mainly due to the difference in heat input. The reduction of heat loss will decrease the heat input which can lead to better agreement with simulation and experiments. In general, the difference between the simulation results and experimental results is small, even through they are larger in magnitude than the uncertainty value. Therefore, the model proposed in Chapter 5 can be used to simulate the heat and mass transfer mechanisms in the adsorbent bed and predict the performance of the adsorption cycle.

Table 7.3 Performance coefficients for experiments and simulation

Driven temperature ($T_{h,in}$), K	COP		SCP, W/kg	
	Experimental	Simulation	Experimental	Simulation
403	0.155	0.182	2.70	2.75
423	0.192	0.219	4.32	4.42
443	0.251	0.285	6.89	6.95

7.6 SUMMARY

This chapter describes an experimental facility set up based on the numerical model described in Chapter 5. Some thermophysical properties (such as thermal conductivity, density, porosity and permeability) of the adsorber bed as inputs to the numerical simulation were determined experimentally. From the comparison of simulation and experimental results, it was verified that the model presented in Chapter 5 can be used to study the heat and mass transfer mechanisms in the adsorber and predict the thermal performance of the adsorption cycle.

CHAPTER 8

MODELLING OF INTERNAL REFORMING SOLID OXIDE FUEL CELL AND ADSORPTION CHILLER COGENERATION SYSTEM

8.1 INTRODUCTION

As mentioned in Chapter 1, compared with the conventional vapour compression refrigeration system, the performance of the adsorption refrigeration system is rather low. This is a big obstacle in large scale application of adsorption refrigeration system. However, there are two advantages of the adsorption refrigeration system. The first is its environmental-friendly properties as they employ safe and non-polluting refrigerants. The other advantage is that it can be driven by low grade energy such as solar energy and waste heat. The latter advantage renders the adsorption refrigeration system to be more promising in application where solar energy or waste heat is available. Solar adsorption refrigeration systems are widely studied by many researchers (Sakoda and Suzuki, 1984; Hu, 1996; Luo and Tondeur, 2000; Li *et al*., 2002). However, there are only limited investigations on waste heat adsorption refrigeration systems. Therefore, the adsorption refrigeration system driven by waste heat from a solid oxide fuel cell (SOFC) is proposed and investigated in this study.

Solid oxide fuel cells have been considered as one of the promising energy conversion technologies because they provide a highly efficient energy conversion rate with low pollutant emissions. The chemical energy of the fuel gas is converted directly to electricity in a SOFC, and hence potentially, high electrical efficiencies can be achieved. The high operating temperature of SOFCs allows the use of cogeneration and hybrid systems. Fuel cell cogeneration systems (FCCS) have been applied successfully in some developed countries. There are increased interests in such a system because it can achieve higher efficiency in electricity production and a higher overall efficiency with a low level of adverse

environmental impact. One type of fuel cell and absorption cogeneration system has been investigated by several researchers (Silveria *et al*., 2001; Burer *et al*., 2003) to produce electrical power and cooling simultaneously. Because the gas-solid adsorption cooling system is more flexible in operation compared with the liquid absorption cooling cycle (Douss and Meunier, 1989), a combined fuel cell and adsorption cooling cogeneration system can be a promising alternative.

In this chapter, an internal reforming solid oxide fuel cell and a zeolite/water adsorption chiller cogeneration system is proposed. A numerical model based on the first law of thermodynamics is developed to simulate this combined system under steady-state operating conditions. The main aim of this work is to investigate the performance of this combined system under different operating conditions and parameters.

8.2 SYSTEM DESCRIPTION

A schematic of the proposed SOFC and adsorption chiller cogeneration system is shown in Figure 8.1. This cogeneration system incorporates a natural gas feed, an internal reforming solid oxide fuel cell (IRSOFC), an adsorption chiller, a DC/AC inverter and two heat exchangers. The system can produce electricity, cooling and heating simultaneously. Air is preheated at the heat exchanger before it enters the IRSOFC generator. Part of fuel gas posterior to the reaction is recirculated and mixed with fresh fuel gas and the mixture re-enters the SOFC. Fuel gas and air flow through the anode and cathode, respectively. Fuel gas is internally reformed in the anode and hydrogen is produced. The electrochemical reaction occurs in the SOFC and electricity is generated together with heat. Subsequently, the non-recirculated portion of the effluent fuel gas and depleted air flow into a combustor. After reacting in the combustor, the fuel-air mixture enters Heat Exchanger 1, where the air is preheated. The combustion gases exiting Heat Exchanger 1 then flows through the

adsorption chiller to drive this cooling system during the heating process. Zeolite/water is used as the working pair for the adsorption chiller. Zeolite has satisfactory adsorption ability and its adsorption properties are also stable under high temperature. Finally, the gases from adsorption chiller are passed through Heat Exchanger 2 for a heating facility and then exhausted to the environment.

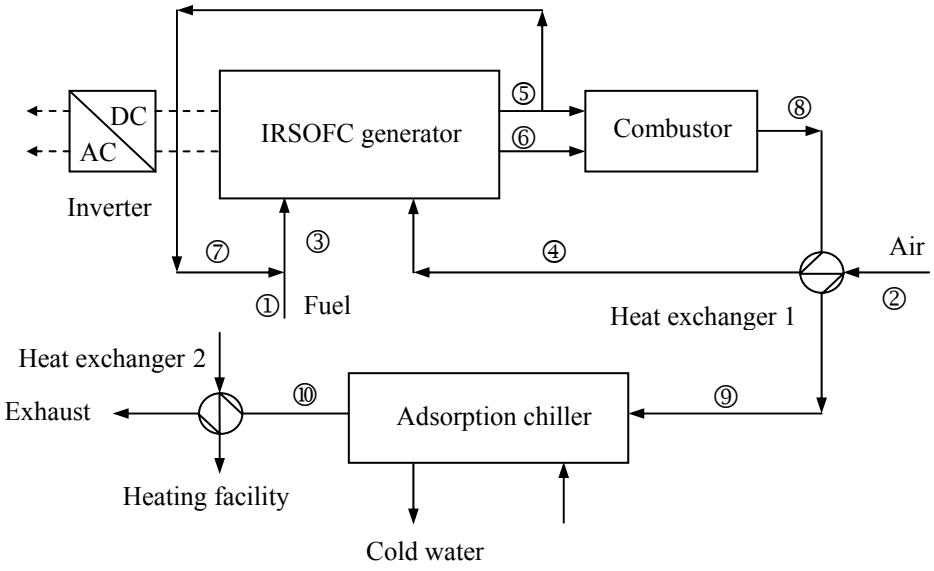

Figure 8.1 Schematic of SOFC and adsorption chiller cogeneration system

8.3 NUMERICAL MODELLING

The numerical model is composed of three parts: internal reforming and electrochemical reaction model, SOFC model and adsorption cooling cycle model. In the development of this model, the following assumptions are made: (1) equilibrium reforming and shifting reactions, (2) the exit temperature of the cathode is equal to that of the anode, (3) the SOFC and heat exchangers are in thermal balance, (4) burner efficiency is 100%, (5) the mass of adsorbent is proportional to the surface area of the adsorber, and (6) no heat loss in this system.

8.3.1 Internal reforming and electrochemical reaction model

The recirculated anode exhaust fuel gas and the high temperature conditions are very helpful to the internal reforming and shifting reactions in a SOFC. The mechanisms for internal reforming and electrochemical reactions for the SOFC are commonly reported in the literature (Massardo and Lubelli, 2000; Campanari, 2001; Chan *et al*., 2002; Zhang *et al*., 2005). The reactions are:

Reforming reaction $CH_4 + H_2O \rightarrow CO + 3H_2$ (8-1)

Shifting reaction $CO + H_2O \rightarrow CO_2 + H_2$ (8-2)

Electrochemical reaction $H_2 + \frac{1}{2}O_2 \rightarrow H_2O$ (8-3)

where the reforming and shifting reactions are assumed to reach thermodynamic equilibrium with equilibrium constants represented by

$$K_{p,r} = \frac{P_{H_2}^3 \cdot P_{CO}}{P_{CH_4} \cdot P_{H_2O}}; K_{p,s} = \frac{P_{CO_2} \cdot P_{H_2}}{P_{CO} \cdot P_{H_2O}} \quad (8\text{-}4)$$

The equilibrium constants are considered as functions of temperature and can be obtained from the following equation:

$$\log K_p = AT^4 + BT^3 + CT^2 + DT + E \quad (8\text{-}5)$$

The values of the parameters in Equation (8-5) are given in Table 8.1 (Bossel, 1992).

Table 8.1 Values of equilibrium constants of reforming and shifting processes

	Reforming	Shifting
A	-2.63121×10^{-11}	5.47301×10^{-12}
B	1.24065×10^{-7}	-2.57479×10^{-8}
C	-2.25232×10^{-4}	4.63742×10^{-5}
D	1.95028×10^{-1}	-3.91500×10^{-2}
E	-6.61395×10^{1}	1.32097×10^{1}

We assumed that the fresh fuel gas is composed of CH_4, N_2 and CO_2. The equilibrium constants can be rewritten as

$$K_{p,r} = \frac{\left(\frac{x-y}{a_t^f+2x}\right)\cdot\left(\frac{3x+y-z}{a_t^f+2x}\right)^3 \cdot P_{cell}^2}{\left(\frac{a_{CH_4}^f-x}{a_t^f+2x}\right)\cdot\left(\frac{z-x-y}{a_t^f+2x}\right)} \tag{8-6}$$

$$K_{p,s} = \frac{\left(\frac{3x+y-z}{a_t^f+2x}\right)\cdot\left(\frac{a_{CO_2}^f+y}{a_t^f+2x}\right)\cdot P_{cell}^2}{\left(\frac{x-y}{a_t^f+2x}\right)\cdot\left(\frac{z-x-y}{a_t^f+2x}\right)} \tag{8-7}$$

where x, y and z are the reactant molar flow rates of CH_4, CO_2 and H_2, respectively and superscript f is fresh fuel gas. a_t^f is the molar flow rate of the fresh fuel gas, $a_{CH_4}^f$ is the mass flow rate of inlet CH_4 from fuel gas, and $a_{CO_2}^f$ is the molar flow rate of inlet CO_2 from fuel gas.

The reactant flow rate z of H_2 can be obtained from the fuel utilisation factor as follows:

$$z = U_f \cdot (4a_{CH_4}^i + a_{H_2}^i + a_{CO}^i) \tag{8-8}$$

where superscript i is inlet cell and U_f is the fuel utilisation factor.

If the value of recirculation ratio r_a is known, Equation (8-8) can be rewritten as

$$z = \frac{4U_f \cdot a_{CH_4}^f}{1-r_a+r_a \cdot U_f} \tag{8-9}$$

where the recirculation ratio, r_a, is defined as the molar flow rate ratio of recirculated fuel gas to total outlet fuel gas.

8.3.2 SOFC model

The cell voltage calculation is the core of the SOFC model. The cell electrical power can be calculated from the product of cell current and the cell voltage while the cell current can

be easily obtained from a known value of the fuel utilisation factor. Based on the work of several researchers (Hall, 1997; Chan *et al*., 2002; Bove, 2005), the cell voltage is given by

$$E = E_{re} - (\eta_{act} + \eta_{ohm} + \eta_{conc}) \tag{8-10}$$

where E_{re} is the ideal reversible cell voltage and the other three terms represent the activation, ohmic and concentration over-potentials.

The ideal reversible cell voltage can be evaluated by the following Nernst equation:

$$E_{re} = E_0 - \frac{RT}{2F}\ln\left(\frac{P_{H_2O}}{P_{H_2} P_{O_2}^{1/2}}\right) = \frac{RT \ln K_{p,e}}{2F} - \frac{RT}{2F}\ln\left(\frac{P_{H_2O}}{P_{H_2} P_{O_2}^{1/2}}\right) \tag{8-11}$$

where $K_{p,e}$ is the electrochemical reaction equilibrium constant. It can be obtained in the following equation given by Shen *et al*. (1983):

$$\ln K_{p,e} = 2.864 + 105.176 \exp(-T/668.154) \tag{8-12}$$

The anode and cathode activation over-potentials can be described by the Bulter-Volmer equation (Bessette, 1994):

$$i = i_0\left[\exp\left((1-\beta)\frac{F\eta_{act}}{RT}\right) - \exp\left(-\beta\frac{F\eta_{act}}{RT}\right)\right] \tag{8-13}$$

where β is the transfer coefficient and i_0 is the apparent exchange current density.

The ohmic over-potential as suggested by Bessette (1994) is given by

$$\eta_{ohmic} = i\sum_j \rho_j \delta_j = i\sum_j A_j \exp\left(\frac{B_j}{T}\right)\cdot\delta_j \tag{8-14}$$

The parameters A_j and B_j are constants for different components and δ_j is the thickness of the cell components. The values of constant A_j and B_j are listed in Table 8.2 (Chan *et al*., 2002).

The concentration over-potential is a result of the reactant diffusion during reaction. According to Bove *et al*. (2005), concentration losses can be ignored under normal operating conditions.

Table 8.2 Values of the constants of ohmic over-potential equations

j	A_j	B_j	Remarks
1	0.00294	10350	Electrolyte constants
2	0.1256	4690	Interconnect constants
3	0.00811	600	Cathode constants
4	0.00298	-1392	Anode constants

The SOFC current can be quantified using the fuel utilisation factor, U_f:

$$I = znF = 2FU_f(4a^i_{CH_4} + a^i_{H_2} + a^i_{CO}) \tag{8-15}$$

The SOFC only converts part of the chemical energy of the fuel into electrical power while the rest will become heat to increase the temperature of the outlet effluent gas. From the following energy balance equation, the temperature of outlet gas is computed.

$$\sum_j a^i_{j,c}\Delta H^i_{j,c} + \sum_j a^i_{j,a}\Delta H^i_{j,a} = \sum_j a^o_{j,c}\Delta H^o_{j,c} + \sum_j a^o_{j,a}\Delta H^o_{j,a} + EI + Q_{loss} \tag{8-16}$$

where i is inlet, o is outlet, a is anode and c is cathode.

As the temperature is known from Equation (8-16) for a specified fuel utilisation factor and inlet conditions, the species concentration in the SOFC can be obtained by solving Equations (8-6)-(8-8).

8.3.3 Adsorption cooling cycle model

After preheating the air, the gas from combustor is directed to the adsorption chiller. The schematic diagram of the adsorber in the adsorption chiller is shown in Figure 8.2. The adsorber consists of a number of adsorption units. Every adsorption unit is a metal tube covered with zeolite adsorbent bed. The configuration of adsorption unit is the same as the adsorber in Chapter 5. Thus, the heat conservation equations for every adsorption unit here are also the same as the heat transfer equations in Chapter 5 [Equations (5-23) – (5-25)]

except that the heat exchange fluid is changed to exhaust gas from Heat exchanger 1(see Figure 8.1). The radial size of the adsorption unit is the same as the adsorber in Chapter 5 while the length is enlarged to 5 m. Adsorption chillers with a continuous adsorption cycle are employed in this system. Hence, the cooling power can be presented as

$$P_{cw} = \frac{N \cdot m_s \Delta q \cdot [L(T_e) - C_{pl}(T_c - T_e)]}{t_h} \tag{8-17}$$

where N is the number of adsorption units, m_s is the mass of the adsorbent for every adsorption unit and t_h is the time of the heating process.

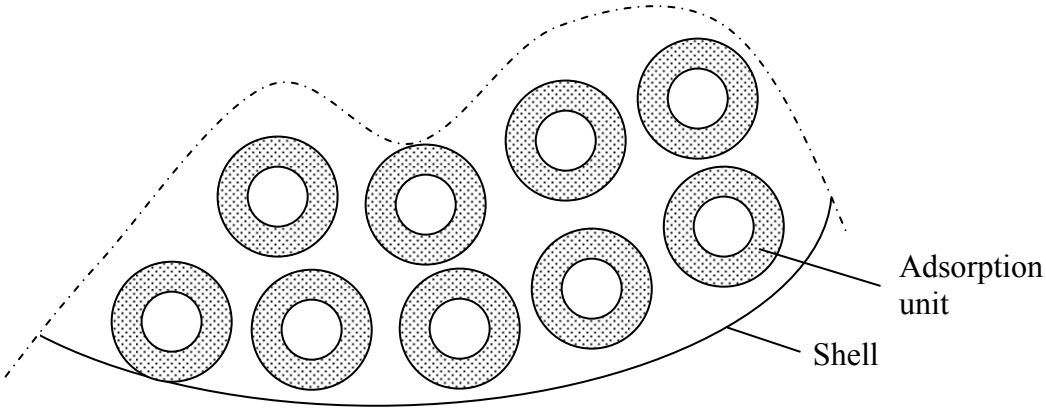

Figure 8.2 Schematic diagram of adsorber in the adsorption chiller

8.3.4 Modelling of combustor and other components

We assume that the exhaust gas from SOFC is completely burned in the combustors, namely CO and H_2 in the exhaust gas is converted to CO_2 and H_2O. Thus the heat balance equation of the combustor is

$$\sum_j a_j^i \Delta H_j^i = \sum_j a_j^o \Delta H_j^o \tag{8-18}$$

The heat balance equation for the heat exchangers is similar to the above equation with no species change in the heat exchangers.

8. 4 CALCULATIONS OF THE SYSTEM MODEL

Figure 8.3 shows the flowchart of the modelling calculations for the SOFC-AC system. The results of every block in the flowchart are the inputs for the next block. After setting the process parameters, the calculation block belonging to SOFC model will be used several times until the error of the energy balance is less than the assigned tolerance (0.1 K). Other blocks in Figure 8.3 will only be executed once. In this study, the SOFC is assumed to be in thermal equilibrium with the exhaust gas. Thus, by making an initial guess of the cell temperature, the equilibrium data for the three reactions in the SOFC can be obtained. All characteristics of the exhaust gas from the anode and cathode can be obtained by solving Equations (8-6)-(8-9). Using this data, the SOFC performance can be obtained in terms of cell voltage and electric current. The energy balance equation can be used to assess the validity of the guessed temperature. When the cell temperature is confirmed and the characteristics of the exhaust gas from SOFC are calculated, the following calculation block will be solved one by one. Every output data of the former block is the input of the next block. The numerical method for the calculation of adsorption cycle block is the same as that in Chapter 5. Visual FORTRAN software is used to develop the simulation code for this SOFC-AC model.

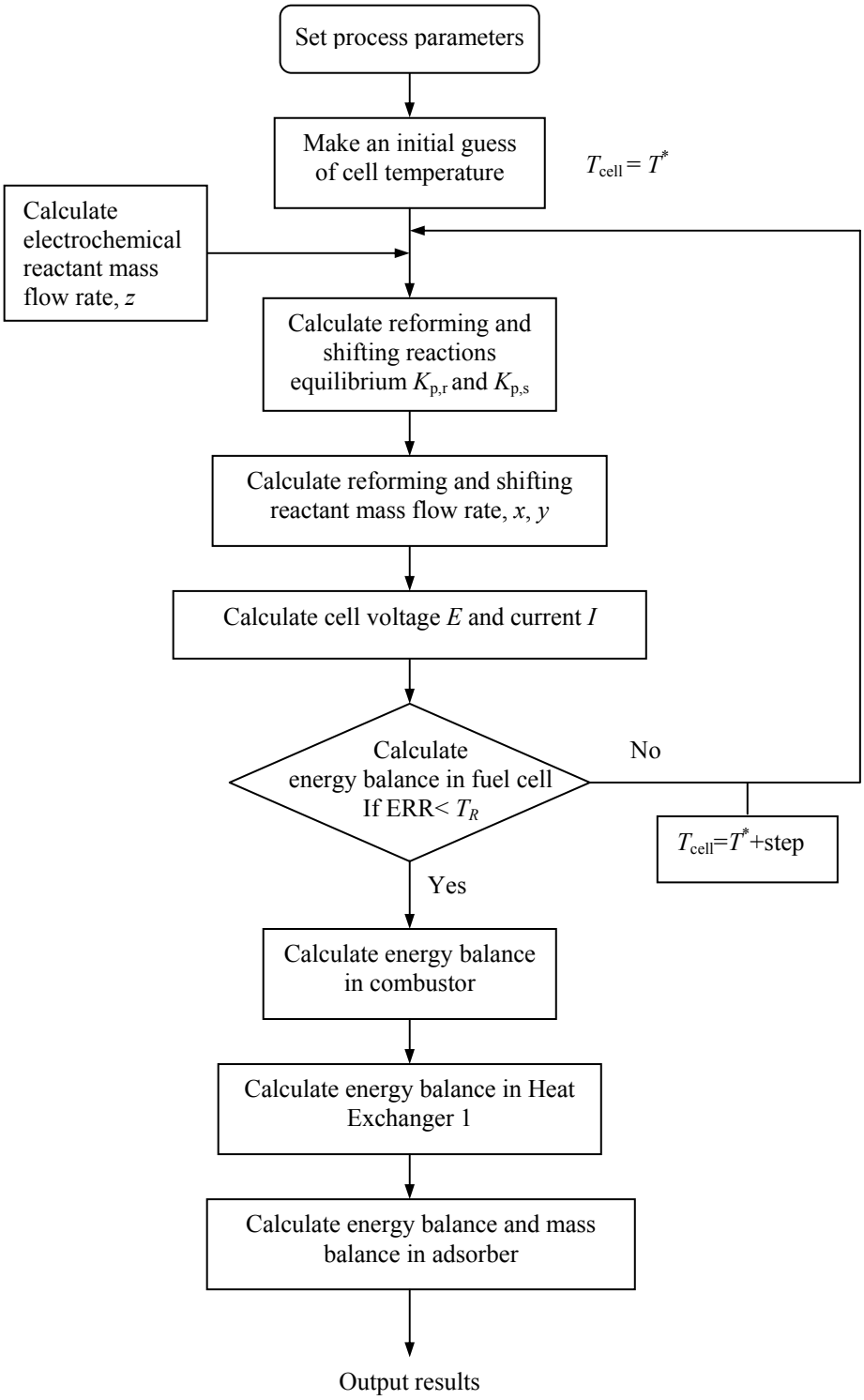

Figure 8.3 Flowchart of calculations for the SOFC-AC system

8.5 RESULTS AND DISCUSSION

The results of the numerical model can be used to carry out a detailed parametric analysis, which can provide an insight into the effects of variation of the operating parameters on the performance of SOFC systems. The operating parameters for the base case are shown in Table 8.3. In this study, heat power is not considered. Thus, the total efficiency of SOFC-AC system is given by

$$\eta_t = \frac{P_{ew} + P_{cw}}{\text{LHV}} \tag{8-19}$$

where P_{ew} is the electrical power delivered by the SOFC and LHV is the lower heating value of the inlet fuel. Simulated results for the base case show that the SOFC operates at a voltage of 0.775 V and a current density of 150 mA/cm^2. It can be seen that the SOFC-AC cogeneration system can achieve a total efficiency of more than 77% (including electrical power 62% and cooling power 15%). About 1800 kW electrical power and 450 kW cooling power can be produced by this system. The simulated stream properties for base case are shown in Table 8.4.

Table 8.3 Prescribed values of parameters for base case

Parameters	Value
Fuel inlet composition	CH_4: 84%, N_2: 15%, CO_2: 1%
Fuel inlet temperature	300 K
Air inlet temperature	300 K
Air temperature after preheat	930 K
Cell operating pressure	101300 Pa
DC/AC inverter efficiency	95%
Burner efficiency	100%
Fuel utilization factor, U_f	0.8
Circulation ratio, r_a	0.2
Electrolyte thickness	0.015 cm
Interconnect thickness	0.010 cm
Cathode thickness	0.20 cm
Anode thickness	0.020 cm
Half cycle time of adsorbent cycle, t_h	1200 s
Mass of the adsorbent, m_s	5 kg
Number of adsorption units, N	250

Table 8.4 Stream properties for SOFC-AC system

	Temperature, K	Gas flow rate, kmol/h	Gas composition, %						
			CH_4	H_2	CO	CO_2	H_2O	N_2	O_2
1	300	16	84.0	-	-	1.0	-	15.0	-
2	300	180	-	-	-	-	-	79	21
3	608	26.7	50.3	5.5	2.9	10.4	19.7	11.2	-
4	930	180	-	-	-	-	-	79	21
5	1118	53.6	-	13.6	7.2	24.5	49	5.7	-
6	1118	157.6	-	-	-	-	-	90.2	9.8
7	1118	10.7	-	13.6	7.2	24.5	49	5.7	-
8	1481	196	-	-	-	6.9	13.7	73.8	5.6
9	934	196	-	-	-	6.9	13.7	73.8	5.6
10	*	196	-	-	-	6.9	13.7	73.8	5.6

* The temperature of Stream 10 will change with time.

8.5.1 Effect of inlet fuel flow rate

The effect of fuel flow rate on the system efficiency is presented in Figure 8.4. Here the ratio of inlet fuel flow rate to the inlet air flow rate was fixed at 0.089. It can be seen from Figure 8.4 that both the electrical efficiency and total efficiency decreases as the fuel flow rate increases while the cooling efficiency has a maximum value for the range of fuel flow rate investigated. Figure 8.5 shows the effects of fuel flow rate on cell voltage and cell temperature. For constant fuel utilisation factor and circulation ratio, a higher rate of fuel flow means that more current will be produced and hence the current density is increased. The higher the current density, the higher the value of the total over-potential produced. The increase in over-potential will result in a reduction in the voltage of SOFC (see Figure 8.5). Since current has a linear relationship with the fuel flow rate, the electrical efficiency will decrease. It is shown in Figure 8.5 that the cell temperature increases linearly with an increase in the inlet flow rate. The increase in over-potential will increase heat generation, which will raise the cell temperature. The effect of inlet fuel flow rate on cooling power is shown in Figure 8.6. The cooling power increases asymptotically to a constant value with an increase in the fuel flow rate. When the fuel flow rate increases, the electrical efficiency will

decrease. This means that more heat can be generated in the combustor. Thus, the driven temperature of adsorption chiller also increases which leads to an increase of cooling power for a fixed cycle time. It also results in an increase in cooling efficiency. When the driven temperature increases to a certain value, no more refrigerant can be drawn from the adsorbent. Thus, the value of cooling power will reach a constant value and cooling efficiency will decrease as a result.

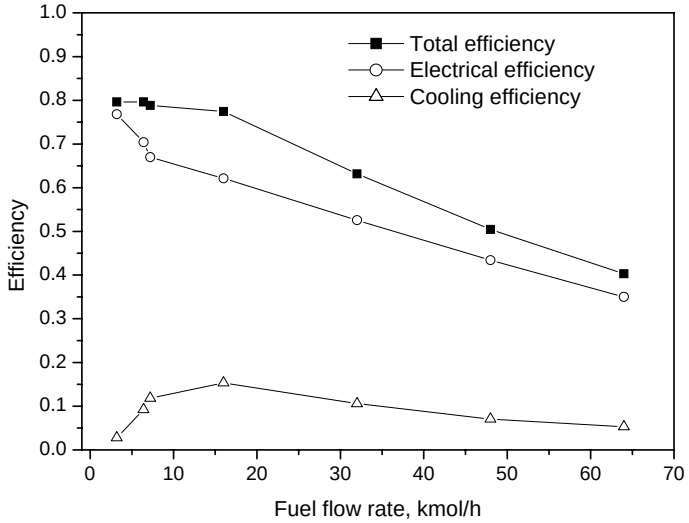

Figure 8.4 Effect of fuel flow rate on efficiency

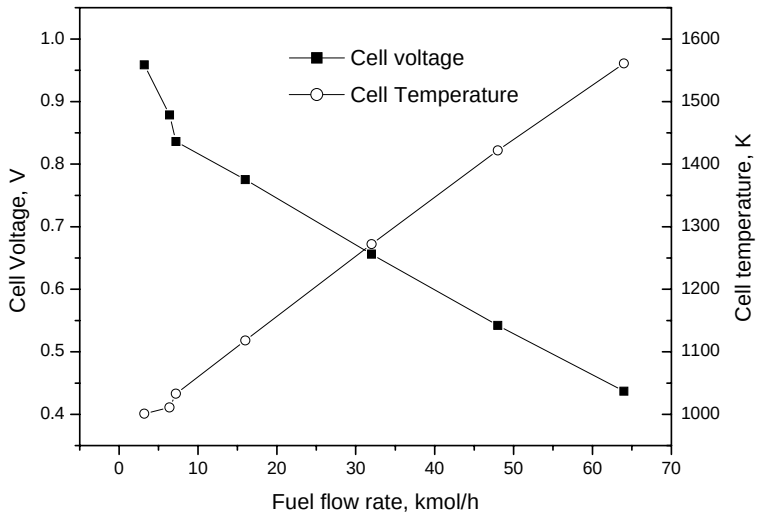

Figure 8.5 Effect of fuel flow rate on cell voltage and cell temperature

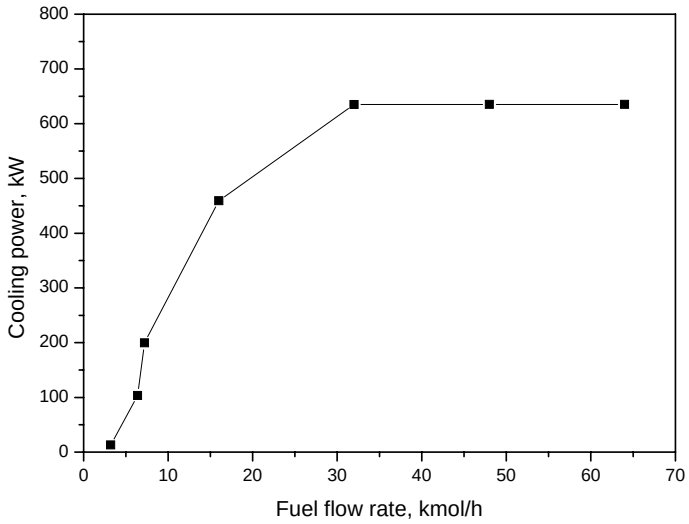

Figure 8.6 Effect of fuel flow rate on cooling power produced

8.5.2 Effect of fuel utilisation factor

Figure 8.7 shows the effect of fuel utilisation factor on system performance. The effect of fuel utilisation factor on cell voltage and cell temperature is given in Figure 8.8. When the fuel utilisation factor increases, the content of hydrogen in the anode is reduced. A higher U_f will lead to a higher value of current and higher cell temperature (see Figure 8.8). The cell temperature causes a reduced over-potential while the current gives rise to an increased over-potential. The SOFC voltage will increase slightly and then decrease quickly with the increase of U_f due to the combined effect of cell temperature and current density. The electrical efficiency, which is proportional to the product of voltage and U_f, has a maximum value for a value of U_f around 0.85. For U_f larger than 0.85, the electrical efficiency will decrease due to the increased effects of the voltage drop. The higher U_f also result in a lower combustion temperature, leading to a lower value of driven temperature for the adsorption chiller. Therefore, the cooling power will decrease with higher U_f. When U_f increases beyond 0.85, the electrical efficiency will decrease, which in turn leads to a higher depleted fuel

heating value. Thus, more heat will be generated in the combustor and the driven temperature of adsorption chiller will increase. Therefore, the cooling power and cooling efficiency will increase with an increase of fuel utilisation factor when $U_f > 0.85$.

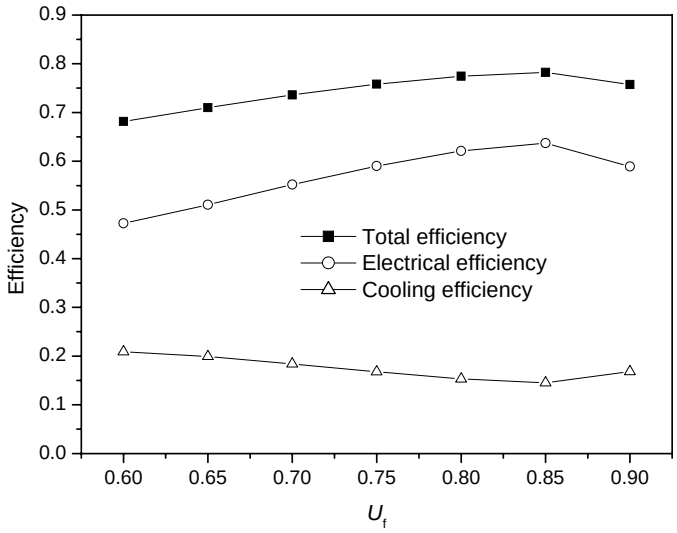

Figure 8.7 Effect of fuel utilisation factor on efficiency

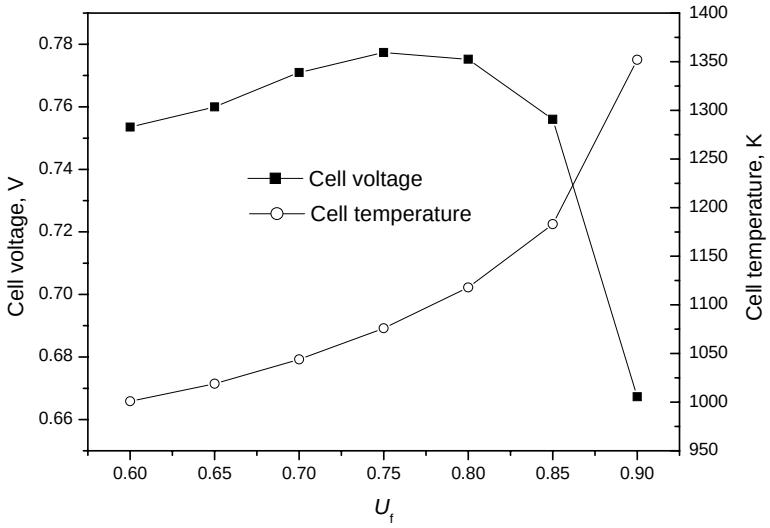

Figure 8.8 Effect of fuel utilisation factor on cell voltage and cell temperature

8.5.3 Effect of circulation ratio

The effects of circulation ratio on system performance are given in Figure 8.9. It can be seen that an increase in the circulation ratio has a positive impact on the system electrical efficiency while adversely affecting the cooling efficiency. The total efficiency can increase slightly with an increase in the circulation ratio. If the circulation ratio increases, the global fuel utilisation factor will also increase. Hence, the electrical efficiency increases for a higher value of circulation ratio. The high circulation ratio also leads to a lower depleted fuel heating value, and hence, a lower driven temperature in the adsorption chiller. The lower driven temperature leads to a decrease in cooling power for a fixed cycle time. Hence, for the fixed inlet fuel flow rate, the cooling efficiency will decrease with an increase in the circulation ratio. Figure 8.10 presents the effect of circulation ratio on cell voltage and cell temperature. The trends of the curves in Figure 8.10 are very similar to those in Figure 8.8 as an increase of circulation ratio leads to a larger global utilisation factor. The effects on cell voltage and cell temperature for these two operating parameters are similar.

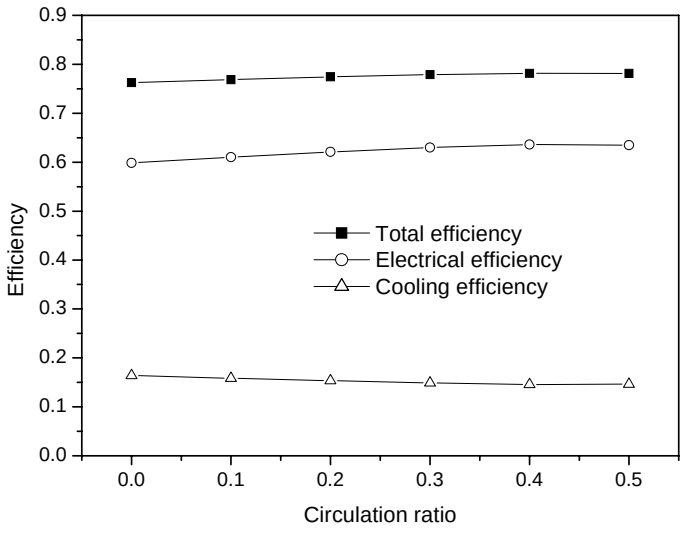

Figure 8.9 Effect of circulation ratio on efficiency

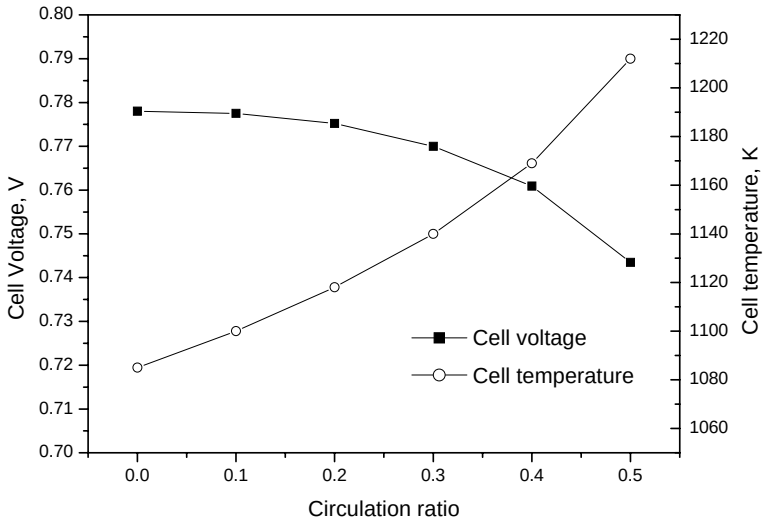

Figure 8.10 Effect of circulation ratio on cell voltage and cell temperature

8.5.4 Effect of inlet air preheat temperature

The inlet air temperature can be increased by increasing the heat exchange efficiency between air and the mixed gas from the combustor in Heat Exchanger 1. Figure 8.11 presents the effect of inlet air temperature on system efficiency. An increase in the inlet air temperature yields an increase in the electrical efficiency and total efficiency which have a negative effect on cooling efficiency. A higher value of inlet air temperature will result in a higher cell temperature, leading to an increase in the voltage (see Figure 8.12). The higher inlet air temperature also leads to a reduction in the temperature of steam, which drives the adsorber. Thus, the cooling power will be reduced with an increase in the inlet air temperature.

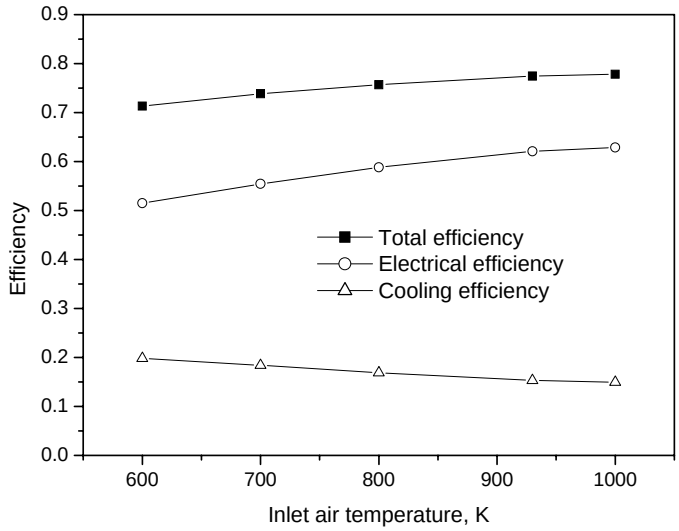

Figure 8.11 Effect of inlet air temperature on efficiency

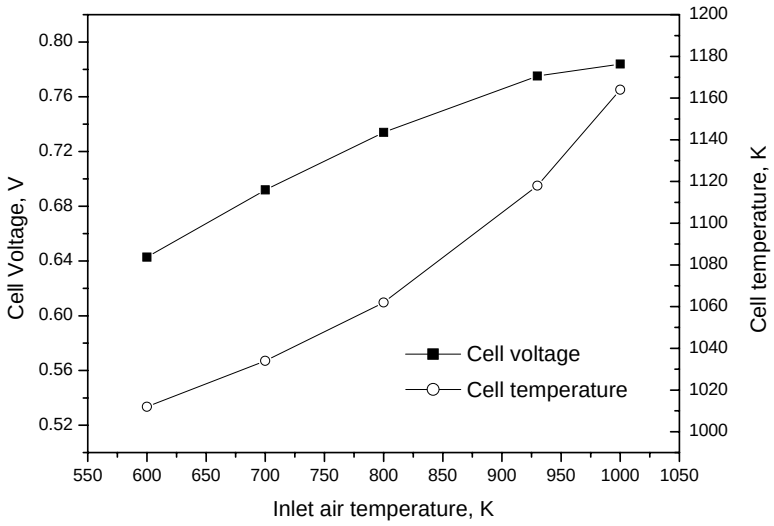

Figure 8.12 Effect of inlet air temperature on cell voltage and cell temperature

8.5.5 Effect of the mass of adsorbent

Figure 8.13 shows the effect of total mass of adsorbent on cooling power. The mass of zeolite adsorbent in adsorber is proportional to the number of adsorption units. Therefore, an

increased mass of zeolite will lead to a reduction of the inlet mass flow of the exhaust gas from Heat Exchanger 1 for every adsorption unit. It is concluded in Chapter 5 that the thermal performance of adsorption cycle will change very little when the mass flow rate of the heat exchange fluid is larger than a certain value. Hence, when the total mass of adsorbent increases, the cycled refrigerant produced by every adsorption unit changes negligibly. Thus the total cycled refrigerant is increased for a larger mass of adsorber, which leads to a higher value of cooling power. With a farther increase in the mass of the adsorbent, the maximum temperatures of adsorbent decrease rapidly, causing a significant reduction in the cycled mass. Thus, the total cycled refrigerant begins to decrease. Therefore, the cooling power has a maximum value with the variation of mass of adsorbent.

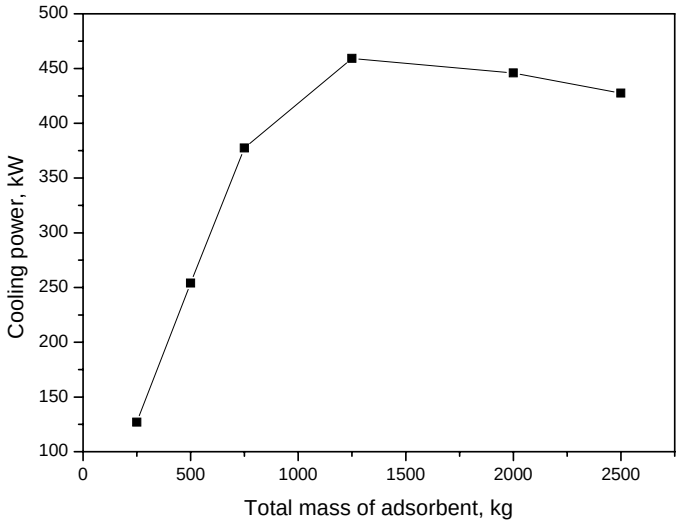

Figure 8.13 Effect of the total mass of adsorbent on cooling power produced

8.6 SUMMARY

In this chapter, the effects of fuel flow rate, circulation ratio, fuel utilisation factor, inlet air temperature and the mass of adsorbent on the system performance are investigated. Based on the simulation results, the following conclusions can be drawn:

(1) The proposed IRSOFC-Adsorption chiller cogeneration system can achieve a total efficiency of more than 77% (including electrical power of 62% and cooling power of 15%).

(2) The electrical efficiency and total efficiency decrease as the fuel flow rate increases. In addition, the cooling power increases asymptotically to a constant value with an increase in the fuel flow rate.

(3) The electrical efficiency has a maximum value for a value of U_f about 0.85 within the investigated range.

(4) An increase in the circulation ratio has a positive impact on the system electrical efficiency while adversely affecting the cooling power.

(5) An increase in the inlet air temperature yields an increase in the electrical efficiency and total efficiency. The cooling power has a maximum value with the variation of mass of adsorbent in the adsorption chiller.

CHAPTER 9

CONCLUSIONS AND RECOMMENDATIONS

9.1 CONCLUSIONS

Several numerical models including thermodynamic model, lumped model and heat and mass transfer model for different zeolite/water adsorption refrigeration cycles were developed and used to investigate the effect of and operating conditions on system performance.

Thermodynamic studies of different adsorption cycles show that COP has a maximum value at a certain value of generation temperature (T_g). Both COP and COP (max) increases as the evaporating temperature (T_e) increases while the optimal value of T_g changes very little with T_e. The reduction of entropy production for the adsorption cycles can result in higher COP. The thermal exchange process in the adsorbent bed is the controlling factor for COP of the adsorption cooling cycle. Both heat and mass recovery results in increased COP for the adsorption cycle. However, the increase of COP is due mainly to heat recovery.

The simulation results for the novel cascading cycle show that the first and second heat recovery processes are very effective thus resulting in a higher COP. The COP for the base case is found to be 1.35, which is much higher than the COP of an intermittent cycle (about 0.5) and a two-bed combined heat and mass recovery cycle (about 0.8). However, its specific cooling power (SCP) is much lower than that of the intermittent cycle. It appears that there is a maximum value of COP within the range of middle temperature (T_m) investigated for a prescribed driven temperature. However, when the COP reaches its highest value, the value of the SCP is at its lowest. Both the COP and SCP increases with an increase in the driven temperature. However, when the driven temperature increases beyond a certain value, the change in COP is negligible.

A two-dimensional non-equilibrium numerical model describing the combined heat and mass transfer in adsorbent bed has been developed. Mass transfer resistances in both micro-pores and macro-pores are considered in the model. COP increases with an increase in adsorbent thickness while SCP reduces with an increase in adsorbent thickness. Particle size has very little effect on the performance of the cooling cycle. The performance of the adsorption cooling cycle can be improved slightly by compressing the adsorbent bed when the adsorbent bed porosity is varied from 0.25 to 0.38. The system performance in terms of both its COP and SCP varies almost linearly with condensing temperature (T_c) and evaporating temperature (T_e). The performance coefficients increase with a reduction in T_c but with an increase in T_e. The adsorption temperature, T_a has an optimal value based on system performance for other operating conditions fixed (T_g = 473 K, T_e = 279 K and T_c = 318 K). SCP has a maximum value within the range of generation temperature (T_g) investigated for a given driven temperature ($T_{h,in}$). COP is directly affected by the generation temperature for different driven temperatures. It increases and tends to a constant value with an increase in T_g. The optimal value of velocity of the heat exchange fluid lies within the range of 0.1 - 0.5 m/s. Heat transfer limitations in condenser do affect the performance of adsorption cycle. The performance will increase with an increase in the inlet cool water ($\dot{m}_{cw}$) in condenser. The experimental study based on this numerical model shows that the model can be used to study the heat and mass transfer mechanisms of the adsorption cycle and predict its system performance.

The heat and mass transfer model is extended to study transfer mechanisms for a combined heat and mass recovery adsorption system. It is concluded that the mass recovery phase is very short (about 50 seconds) compared to the whole cycle time for the specified operating conditions. By using only mass recovery, the COP and SCP can be improved by about 6% and 7%, respectively compared to the basic cycle. The COP will increase and tend

to a constant value while the SCP reduces with an increase in heat recovery time for the combined heat and mass recovery cycle. For the combined heat and mass recovery cycle with the given conditions, the calculated values of the COP and SCP are 0.65 and 27.58 W/kg, respectively. Although there is a significant increase in COP (by about 47%) compared to the basic cycle, there is an accompanied reduction in SCP by about 40%. The COP value of the system increases while its SCP decreases with an increase in the degree of heat recovery (D_{hr}). When D_{hr} becomes greater than 90%, the increase of COP results in a severe decrease in the SCP. Both COP and SCP increase with an increase in the driven temperature of heat exchange fluid. The SCP of the system can be severely deteriorated when the fluid velocity is below 0.1 m/s. However, for velocities larger than 0.5 m/s, any change in fluid velocity will result in negligible change in the SCP. The COP of the system increases while its SCP decreases with an increase in adsorbent bed thickness.

Finally, a zeolite/water adsorption refrigeration and internal reforming solid oxide fuel cell (IRSOFC) cogeneration system was studied numerically. The results show that this system can achieve a total efficiency of more than 77% (including electrical power of 62% and cooling power of 15%). The electrical efficiency and total efficiency of this cogeneration system decrease as the fuel flow rate increases. In addition, the cooling power increases asymptotically to a constant value with an increase in the fuel flow rate at a given ratio of inlet fuel flow rate to inlet air flow rate of 0.089. The electrical efficiency has a maximum value for a value of U_f about 0.85 within the investigated range. An increase in the circulation ratio has a positive impact on the system electrical efficiency while adversely affecting the cooling power. An increase in the inlet air temperature yields an increase in the electrical efficiency and total efficiency. The cooling power has a maximum value with the variation of mass of adsorbent in the adsorption chiller.

9.2 RECOMMENDATIONS FOR FUTURE WORK

The entropy production in the adsorbent process is dominant in the adsorption cycle. Thus, reducing the entropy production in the adsorbent bed is a useful way to improve the coefficient of performance. Therefore, a comparison of entropy production for the four phases with different conditions can be considered in future research to provide a better understanding on the performances.

In most heat and mass transfer models, adiabatic boundary conditions are assumed. However, from the author's experimental results, the main cause for deviation between the simulated and experimental results may be heat loss from the boundary. Future efforts should be focused on developing a more detailed numerical model by including the effect of heat loss.

Although many advanced cycles have been proposed to improve system performance, most of these cycles focus on improving COP. Unfortunately, an increase in COP is often accompanied by a reduction in SCP. It is therefore necessary to intensify research efforts on the design of the adsorber to improve the heat transfer coefficient between the adsorbent bed and heat exchange fluid. This will lead to an increase in SCP.

Experimental studies for the advanced cycle proposed in this project such as the cascading cycle and combined heat and mass recovery cycle should be carried out to compare with the numerical results. Compared with the traditional vapour compression refrigeration system, one advantage of the adsorption refrigeration system is that it can be driven by free or cheap heat sources such as waste heat and solar energy. Thus the adsorption refrigeration and SOFC cogeneration system proposed by the author has a good potential for future applications. An experimental study on such system should also be carried out in the future to yield more insight on the actual system.

Since the temperature of exhaust gas from the adsorber in SOFC-AC cogeneration system is still very high, a Rankine cycle can be incorporated into this system to generate more electrical power.

References

Alam K.C.A., Saha B.B., Kang Y. T., Akisawa A. and Kashiwagi T., Heat exchanger design effect on the system performance of silica gel adsorption refrigeration systems, *International Journal of Heat and Mass Transfer*, Vol. 43, pp. 4419-4431, 2000

Aittomäki A. and Härkönen M., Internal regeneration of the adsorption process, *Solid Sorption Refrigeration Symposium*, Paris, France, November 1992

Ben Amar N., Sun L. M. and Meunier F., Numerical analysis of adsorptive temperature wave regenerative heat pump, *Applied Thermal Engineering*, Vol. 16, No. 5, pp. 405-418, 1996

Bessette N. F., *Modeling and Simulation of a Solid Oxide Fuel Cell Power System*, PhD Thesis, Georgia Institute of Technology, 1994

Bird R. B., Stewart W. E. and Lightfoot E. N., *Transfer Phenomena*, New York, John Wiley & Sons, 1960

Bossel U. G., *Final Report on SOFC Data Facts and Figures*, Swiss Federal Office of Energy, Berne, CH, 1992

Bove R., Lunghi P. and Sammes, N. M., SOFC Mathematical model for systems simulation. part one: from a micro-detailed to macro-black-box model, *International Journal of Hydrogen Energy*, Vol. 30, pp. 181 – 187, 2005

Burer M., Tanaka K., Favrat D. and Yamada K., Multi-criteria optimization of a district cogeneration plant integrating a solid oxide fuel cell-gas turbine combined cycle, heat pumps and chillers, *Energy*, Vol.28, pp. 497-518, 2003

Cacciola G., Czepirskik L., Restuccia G., and Giordano N., Preformed zeolite products to be used in adsorption heat pump: Part 1. *Preparation Methodology and Adsorption Measurement*, 1993

Cacciola G. and Restuccia G., Reversible adsorption heat pump: a thermodynamic model, *International Journal of Refrigeration*, Vol. 18, pp. 100-106, 1995

Carman P. C., Fluid flow through a granular bed, *Transactions of Institution of Chemical Engineers*, London, 1937

Campanari S., Thermodynamic model and parametric analysis of a tubular SOFC module, *Journal of Power Sources*, Vol. 92, pp. 26-34, 2001

Chahbani M. H., Labidi J. and Paris J., Effect of mass transfer kinetics on the performance of adsorptive heat pump systems, *Applied Thermal Engineering*, Vol. 22, pp. 23-40, 2002

Chandra I. and Patwardhan V. S., Theoretical studies on adsorption heat transformer using zeolite-water vapour pair, *Heat Recovery Systems & CHP*, Vol. 10, No. 5, pp. 527-537, 1990

Chan S. H., Ho H. K. and Tian Y., Modeling of simple hybrid solid oxide fuel cell and gas turbine power plant, *Journal of Power Sources*, Vol. 109, pp.111-120, 2002

Chen L. and Tan Y. K., Study on the adsorption characteristics of $SrCl_2$-NH_3 chemisorption refrigeration working pair, *ACTA ENERGIAE SOLARIS SINICA*, Vol. 22, No. 1, pp. 31-34, 2001(Chinese)

Cho S. H., Kim J. N. and You Y. J., Silica gel/water adsorption cooling system, *Solid Sorption Refrigeration Symposium*, Paris, France, November 1992

Chua H. T., Ng K. C., Malek A., Kashiwag T., Akisawa A. and Saha B. B., Entropy generation analysis of two-bed, silica gel-water, non-regenerative adsorption chillers, *Journal of Applied Physics*, Vol. 31, pp.1471-1477, 1998

Critoph R. E., Activated carbon adsorption cycles for refrigeration and heat pumping, *Carbon*, Vol. 27, pp. 63-70, 1989

Critoph R. E., Forced convection adsorption cycles, *Applied Thermal Engineering*, Vol. 18, pp. 799-807, 1998

Critoph R. E.**,** Simulation of a continuous multiple-bed regenerative adsorption cycle, *International Journal of Refrigeration*, Vol. 24, No. 5, pp. 428-437, 2001

Critoph R. E., Multiple bed regenerative adsorption cycle using the monolithic carbon-ammonia pair, *Applied Thermal Engineering*, Vol. 22, pp. 667-677, 2002

Critoph R. E., Metcalf S. J., Specific cooling power intensification limits in ammonia-carbon adsorption refrigeration systems, *Applied Thermal Engineering*, Vol. 24, pp.661-678, 2004

Coulibaly Y., Bambang Teguh P., Diny M., Boussehain R. and Feidt M., Thermal behaviour of a solid sorption generator, *Revue Générale de Thermique*, Vol. 37, pp. 818-826, 1998 (in French)

Douss N., Meunier F. E. and Sun L. M., Predictive model and experimental results for a two-adsorber solid adsorption heat pump, *Industrial & Engineering Chemistry Research*, Vol. 27, pp. 310-316, 1988

Douss N. and Meunier F., Experimental study of cascading adsorption cycle, *Chemical Engineering Science*, Vol. 44, pp. 225-235, 1989.

E. Gluekauf, Theory of Chromatography, Part 10: Formula for diffusion into spheres and their application to chromatography, *Transaction Faraday Society*, Vol. 51, pp. 1540-1551, 1955

Grenier Ph., Guilleminot J. J., Meunier F., and Pons M., Solar powered solid adsorption cold store, *Transactions of the ASME*, Vol. 110, pp. 192-197, August 1988

Groll M., Reaction beds for dry sorption machines, *Heat Recovery Systems & CHP*, Vol. 13, No.4, pp. 341-346, 1993

Guilleminot J. J. and Meunier F., Heat and mass transfer in a non-isothermal fixed bed solid adsorbent reactor: a uniform pressure non-uniform temperature case, *International Journal of Heat and Mass Transfer*, Vol. 30, No. 8, pp. 1595-1606, 1987

Gui Y. B., Wang R. Z., Wang W., Wu J. Y. and Xu Y. X., Performance modeling and testing on a heat-regenerative adsorptive reversible heat pump, *Applied Thermal Engineering*, Vol. 22, pp. 309-320, 2002

Hall D. J., *Transient Modeling and Simulation of a Solid Oxide Fuel Cell*, PhD Thesis, University of Pittsburgh, 1997

Hajji A. and Worek W M., Simulation of a regenerative, closed-cycle adsorption cooling/heating system, *Energy*, Vol. 16, No. 3, pp. 643-654, 1991

Härkönen M. and Aittomäki A., The principle of internal regeneration as applied to the adsorption heat pump process, *Heat Recovery Systems & CHP*, Vol. 11, No. 4, pp. 239-248, 1991

Hsu, C. T., Cheng, P. and Wong, K. W. A lumped parameter model for stagnant thermal conductivity of spatially periodic porous media. *International Journal of Heat and Mass Transfer*, Vol.37, pp.2751-2759, 1995

Hu E. J., Simulated results of a non-valve, daily-cycled, solar-powered carbon/methanol refrigerator with a tubular solar collector, *Applied Thermal Engineering*, Vol.16, pp. 439-445, 1996

Li Y. and Sumathy K., Review of mathematical investigation on the closed adsorption heat pump and cooling systems, *Renewable & Sustainable Energy Reviews*, Vol. 6, pp. 305-337, 2002

Li M., Wang R. Z. and Shi F., Thermodynamics analysis of a solid adsorption refrigeration ice-maker model and experiment validation, *ACTA ENERGIAE SOLARIS SINICA*, Vol. 22, No. 3, pp. 274-279, 2001(Chinese)

Li M., Wang R. Z., Xu Y. X., Wu J. Y. and Dieng A. O., Experimental study on dynamic performance analysis of a flat-plate solar solid-adsorption refrigeration for ice maker, *Renewable Energy*, Vol. 27, No. 2, pp. 211-221, 2002

Liu Z. Y., Fu Z. M., Ge X. S., Su Y. H. and Wang Y. T., Experimental and numerical investigation of enhancement of heat and mass transfer in adsorption beds, *Journal of Thermal Sciences*, Vol. 3, No. 2, pp. 187-190, 1994

Liu Z. Y., Lu Y. Z. and Zhao J. X., Zeolite-active carbon compound adsorbent and its use in adsorption solar cooling tube, *Solar Energy Materials and Solar Cells*, Vol. 52, pp. 45-53, 1998

Llobet J. and Goetz V., Rotary system for the continuous production of cold by solid-gas sorption: modeling and analysis of energy performance, *International Journal of Refrigeration*, Vol. 23, pp. 609-625, 2000

Lu G. Q. and Leong K. C., Adsorption cycles for refrigeration and heat pump systems, *Journal of the Institution of Engineers*, Singapore, Vol. 33, No. 5, September 1993

Luo L., Lecomte D. and Feidt M., A review of solid-vapour adsorbent data with respect to solar refrigeration, *International Symposium on Thermodynamic Analysis and Improvement of Energy System*, Beijing, China, 1989

Luo L. and Feidt M., Thermodynamics of adsorption cycles: a theoretical study, *Heat Transfer Engineering*, Vol.13, No. 4, 19-31, 1992

Luo L. and Tondeur D., Transient thermal study of an adsorption refrigeration machine, *Adsorption*, Vol. 6, pp. 93-104, 2000

Marletta L., Maggio G., Freni A., Ingrasciatta M. and Restuccia G., A non-uniform temperature non-uniform pressure dynamic model of heat and mass transfer in compact adsorbent beds, *International Journal of Heat and Mass Transfer*, Vol. 45, pp. 3321-3330, 2002

Massardo A. F., Lubelli F., Internal reforming solid oxide fuel cell-gas turbine combined cycles (IRSOFC-GT): Part A-cell model and cycle thermodynamic analysis, *Transactions of the ASME*, Vol.122, pp.27-35, 2000

Meunier F., Solid sorption: an alternative to CFCs, *Heat Recovery Systems & CHP*, Vol. 13, No. 4, pp. 289-295, 1993

Meunier F., Solid sorption heat powered cycles for cooling and heat pumping applications, *Applied Thermal Engineering*, Vol. 18, pp. 715-729,1998.

Meunier F., Poyelle F. and Levan M. D., Second-law analysis of adsorptive refrigeration cycles: the role of thermal couple entropy production, *Applied Thermal Engineering*, Vol. 17, No. 1, pp. 43-55, 1997

Miles D. J., Sanborn D. M., Nowakowski G. A. and Shelton S. V., Gas fired sorption heat pump development, *Heat Recovery Systems & CHP*, Vol. 13, No. 4, pp. 347-351, 1993

Miles D. J., *Analysis and Design of a Solid Adsorption Heat Driven Heat Pump*, Georgia Institute of Technology, Ph.D. Thesis, 1989

Miltkau T. and Dawoud B., Dynamical modeling of the combined heat and mass transfer during the adsorption/desorption of water vapor into/from a zeolite layer of an adsorption heat Pump, *International Journal of Thermal Sciences*, Vol. 24, pp. 753-762, 2002

Onyebueke L., Feidt M., Apparent thermal diffusivity of active charcoals in presence of alcohol vapours, 18th International Congress of Refrigeration, Montreal, Canada, pp. 1084-1087, 1991

Passos E., Meunier F. and Gianola J. C., Thermodynamic performance improvement of an intermittent solar-power refrigeration cycle using adsorption of methanol on activated carbon, *Heat Recovery Systems & CHP*, Vol. 6, No. 3, pp. 259-264, 1986

Passos E. F., Escobedo J. F. and Meunier F., Simulation of an intermittent adsorptive solar cooling system, *Solar Energy*, Vol. 42, No. 2, pp 103-111, 1989

Patankar S. V., *Numerical Heat Transfer and Fluid Flow*, Hemisphere Publication Corporation, 1980

Picard P., Sorption systems: the point of view of a gas utility, *Heat Recovery Systems & CHP*, Vol. 13, No. 4, pp. 329-334, 1993

Pons M., Laurent D. and Meunier F., Experimental temperature fronts for adsorptive heat pump applications, *Applied Thermal Engineering*, Vol. 16, pp. 395-404, 1996

Pons M. and Feng Y., Characteristic parameters of adsorptive refrigeration cycles with thermal refrigeration, *Applied Thermal Engineering*, Vol. 17, No. 3, pp. 289-298, 1997

Poyelle F., Guilleminot J. J. and Meunier F., Experimental tests and predictive model of an adsorptive air conditioning unit, *Industrial and Engineering Chemistry Research*, Vol. 38, pp. 298-309, 1999

Qu T. F., Wang R. Z. and Wang W., Study of heat and mass recovery in adsorption refrigeration cycles, *Applied Thermal Engineering*, Vol. 21, pp.439-452, 2001

Restuccia G., Freni A. and Maggio G., A zeolite-coated bed for air conditioning adsorption systems: paramedic study of heat and mass transfer by dynamic simulation, *Applied Thermal Engineering*, Vol. 22, pp. 619-630, 2002

Ruthven D. M., *Principles of Adsorption and Adsorption Process*, Wiley, New York, 1984

Saha B. B., Boelman E. and Kashiwagi T., Computer simulation of a silica gel-water adsorption refrigeration cycle-the influence of operating conditions on cooling output and COP, *ASHRAE Transactions: Research*, Vol.101, No.2, pp. 348-357,1995

Schwarz J., Keller C. and Soltes J., Adsorption cycles with the working fluid zeolite/water, *ASHRAE Transactions*, Vol. 97, 1991

Silveria J. L., Leal E. M. and Ragonha J. L., Analysis of a molten carbonate fuel cell: cogeneration to produce electricity and cold water, *Energy*, Vol., 26, pp.891-904, 2001

Shelton S. V., Residential Space Conditioning with Solid Sorption Technology, *Heat Recovery Systems & CHP*, Vol. 13, No. 4, pp. 353-361, 1993

Shen W. D., Zhen P. Z. and Jiang D. A., *Engineering Thermodynamics*, Higher Education Press, Beijing, 1983 (in Chinese)

Sakoda A. and Suzuki M., Fundamental study on solar power adsorption cooling system, *Journal of Chemical Engineering of Japan*, Vol. 17, No. 1, pp. 52-57, 1984

Sami S. M. and Tribes C., An improved model for predicting the dynamic behavior of adsorption systems, *Applied Thermal Engineering*, Vol. 16, No. 4, pp. 327-338, 1997

San J. Y., Ni C. C. and Hsu S. H., Validity of solid side mass diffusivity in simulation of water vapor adsorbed by silica gel in packed beds, *International Journal of Thermal Sciences*, Vol. 41, pp. 41-49, 2002

Srivastava N. C. and Eames L. W., A review of adsorbents and adsorbates in solid-vapour adsorption heat pump systems, *Applied Thermal Engineering*, Vol. 18, pp. 707-714, 1998

Stitou D, Spinner B., Satzger P. and Ziegler F., Development and comparison of advanced cascading cycles coupling a solid/gas thermochemical process and a liquid/gas absorption process, *Applied Thermal Engineering*, Vol. 20, pp.1237-1269, 2000

Sun L. M. and Meunier F., A detailed model for non-isothermal sorption in porous adsorbents, *Chemical Engineering Science*, Vol. 42, No. 7, pp. 1585-1593, 1987

Sun L. M., Ben Amar N. and Meunier F., Numerical study on coupled heat and mass transfers in an adsorber with external fluid heating, *Heat Recovery Systems & CHP*, Vol. 15, No. 1, pp. 19-29, 1995

Sun L. M., Feng Y. and Pons M., Numerical investigation of adsorptive heat pump systems with thermal wave heat refrigeration under uniform-pressure conditions, *International Journal of Heat and Mass Transfer*, Vol. 40, No. 2, pp. 281-293, 1997

Suzuki M., Application of adsorption cooling system to automobiles, *Solid Sorption Refrigeration Symposium*, Paris, France, November 1992

Suzuki M., *Adsorption Engineering*, Kodansha Ltd, Tokyo, 1990

Sward B. K., Douglas L. M. and Meunier F., Adsorption heat pump modeling: the thermal wave process with local equilibrium, *Applied Thermal Engineering*, Vol. 20, pp. 759-780, 2000

Tamainot-Telto Z. and Critoph R. E., Monolithic carbon for sorption refrigeration and heat pump applications, *Applied Thermal Engineering*, Vol. 21, pp. 37-52, 2001

Tao W. Q., *Numerical Heat Transfer (Second Edition)*, Xi'an Jiaotong University, Xi'an, China, 2001 (in Chinese)

Teng Y., Wang R. Z. and Wu J. Y., Study of the fundamentals of adsorption systems, *Applied Thermal Engineering*, Vol. 17, No. 4, pp. 327-338, 1997

Turner L., *Improvement of Activated Charcoal-Ammonia Adsorption Heat Pumping/Refrigeration Cycles. Investigation of Porosity and Heat/Mass Transfer Characteristics*, University of Warwick, Ph.D. Thesis, July 1992

Wang Q., Chen G., and Han B., Measurement and analysis of efficient diffusivity for adsorbent /adsorbate pairs in adsorption refrigeration process, *ACTA ENERGIAE SOLARIS SINICA*, Vol. 22, No. 2, pp. 187-190, 2001(in Chinese)

Wang R. Z., Wu J. Y., Teng Y., Xu Y., Shi W., Yang L. and Wang Q., Research on the key technologies of solid sorption refrigeration, *ACTA ENERGIAE SOLARIS SINICA*, Vol. 19, No. 1, 1998 (in Chinese)

Wang R. Z., Performance improvement of adsorption cooling by heat and mass recovery operation, *International Journal of Refrigeration*, Vol. 24, pp. 602-611, 2001

Wang R. Z., Xu Y. X., Wu J. Y., Li M., and Shou H. B., Research on a combined adsorption heating and cooling system, *Applied Thermal Engineering*, Vol. 22, No. 6, pp 603-617, April 2002 A

Wang W., Qu T. F. and Wang R. Z., Influence of degree of mass recovery and heat regeneration on adsorption refrigeration cycles, *Energy Conversion and Management*, Vol. 43, pp. 733-741, 2002 B

Worsøe-Schmidt P., Solar refrigeration for developing countries using a solid-absorption cycle, *International Journal of Ambient Energy*, Vol. 4, No. 3, 1983

Yang R. T., *Gas Separation by Adsorption Process*, Butterworths, Boston, 19987

Zanifé T. and Meunier F., Experimental results of a zeolite-water heat pump installed in a slaughter house, *Heat Recovery Systems & CHP*, Vol. 12, No. 2, pp. 131-142, 1992

Zhang L. Z. and Wang L., Effects of coupled heat and mass transfers in adsorbent on the performance of a waste heat adsorption cooling unit, *Applied Thermal Engineering*, Vol.19, pp. 195-215, 1999

Zhang L. Z., A three-dimensional non-equilibrium model for an intermittent adsorption cooling system, *Solar Energy*, Vol. 69, No. 1, pp. 27-35, 2000

Zhang W., Croiset E., Douglas P. L., Fowler M. W., Entchev E., Simulation of a tubular solid oxide fuel cell stack using AspenPlusTM unit operation models, *Energy Conversion and Management* , Vol. 46, pp. 181-196, 2005

Zhu D. and Wang S., Experimental investigation of contact resistance in absorber of solar adsorption refrigeration, *Solar Energy*, Vol. 73, No. 3, pp. 177-185, 2002

Zhu R. Q., Han B. Q., Lin M. Z. and Yu Y. Z., Experimental investigation on an adsorption system for producing chilled water, *International Journal of Refrigeration*, Vol. 15, No. 1, pp. 31-34, 1992

APPENDIX

PROGRAMME LISTING FOR CALCULATION OF NUMERICAL MODEL IN CHAPTER 5

The FORTRAN code list below is the main subroutine of the full programme

```
CCCCCCCCCCCCCCCCCCCCCCCCCCCCCCCCCCCCCCCCCCCCCCCCCCCCCCCCCCCCCCCCCCCCCCCCCCCCCCC
      SUBROUTINE USER
C*****************************************************************
      INCLUDE 'PARAM.FOR'
      INCLUDE 'COMMON.FOR'
C-*-*-*-*-*-*-*-*-*-*-*-*-*-*-*-*-*-*-*-*-*-*-*-*-*-*-*-*-*-*-*-*-*-*-*-*-*-*
      DIMENSION TEM(NI,NJ),T2(NI,NJ),PF(NI,NJ),Q(NI,NJ),
      1DQDT(NI,NJ),ERRPR(NI,NJ),PFHOLD(NI,NJ)
      EQUIVALENCE (F(1,1,5),TEM(1,1)),(F(1,1,6),PF(1,1)),
      1(F(1,1,7),Q(1,1))
C*****************************************************************
C                       U S E R   P R O B L E M
C-----------------------------------------------------------------
      ENTRY GRID
C
      TITLE(5)='TEMP'
      TITLE(6)='PRESSURE'
C     PRINTF='PROB4.DAT'

      KSOLVE(5)=1
      KSOLVE(6)=2
C
      KPRINT(5)=1
      KPRINT(6)=1

      RELAX(5)=0.8
      RELAX(6)=0.8
C
      MODE=2
      R(1)=0.

      NZX=1
      XZONE(1)=0.6
      POWRX(1)=1.0
      NCVX(1)=40

C
      NZY=3
      YZONE(1)=0.020
      POWRY(1)=1.0
      NCVY(1)=10
      YZONE(2)=0.001
      POWRY(2)=1.0
      NCVY(2)=2
      YZONE(3)=0.015
      POWRY(3)=1.0
      NCVY(3)=12
```

```
C
      CALL ZGRID

      YSTR=YZONE(1)
      YEND=YSTR+YZONE(2)


C
      NSTPS=20000
      NREPT=500
      DT=0.1

C
      RETURN
C-----------------------------------------------------------------------
      ENTRY BEGIN
C
      R0=20E-3
      R1=21E-3
      R2=41E-3
      LENTH=0.6
      UF=1
C
      T0=318
      T1=473
      TIN=523
      P0=1000
      P1=10000
C
      VOIDA=0.38
      VOIDI=0.42
      VOIDT=0.64
      DDP=0.0002
      RHOADS=620
      RHOMET=7850
      RHOFLD=800
      KADS=0.2
      KMET=15.6
      KFLD=0.1
      CPADS=836
      CPMET=460
      CPFLD=2090
C
      CPG=1880
      CPL=4180
      VIS=9.09E-6
      HEATADS=3.2E6
C
      DO 200 J=1,M1
         YJ=Y(J)
      DO 201 I=1,L1
      XI=X(I)
      TEM(I,J)=318.0
C
      IF(YJ.LE.YSTR) IMAT(I,J)=1
      IF(YJ.GT.YSTR.AND.YJ.LE.YEND)       IMAT(I,J)=2
       IF(YJ.GT.YEND) IMAT(I,J)=3
 201     CONTINUE
 200    CONTINUE
```

```
      DO 211 I=1,L1
      DO 210 J=1,M1
      Q(I,J)=0.
      PF(I,J)=0.
      IF(IMAT(I,J).EQ.1) THEN
      TEM(1,J)=493
C
      U(I,J)=1
      ENDIF
      IF(IMAT(I,J).EQ.3) THEN
      Q(I,J)=0.2447300
C     Q(I,J)=0.2233977
      PF(I,J)=1000
       ENDIF

 210  CONTINUE
 211   CONTINUE


C
      RETURN
C-----------------------------------------------------------------------
      ENTRY DENSE
      DO 300 I=1,L1
      DO 301 J=1,M1
       IF(IMAT(I,J).EQ.1) THEN
       RHO(I,J)=167200
      RHON(I,J)=167200
      ENDIF
      IF(IMAT(I,J).EQ.2) THEN
      RHO(I,J)=3611000
      RHON(I,J)=3611000
      ENDIF
      IF(IMAT(I,J).EQ.3)THEN
      RHO(I,J)=PF(I,J)*0.018*1880/(8.314*TEM(I,J))

      RHON(I,J)=518320+620*4180*Q(I,J)+VOIDT*PF(I,J)*0.018*1880/(8.314
      1*TEM(I,J))

      ENDIF
301    CONTINUE
300   CONTINUE
C
      RETURN
C-----------------------------------------------------------------------
      ENTRY DENSE2
C
      DO 302 I=1,L1
         DO 303 J=1,M1
       IF(IMAT(I,J).EQ.1) THEN
       RHO(I,J)=167200
      RHON(I,J)=167200
      ENDIF
      IF(IMAT(I,J).EQ.2) THEN
      RHO(I,J)=3611000
      RHON(I,J)=3611000
      ENDIF
      IF(IMAT(I,J).EQ.3) THEN
      RHO(I,J)=SMALL
```

```
      RHON(I,J)=0.64*318/TEM(I,J)
C     RHON(I,J)=VOIDT*0.018/(8.314*TEM(I,J))
      ENDIF
 303   CONTINUE
 302  CONTINUE

      RETURN
C-----------------------------------------------------------------------
      ENTRY GTIME
C
C      IF(ISTEP.GT.10) DT=0.02
      IF(TIME.GT.300) DT=1.0
      IF(TIME.GT.1300)DT=2.0
      RETURN
C-----------------------------------------------------------------------
      ENTRY BOUND
      IF(ITER.GT.1) THEN
      DO 500 I=1,L1
      TEM(I,M1)=TEM(I,M2)
      TEM(I,1)=TEM(I,2)
      IF(AVGP.LT.10000) THEN
      PF(I,M1)=PF(I,M2)
      ELSE
      PF(I,M1)=10000
      ENDIF
 500   CONTINUE

      DO 511 I=1,L1
      DO 510 J=1,M1
      TEM(L1,J)=TEM(L2,J)
      IF(IMAT(I,J).NE.1) THEN
      TEM(1,J)=TEM(2,J)
      ENDIF
      IF(IMAT(I,J).EQ.3) THEN
       IF(AVGP.LT.10000) THEN
      PF(1,J)=PF(2,J)
      PF(L1,J)=PF(L2,J)
      ELSE
      PF(1,J)=10000
      PF(L1,J)=10000
      ENDIF
      ENDIF
 510   CONTINUE
 511   CONTINUE
      ENDIF
C
      RETURN
C-----------------------------------------------------------------------
      ENTRY OUPT1
      AREA1=0.
      VOLT=0.
      VOLP=0.
      VOLQ=0.
      AREA2=0.
      VOL2=0.
      TOUT=0.
      AREA3=0
      VOL3=0.
      AREAN3=0.
      VOLN3=0.
```

```
      DO 602 I=2,L2
      DO 603 J=2,M2

       IF(IMAT(I,J).EQ.3)     THEN

      AREA1=AREA1+XCV(I)*YCV(J)*Y(J)
      VOLT=VOLT+TEM(I,J)*XCV(I)*YCV(J)*Y(J)
      VOLP=VOLP+PF(I,J)*XCV(I)*YCV(J)*Y(J)
      VOLQ=VOLQ+Q(I,J)*XCV(I)*YCV(J)*Y(J)

      ENDIF
      IF(IMAT(I,J).EQ.1) THEN
      TOUT=TOUT+TEM(L1,J)*YCV(J)*Y(J)
      AREA3=AREA3+XCV(I)*YCV(J)*Y(J)
      VOL3=VOL3+TEM(I,J)*XCV(I)*YCV(J)*Y(J)
      AREAN3=AREAN3+YCV(J)*Y(J)
C     VOLN3=VOLN3+FOLD(I,J,5)*XCV(I)*YCV(J)*Y(J)
      ENDIF

      IF(IMAT(I,J).EQ.2) THEN
      AREA2=AREA2+XCV(I)*YCV(J)*Y(J)
      VOL2=VOL2+TEM(I,J)*XCV(I)*YCV(J)*Y(J)
      ENDIF
 603   CONTINUE
 602  CONTINUE
      AVGTEM=VOLT/AREA1
      AVGP=VOLP/AREA1
      AVGQ=VOLQ/AREA1
      TMET=VOL2/AREA2
      TOUT=TOUT/AREAN3
      TFLD=VOL3/AREA3
C     TFLDOLD=VOLN3/AREA3

      QINSUM=QINSUM+QIN

      WRITE(*,600) TIME,AVGTEM,AVGP,AVGQ,TMET,TFLD,QIN,TOUT
      CALL TCPLT
      WRITE(100,600) TIME,AVGTEM,AVGP,AVGQ,TMET,TFLD,QIN,QINSUM
600   FORMAT(1X,8F16.7)



      RETURN
C-----------------------------------------------------------------------
      ENTRY OUTPUT
C
C      IF(ITER.EQ.1) WRITE(6,790)
C      WRITE(6,791) ITER,TEM(8,15),PF(8,15),ERRMAX,V(8,15)
C      WRITE(6,791) ITER,TEM(8,14),PF(8,14),Q(8,14),DQDT(8,14)


C
C 790  FORMAT('   ITER',8X,'TEM(8,14)',8X,'P(8,14)',8X,'U(8,14)',
C     18X,'V(8,14)')
C 791  FORMAT(I4,4F18.9)
      ERRMAX=0.
      QIN=0.
      DO 780 I=2,L2
      DO 781 J=2,M2
      ERRPR(I,J)=ABS((PF(I,J)-PFHOLD(I,J))/(PF(I,J)-FOLD(I,J,6)+SMALL))
```

```
      PFHOLD(I,J)=PF(I,J)
      IF(ERRPR(I,J).GT.ERRMAX) ERRMAX=ERRPR(I,J)
      IF(IMAT(I,J).EQ.3) THEN
      QIN=QIN+(518320+620*4180*Q(I,J)+VOIDT*PF(I,J)*0.018*1880/(8.314
      1*TEM(I,J)))*(TEM(I,J)-FOLD(I,J,5))*XCV(I)*YCV(J)*Y(J)*3.14159*2
      2+3.2E6*620*(FOLD(I,J,7)-Q(I,J))*XCV(I)*YCV(J)*Y(J)*3.14159*2
      ENDIF
781   CONTINUE
780   CONTINUE



      RETURN
C-----------------------------------------------------------------------
      ENTRY GAMSOR
C
      IF(NF.EQ.5) THEN
      DO 800 J=1,M1
         DO 801 I=1,L1
      IF(IMAT(I,J).EQ.1) THEN
            GAM(I,J)=0.1
      ENDIF
      IF(IMAT(I,J).EQ.2) THEN
      GAM(I,J)=15.6
      ENDIF
       IF(IMAT(I,J).EQ.3) THEN
      GAM(I,J)=0.2
      ENDIF

 801     CONTINUE
 800  CONTINUE
C
      DO 810 J=2,M2
      DO 811 I=2,L2
      IF(IMAT(I,J).EQ.3) THEN
      CON(I,J)=HEATADS*RHOADS*DQDT(I,J)
      AP(I,J)=0.
      ENDIF
 811  CONTINUE
 810  CONTINUE
      ENDIF

      IF(NF.EQ.6) THEN
      DO 812 I=1,L1
         DO 813 J=1,M1
            GAM(I,J)=0
      IF(IMAT(I,J).EQ.3)THEN
      DC=4.73E-4*VOIDA*(0.45+0.55*VOIDA)*SQRT(TEM(I,J)**3)/
     1PF(I,J)**2+VOIDA**3*DDP**2/(150*(1-VOIDA)**2*VIS)
C
      GAM(I,J)=318*PF(I,J)*DC/TEM(I,J)
C     IF(ITER.GT.50.AND.ITER.LE.150) THEN
C     GAM(I,J)=GAM(I,J)+0.99*GAM(I,J)*(ITER-20)
C     ENDIF
C     IF(ITER.GT.20) THEN
C     GAM(I,J)=GAM(I,J)*100
C     ENDIF
C      GAM(I,J)=PF(I,J)*0.018*DC/(8.314*TEM(I,J))
      ENDIF
 813     CONTINUE
 812  CONTINUE
```

```
      DO 814 I=2,L2
         DO 815 J=2,M2
            CON(I,J)=0.
            AP(I,J)=0.
      IF(IMAT(I,J).EQ.3) THEN
      CON(I,J)=-1*318*8.314*RHOADS*DQDT(I,J)/0.018
      ENDIF

 815      CONTINUE
 814  CONTINUE
      ENDIF


      RETURN

C-----------------------------------------------------------------------

      ENTRY QCOM
      DO 903 I=1,L1
         DO 904 J=1,M1
      IF(IMAT(I,J).EQ.3) THEN
C     QS1=0.0467-79.72/TEM(I,J)+4.233E4/TEM(I,J)**2-5.617E6/TEM(I,J)**3
C     QS2=-0.456+5.157E2/TEM(I,J)-1.69E5/TEM(I,J)**2+1.845E7/TEM(I,J)**3
C     QS3=0.1776
      QS1=0.07-119.9/TEM(I,J)+6.369E4/TEM(I,J)**2-8.450E6/TEM(I,J)**3
      QS2=-0.687+7.757E2/TEM(I,J)-2.542E5/TEM(I,J)**2+2.775E7/
     1TEM(I,J)**3
      QS3=0.267-QS1-QS2
      B1=1.508E-10*EXP(7726.58/TEM(I,J))
      B2=5.417E-10*EXP(6074.71/TEM(I,J))
      B3=1.707E-10*EXP(5392.17/TEM(I,J))
      QEQ=QS1*B1*PF(I,J)/(1+B1*PF(I,J))+QS2*B2*PF(I,J)/(1+B2*
     1PF(I,J))+QS3*B3*PF(I,J)/(1+B3*PF(I,J))


      DIFG=3.92E-6*60*EXP(-28036/(8.314*TEM(I,J)))/DDP**2
      Q(I,J)=(DIFG*DT*QEQ+FOLD(I,J,7))/(1+DIFG*DT)
      DQDT(I,J)=DIFG*(QEQ-FOLD(I,J,7))/(1+DIFG*DT)


      ENDIF
904     CONTINUE
903   CONTINUE
C      PAUSE
C
      RETURN


C-----------------------------------------------------------------------
      ENTRY UVCOM
      DO 900 I=3,L2
      DO 901 J=2,M2

      IF(IMAT(I,J).EQ.3) THEN
      DC=4.73E-4*VOIDA*(0.45+0.55*VOIDA)*SQRT(TEM(I,J)**3)/
     1PF(I,J)**2+VOIDA**3*DDP**2/(150*(1-VOIDA)**2*VIS)

      U(I,J)=-1.*DC*(PF(I,J)-PF(I-1,J))/XDIF(I)

      ENDIF
```

```
 901  CONTINUE
 900  CONTINUE

      DO 910 I=2,L2
      DO 911 J=2,M3
      IF(IMAT(I,J).EQ.3) THEN
      DC=4.73E-4*VOIDA*(0.45+0.55*VOIDA)*SQRT(TEM(I,J)**3)/
     1PF(I,J)**2+VOIDA**3*DDP**2/(150*(1-VOIDA)**2*VIS)

      V(I,J+1)=-1.*DC*(PF(I,J+1)-PF(I,J))/YDIF(J+1)
      ENDIF
911   CONTINUE
910   CONTINUE


C
      RETURN
C-----------------------------------------------------------------------

      ENTRY LC
C
      RETURN
      END
C***********************************************************************
```